INVESTIGATING THE POTENTIAL ROLE OF DNA HYDROXYMETHYLATION IN THE CONTROL OF POST-STROKE AXON GROWTH

Marcus Dean Wallis, BSc.

Submitted to The University of Nottingham for the degree of Doctor of Philosophy

October 2019



University of Nottingham
UK | CHINA | MALAYSIA

ABSTRACT

An important mechanistic factor of functional recovery following ischemic stroke is the sprouting of new axons and repair of damaged axons in the region around the infarct. To induce this axonal growth, regulation of gene expression is required. Whilst some previous research has characterised a role of DNA methylation (5-methylcytosine, 5mC) in this regulation, less is known about what role, if any, oxidised forms of 5mC perform. 5mC is oxidised by Tet enzymes to form 5-hydroxymethylcytosine (5hmC), which acts mainly as an intermediate of demethylation and is therefore associated with increased gene expression. It has been previously shown that global 5hmC levels increase following ischemic stroke, although no determination has been made as to how this increase influences post-stroke axon growth.

The use of an *in vivo* model of ischemic stroke helped to determine that post-stroke increases in global 5hmC are delayed, peaking at 2-7 days post-stroke, and return to baseline after 1 month. The temporal peak in 5hmC coincides with previously determined peak expression of axon growth-related genes, suggesting a potential role of DNA hydroxymethylation in the regulation of post-stroke axon growth via altered gene expression. Furthermore, isolation of specific cell types from the post-ischemic brain revealed that post-stroke increases in 5hmC are observed not only in the total cell population, but also in microglial cells specifically. These post-stroke increases in 5hmC are accompanied by significantly increased expression of microglial activation markers. This therefore suggests that DNA hydroxymethylation is involved in the regulation of the brains innate immune response to ischemic stroke, which in itself has implications on post-stroke axon growth.

An *in vitro* model of ischemic stroke and reperfusion was also used to determine a direct effect of Tet enzyme expression on axon growth, with decreased expression of Tet2 and Tet3 each leading to significantly reduced axon growth. Additionally, it was seen that global 5hmC levels and Tet3 expression are significantly increased following hypoxic insult. Taken together, this suggests that ischemia may act to induce Tet3 expression in the brain, which subsequently acts to promote axonal growth as part of the central nervous system's endogenous repair response.

Overall, the body of work detailed in this thesis has revealed a potential role of 5hmC, and the Tet family of enzymes that catalyse its formation, in the regulation of post-stroke axonal growth. Though the novelty of these findings necessitates that further research be performed to consolidate this effect, it is hoped that this methylomic response to ischemic stroke can be used to develop delayed therapeutic treatments aimed at promoting post-stroke axonal growth and functional recovery.

ACKNOWLEDGEMENTS

There are so many people to whom I am very thankful for their role in helping me complete this body of work over the last 4 years; be it through technical advice/assistance, moral support, or just being there to listen to me complain about PhD life for years on end.

First thanks go to my family – Mum, Dad, Tayla, and all the rest – for always providing love & support and having no doubts in my ability to complete this PhD at times when I was doubting myself.

Thank you to the members of my lab – Jewel, Ged, Tracy, and all the students of E27 – for providing such a fun and friendly work environment… and also helping me believe I could overcome any obstacle the PhD threw my way by gifting me with my alter ego "Big Marco"!

Thank you to my best friends Colman and Emily for not only providing countless moments of fun and laughter over the last several years, but also being willing participants in my not-so-healthy coping mechanism of ordering takeaway food & binging TV shows.

Thank you to all of the staff and colleagues – Alexey, Maxine, David, Nicki, Mark, Simon, Raquel, Federico and many others – that have helped me with my various experiments, always doing so with patience and a smile.

My final and biggest thanks go to my supervisor, Becky – completing this PhD has certainly not been easy, but I know that it would have been infinitely harder if I wasn't lucky enough to have such a knowledgeable, kind and understanding supervisor.

CONTENTS

ABSTRACT ..... **i**

ACKNOWLEDGEMENTS ..... **iii**

CONTENTS ..... **iv**

LIST OF FIGURES ..... **x**

LIST OF TABLES ..... **xii**

ABBREVIATIONS ..... **xiii**

Chapter 1: General Introduction **1**

1.1: Ischemic stroke 1

1.1.1: Timeline of ischemic stroke events 1

1.1.2: Post-stroke immune response 4

1.1.3: Timeline of ischemic stroke recovery 7

1.1.4: Genes influencing post-stroke axonal sprouting 9

1.2: DNA (hydroxy)methylation 11

1.2.1: DNA Methyltransferases 11

1.2.2: Function of 5-methylcytosine 13

1.2.3: DNA demethylation 14

1.2.4: Tet Enzymes 15

1.2.5: Oxidised 5mC as demethylation intermediates 18

1.2.6: Alternative roles of oxidised 5mC 20

1.2.7: Distribution of 5hmC 21

1.2.8: Role of Tet enzymes in brain development & function 22

1.3: The role of DNA (hydroxy)methylation in ischemic stroke 23
1.3.1: Oxidised 5mC in neurodegenerative disorders 23
1.3.2: The role of oxidised 5mC in ischemic stroke 24
1.4: Modelling ischemic stroke in rodents 28
1.5: Summary 32
1.6: Thesis aims 33

Chapter 2: Timeline of post-stroke DNA hydroxymethylation 34
2.1: Introduction 34
2.1.1: Post-stroke DNA (hydroxy)methylation 34
2.1.2: Ischemic stroke across brain regions 36
2.1.3: Secondary degeneration in exfocal brain regions 37
2.1.4: Methods of quantifying global 5hmC 39
2.1.5: Objectives & Hypotheses 42
2.2: Methods 43
2.2.1: Experimental design 43
2.2.2: Surgical procedures 44
2.2.3: Tissue collection 45
2.2.4: Immunohistochemical staining 46
2.2.5: Image Analysis 48
2.2.6: Statistical Analysis 52
2.3: Results 53
2.3.1: Review of fluorescent staining quality 53
2.3.2: Post-stroke 5hmC levels in the cortex 57
2.3.3: Post-stroke 5hmC levels in the striatum 57
2.3.4: Post-stroke 5hmC levels in the substantia nigra pars compacta 61

2.3.5: Loss of dopaminergic cells in substantia nigra 63

2.3.6: Correlations between infarct size and 5hmC levels 64

2.3.7: 5hmC levels in the medial geniculate nucleus 66

2.4: Discussion 68

2.4.1: Limitations 72

2.4.2: Summary 74

Chapter 3: Developing a method of isolating neurons & microglia from ischemic rat brain 75

3.1: Introduction 75

3.1.1: Methods of cell isolation 75

3.1.2: Flow cytometry & FACS 77

3.1.3: Consideration & requirements of planned experiment 80

3.1.4: Previous research performing FACS on brain tissue 82

3.1.5: Objectives 84

3.2: Developing FACS protocol 84

3.2.1: Methods of cell homogenisation 84

3.2.2: Methods of cell fixation 87

3.2.3: Developing panel of antibodies 89

3.2.4: Development of final protocol 92

3.2.5: DNA & RNA quality check 107

3.3: Discussion 110

Chapter 4: Methylomic response to stroke in specific cell types 114

4.1: Introduction 114

4.1.1: Importance of isolating and analysing neurons 114

4.1.2: Importance of isolating and analysing microglia 115
4.1.3: Objectives & Hypotheses 117
4.2: Methods 119
4.2.1: Experimental design 119
4.2.2: Surgical procedures 120
4.2.3: MRI scanning & infarct volume analysis 121
4.2.4: Tissue collection 122
4.2.5: Staining & FACS 122
4.2.6: Issue with neuronal cell isolation 124
4.2.7: DNA & RNA extraction 125
4.2.8: 5mC & 5hmC quantification 126
4.2.9: Reverse transcription & qPCR 126
4.2.9: Statistical analysis 128
4.3: Results 129
4.3.1: Infarct volumes 129
4.3.2: Microglial staining & sorting 131
4.3.3: Microglial CD11b expression 131
4.3.4: 5mC and 5hmC levels in total cell populations 133
4.3.5: 5mC and 5hmC levels in microglia/macrophage cells 136
4.3.6: mRNA expression levels of BDNF, Ttll7 and Tet enzymes 139
4.4: Discussion 141
4.4.1: Post-stroke (hydroxy)methylation in total cell population 141
4.4.2: Post-stroke (hydroxy)methylation in microglia/macrophage cells 143
4.4.3: Limitations 144
4.4.4: Summary 145

Chapter 5: Determining role of Tet enzymes in control of axon growth *in vitro* 147

5.1: Introduction 147

5.1.1: The role of DNA methylation in axon growth 147

5.1.2: The role of Tet enzymes in axon growth 150

5.1.3: The role of hypoxia in axon growth 151

5.1.4: Objectives & Hypotheses 152

5.2: Methods 153

5.2.1: Experimental design 153

5.2.2: Culture preparation 154

5.2.3: Plasmid preparation 155

5.2.4: Cell transfection 156

5.2.5: Oxygen-glucose deprivation (OGD) 157

5.2.6: MTT reduction assay 158

5.2.7: Fixation & staining 158

5.2.8: Image analysis 159

5.2.9: DNA extraction and 5mC + 5hmC quantification 160

5.2.10: Statistical analysis 161

5.3: Results 162

5.3.1: The effect of hypoxia on cell viability 162

5.3.2: The effect of hypoxia on Hif1α and Tet protein expression 162

5.3.3: The effect of hypoxia on 5mC and 5hmC levels 164

5.3.4: Effects of decreased Tet enzyme expression 165

5.3.5: Effects of increased Tet enzyme expression 169

5.4: Discussion 174

5.4.1: Hypoxia and cell viability 174

5.4.2: The effects of Tet enzyme expression on neuronal growth 175

5.4.3: The effects of hypoxia on neuronal growth 177

5.4.4: Potential role of ascorbate 178

5.4.5: Limitations & future research 179

5.4.6: Summary 183

Chapter 6: General Discussion 184

6.1: Summary and overall relevance 184

6.1.1: Methylomic response to ischemic stroke 184

6.1.2: Tet-mediated regulation of axon growth 187

6.2: Areas for future research 190

6.3: Conclusion 193

APPENDIX 195

A1: Comparing sham & naïve animal data from Chapter 2 195

A2: Standard curves for 5mC and 5hmC ELISAs 197

A3: qPCR Housekeeping Gene 198

A4: Specificity of Tet-targeting siRNAs 199

A5: Comparing GFP only and NT siRNA data from Chapter 5 201

A6: Post-hoc power analyses 203

A7: PIP Reflection 205

REFERENCES 206

LIST OF FIGURES

Figure 1.1: Broad timeline of events that occur during the post-ischemic cascade 3
Figure 1.2: The innate immune response to ischemic stroke 6
Figure 1.3: Methylation of cytosine bases 13
Figure 1.4: Oxidation of methylated cytosine by Tet enzymes.....16
Figure 1.5: Structure and function of the mouse Tet proteins 17
Figure 1.6: DNA methylation and demethylation pathways in mammals 19
Figure 1.7: Timeline of epigenomic, molecular & cellular changes post-stroke 26
Figure 2.1: The nigrostriatal dopaminergic pathway & motor basal ganglia circuitry 38
Figure 2.2: Brain areas analysed for post-stroke 5hmC levels 50
Figure 2.3: Example images of 5mC, 5hmC + 5caC immunohistochemical staining 54
Figure 2.4: Staining of various cell types 56
Figure 2.5: Immunohistochemical staining for NeuN + 5hmC in mouse tissue 58
Figure 2.6: Timeline of post-stroke cortical 5hmC levels.....59
Figure 2.7: Timeline of post-stroke striatal 5hmC levels 60
Figure 2.8: Post-stroke 5hmC levels of dopaminergic cells in the SNc 61
Figure 2.9: Immunohistochemical detection of TH and 5hmC 62
Figure 2.10: Count of TH+ cells of substantia nigra pars compacta following MCAO.....63
Figure 2.11: Correlation between infarct volume and 5hmC level in various brain areas.....65
Figure 2.12: Post-stroke 5hmC levels of the medial geniculate nucleus 66
Figure 2.13: Immunohistochemical detection of 5hmC in MGN 67
Figure 3.1: Fluorescence-activated cell sorting (FACS) 78
Figure 3.2: Detection of forward and side scatter in flow cytometry.....79
Figure 3.3: Testing methods of fixation & permeabilisation for FACS 88
Figure 3.4: Outcome of first round of FACS protocol testing 94
Figure 3.5: Outcome of second round of FACS protocol testing 95
Figure 3.6: Outcome of third round of FACS protocol testing 99
Figure 3.7: Outcome of fourth round of FACS protocol testing.....101
Figure 3.8: Outcome of fifth round of FACS protocol testing 102
Figure 3.9: Outcome of sixth round of FACS protocol testing 104
Figure 3.10: Analysis of $CD11b^{+}/CD45^{high}$ population 106
Figure 3.11: Testing purity of FACS-sorted cells 107

Figure 4.1: Infarct volumes of rats that have undergone MCAO surgery 129
Figure 4.2: T_2 weighted images of rats that have undergone MCAO surgery 130
Figure 4.3: Phenotypic profile of microglia analysed by flow cytometry 132
Figure 4.4: Proportions of CD11b-high populations 133
Figure 4.5: 5mC and 5hmC content of DNA from total cell population 134
Figure 4.6: Correlation between infarct volume and 5mC and 5hmC content in total cell population 135
Figure 4.7: 5mC and 5hmC content of DNA from microglia 137
Figure 4.8: Correlation between 5mC & 5hmC content of microglia/macrophage cells and proportion of CD11b-high cells 138
Figure 4.9: Relative expression levels of genes of interest 140
Figure 5.1: Timeline of cell culture experiments 154
Figure 5.2: Viability of mouse cortical neurons following 2.5h of OGD 162
Figure 5.3: Images of normoxic and hypoxic cultures stained for Tet and Hif1α proteins . 163
Figure 5.4: The effect of hypoxia on expression of Tet enzymes and Hif1α 164
Figure 5.5: The effect of hypoxia on 5mC and 5hmC content 165
Figure 5.6: Images of neuronal cultures transfected with siRNAs targeting Tet1-3 166
Figure 5.7: The effects of hypoxia and knocking down Tet enzymes on axon length 167
Figure 5.8: The effects of hypoxia and knocking down Tet enzymes on number of neurites 168
Figure 5.9: The effects of hypoxia & knocking down Tet enzymes on total neurite length 169
Figure 5.10: Images of neuronal cultures transfected with plasmid constructs of Tet1-3 . 170
Figure 5.11: The effects of hypoxia and increasing Tet enzyme expression on axon length 171
Figure 5.12: The effects of hypoxia and increasing Tet enzyme expression on number of neurites 172
Figure 5.13: The effects of hypoxia and increasing Tet enzyme expression on total neurite length 173
Figure A1: Comparing sham and naïve animal data from Chapter 2 196
Figure A2: Standard curves for 5mC and 5hmC ELISA kits 197
Figure A3: Expression of HPRT1 198
Figure A4: Analysing specificity of Tet-targeting siRNAs 200
Figure A5: Comparing GFP only and NT siRNA data from Chapter 5 202

LIST OF TABLES

Table 1.1: Differentially expressed post-stroke axon growth related genes 10

Table 1.2: Rodent models of MCAO 29

Table 2.1: Methods of quantifying global 5hmC 41

Table 2.2: The number of mice used to assess post-stroke levels of 5hmC 44

Table 3.1: Testing various methods of tissue homogenisation on adult rat striatum 86

Table 3.2: Panel of antibodies chosen for development of protocol 92

Table 3.3: DNA & RNA analysis from test samples 110

Table 4.1: The number of rats used to assess cell-specific post-stroke 5mC/5hmC levels ..120

Table A1: Post-hoc analyses of experiments from Chapters 2, 4 and 5 204

ABBREVIATIONS

5caC	5-carboxylcytosine
5fC	5-formylcytosine
5hmC	5-hydroxymethylcytosine
5hmU	5-hydroxymethyl uracil
5mC	5-methylcytosine
AMPA	α-amino-3-hydroxy-5-methyl-4-isoxazolepropionic acid
APC	Allophycocyanin
ATP	Adenosine triphosphate
BDNF	Brain-derived neurotrophic factor
BSA	Bovine serum albumin
CCA	Common carotid artery
CD11b	Cluster of differentiation molecule 11b
CD45	Cluster of differentiation molecule 45
CD68	Cluster of differentiation molecule 68
CNS	Central nervous system
CpG	Cytosine-guanine dinucleotide
CTF	Corrected total fluorescence
DAB	3,3'-Diaminobenzidine
DAPI	4',6-diamino-2-phenylindole
DhMRs	Differentially hydroxymethylated regions
DIV	Days *in vitro*
DMEM	Dulbecco's Minimal Essential Medium
DMSO	Dimethyl sulfoxide
DNA	Deoxyribonucleic acid
DNMT	DNA methyl transferase
DRG	Dorsal root ganglion
ECA	External carotid artery
ELISA	Enzyme-linked immunoabsorbent assay
FACS	Fluorescence-activated cell sorting
FITC	Fluorescin isothiocyanate
Gadd45	Growth arrest and DNA-damage-inducible protein

GFP	Green fluorescent protein
H3K27me3	Trimethylation at lysine 27 of histone H3
HBSS	Hank's Bufered Salt Solution
HDAC	Histone deacetylase
Hif1α	Hypoxia-inducible factor 1-alpha
HPLC	High performance liquid chromatography
Iba1	Ionised calcium binding adaptor molecule 1
ICA	Internal carotid artery
IHC	Immunohistochemistry
IMPROVE	Ischaemia Models: Procedural Refinements Of *in vivo* Experiments
IVC	Individually ventilated cages
KO	Knockout
LF2000	Lipofectamine 2000
LPS	Lipopolysaccharide
MBD	Methyl-binding domain
MCA	Middle cerebral artery
MCAO	Middle cerebral artery occlusion
MECP2	Methyl-CpG binding protein 2
MeDIP	Methylated DNA immunoprecipitation
mESC	Mouse embryonic stem cell
MGN	Medial geniculate nucleus
miRNA	Micro-RNA
MRI	Magnetic Resonance Imaging
mRNA	Messenger RNA
MTT	Methylthiazolyldiphenyl-tetrazolium bromide
NeuN	Neuron specific nuclear protein (Fox-3)
NMDA	N-methyl-D-aspartate
NT	Non-targeting (siRNA)
OCT	Optimal cutting temperature compound
OGD	Oxygen-glucode deprivation
PBS	Phosphate-buffered saline
PE	Phycoerythrin
PFA	Paraformaldehyde
RIN	RNA integrity number
RNA	Ribonucleic acid

ROI	Region of interest
RT-qPCR	Reverse transcription - quantitative polymerase chain reaction
SAH	S-adenosyl homocysteine
SAM	S-adenosyl methionine
SD	Standard deviation
SIP	Stock isotonic Percoll
siRNA	Short-interfering RNA
SNc	Substantia nigra pars compacta
TDG	Thymine DNA glycosylase
Tet	Ten-eleven translocation enzyme
TH	Tyrosine hydroxylase
TLC	Thin-layer chromatography
TNF-α	Tumor necrosis factor alpha
tPA	Recombinant tissue plasminogen
VTA	Ventral tegmental area
WT	Wild-type

Chapter 1: General Introduction

1.1: Ischemic stroke

Ischemic stroke occurs when blockage of a blood vessel causes a loss of blood supply to brain tissue, resulting in tissue death. Ischemic stroke is a hugely prevalent disorder, with over 100,000 cases in the UK every year, making it the second leading cause of death and the leading cause of adult disability (Stroke Association, 2018). Ischemic stroke is therefore a source of huge costs for the NHS, which emphasises the importance of finding effective, novel treatments for the disorder. The only licensed drug for use in stroke patients, tissue plasminogen activator (tPA) (O'Collins et al., 2006), works by breaking down the offending blood clot via thrombolysis, meaning it is most effective in the few hours following the onset of stroke symptoms. Therefore, its main disadvantage is a narrow therapeutic window (Hacke et al., 1999). Developing a therapeutic treatment for ischemic stroke that is aimed at promoting mechanisms of functional recovery, such as axonal sprouting, could present a treatment with a much wider therapeutic window, thereby addressing the main disadvantages of currently used treatments.

1.1.1: Timeline of ischemic stroke events

In order to better understand the pathophysiology of ischemic stroke and begin to assess areas of therapeutic interest, it is important to consider the timeline of events that occur during the post-stroke cascade. A broad timeline of post-stroke events is outlined in Figure 1.1.

Within minutes of ischemic onset, the core of the lesion experiences fast and irreversible damage that results in cell necrosis. Reduced blood flow results in failure of energy-dependent ion channels and pumps due to a reduction in ATP production. The failure of these channels and pumps causes transmembrane potentials to collapse as Na^+, K^+ and Ca^{2+} ions flow freely along their concentration gradient, subsequently causing depolarisation and the release of excitatory neurotransmitters (primarily glutamate) (Dirnagl et al., 1999). This is accompanied by activation of proteolytic enzymes, cytotoxic swelling, degradation of the cytoskeleton and peroxidation of membrane lipids (Witte et al., 2000). The tissue immediately surrounding the core is known as the ischemic penumbra, an area that experiences constrained blood flow and, without treatment, can progress to infarction due to ongoing excitotoxicity (Hossmann, 1994). The release of glutamate from the ischemic core activates NMDA and AMPA receptors, causing excitotoxicity and triggering a propagating wave of depolarisation that places additional metabolic stress on the compromised cells in the penumbra (Mergenthaler et al., 2004).

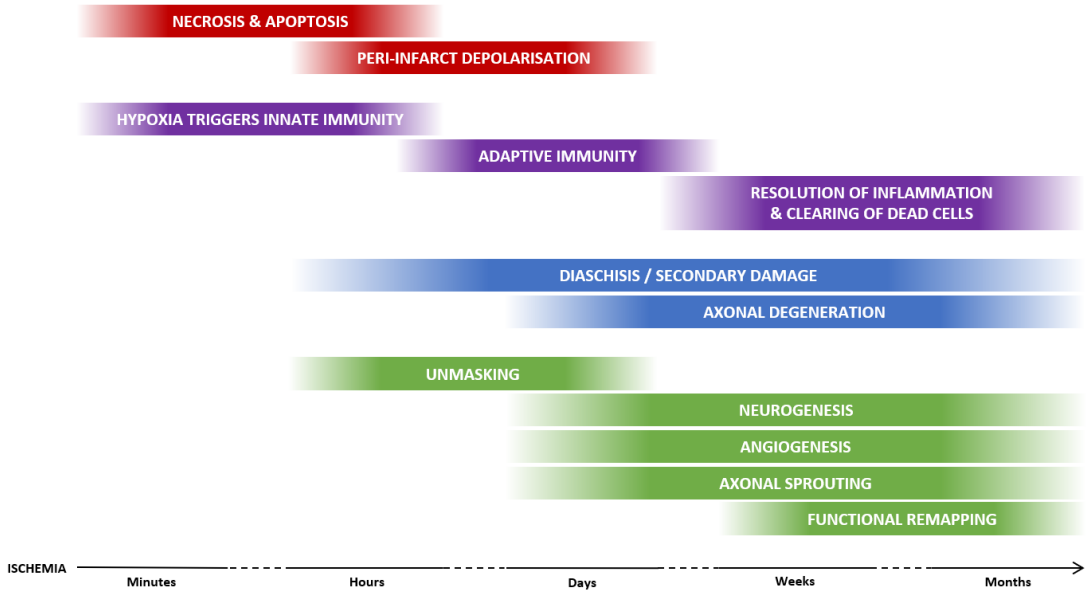


Figure 1.1: Broad timeline of events that occur during the post-ischemic cascade
Following the onset of ischemia, necrosis, apoptosis and depolarisation of penumbral neurons contribute to the growth of the infarct (red bars). Immediately following the onset of hypoxia, the immune response is triggered (purple bars). Hypoxia immediately triggers the innate immune response, which then activates the adaptive immune response in the days following stroke. Inflammation is eventually resolved in the followings weeks/months as cellular debris is cleared. Regions far from the infarct also experience damage (blue bars) as dysfunction of connected regions distal to the infarct (diaschisis) occurs hours after onset and persists for weeks. Axonal degeneration and further secondary damage are initiated in the days/weeks following the ischemic event and can persist for months. Functional recovery in the form of adaptive plasticity (green bars) begins hours after injury in the form of neurogenesis and angiogenesis. In the days/weeks following the ischemic event, enhanced axonal growth allows for neuroanatomical remodelling and functional remapping of functions lost to stroke to new locations, a process which persists for months.

Necrotic cell death is not solely responsible for infarct growth, with apoptosis also occurring following ischemic injury albeit in the hours/days following injury. Post-ischemic apoptosis can be triggered by the influx of Ca^{2+} and persistent activation of NMDA receptors, subsequently altering mitochondrial membrane potentials and triggering the release of pro-apoptotic factors such as cytochrome c (Garrido et al., 2006). Apoptosis can also be initiated via the release of pro-inflammatory cytokines such as TNF-α during the post-stroke inflammatory response (Pettigrew et al., 2008). Following ischemic injury, the innate and adaptive immune responses are initiated within hours and can persist for weeks (Figure 1.1).

Whilst much of the disability due to stroke is caused by cell death within the infarct, some dysfunction is due to degradation in areas that are distal to the site of injury but still anatomically connected to the infarcted area (defined as diaschisis), which occurs within days of the ischemic event. The main contributing factor to diaschisis is thought to be functional deafferentation, although brain swelling and altered inhibitory neurotransmitter signalling have also been shown to be responsible (Finger et al., 2004). Alongside diaschisis, degeneration of axonal afferents from within the infarct occurs, which causes increased release of pro-inflammatory cytokines and subsequent secondary damage and atrophy of peri-infarct tissue (Wang et al., 2007).

1.1.2: Post-stroke immune response

In ischemic stroke, hypoxia caused by a lack of blood flow leads to the activation of the central nervous system's immune response, which involves an immediate innate response followed by a delayed adaptive response that can persist for days/weeks post stroke. The broad immune changes that occur post-stroke are illustrated in Figure 1.1.

1.1.2.1: Innate immune response

The tissue damage caused by ischemic stroke leads to activation of the innate immune response within the CNS, initiating a cascade of events including the activation of resident astrocytes and microglia (Figure 1.2). Ischemic stroke also causes a decrease in the integrity of the blood-brain-barrier (Jiang et al., 2005), which allows peripheral neutrophils and macrophages to infiltrate and accumulate in the ischemic tissue (Gelderblom et al., 2009). All of these events lead to inflammation of the brain tissue, which causes further tissue damage

and impaired recovery. This is evidenced by the fact that immunodeficient mice experience a reduced infarct size after transient MCAO (Hurn et al., 2007) and that increased activation of toll-like receptors on activated microglia causes a decrease in numbers of sprouting axons (Cameron et al., 2007). However, some of the immune cells upregulated following ischemic injury have been shown to demonstrate anti-inflammatory activity and promote tissue repair.

"Activated" microglia can exist along a phenotypic spectrum of pro-inflammatory and anti-inflammatory states, with M1 phenotype microglia producing various pro-inflammatory cytokines via iNOS and NF-κB pathways, whereas M2 microglia facilitate phagocytosis of cell debris and promote neuronal reconstruction and tissue repair via the release of neurotrophic factors (Loane & Byrnes, 2010). This dichotomous classification of microglia into M1 and M2 states was applied as a way to structure the complexity of microglial activation. The M1 phenotype is characterised by the production of many pro-inflammatory cytokines (including IL-6, IL-1β, and TNF-α), reactive oxygen species and chemokines, all leading to acute immune responses. Conversely, M2 phenotype microglia are characterised by the expression of anti-inflammatory cytokines (including IL-13 and IL-4) and their involvement in promoting cellular debris clearance and wound healing (Cherry et al., 2014). However, more recent studies have led to the criticism of this static classification by determining that cytokines previously thought to be exclusive to each polarisation state are co-expressed by microglia in the context of traumatic brain injury (Kim et al., 2016).

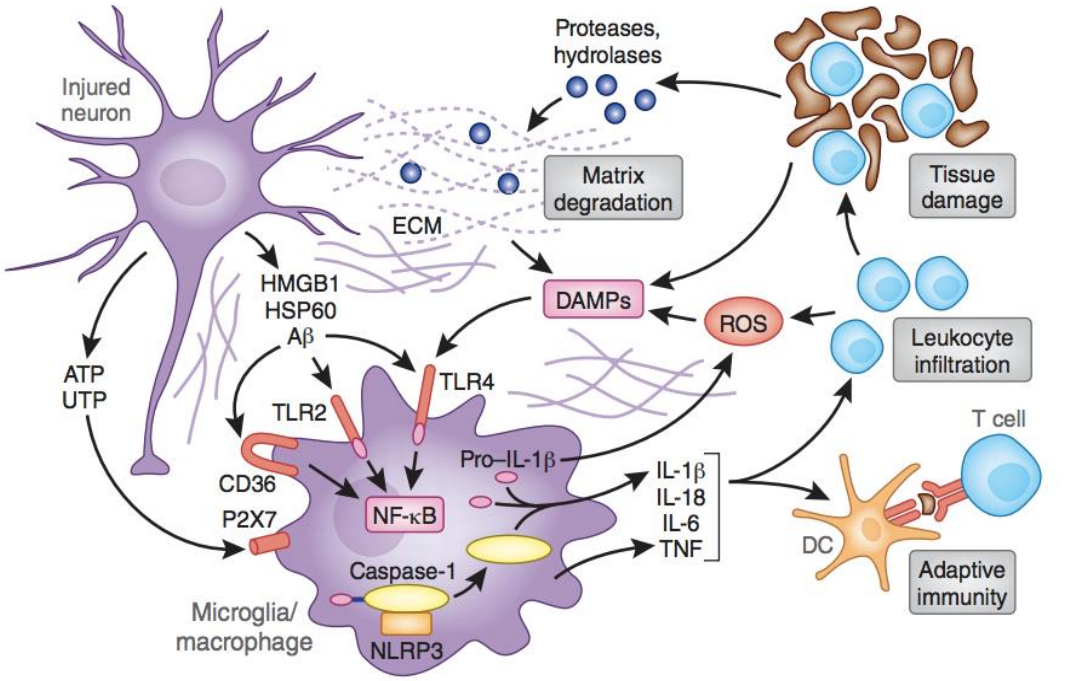


Figure 1.2: The innate immune response to ischemic stroke
Nucelotides (ATP, UTP) released from injured neurons activate microglia and infiltrating macrophages via purinergic receptors (eg. P2X7). Activated microglia/macrophages then release proinflammatory cytokines such as IL-1β, which facilitate leukocyte infiltration. Most of these cytokines are transcriptionally induced by nuclear factor-κB (NF-κB), IL-1β is processed from its propeptide via caspase-1. Infiltrating leukocytes cause further tissue damage and produce reactive oxygen species (ROS), which leads to the production of danger-associated molecular pattern molecules (DAMPs) such as β-amyloid (Aβ) and high mobility group protein B1 (HMGB1). Tissue damage via leukocytes also causes the release of proteases & hydrolases, which break down the extracellular matrix (ECM) and produce more DAMPs. DAMPs activate toll-like receptors (TLRs) on microglia/macrophages to cause further activation. Finally, pro-inflammatory cytokine release from microglia/macrophages facilitates the infiltration of dendritic cells (DCs), which present antigens to T cells, thereby initiating the adaptive immune response. (Image taken from Iadecola & Anrather, 2011)

1.1.2.2: Adaptive immune response

Whilst the innate immune response is important in influencing the extent of tissue damage in the acute phase of ischemic injury, later stages of stroke involve the activation of the adaptive immune response. Following a stroke, damaged neurons release antigens which are presented to T-cells, causing them to become primed. Antigens are also presented to T-cells by invading dendritic cells (Figure 1.2). In the acute phase of ischemic injury, unprimed T-cells

contribute to tissue damage in an antigen-independent manner via the production and release of reactive oxygen species (Brait et al., 2010). However, primed T-cells can be neuroprotective in the later stages of ischemic stroke. The release of transforming growth factor-β from surviving neurons and microglia causes the upregulation of primed T-cells, which in turn release the protective cytokine interleukin-10 and suppresses the activity of the detrimental T1 and T2 T-cell subtypes (Liesz et al., 2009).

1.1.3: Timeline of ischemic stroke recovery

Whilst immune cell activation, cell death and infarct growth begin immediately following ischemic injury, the cellular mechanisms that initiate recovery are somewhat more delayed. These include processes such as neurogenesis, which involves the proliferation of newly divided neurons in the subventricular zone in the days/weeks following the onset of stroke. This is followed by migration of these immature neurons as they localise towards peri-infarct tissue, eventually maturing and forming functional connections that can manifest as functional motor or sensory recovery. The process of proliferation requires the involvement of cellular signalling proteins such as brain-derived neurotrophic factor (BDNF), whereas the migration of neurons towards peri-infarct tissues relies more upon metalloproteinases that are also involved in angiogenesis (Ohab & Carmichael, 2008). Angiogenesis is another cellular mechanism of post-stroke recovery, which similarly to neurogenesis is initiated in the days/weeks following the ischemic insult. It involves the formation of new blood vessels from pre-existing vessels, and occurs in the peri-infarct tissue as a means of returning a supply of blood flow to the ischemic penumbra (Yanev & Dijkhuizen, 2012). It is also believed that vasculogenesis, which is the development of blood vessels from endothelial precursor cells as opposed to pre-existing vessels, may also occur in the adult brain and contribute to ischemic

stroke recovery (Ishikawa et al., 2013), although this phenomenon remains largely unexplored.

Although the initiation of neurogenesis, angiogenesis and vasculogenesis are somewhat delayed from the onset of ischemic stroke, other mechanisms of recovery are triggered much sooner. For example, the remapping of functions that were lost due to stroke can occur very soon after the ischemic event, as evidenced by the fact that forelimb-specific somatosensory cortex function has been found to be partially redistributed within 1 hour of stroke (Winship & Murphy, 2008). This rapid remapping of function is due to the activation of previously dormant or ancillary connections as opposed to the formation of new connections. In the first few days following ischemic injury, increased NMDA signalling and long term potentiation of peri-infarct neurons persists for up to four weeks, which provides a favourable environment for functional rewiring of connections that were lost due to necrosis/apoptosis (Centonze et al., 2007).

Although this rapid potentiation of signalling and unmasking of pre-existing connections has some positive effect on functional recovery, the majority of recovery seen in patients is due to the growth of new axons from the peri-infarct and contralateral regions (Murphy & Corbett, 2009). Following stroke, neurons in the peri-infarct cortex form new connections with motor, premotor and sensory areas in the ipsilateral cortex. These new connections can remain local to the peri-infarct region or can even connect brain areas within different lobes (Brown et al., 2009). The initiation phase for axonal sprouting within the peri-infarct area is within the first 7 days after stroke (Li et al., 2010), with functional connections formed around 3 weeks post-injury. Using tracer injections and quantitative mapping, it has been shown that strokes in the motor or somatosensory cortex of mice causes the formation of new and significantly

different connections from the motor cortex to premotor cortex 1 month post-stroke (Clarkson et al., 2011).

1.1.4: Genes influencing post-stroke axonal sprouting

The process of axonal sprouting post-stroke is a profound phenomenon in the cortex of the adult brain, a region in which the formation of substantial new connections is not usually seen. To fully understand the molecular mechanisms behind the initiation of axonal growth, studies have been carried out to determine which genes are differentially regulated in sprouting neurons following ischemic injury. In an attempt to determine a gene expression program that underlies post-stroke axonal growth, Li et al. (2010) developed a method to selectively label sprouting neurons in a rat model of stroke and found a number of genes linked to axonal growth and synaptogenesis that were differentially regulated in comparison to non-sprouting neurons at 7 days post-ischemic injury. Interestingly, they compared the differentially regulated genes found in young adult and aged adult rats and found that there was little overlap in the two transcriptomes, with just 79 genes commonly regulated post-stroke. 13 of these genes are related to axon growth and neuronal plasticity, and are summarised in Table 1.1.

Name	Function	Up- or down- regulated post-stroke
Eph receptor A4 (Epha4)	Axonal guidance	Up
Leucine-rich repeat & Ig domain containing 1 (Lingo1)	Axonal guidance	Up
Insulin-like growth factor (Igf1)	Growth factor	Up
Epidermal growth factor receptor (Egfr)	Growth factor	Up
Glial cell line-derived neurotrophic factor family receptor alpha 3 (Gfra3)	Growth factor	Up
Sortilin-related VPS10 domain containing receptor 3 (Sorcs3)	Growth factor	Up
Piccolo (Pclo)	Synaptogenesis	Up
Synaptotagmin 1 (Syt1)	Synaptogenesis	Up
Synaptic vesicle glycoprotein 2b (Sv2b)	Synaptogenesis	Up
Protocadherin 11 X-linked; Pcdhx (Pcdh11x)	Synaptogenesis	Up
Synaptophysin (Syp)	Synaptogenesis	Down
Homer homolog 1; Homer (Homer1)	Neuronal plasticity	Down
Activity-regulated cytoskeletal-associated protein (Arc)	Neuronal plasticity	Down

Table 1.1: Differentially expressed post-stroke axon growth related genes
List of axonal sprouting-related genes that are differentially regulated in sprouting cortical neurons post-stroke in both young and aged individuals. Data taken from Li et. al (2010).

The differential gene expression with age observed by Li et al. reflects what has been seen in human stroke patients; that there are differential recovery mechanisms between young and aged individuals that mean young individuals show greater recovery, even though stroke is more prevalent in aged individuals. Possible explanations for this include increased incidence of ischemic stroke risk factors, comorbidities, or changes to the epigenome that occur with age.

1.2: DNA (hydroxy)methylation

Epigenetic changes are defined as heritable changes to the DNA molecule that do not alter the base pair sequence, examples of which include histone modifications such as acetylation and ubiquitination; micro-RNA (miRNA) interference; and DNA methylation. The discovery of methylated DNA bases occurred around 70 years ago when the presence of so-called 'minor bases' was found in the DNA molecule alongside the four classical bases (Hotchkiss, 1948), with the first 'minor base' identified as 5-methyl-cytosine (5mC) – a cytosine residue with an attached methyl group. The mechanism underlying the formation of 5mC in the DNA molecule remained unknown until studies carried out in the 1960s identified specific enzymatic activity that involved the transferal of methyl groups from S-adenosyl-L-methionine (SAM) to cytosine residues on the DNA molecule (Gold & Hurwitz, 1963) (Figure 1.3). From this, it became apparent that 5mC is not incorporated into the DNA molecule during synthesis but is instead formed as a result of the enzymatic modification of pre-existing bases. The enzymes responsible for this activity became known as the DNA methyltransferase family of enzymes (DNMTs), and although their existence was determined in the 1960s, their specific function and importance was not discovered for many years

1.2.1: DNA Methyltransferases

The human genome codes for 5 DNA methyltransferase enzymes – DNMT1, DNMT2, DNMT3a, DNMT3b and DNMT3L. DNMT1, DNMT3a and DNMT3b are all canonical methyltransferases that have been shown to catalyse the addition of methyl groups to genomic DNA, whereas DNMT2 and DNMT3L do not possess catalytic methyltransferase activity but do have high sequence conservation with the canonical methyltransferases (Lyko, 2017). DNMT4, DNMT5

and DNMT6 have been identified in algae and fungi (Huff & Zilberman, 2014), though are not known to be conserved in animals.

DNMT1 is known as the maintenance methyltransferase enzyme, with its main function being to reproduce the methylome on hemi-methylated daughter strands of DNA following DNA replication. DNMT1 was the first human methyltransferase to be cloned (Yen et al., 1992) and targeted mutation of *Dnmt1* (the mouse homologue of DNMT1) was found to cause severe developmental abnormalities and lethality in mouse embryos (Li et al., 1992). *Dnmt2* was first cloned in 1998 (Okano et al., 1998b) and despite containing conserved methyltransferase motifs, was found to have very weak DNA methylation activity although with slight methylation activity on tRNA (Jeltsch et al., 2006). The *Dnmt3a* and *Dnmt3b* genes were cloned in 1998 (Okano et al., 1998a) and found to code for two highly similar proteins that were both found to be required for *de novo* genome-wide methylation and essential for development (Okano et al., 1999). Whilst structurally similar to DNMT3a/b, the DNMT3L protein lacks a conserved catalytic domain and is not required for *de novo* DNA methylation nor is it essential for development, although research has shown that it can bind to the catalytic domain of DNMT3a/b to regulate *de novo* DNA methylation (Cheng & Blumenthal, 2008) (Figure 1.3).

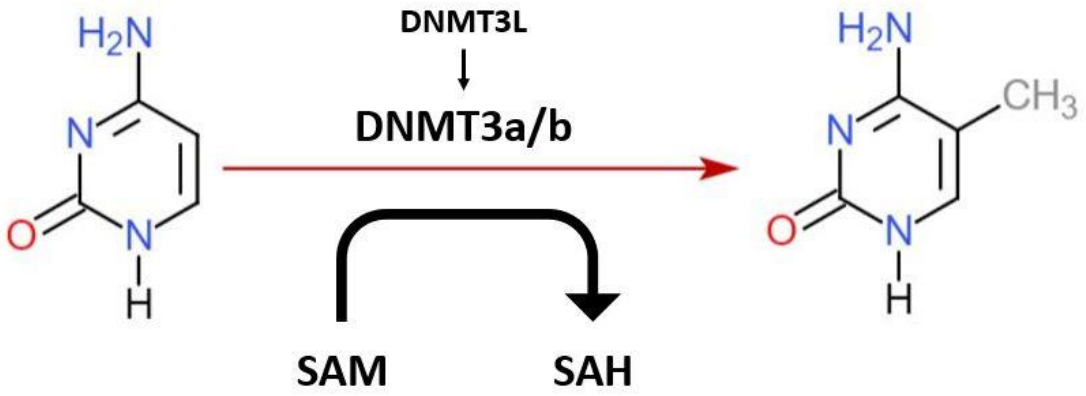


Figure 1.3: Methylation of cytosine bases
DNMT3L binds the de novo methyltransferases DNMT3a/b and regulates their ability to transfer a methyl group from S-adenosyl-L-methionine (SAM) to cytosine. The products are 5-methylcytosine and S-adenosyl-homocysteine (SAH).

1.2.2: Function of 5-methylcytosine

Cytosine methylation is both stable and heritable and is therefore considered to be a form of 'cellular memory'. 5mC is most commonly found at CpG islands, regions of high cytosine-phosphate-guanine (CpG) dinucleotide density (>50%) between 200bp-2kb in length that are typically found at the promoter region of 70% of human genes (Takai & Jones, 2002). In the mammalian genome, 5% of all C and 85% of all CpGs are methylated (Lister et al., 2013). Increased levels of cytosine methylation at promoter-region based CpG islands are associated with decreased gene transcription, as the methyl group of 5mC prevents transcriptional machinery from effectively binding to the DNA molecule, particularly transcriptional enzymes which have a CpG-rich motif (Watt & Molloy, 1988). Furthermore, proteins containing a methyl-CpG-binding domain (MBD) such as MECP2 can bind specifically to methylated CpG sites and further exclude transcriptional machinery and silence genes (Akintola & Parrish, 2010). Some non-MDB-containing proteins, such as the Kaiso-related proteins, contain a zinc finger which binds to methylated cytosine residues and represses gene transcription by

interacting with histone deacetylases and remodelling chromatin to a repressive state (Parry & Clarke, 2011).

Unlike methylation of gene promoter regions, methylation in the gene body does not block transcription or silence genes (Maunakea et al., 2010), although cytosine methylation at any loci can have a profound effect on the structure of the genome by producing mutational hotspots in the DNA (Coulondre et al., 1978). The application of a methyl group to a cytosine residue in DNA increases the probability of spontaneous deamination by around 2.5 fold and produces a thymine residue as a product as opposed to a uracil residue. (Shen et al., 1994). As thymine is a normal component of DNA, it is not as easily recognised by regulatory DNA machinery and is therefore more difficult to repair.

1.2.3: DNA demethylation

Whilst the addition of a methyl group to cytosine residues is always an active enzymatic process, the loss or removal of these groups, known as DNA demethylation, can be either a passive or active process. Passive demethylation involves the loss of conservation of methylated sites during DNA replication, due to either the loss or inhibition of DNMT1 (Bhutani et al., 2011). In contrast, active DNA demethylation involves the enzymatic removal of the methyl group from 5mC and is observed in somatic cells in a locus-specific manner. For example, Paroush et al. (1990) demonstrated that demethylation occurs in the absence of DNA replication in L8 myoblasts, with this process occurring in two steps: loss of 5mC within a few hours on one strand, and a ~48h delay before loss of 5mC on the complimentary strand. Observations such as this led to the search for putative demethylation enzymes.

Breakthroughs in the study of the active demethylation process were first made around 30 years ago when it was found that the process of DNA methylation allows for incorporation of radio-labelled cytidine, but not adenosine, into pre-existing DNA strands (Razin et al., 1986), thereby demonstrating that active DNA demethylation is achieved by an enzymatic process in which 5mC is replaced by unmodified cytosine, known as base excision repair. Further developments soon followed when purification of the base excision repair activity revealed that it involved a combination of thymine-DNA glycosylase and apyrimidinic endonuclease activity (Jost et al., 1995).

1.2.4: Tet Enzymes

Research in the years following these discoveries focused on further detailing the base excision repair mechanism that replaces 5mC with unmethylated cytosine, until another breakthrough was made with the discovery of the oxidised form of 5mC, 5-hydroxymethylcytosine (5hmC) (Kriaucionis & Heintz, 2009), and the family of Ten-eleven translocation (Tet) enzymes that catalyse the reaction (Tahiliani et al., 2009). This enzymatic activity was discovered in all 3 members of the Tet family of enzymes (Tet1-3) (Ito et al., 2010) and the theory that these enzymes further sequentially oxidise 5hmC to 5-formylcytosine (5fC) and 5-carboxylcytosine (5caC) were later confirmed both *in vitro* and *in vivo* (He et al., 2011; Ito et al., 2011) (Figure 1.4). In the brain, Tet3 is the most highly expressed member of the family of enzymes, followed by Tet2; Tet1 has significantly lower levels of expression than the other two Tets (Szwagierczak et al., 2010).

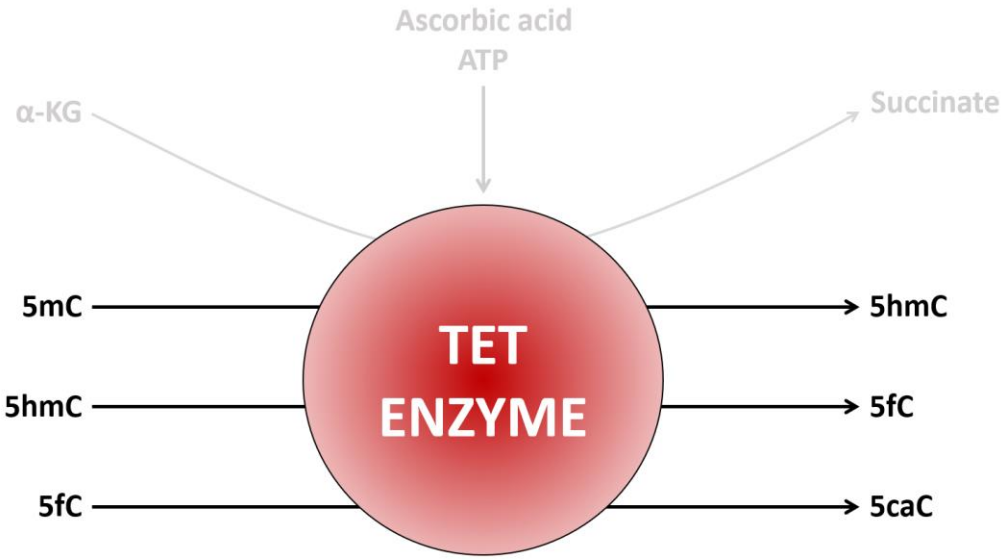


Figure 1.4: Oxidation of methylated cytosine by Tet enzymes
Tet enzymes sequentially oxidise 5mC to 5hmC, 5fC and 5caC. The reaction depends on the presence of, alpha-ketoglutarate (often referred to as 2-oxoglutarate) as a co-substrate, converting it to succinate. Ascorbic acid (Vitamin C) and ATP enhance the catalytic activity of Tet enzymes.

All 3 members of the Tet family of proteins contain a catalytic C-terminal CD domain that exhibits dioxygenase activity that is 2-oxoglutarate (2-OG) and iron (II)-dependent (Tahiliani et al., 2009), with this being the domain responsible for the oxidisation of 5mC to 5hmC. Using radiolabelled thin-layer chromatography, it was later discovered that this same domain was also responsible for the subsequent oxidisation of 5hmC to 5fC and 5caC in the presence of ATP *in vitro* (He et al., 2011).

Another functional domain found within the structure of Tet proteins is the zinc-finger CXXC domain, which was first identified in the DNMT1 protein (Bestor, 1992). Although this domain is found at the N-terminal of Tet1 and Tet3, it is absent from Tet2 (Figure 1.5). The exact function of this domain is debated, as it has been determined that the CXXC domain of Tet1 can bind to 5mC and 5hmC (Zhang et al., 2010), therefore suggesting that this domain aids direct DNA binding. However, research has also found that this domain is not required for

catalytic activity of Tet1 *in vivo* (Frauer et al., 2011); taken together with the fact that Tet2 is missing this domain and is still catalytically active *in vivo*, this suggests that the zinc-finger domain is non-essential to the activity of the Tet enzymes.

In addition to the functional CD and CXXC domains, all 3 members of the Tet family of proteins contain a spacer region that interrupts the CD domain. Whilst the dioxygenase function of the CD domain has been established, the importance of the spacer region remains unclear (Tan & Shi, 2012). Attempts at discerning the function of this spacer region have found that the spacer region of Tet1 has extremely high similarity to the C-terminal domain of RNA polymerase II of *S. cerevisiae* (Upadhyay et al., 2011). Whilst not identical, the conserved regions contain key residues that are important for post-translational modification, suggesting that the spacer region found in Tet proteins may act as a post-translational 'switch' that allows for modification of Tet enzyme activity. However, further research is required to fully conclude that this function exists.

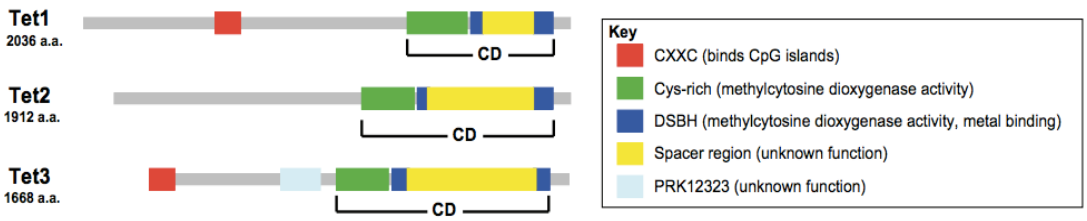


Figure 1.5: Structure and function of the mouse Tet proteins
All 3 members of the Tet family of proteins contain the CD domain, which exhibits dioxygenase activity and is responsible for the oxidation of 5mC. Within the CD domain is the spacer region, which interrupts the DSBH subdomain. The CXXC domain is found only at the N-termini of Tet1 and Tet3, and is believed to be non-essential for catalytic activity. The PRK12323 domain is found only in Tet3, does not belong to a superfamily of domains and currently has no known function. a.a. = amino acids. (Image adapted from Tan & Shi, 2012)

1.2.5: Oxidised 5mC as demethylation intermediates

The oxidation of 5mC by Tet enzymes is considered to prohibit maintenance of existing DNA methylation patterns due to the fact that no oxidised form of 5mC is recognised by the regulatory methyltransferase DNMT1 (Valinluck & Sowers, 2007), thereby leading to loss of methylation during DNA replication. This loss of DNA methylation is still considered passive DNA demethylation although the initial step requires Tet-mediated oxidation of 5mC. With regard to active demethylation, 5fC and 5caC are thought to act as intermediates of enzymatic 5mC removal as both of these derivatives are able to be cleaved by thymine-DNA glycosylase (TDG) (Maiti & Drohat, 2011). These findings have led to the belief that Tet-mediated oxidation of 5mC to 5fC and 5caC followed by TDG excision and subsequent base excision repair may be one of the pathways of active DNA demethylation (Figure 1.6), which is evidenced by the finding that TDG knockout mice show increased DNA methylation at certain genomic loci (Cortázar et al., 2011).

Additionally, recent research has identified a protein acting as a nonenzymatic supporting factor of the excision of 5fC and 5caC by TDG; namely, a member of the Growth arrest and DNA-damage-inducible protein 45 family (Gadd45a). A demethylating effect of Gadd45a was first determined when overexpression of the protein in *Xenopus laevis* oocytes led to reactivation of methylation-silenced plasmids (Barreto et al., 2007), and the relationship between Gadd45a and TDG activity was identified when knockout of Gadd45a in mouse embryonic stem cells (mESCs) caused genome-wide hypermethylation and 5fC enrichment in TDG deficient cells (Li et al., 2015). This therefore led to the conclusion that Gadd45a facilitates Tet-mediated DNA demethylation by interacting directly with TDG and positively regulating the cleavage of 5fC and 5caC.

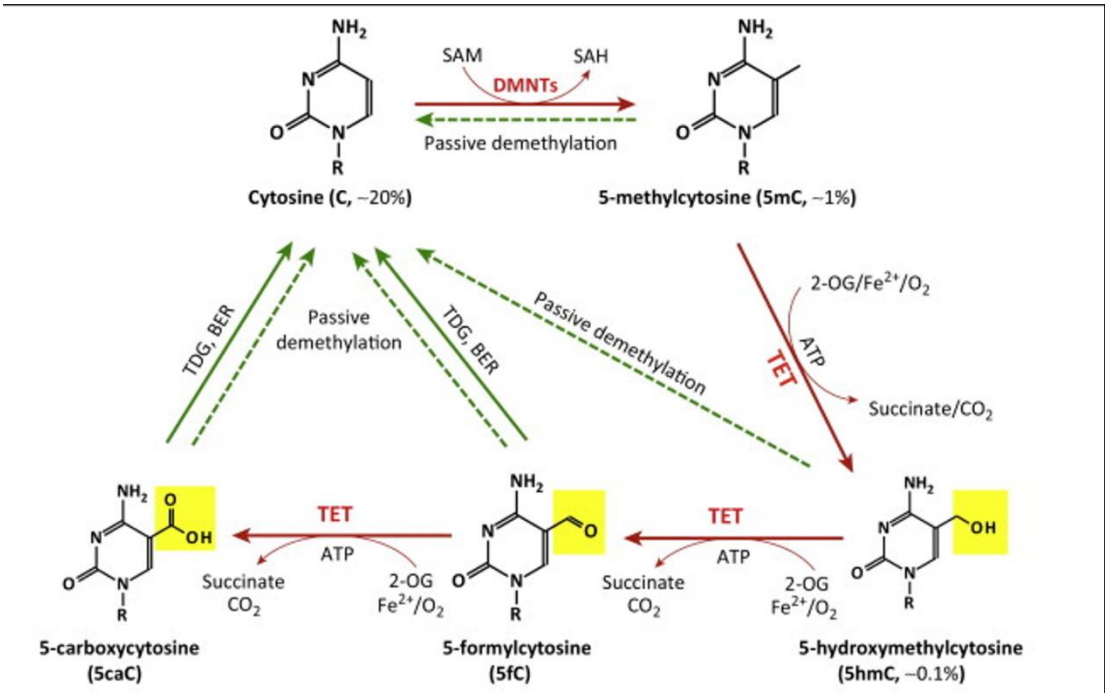


Figure 1.6: DNA methylation and demethylation pathways in mammals
DNA methylation occurs as transfer of a methyl group from SAM to a cytosine residue to form 5mC, catalysed by DNMTs. Tet enzymes sequentially oxidise 5mC to 5hmC, 5fC and 5caC; the oxidised derivatives of the methyl group are shown in yellow. Numerous demethylation pathways exist from these forms of methylcytosine; formation of 5hmC, 5fC and 5caC all lead to passive demethylation as the regulatory methyltransferase DNMT1 is unable to recognize these oxidised motifs. 5fC and 5caC also have the potential to be cleaved by thymine DNA glycosylase (TDG) and undergo base-excision repair (BER), being replaced by an unmethylated cytosine in the process of active demethylation. SAM = S-adenosyl-L-methionine; SAH = S-adenosyl-homocysteine; DNMTs = DNA methyltransferases; ATP = adenosine triphosphate. (Image adapted from Huang & Rao, 2014)

Whilst base excision repair is the most widely studied mechanism of Tet-mediated demethylation, alternative mechanisms have been suggested and investigated in recent years. For example, it has been put forward that 5hmC can be deaminated by enzymes such as activation-induced deaminase to form 5-hydroxymethyluracil (5hmU), which itself can then be cleaved by TDG (Guo et al., 2011), although formation of 5hmU in this manner has not yet been identified within a mammalian genome. Alternatively, mouse embryonic stem cells have been used to demonstrate that putative decarboxylases are capable of directly converting 5caC to cytosine (Schiesser et al., 2012), which serves as a method of demethylation that is

more energy efficient than base excision repair whilst also reducing the risk of mutations caused by DNA lesions. This research has made it clear that there are varying mechanisms of oxidation-dependent demethylation which make oxidised forms of 5mC, as well as the Tet enzymes that catalyse their production, key players in the dynamic process of epigenetic regulation.

1.2.6: Alternative roles of oxidised 5mC

Whilst the roles of 5hmC, 5fC and 5caC as intermediates of demethylation have been well documented in recent years, their potential functional roles as regulatory epigenetic markers are still relatively unknown. 5hmC levels in nervous tissue have also been found to increase with age, which suggests a potential role as a stable epigenetic marker (Szulwach et al., 2011). Mellen et al. (2012) found that in neurons, 5hmC is enriched at the bodies of genes which are related to neuronal function, with the ratio of 5hmC:5mC strongly correlating with levels of gene transcription. In the same study it was found that 5hmC is capable of binding to MECP2, similarly to 5mC, in order to affect chromatin structure and decrease gene transcription. This therefore suggests that 5hmC is not a committed demethylation intermediate and is instead somewhat stable and capable of recruiting proteins to initiate either demethylation or gene transcription regulation, revealing a potential dynamic role of the oxidised 5mC derivative.

In contrast to the relatively high expression of 5hmC in nervous tissue, 5fC and 5caC are 10-1,000 fold less abundant than 5hmC in neurons and are found to have consistently low expression across all tissues (Ito et al., 2011). Given their low abundance and the fact that they are further oxidised derivates of 5hmC, 5fC and 5caC are widely regarded to act exclusively as active demethylation intermediates, although recent studies have begun to elucidate some potential functions of these markers that are coupled with demethylation. For example,

increased 5fC levels at enhancer sites are found in the absence of TDG, and this is associated with increased binding of the transcriptional coactivator p300 (Song et al., 2013). p300 enhances the binding of transcription factors and increases the likelihood of gene transcription, therefore suggesting that 5fC could play a role in the epigenetic priming of certain genes. However, the experiments performed to examine this have been performed exclusively in mESCs and given that the pattern of oxidised 5mC derivatives varies between different tissues, these conclusions cannot be applied to cells such as neurons.

1.2.7: Distribution of 5hmC

Unlike 5mC, which is evenly distributed across different cells and tissues, 5hmC expression is extremely variable with the highest abundance of 5hmC found in the central nervous system, where it accounts for ~1% of total cytosine (Ito et al., 2011). 5hmC levels in the central nervous system are also brain-region specific, with 5hmC constituting 0.7% of total cytosine bases in the cortex and hypothalamus; 0.6% in the olfactory bulb, hippocampus and brainstem; 0.5% in the spinal cord; 0.4% in the midbrain; and 0.3% in the cerebellum (Kriaucionis & Heintz, 2009; Münzel et al., 2010). In the pituitary gland, which is a non-neuronal structure within the brain, 5hmC has been found to constitute only 0.06% of total cytosine (Münzel et al., 2010), which supports the idea that high levels of 5hmC are specific to neural tissues.

It remains unclear why 5hmC levels are so abundant in neural tissue or why they vary between different brain regions; since Tet enzyme expression levels are similar across tissue types with varying levels of 5hmC, overall expression of these enzymes cannot account for the difference. It is possible that the determining factor of 5hmC concentration is the availability of required cofactors such as alpha-ketoglutarate or ascorbic acid (Vitamin C). In mESC culture, supplementation of ascorbic acid significantly decreased 5mC levels whilst increasing 5hmC

levels (Blaschke et al., 2013), and considering that the brain has the highest levels of ascorbic acid in the body (May, 2012) this could account for the observed abundance of 5hmC. However, further research is needed to fully elucidate this effect.

1.2.8: Role of Tet enzymes in brain development & function

The observation that 5hmC is highly abundant in the CNS has led researchers to attempt to determine what functional roles the Tet enzymes play in brain development & the function of the adult brain. It has been found that Tet1 knockout (KO) mice are viable and fertile, albeit with smaller body weight than wild type (WT) animals (Dawlaty et al., 2011). These Tet1-KO animals exhibit no morphological brain abnormalities but do posess slightly lower 5hmC levels in the CNS (Rudenko et al., 2013), thereby suggesting that Tet1 is not necessary to functional brain development. The fact that a larger change is not seen is most likely due to the fact that Tet2 and Tet3 are still present and are more highly expressed in the healthy brain. In confirmation of this compensation effect, double KO of Tet1 and Tet2 in mice results in almost certain perinatal death, although some mice survived without any gross abnormalities (Dawlaty et al., 2013). The surviving mice exhibited decreased 5hmC levels (-34%) and slightly increased 5mC levels (+5%), suggesting that Tet3 is still compensating in the oxidation of 5mC to 5hmC. In terms of adult brain function, KO in rodent studies have elucidated a role for Tet1 in spatial learning & memory (R. Zhang et al., 2013) and have also revealed that loss of Tet1 results in electrophysiological deficits in the hippocampus (Rudenko et al., 2013).

The roles of Tet2 and Tet3 in brain development and function are less widely studied, but it has been determined that similarly to Tet1, Tet2 KO does not result in brain abnormalities or dysfunction in mice (Li et al., 2011). A potential role for Tet3 in fear memory was identified when Tet3 KO had no effect on fear memory acquisition but impaired fear memory extinction

(Li et al., 2014), whilst a potential role in the regulation of synaptic transmission was revealed when Tet3 knockdown was found to significantly increase the number of glutamate receptor 1 (GluR1) on the surface of hippocampal neurons *in vitro* (Yu et al., 2015), which had a negative downstream effect on the amplitude of electrical signals.

1.3: The role of DNA (hydroxy)methylation in ischemic stroke

1.3.1: Oxidised 5mC in neurodegenerative disorders

Whilst the mechanisms behind Tet-mediated active demethylation are becoming clearer, the role that this process plays in the pathophysiology of neurodegenerative disorders and how this could possibly translate into therapeutic treatments remains an area of great interest. Wang et al. (2013), using a mouse model of Huntington's disease, found that 5hmC levels are significantly lower in the striatum and cortex in comparison to age-matched controls. The same study also found that differentially hydroxymethylated regions (DhMRs) were acquired at the bodies of genes important in neuronal development and growth. They therefore speculate that encouraging the acquisition of DhMRs through manipulation of Tet enzymes could have the potential to slow or halt the progression of Huntington's disease, which is the focus of their future studies. 5mC and 5hmC may also have a role in the development of Alzheimer's disease, as evidenced by the fact that the middle temporal gyrus and middle frontal gyrus in a mouse model of Alzheimer's express significantly higher levels of both 5mC and 5hmC in comparison to controls (Coppieters et al., 2014). This increase in hydroxymethylation was found to occur only in neurons and was not seen in astrocytes or microglia, suggesting that differential expression of 5hmC and the subsequent effects on gene expression may play a role in the neurodegeneration that occurs in Alzheimer's pathophysiology.

Previous research has shown that the epigenetic events following ischemic stroke are complex and extremely varied. Early studies revealed an overall increase in levels of 5mC in infarcted tissue when compared to the healthy contralateral hemisphere (Endres et al., 2000), although the relationship is not quite that simple as evidenced by the fact that DNMT1 reduction protects against the damaging effects of ischemic stroke, whereas complete loss of the enzyme does not (Endres et al., 2001).

1.3.2: The role of oxidised 5mC in ischemic stroke

This relationship between DNA methylation and ischemic injury only becomes more complicated when considering the oxidised derivatives of 5mC. Miao et al. (2015), using a middle cerebral artery occlusion (MCAO) model of stroke in mice, discovered that levels of 5hmC in the infarcted hemisphere were significantly increased after ischemic stroke, although not until at least 36 hours after the injury occurred and with peak expression occurring at 48h post-stroke. Alternatively, very recent research by Morris-Blanco et al. (2019) determined a significant increase in 5hmC levels as soon as 5 minutes after the conclusion of a transient ischemic stroke, although these levels remained significantly increased for at least 24 hours.

Both Miao et al. and Morris-Blanco et al. also found increases in 5mC, although expression of this marker peaked at 12-24h post-stroke and by 7 days the expression of 5mC had reduced to significantly below that of control animals. This therefore seems to suggest a timeline of events occurring post-stroke, with the immediate response being an increase in DNMT3a/b activity resulting in increased 5mC, with subsequent increased activity of Tet enzymes then oxidising the 5mC to 5hmC, leading to the observed decrease and increase in expression of 5mC and 5hmC, respectively. The research carried out by Miao et al. seems to provide further evidence for this as inhibition of the Tet2 enzyme *in vivo* prevented the 5hmC increase in the

infarcted hemisphere, whereas 5mC levels still increased. This was accompanied by significant increases in infarct volume which suggests that the oxidisation of 5mC to 5hmC post-stroke has a neuroprotective effect and could therefore be an interesting target for future therapeutic treatments. Additionally, Morris-Blanco et al. determined that knocking down expression of Tet3 through administration of short-interfering RNAs (siRNAs) also caused increased infarct volumes, further suggesting that oxidation of 5mC provides a neuroprotective effect.

It has been found that increased axonal sprouting and synaptogenesis is initiated by the end of the first week post-stroke and persists for several more weeks (Brown et al., 2009), whilst gene studies have found that increased expression of genes associated with axon growth occurs in the week following injury and can persist for months (Carmichael et al., 2005). This is very interesting when compared to the previously described finding that post-stroke 5hmC expression peaks at 48h following injury and remains significantly increased at 7 days (Miao et al., 2015). The fact that peak 5hmC expression coincides with the increase in expression of pro-axon growth genes suggests a potential role of 5hmC in controlling the expression of these genes. However, it is not yet known what the levels of 5hmC expression are at longer time periods following injury, such as 1 month, and no studies have determined the genomic loci at which 5hmC is increased following ischemic injury. The supposed timeline of global 5mC and 5hmC changes in the brain post-stroke, based on the currently available literature, as well as how they coincide with broad molecular & cellular changes in ischemic stroke pathophysiology can be seen in Figure 1.7.

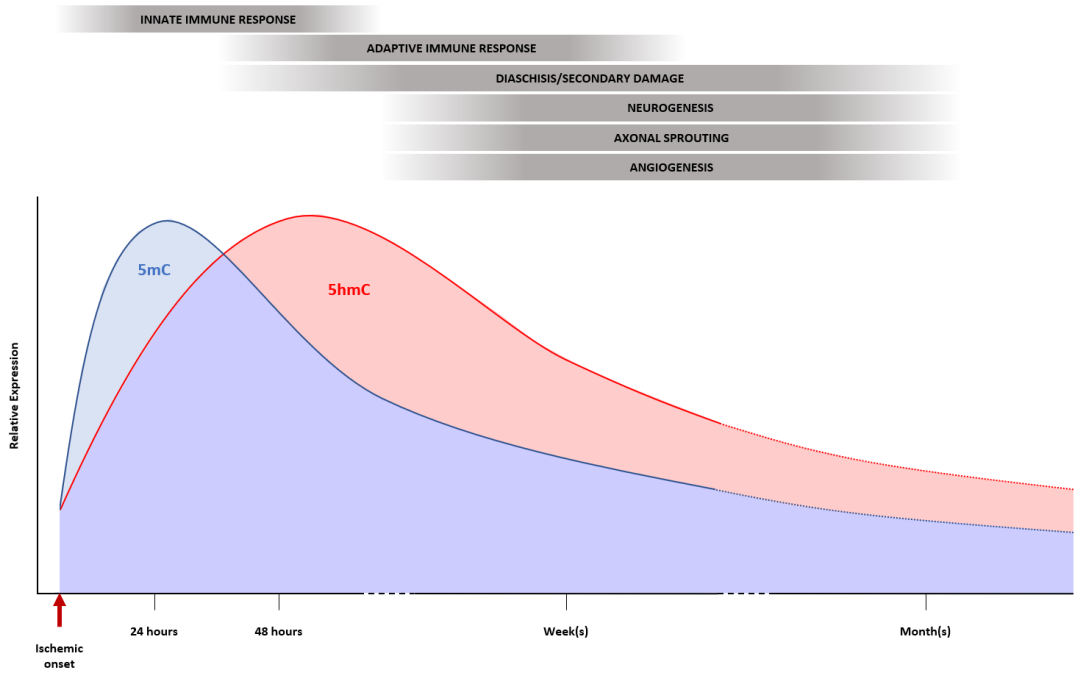


Figure 1.7: Timeline of epigenomic, molecular & cellular changes post-stroke
Based on the currently available research focused on assessing global changes to 5mC and 5hmC levels post-stroke (from Miao at al. (2015) and Morris-Blanco et al. (2019)), it is supposed that both 5mC and 5hmC levels increase significantly following ischemic onset, with 5mC levels peaking at around 24 hours post-stroke, whereas 5hmC levels peak at around 48 hours post-stroke. These peaks coincide with several major molecular and cellular changes in the ischemic cascade, including the innate immune response and the onset of the adaptive immune response and diaschisis. These peaks also precede several other broad changes, including neurogenesis, axonal sprouting and angiogenesis. However, levels of 5mC and 5hmC have not been determined for later time points, in the order of months post-stroke.

Whilst this new research suggests that increased Tet activity and oxidisation of 5mC has a positive effect on ischemic injury, the mechanism behind this observed effect is yet to be fully elucidated. In their same study, Morris-Blanco et al. determined that knocking down expression of Tet3 led to differential post-stroke expression of oxidative stress-related genes. Alternatively, Miao et al. found that post-stroke 5hmC levels were particularly increased at the promoter regions of genes involved in axonal growth, neuronal morphogenesis and neurodevelopment. One such gene was the gene coding for brain-derived neurotrophic factor (BDNF), a protein that encourages the growth of new neurons and synapses. Ischemic injury caused a significant increase in hydroxymethylation of the BDNF gene, whereas inhibiting Tet2

caused no increase in 5hmC levels and led to reduced levels of BDNF mRNA and protein in comparison to control animals. This therefore suggests that oxidisation of 5mC by the Tet family of enzymes is responsible for modulating the severity of ischemic injury by increasing the expression of various neurotrophic factors, thereby promoting neuronal growth and proliferation. As of yet there are no studies which confirm that altered levels of 5mC or its oxidised derivatives are directly responsible for the altered expression of these axon sprouting-related genes, although given the available evidence that demonstrates the changes in 5mC/5hmC levels and Tet activity post-stroke, it is plausible. The previously established changes in global hydroxymethylation patterns with age (Szulwach et al., 2011) could also offer a potential explanation as to why the axon sprouting response differs between young and aged individuals.

Whilst studies have begun to elucidate the potential role of epigenetic modifications in regulating post-stroke axonal sprouting by influencing gene expression within neurons, a newly emerging field of research has begun to highlight a potentially more indirect role of epigenetic modifications in regulating post-stroke injury severity. Mounting evidence suggests that epigenetic modifications to DNA in microglia and peripheral macrophages can influence the cascade of immune response events that occur following ischemic injury by controlling the release of pro- and anti-inflammatory cytokines (Picascia et al., 2015). Further research into how epigenetic modifications alter this complex post-ischemic innate immune response has revealed that inhibiting histone deacetylase enzymes (HDACs) prevents the release of M1 microglia activation markers (Kannan et al., 2013), as does overexpression of the micro RNA miR-424 (Zhao et al., 2013). However, no current research has aimed to determine a role of DNA methylation or 5mC oxidation in the regulation of this immune response.

Whilst this new research is beginning to shed light on the role of 5hmC in stroke, there is no research at present that has aimed to determine a role of 5fC or 5caC in stroke pathophysiology. Given the previously established different demethylation mechanisms and potential regulatory roles of 5hmC and 5fC/5caC, discovering the role that these further oxidised 5mC derivatives play in influencing neuronal plasticity and determining ischemic injury severity is an area of great interest that could offer even more potential therapeutic targets.

1.4: Modelling ischemic stroke in rodents

Preclinical research to determine the potential role of DNA (hydroxy)methylation in the pathophysiology of ischemic stroke requires the use of an *in vivo* rodent model. There are a wide number of available techniques to induce focal ischemia, however most focus on occlusion of the middle cerebral artery (middle cerebral artery occlusion; MCAO). This is because the middle cerebral artery (MCA) is the most commonly occluded blood vessel in human ischemic stroke patients (Bogousslavsky et al., 1988), and occlusion of the MCA affects the same main brain regions in rodents and human patients, with minor anatomical differences (Howells et al., 2010). A variety of MCAO rodent models have been previously established; a brief summary of the most commonly used, as well as their advantages and disadvantages, are listed in Table 1.2.

Method	Description	Advantages	Disadvantages	References
Filament Occlusion	Filament is inserted into the CCA and advanced into Circle of Willis until MCA is blocked at point of origin. Can be temporary or permanent.	Less invasive (no craniotomy) Shorter surgery times Can control occlusion length Consistent location of occlusion	Possibility of damage to hypothalamus & hippocampus High variability between and within strains Occlusion cannot be visually confirmed If permanent, causes large infarct and high mortality rate	Koizumi et al. (1986) Connolly et al. (1996)
Transcranial Occlusion	Following craniotomy, the distal portion of the MCA is occluded, either temporarily or permanently. Can be occluded via: ligation, application of a clip, electrocoagulation, or injection of a vasoconstrictor (endothelin-1).	Visual confirmation of occlusion Location of occlusion is controllable Small, reproducible infarcts	Invasive (craniotomy is required) Cannot be used to study thrombolysis Reduced functional deficits	Robinson et al. (1975) Tamura et al. (1981) Buchan et al. (1992) Sharkey (1993)
Clot Embolism	Laboratory-created clots are carefully inserted into the CCA, or directly into the MCA.	Most clinically relevant Can be used to study thrombolysis No craniotomy required if inserted into CCA	Invasive (craniotomy required) if inserted directly into MCA Variable occlusion lengths & infarct sizes Variable infarct location if injected into CCA	Kudo et al. (1982) Kilic et al. (1998) Orset et al. (2007)

Table 1.2: Rodent models of MCAO
A number of techniques are available to induce middle cerebral artery occlusion in rodents. This table briefly describes the most commonly used as well as their main advantages and disadvantages. Included are references to published studies that have used the technique. MCA = middle cerebral artery; CCA = common carotid artery.

The most widely used technique of inducing MCAO is the filament occlusion model, which involves the insertion of a monofilament into the common carotid artery (CCA) which is then moved up the internal carotid artery and into the Circle of Willis until it blocks MCA at its origin (Connolly et al., 1996; Koizumi et al., 1986). Doing so means that the entire territory of the vessel, including both the cortex and striatum, are affected (Bederson et al., 1986). Additionally, it has been shown that filament occlusion of the MCA can also cause ischemic damage to the hypothalamus and hippocampus (Özdemir et al., 1999) since these brain regions receive collateral blood supply from arteries originating from the internal carotid artery. Occlusion of the MCA with a filament can block the origins of these arteries, leading to reduced blood flow and possible ischemia. This not only leads to functional deficits, but can also cause hyperthermia, which further exacerbates ischemia-related cell death (Li et al., 1999). However, transient occlusion of the MCA (in which the filament is removed after 60-90 minutes) has been shown to prevent most of this hypothalamic damage (Li et al., 1999).

The main advantages of the filament model of MCAO are that the surgery is relatively non-invasive, not requiring a craniotomy, and the location of the resulting infarct is relatively consistent. Conversely, the main disadvantage of the filament model of MCAO is that it produces highly variable infarct sizes both between and within strains. Variability from within strains arises from the difficulty in reliably placing the occluding filament in the exact same position in each animal, thereby leading to differences in blood flow and subsequent ischemic damage. Variability between strains arises from differences in blood vasculature; for example, in the MCAO model of ischemic stroke, it has been found that C57BL/6 mice exhibit significantly larger infarcts than Sv129 or BALBc mice due to the fact that they have poorly developed posterior communicating arteries, which limits collateral blood flow to the occluded brain areas (Carmichael, 2005). An alternative model that is often used in order to reduce this variability is the transcranial occlusion of the MCA, in which only the distal portion

of the MCA is occluded. This method produces smaller, more reliable cortical infarcts, although the surgery is more invasive as it requires craniotomy and also produces less functional deficits than the filament model (Howells et al., 2010).

Another disadvantage of the filament model of MCAO is that it is not truly representative of the thromboembolic occlusions that occur in human stroke patients. Mechanical occlusion of the MCA with filaments as opposed to blood clots means that thrombolysis cannot be examined in this model. Currently, there is only one licensed drug for use in stroke patients: recombinant tissue plasminogen activator (tPA) (O'Collins et al., 2006), which acts to break down ischemia-causing clots through the activation of plasmin. The fact that this is the only preclinical treatment that has advanced to become a licensed drug highlights the importance of being able to test thrombolysis in ischemic stroke models. Clot embolism models of MCAO are established in which laboratory-made clots are placed into the CCA or MCA directly (Kudo et al., 1982; Orset et al., 2007). However, these models can require invasive surgery and given that the clots are prone to dissolution, they can create infarcts of varying sizes and in various locations, producing varied and often undetectable functional deficits. It is for these reasons that the filament model of MCAO remains the most widely used in preclinical ischemic stroke research.

A further aspect of modelling ischemic stroke in rodents that is important to consider is its translatability to humans. For example, it is known that stroke occurrence and severity both increase with age (Mogensen et al., 2013), and there exist differences in stroke outcomes between sexes, with women tending to experience worse functional outcomes and quality of life following stroke even after adjusting for other factors such as age (Reeves et al., 2008). Furthermore, comorbidities such as diabetes, obesity and hypertension are all known to worsen stroke severity and functional outcomes (Bushnell et al., 2008), so it is often stated

that in order to pre-clinically assess potential stroke therapeutics, the animal models utilised must also account for these comorbidities. Considering the number of factors that can affect stroke severity in humans, it is important that in order to produce results that are translatable to humans, these factors need to be considered when producing the animal model. However, producing animal models that are aged and/or have comorbidities increases cost as well as the number of animals required, as more are likely to be lost to stroke-related death during the study. It is therefore important to consider which, if any, factors to include in an animal model when designing *in vivo* stroke studies.

1.5: Summary

Having considered recent research into post-stroke axonal sprouting and the role of oxidised 5mC derivatives in the demethylation of DNA, it appears that these derivatives and the Tet enzymes that produce them are potentially responsible for the initiation of axon growth following ischemic injury. Studies have shown that 5hmC, 5caC and 5fC are all involved in one or more mechanisms of DNA demethylation and are subsequently responsible for increased gene expression. Increased expression of 5hmC is observed in the brain following ischemic injury, with expression peaking at 48h and persisting for 7 days. This coincides with post-ischemic increased expression of genes associated with axonal growth, suggesting that 5hmC could potentially be responsible for the increased expression of these genes. However, a number of things remain to be seen before such a relationship can be ascertained. For example, there is no current research that determines which genes or genomic loci in particular express increased 5hmC levels post-stroke. Furthermore, the post-stroke inflammatory response has been shown to have a negative effect on axonal growth, and whilst some research has determined an effect of epigenetic modifications such as histone acetylation or micro-RNA interference in the control of the post-stroke inflammatory

response, the effect that DNA methylation has on this response also remains unknown. Determining the potential role of 5hmC in the control of post-stroke axonal sprouting is clinically important as it could provide potential therapeutic treatments for stroke patients, which there is a severe lack of as evidenced by the high mortality rate of stroke.

1.6: Thesis aims

The ultimate aim of this thesis is to investigate the potential roles of DNA (hydroxy)methylation and the Tet family of enzymes in the control of post-stroke axonal growth. The main part of this thesis focuses on ascertaining the methylomic response of the brain to ischemic stroke using rodent models of MCAO; first developing on the small amount of previously published research by determining post-stroke global 5hmC levels in distinct brain areas and at delayed time points (Chapter 2). This is then further elaborated upon by analysing levels of DNA (hydroxy)methylation in specific cell types, namely neurons and microglia, in the hopes of elucidating a potential role of the epigenetic modification in the brains inflammatory response to stroke (Chapters 3 and 4). Focus then shifts to the use of an *in vitro* model of ischemic stroke, with the aim of determining a direct effect of Tet enzyme expression on neuronal growth (Chapter 5). The resulting findings are then collated and considered within the context of previously published research, determining how they can inform future research and possibly lead to the development of new therapeutic interventions for ischemic stroke (Chapter 6).

Chapter 2: Timeline of post-stroke DNA hydroxymethylation

2.1: Introduction

Evidence from previous research has elucidated a potential role of DNA (hydroxy)methylation in neurodegenerative diseases such as Alzheimer's, Huntington's and Parkinson's (Bradley-Whitman & Lovell, 2013; Stöger et al., 2017; Wang et al., 2013). Whilst the pathophysiology of ischemic stroke is vastly different to that of these neurodegenerative diseases, these findings hint at a highly dynamic role of (hydroxy)methylation in the pathophysiology of these diseases that could potentially translate to the neurodegeneration that occurs following an ischemic stroke. Any potential role of (hydroxy)methylation in ischemic stroke or post-stroke neuroplasticity could form the basis of novel treatments; however, before such a role can be elucidated, it is important to examine how endogenous levels of (hydroxy)methylation are affected by ischemic stroke.

2.1.1: Post-stroke DNA (hydroxy)methylation

Previous studies focusing on the post-stroke expression of 5mC and DNMTs (the enzymes responsible for adding methyl groups to cytosine residues on the DNA molecule) have given varied results. Early research discovered that following middle cerebral artery occlusion (MCAO) in mice, 5mC levels were significantly increased in infarcted tissue in comparison to healthy tissue, which may be responsible for promoting cell death (Endres et al., 2000). However, the role of this increased DNA methylation in stroke pathophysiology appears to be multifaceted, as evidenced by subsequent research finding that animals engineered to express

low levels of DNMT1 experienced smaller infarcts and increased functional recovery post-MCAO, whereas mice that expressed no DNMT1 did not experience a protective effect (Endres et al., 2001). More recent research concurs that increased 5mC levels post-stroke appear to play a detrimental role in the pathophysiology of ischemic stroke, with Choi et al. (2018) finding that post-stroke administration of the cytidine analogue 5-Azacytidine, an inhibitor of DNA methylation, improves functional recovery and increases axonal sprouting in a photothrombotic model of stroke in rats. Similarly, Dock et al. (2015) found that infarct size was significantly decreased in rats that were treated with Zebularine, a DNMT1 inhibitor, following MCAO.

Whilst various studies focusing on the post-stroke expression of 5mC and its impact on stroke severity have been carried out since the early 21st century, very little research has been done to elucidate the same information regarding the more recently discovered oxidised forms of 5mC. Miao et al. (2015) found that 5hmC expression was significantly increased in the infarcted hemisphere of mice that underwent MCAO, with a significant increase found at 36 hours post-stroke and peak levels occurring 48 hours post-stroke. The same study also found that intracerebroventricular administration of the Tet2 inhibitor SC1 (Pluripotin) caused significantly increased infarct volumes, suggesting that the oxidisation of 5mC to 5hmC in the days following ischemic stroke has a neuroprotective effect. Additionally, Morris-Blanco et al. (2019) also discovered that 5hmC levels are increased following transient MCAO, peaking at 12-24h, and that knockdown of Tet3 leads to increased infarct size.

Although this research is beginning to illustrate the timeline of post-stroke 5hmC levels and its potential role in stroke pathophysiology, there are still a number of factors that have yet to be investigated. Namely, no studies have aimed to analyse post-stroke 5hmC levels in different brain areas; whether changes in 5hmC levels are local to the infarct and/or peri-

infarct area; or whether any changes in the further oxidised derivatives of 5mC (5fC and 5caC) are observed post-stroke. There is also no research that has yet determined if increased post-stroke levels of (hydroxy)methylation are observed in the long term (> 1 week post-stroke), or if there are differences in 5mC/5hmC levels between different cell types. This information is necessary in order to detail the role of (hydroxy)methylation in stroke pathophysiology and recovery as axonal sprouting & functional remapping does not occur until several weeks after the ischemic event, with various different cell types contributing to this process of recovery (Sist et al., 2012).

2.1.2: Ischemic stroke across brain regions

When studying the pathophysiology of ischemic stroke, it is important to consider differences in brain regions as a stroke can affect various brain structures and the resulting deficits are dependent on the areas of the brain that are damaged. The artery that is most commonly obstructed in large vessel occlusion in stroke patients is the MCA, which causes damage to the somatosensory and motor cortices. Damage to these areas leads to the deficits in sensory, motor and speech functions that are commonly observed in ischemic stroke patients. As well as supplying these cortical structures, the MCA also supplies a number of deeper brain structures, including the striatum, through penetrating blood vessels known as lenticulostriate arteries (Donzelli et al., 1998).

Whilst occlusion of the MCA causes direct damage to the striatum and portions of the cortex, other brain regions that are functionally connected to these structures can also become damaged due to secondary degeneration. In the case of ischemic stroke involving occlusion of the MCA, secondary degeneration of cells has been observed in the substantia nigra pars compacta (SNc) following MCAO in rodents (Tamura et al., 1990; Winter et al., 2005), with

later studies utilising MRI to elucidate the same phenomenon in human patients (Abe et al., 2003; Nakajima et al., 2010). This is due to the presence of dopaminergic cells projecting directly from the SNc and ventral tegmental area (VTA) to the striatum as part of the nigrostriatal pathway (Figure 2.1), forming part of the basal ganglia circuitry (Haber, 2016). Due to the loss of their striatal target cells and/or damage to the axons that connect them, these dopaminergic neurons undergo secondary degeneration in the weeks following the ischemic event.

2.1.3: Secondary degeneration in exfocal brain regions

The exact mechanisms that underly this post-ischemic neurodegeneration in the SNc are unclear as there is evidence for several cellular mechanisms contributing to cell death in exfocal brain areas. Early studies identified several markers of necrotic cell death in areas of post-ischemic degeneration (Fujie et al., 1990), whereas studies carried out in the following years identified markers of apoptosis, such as DNA fragmentation and nuclear fragmentation, in the same brain areas (Soriano et al., 1996). However, subsequent recent research has analysed these markers on a cell-by-cell basis and found markers for both apoptosis and necrosis, suggesting that cells functionally connected to the ischemic infarct may undergo a "hybrid" death following damage to their infarcted targets as opposed to a purely apoptotic or necrotic death (Wei et al., 2004).

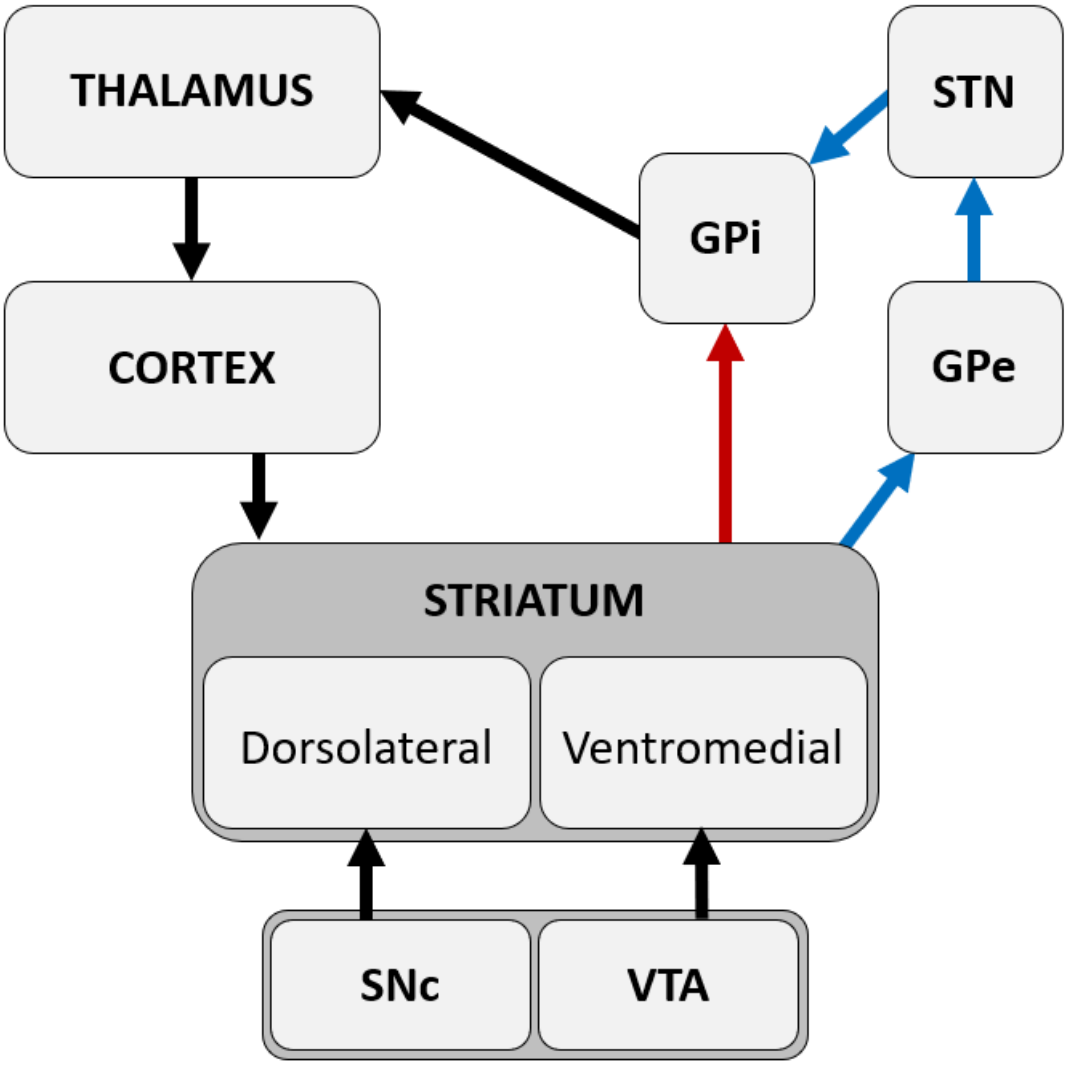


Figure 2.1: The nigrostriatal dopaminergic pathway & motor basal ganglia circuitry
The nigrostriatal pathway consists of direct dopaminergic output from the substantia nigra pars compacta (SNc) to the dorsolateral striatum. Alongside this, the ventral tegmental area (VTA) projects directly to the ventromedial striatum via dopaminergic neurons. These dopaminergic inputs synapse with GABAergic neurons in the striatum, which themselves project to the globus pallidus interna (GPi) either directly (red arrows) or indirectly (blue arrows) through the globus pallidus externa (GPe) and subthalamic nucleus (STN). The output from the globus pallidus interna to the thalamus is inhibitory and modulates normal motor function through direct projections from the thalamus to the motor cortex. This circuitry as a whole comprises the motor circuitry of the basal ganglia. Additionally, there exists input from the cortex to the striatum via glutamatergic neurons, forming the well characterised corticostriatal pathway.

The cellular mechanisms triggered by ischemic stroke that lead to this “hybrid” death in exfocal regions are also varied and not entirely clear. Previous research into these mechanisms has suggested that oxidative stress may trigger this degeneration, with cells undergoing post-ischemic secondary degeneration in the thalamus of a rat model of stroke exhibiting increased expression oxidative stress markers (Ohba et al., 2004). Conversely, other studies have found that the axonal damage caused to cells of the thalamus and SNc during ischemic stroke can cause dysregulation of cell membrane potentials and trigger excitotoxicity (Zhao et al., 2001); and that ischemic stroke can lead to build-up of the well-characterised neurotoxic peptide amyloid beta in areas of exfocal neuronal degeneration (Zhang et al., 2011). Taken together, this research clearly demonstrates that the cellular mechanisms underlying post-stroke secondary degeneration in exfocal brain areas are varied and multifaceted. It is therefore possible that (hydroxy)methylation could play a role in this process, although there is no research to date that has attempted to investigate this.

2.1.4: Methods of quantifying global 5hmC

Since the discovery of 5hmC around a decade ago, numerous methods have been developed in order to determine global levels of 5hmC across the genome, each with various strengths and weaknesses in terms of their assay design. The most easily accessible and widely used methods utilise antibodies targeting 5hmC, examples of which include immuno-dot-blot and immunohistochemistry (IHC). Although more accurate procedures are available, these methods remain popular due to their simple assay design and relatively low cost. Other available methods, such as [3H]-glucose labelling and thin layer chromatography (TLC) involve the use of radioactive isotopes in order to label the hydroxylated cytosine bases. Whilst widely considered more accurate than immuno-dot-blot and IHC, the use of isotopes makes these

methods more expensive to run and a higher safety risk. An alternative, highly accurate method of quantifying global 5hmC levels is high performance liquid chromatography (HPLC). However, in order to obtain the most accurate and informative data from this method, specialist equipment such as mass spectrometers are needed. This therefore makes HPLC a relatively expensive assay to run that also requires expert knowledge of the specialist equipment needed. An overview of each aforementioned method, as well as various pros, cons and references to papers utilising these methods, are included in Table 2.1.

Considering the benefits and drawbacks of each available method, the technique chosen to investigate post-stroke levels of DNA methylation in this thesis chapter is IHC. IHC allows for the visualisation and analysis of post-stroke DNA methylation in the actual biological environment and also allows for analysis of the infarcted and peri-infarct tissue simultaneously.

Method	Description	Advantages	Disadvantages	References
Immunohistochemistry (IHC)	Antibodies targeting 5hmC are used to stain fixed cells or tissue	Allows for visualisation of 5hmC distribution in biological sample; can analyse across tissue types (i.e. diseased & healthy); tissue preparation allows for other tests to be performed using same samples	Sensitive to sample preparation	Haffner et al. (2011); Szulwach et al. (2011)
Immuno dot-blot	DNA is immobilised on a surface and probed with an antibody targeting 5hmC	Simple & rapid technique; can be adapted to ELISA format for high throughput; can be quantitatively analysed through use of calibration curves	Requires µg quantities of DNA; can be affected by non-specific antibody binding	Thomson et al. (2012); Miao et al. (2015)
[3^{H}]-glucose labelling	[3^{H}]-glucose is transferred to genomic 5hmC, with incorporation measured by scintillation counting	Simple assay design; can determine absolute 5hmC levels through use of calibration curves	Requires large amount of DNA; requires use of radioactive isotopes	Terragni et al. (2012); L. Zhang et al. (2013)
Thin-layer chromatography (TLC)	DNA is enzymatically digested and radioactively labelled before being hydrolysed, after which nucleosides are separated on TLC plates	The use of different restriction enzymes allows for analysis of 5hmC content in different sequence contexts	Requires large amount of DNA; requires use of radioactive isotopes	Tahiliani et al. (2009); Ficz et al. (2011)
High-performance liquid chromatography (HPLC)	Hydrolysed nucleosides are resolved by liquid chromatography and then detected by adsorption analysis or mass spectrometry	Very accurate and sensitive; can use reference compounds to quantitatively analyse 5hmC content	Requires large amount of DNA; often expensive and requires expert knowledge of equipment	Xu et al. (2011); Yin et al. (2015)

Table 2.1: Methods of quantifying global 5hmC
Widely used methods of detecting and quantifying global levels of 5hmC, including references to published studies that have used the technique.

2.1.5: Objectives & Hypotheses

The objectives of this chapter are as follows:

- To determine the time course of changes in global 5mC, 5hmC & 5caC levels in the brain up to 1 month post-ischemic stroke
- To determine differences in post-stroke global 5mC, 5hmC & 5caC in various cell types; namely neurons, microglia & dopaminergic neurons of the substantia nigra pars compacta
- To determine differences in post-stroke global 5mC, 5hmC & 5caC levels in various brain areas affected by MCAO; namely the cortex and striatum (directly affected) and the substantia nigra pars compacta (indirectly affected) and compare to a brain area not affected by ischemic stroke (medial geniculate nucleus)

Based on previous research carried out in this area, the hypotheses for the findings of this chapter are as follows:

- Levels of global 5mC and 5hmC will increase in both the cortex and striatum, peaking at between 24 hours and 7 days
- Global levels of 5mC and 5hmC will differ between neurons and microglia
- Significant changes in global 5hmC levels in dopaminergic cells of the substantia nigra and ventral tegmental area will also be observed
- No changes in global levels of 5mC or 5hmC levels will be observed in the medial geniculate nucleus

2.2: Methods

All surgical procedures and tissue collection (sections 2.2.2 + 2.2.3) were performed by Rebecca Trueman and Annastazia Learoyd. Infarct volume analysis was performed by Annastazia Learoyd (section 2.2.5.2).

2.2.1: Experimental design

All experiments were performed according to the UK Animals (Scientific Procedures) Act 1986 under a project license from the UK Home Office.

Male C57BL/6 mice weighing 25-30g (Charles River, UK) were housed in IVC cages in groups of four under standard conditions (aspen chip bedding (depth of 3-5cm), sizzlenest material, cardboard tube and a wooden stick for chewing). Room conditions were kept to 21-23^{o}C with 12h light-dark cycle. All experimental procedures were completed during light hours (7am-7pm). Animals had unlimited access to food and water throughout the study with supplementary softened food being provided once prior to surgery and daily post-surgery for 7 days. Paracetamol was added to the drinking water (1mg/ml) for the day before and 48h following surgery.

Animals (n=44) underwent 30 minute MCAO, an equivalent sham surgery, or no surgery (naive animals). At varying time points after surgery (1, 2, 7 or 28 days) animals were euthanised and perfused. Brains were collected for the analysis of infarct volume and expression of 5hmC. The number of animals used for each experimental group is shown in Table 2.2.

Time point after MCAO (days)	Initial Number of Animals	Animals Excluded	Final Number of Animals
Stroke Groups			
1	8	4	4
2	8	3	5
7	8	3	5
28	9	4	5
Control Groups			
Sham	6	2	4
Naïve	5	0	5

Table 2.2: The number of mice used to assess post-stroke levels of 5hmC
Mice underwent 30 minute middle cerebral artery occlusion (n=33), an equivalent sham surgery (n=6) or no surgery at all (n=5). Animals were excluded due to anaesthetic related death (n=3), severity of stroke (n=4), lack of stroke (no stroke symptoms during occlusion or infarct < 5mm^3; n=8) or damage to brain during tissue collection (n=1).

2.2.2: Surgical procedures

The filament occlusion model was used to induce a stroke (originally developed by Longa et al. (1989), modified in this study by not cauterising external carotid artery). Animals were anaesthetised using 5% isoflurane (100% w/w, 250ml; Abbott, US) in 1NLt/min O2 and maintained using 1-2.0% isoflurane in 0.6 NLt/min O2 and 0.8NLt/min N2O. Prior to the start of surgery, animals were shaved and the surgical site cleaned. Local anaesthetic (EMLA Cream (5%, 5g; AstraZeneca, UK)) was applied to the neck and lubricant was applied to the eyes. During surgery, core temperature was maintained at 37±0.5^{o}C through the use of a homeothermic blanket (Harvard Apparatus, US). Sterile conditions were maintained throughout the procedure.

Surgery to induce the stroke involved the dissection of tissue in the neck to expose the right common carotid artery (CCA) and its bifurcation into the external carotid artery (ECA) and internal carotid artery (ICA). All vessels were dissected from the surrounding tissue and a hole was made in the CCA to allow insertion of a silicone-coated filament (diameter of 0.19mm;

Doccol, US). The filament was inserted up the CCA and the ICA until a mild resistance was felt. At this point if the filament had moved a sufficient length up the artery and none of the white silicone of the filament was visible, the MCA was deemed occluded. The filament was secured in place, occluding the MCA, for 30 minutes. Animals were allowed to recover from the anaesthetic for the duration of the occlusion period. During this time animals were placed in a box heated to 32^{o}C and monitored for stroke symptoms. Symptoms included circling and unilateral loss of sensation (assessed through whisker stimulation and paw placement). Complete lack of stroke symptoms led to exclusion from the experiment. At the end of the occlusion period, after a stroke had been confirmed, animals were re-anaesthetised and the filament removed.

Animals undergoing sham operations underwent the same procedures including the dissection and ligation of blood vessels. A filament was not inserted into the CCA of sham animals. These animals were also re-anaesthetised 30 minutes post-surgery to maintain the time spent under anaesthesia.

2.2.3: Tissue collection

At various time ponts post-MCAO (24 hours, 48 hours, 7 days or 1 month), animals were euthanised using intraperitoneal injection of Euthatal (0.1ml; 200mg/ml, Merial Animal Health Ltd, UK). After injection, animals were left in their home cage until they had no toe or corneal reflexes and breathing had ceased. At this point animals were perfused via the left ventricle with 250ml phosphate buffered saline (PBS) followed by 250ml of 1.5% paraformaldehyde (PFA). Brains were then removed and placed in 1.5% PFA for 24 hours followed by 25% sucrose for 24 hours. Following incubation in sucrose brains were mounted using mounting medium (OCT) onto a freezing platform of a freezing sledge microtome

(AS200; Anglia Scientific, UK). Once frozen, brains were cut into 40µm thick sections. The sections were placed in anti-freeze solution in 24 well plates and stored at -20°C.

2.2.4: Immunohistochemical staining

2.2.4.1: Fluorescent Staining for 5mC, 5hmC, NeuN, Iba1 & Tyrosine Hydroxylase

Sections were fluorescently stained to detect 5-methylcytosine (antibody raised in rabbit; Active Motif, USA), 5-hydroxymethylcytosine (antibody raised in mouse; Active Motif, USA), NeuN+ neurons (antibody raised in guinea-pig; Abcam, UK), Iba1+ microglia (antibody raised in goat; Abcam, UK) and TH+ dopaminergic neurons (antibody raised in rabbit; Millipore, USA). For sections undergoing double staining, primary antibodies were added at the same time, not in series.

Tissue sections stained for 5mC and/or NeuN first underwent antigen retrieval, which involved incubation in 15mM sodium citrate buffer (adjusted to pH 6.0 with citric acid) at 80°C for 20 minutes followed by three washes in PBS.

All tissue sections were then permeabilised by incubating in PBS containing 0.5% Triton X-100 for 30 minutes, followed by incubation in 2N HCl for one hour in order to denature DNA. Sections were then neutralised via incubation in 10mM Tris-HCl for 30 minutes before being placed in a blocking solution consisting of PBS with 0.3M glycine, 0.5% Triton X-100 and 0.5% low endotoxin bovine serum albumin (BSA; Sigma-Aldrich, UK) in order to prevent nonspecific binding of antibodies. Sections were then incubated overnight at 4°C with primary antibodies diluted in blocking solution (rabbit anti-5mC, 1 in 500; mouse anti-5hmC, 1 in 2000; guinea-pig anti-NeuN, 1 in 500; goat anti-Iba1, 1 in 500; and rabbit anti-TH, 1 in 500). Three washes

in PBS were performed before incubation in fluorescent marker-conjugated secondary antibodies (goat-anti-mouse AlexaFluor 568, Thermo Fisher, UK; goat-anti-rabbit AlexaFluor 594, Invitrogen, UK; goat anti-guinea-pig AlexaFluor 405, Thermo Fisher, UK; donkey anti-goat AlexaFluor 488, Invitrogen, UK) at a dilution of 1 in 400 in blocking buffer for 2 hours at room temperature. Sections underwent one final round of PBS washes before being mounted onto gelatinised microscope slides and allowed to air dry in the dark. All sections then underwent serial dehydration via incubations in increasing concentrations of ethanol (70%, 90% and 100%). Slides were then cleared with a rinse in xylene before being coverslipped with DPX (non-aqueous mounting medium; Millipore, USA). Coverslipped slides were stored at 4°C in the dark until imaging took place.

2.2.4.2: Fluorescent Staining for 5caC

Immunohistochemical detection of 5caC used a horseradish peroxidase-conjugated antibody; therefore, endogenous peroxidase activity was blocked by incubation in 3% hydrogen peroxide for 10 minutes. This was followed by cell membrane permeabilisation via incubation in PBS containing 0.5% Triton X-100 for 30 minutes. Sections were then incubated in 2N HCl for 30 minutes to denature DNA before being neutralised via incubation in 10mM Tris-HCl for 30 minutes. Tissue sections were then incubated in a blocking solution (PBS containing 0.3M glycine and 0.5% BSA) containing a 1 in 1000 dilution of rabbit-anti-5caC antibody (Active Motif, USA) at 4°C overnight. Following 3 washes in PBS, sections were then incubated in blocking solution containing a 1 in 400 dilution of goat-anti-rabbit HRP-conjugated secondary antibody (Vector Laboratories, UK) at room temperature for 2 hours. Following a further 3 washes in PBS, sections were then incubated in tyramide signal amplification buffer containing a 1 in 200 dilution of tyramide (Perkin Elmer, USA) for 2 minutes. Sections then

underwent 3 final washes in PBS before being dehydrated and coverslipped as previously described in section 2.2.4.1.

2.2.4.3: DAB Staining for NeuN

Briefly, endogenous peroxidase activity was blocked by incubation in 3% hydrogen peroxide for 10 minutes before nonspecific binding of antibodies was blocked by incubation in 3% normal serum. Tissue was then incubated with mouse-anti-NeuN antibody (Millipore, USA) diluted to 1 in 3000 overnight at 4°C. This was followed by incubation in a 1 in 400 dilution of biotinylated secondary antibody (goat-anti-mouse; Vector Laboratories, UK) for 2 hours. Sections were then incubated in Avidin/Biotin complex (Vectastain Elite ABC kit; Vector Laboratories, UK) for 2 hours followed by 3,3' Diaminobenzidine (DAB) in order for the stained cells to be detected. Sections were then serially dehydrated and coverslipped as described in section 2.2.4.1.

2.2.5: Image Analysis

2.2.5.1: Fluorescent Intensity Analysis

Fluorescently stained sections were imaged at either x10 magnification (when analysing the substantia nigra pars compacta) or x20 magnification (when analysing the cortex, striatum and medial geniculate nucleus) using a Zeiss 200M microscope (Zeiss, Germany). To create composite images of the entire infarcted hemisphere, x20 magnification images were stitched together using Volocity software (Leica, Germany).

Images of sections stained for 5hmC were analysed using ImageJ software (Abràmoff et al., 2004). Images were converted from colour to greyscale before regions of interest (ROIs) were

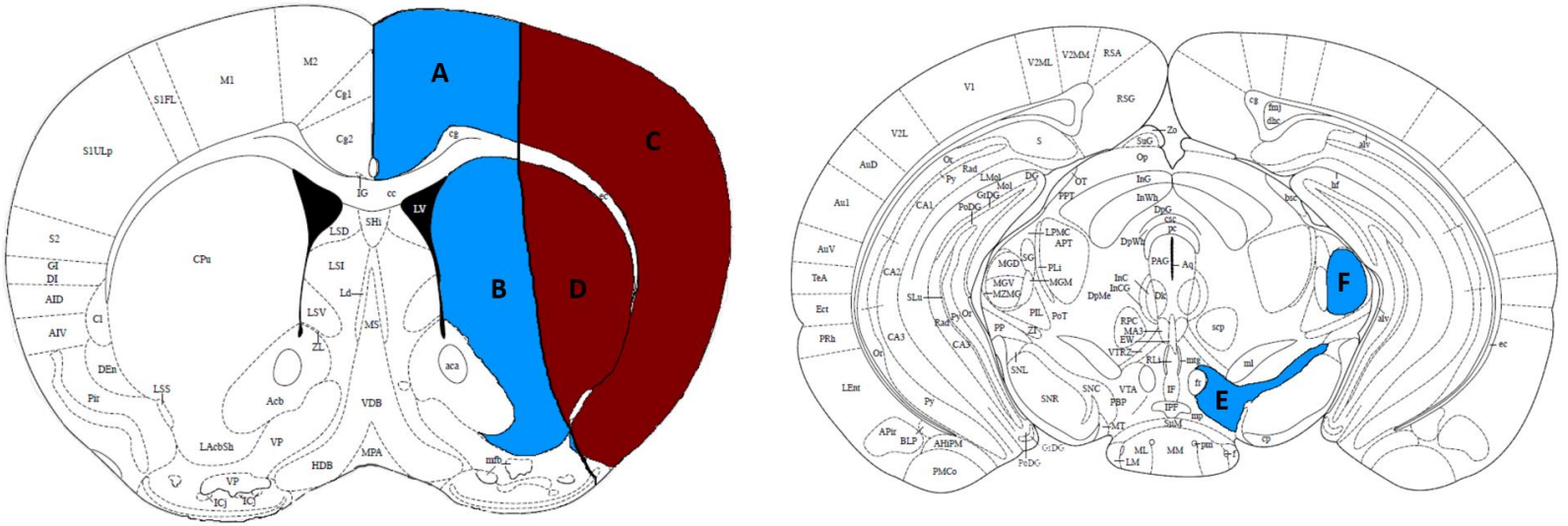
drawn and integrated density (a measure of average intensity across the entire region) measured. These measures of integrated density were then used to calculate Corrected Total Fluorescence (CTF), as detailed by McCloy et al. (2014). CTF is calculated as follows:

CTF = Integrated Density of ROI – (area of ROI x mean fluorescence of background readings)

As such, for each region of interest, the fluorescent intensity (defined as Mean Gray Value in ImageJ) was measured for 5 separate small non-nuclear areas within the ROI. These were then averaged to give a mean fluorescent reading of the background. The calculated CTF is thereby a measure of intensity of nuclear staining and is used as an indirect measure of 5hmC levels.

The regions of interest that were measured in this study include the cortex and striatum, which are directly affected by the infarct. As such, infarcted and non-infarcted areas of these brain regions were analysed separately. To determine borders of the infarct in the 5hmC stained tissue sections, ROIs were drawn around the infarct of directly adjacent tissue sections that were stained for NeuN. These ROIs were then mapped onto the corresponding sections stained for 5hmC.

Other brain regions analysed were the substantia nigra pars compacta and the medial geniculate nucleus. For analysis of the substantia nigra pars compacta, only dopaminergic (TH+) cells were of interest. Therefore, the nucleus of each TH+ cell was defined as a ROI, and the CTF of all nuclei were averaged for each animal. Figure 2.2 shows the regions of interest analysed in this study.



Bregma = ~0.74 **Bregma = ~-3.08**

Figure 2.2: Brain areas analysed for post-stroke 5hmC levels

To determine the timeline of post-stroke 5hmC expression, several brain areas were analysed. An example of an infarct produced by MCAO is shown in dark red. Brain areas directly affected by stroke were analysed, with infarcted and non-infarcted areas analysed separately. A = non-infarcted cortex; B = non-infarcted striatum; C = infarcted cortex; D = infarcted striatum. A brain area indirectly affected by stroke, dopaminergic neurons of the substantia nigra pars compacta and ventral tegmental area (E) was also analysed. As a control, a brain area that is not directly or indirectly affected by stroke, the medial geniculate nucleus (F) was also analysed. Image adapted from Franklin and Paxinos (2008).

2.2.5.2: TH+ Cell Count

One brain section from each mouse (bregma point ~-3.08; Figure 2.2) was fluorescently stained with antibodies targeting TH and subsequently imaged at x10 magnification. ImageJ software was then used to count the number of positively stained cell bodies in the substantia nigra pars compacta and ventral tegmental area of the hemisphere ipsilateral to the infarct in each section.

2.2.5.3: Infarct Volume Analysis

Sections stained for NeuN were imaged at x10 magnification using a slide scanner (Axioscan Z1; Zeiss, Germany). This scanner automated the process of taking x10 magnification images and stitching to produce a composite image of the entire section. Images of sections between Bregma 0.98 to -0.94mm were used to determine infarct volume. The area of intact tissue on both the ipsilateral and contralateral hemispheres was measured using ImageJ. Infarcted tissue was identified as tissue in which NeuN staining became non-specific (no longer localised to within the nucleus) or notably decreased. Previous studies using NeuN staining to identify infarcted tissue have used the same criteria, with accurate delineation of infarct borders possible as soon as 6h post-ischemia (Liu et al., 2009). It is important to note that at the earliest timepoints in this study, a reduction in NeuN staining intensity may not necessarily be indicative of neuronal cell loss as previous research has found that ischemia can cause a transient reduction in antigenicity in neuronal cells destined to survive (Ünal-Çevik et al., 2004), although this is not likely to be an issue in the later timepoints used in this study.

The calculated area of intact tissue for the ipsilateral hemisphere was subtracted from that for the contralateral hemisphere to create an indirect measure of the infarct which accounted for both oedema in the first few days post-MCAO and atrophy at 28 days post-MCAO. These

areas were then multiplied by the section thickness (40µm) and the number of sections in a series (12) to calculate the infarct volume. Infarct volumes are presented as a percentage of the volume of the contralateral hemisphere.

2.2.6: Statistical Analysis

Data is presented as mean ± standard deviation (SD). Statistical analysis was performed using GraphPad Prism 7. Naïve and Sham groups were combined for all analyses into the "Controls" group due to the similar results obtained by both (see Appendix A1). D'Agostino normality test revealed that all data was not normally distributed; therefore, the Kruskal-Wallis test was used to detect differences between groups. Dunn's multiple comparisons test was used to perform post-hoc analysis and compare groups. For correlational analysis, Spearman's rank correlation coefficient was utilised. Differences were considered significant if $p \leq 0.05$.

2.3: Results

2.3.1: Review of fluorescent staining quality

2.3.1.1: 5mC, 5hmC + 5caC

Antibodies were used to stain mouse brain tissue for the quantification of 5mC, 5hmC and 5caC in various cell types. Considering that these antibodies were being used to quantify levels of (hydroxy)methylation, the quality of staining needed to be of a high standard (ie. localised to the nucleus, with low background staining and consistent across brain areas).

Figure 2.3 shows example images of the quality of staining obtained by using the antibodies targeting 5mC, 5hmC and 5caC. It can be seen that the quality of 5mC staining is not of a high standard, as some areas of the brain appear to stain well (low background fluorescence) whereas other brain areas within the same section appear to have high background, even with sections having undergone antigen retrieval. Staining for 5hmC appears to be of much higher quality, with low background fluorescence and consistent quality staining across the section. Confocal microscopy also reveals that the staining is localised to the nucleus (Figure 2.3). Similarly, staining for 5caC is consistent across the brain, albeit with moderate background fluorescence. However, confocal microscopy reveals that the staining is not localised to the nucleus, instead having appeared to stain around the nucleus. This is not consistent with other research that has immunohistochemically detected 5caC in neural and glial cells (Abakir et al., 2016; Wheldon et al., 2014). Considering this, it was concluded that the staining of 5mC and 5caC was not of a high enough quality to reliably use for quantification. Numerous modifications to the protocol (including antigen retrieval, various blocking buffers, and various antibody concentrations) were attempted, though staining quality did not improve. Therefore, only immunohistochemical staining of 5hmC was used for subsequent analysis.

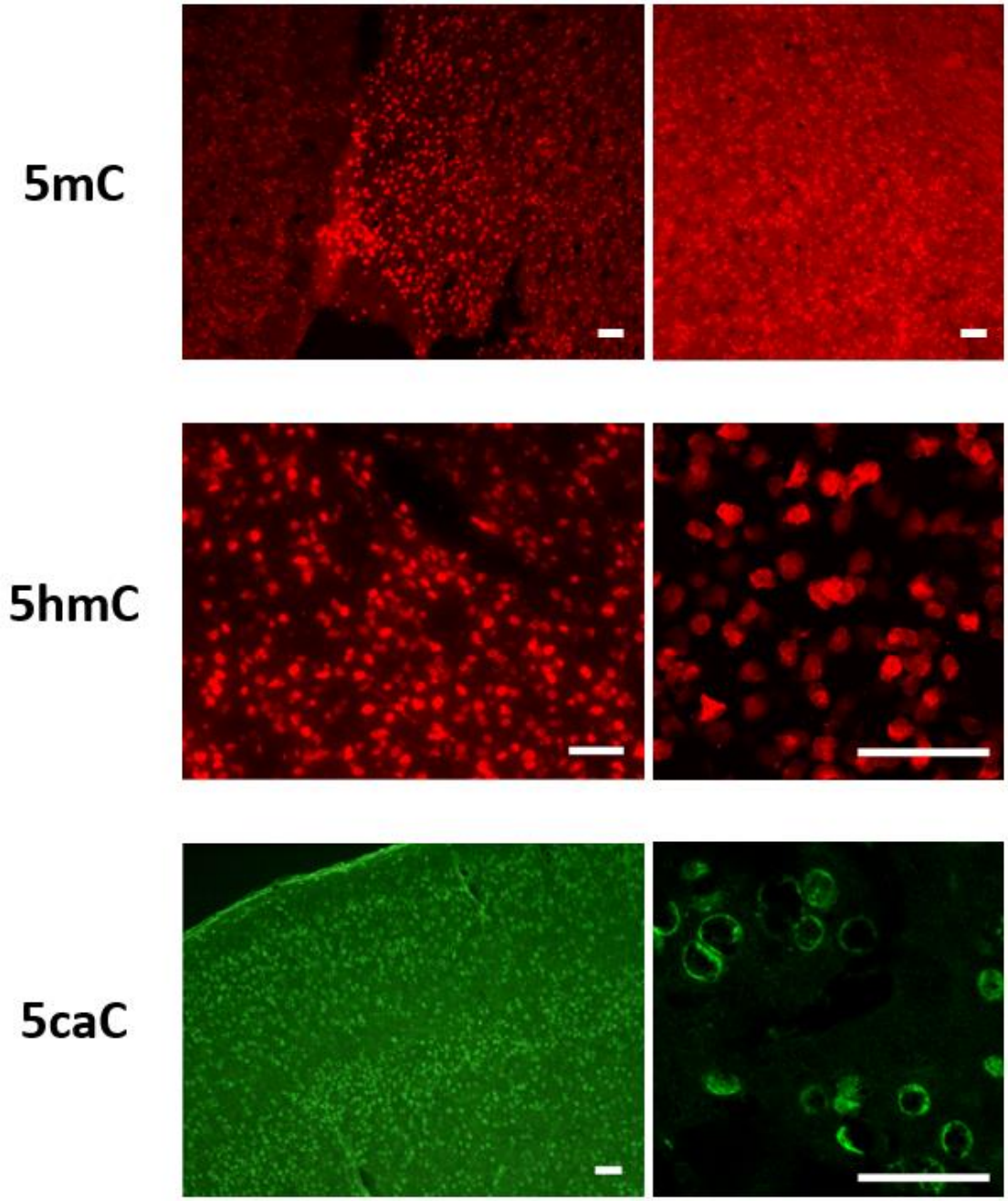


Figure 2.3: Example images of 5mC, 5hmC + 5caC immunohistochemical staining
Primary antibodies targeting 5mC, 5hmC and 5caC were used in conjunction with fluorescent secondary antibodies for immunohistochemical detection in mouse brain tissue. Quality of 5mC staining is inconsistent, as some brain areas stained well with low background fluorescence (*top left*), whereas other brain areas within the same sections exhibited high levels of background fluorescence (*top right*). 5hmC staining is of much higher quality, with low background fluorescence (*middle left*) and staining localised to the nucleus (*middle right*). 5caC staining was also consistent across brain areas, albeit with high background fluorescence (*bottom left*) and confocal microscopy revealed that staining was not localised to within the nucleus (*bottom right*). Scale bar = 50µm in each image.

2.3.1.2: Iba1, TH + NeuN

In order to quantify 5hmC levels in various cell types, mouse brain tissue sections were co-stained with 5hmC antibodies and antibodies targeting various cell types: microglia (anti-Iba1); neurons (anti-NeuN); and dopaminergic neurons (anti-tyrosine hydroxylase; TH).

Figure 2.4 shows example images of the quality of staining of each of these antibodies. It can be seen that although the Iba1 antibody appears to have successfully stained microglia, there appears to be no cells that are positively stained for both Iba1 and 5hmC. Therefore 5hmC content of microglia was not analysed.

Dopaminergic neurons of the substantia nigra pars compacta were stained using an antibody targeting tyrosine hydroxylase (TH), with staining appearing to work well with many cells positively staining for both TH and 5hmC (Figure 2.4). 5hmC content of these dopaminergic neurons was therefore subsequently analysed.

Neurons of the cortex and striatum were stained using an antibody targeting NeuN, a nuclear neuronal protein. However, the staining produced with this antibody was not of a high quality, with low fluorescent intensity compared to background (Figure 2.4). Though numerous attempts were made to improve staining quality (including antigen retrieval, use of different blocking buffers, increasing antibody concentration), these proved unsuccessful. This therefore makes it difficult to accurately determine positively stained cells and as such, the 5hmC content of NeuN+ cells was not analysed.

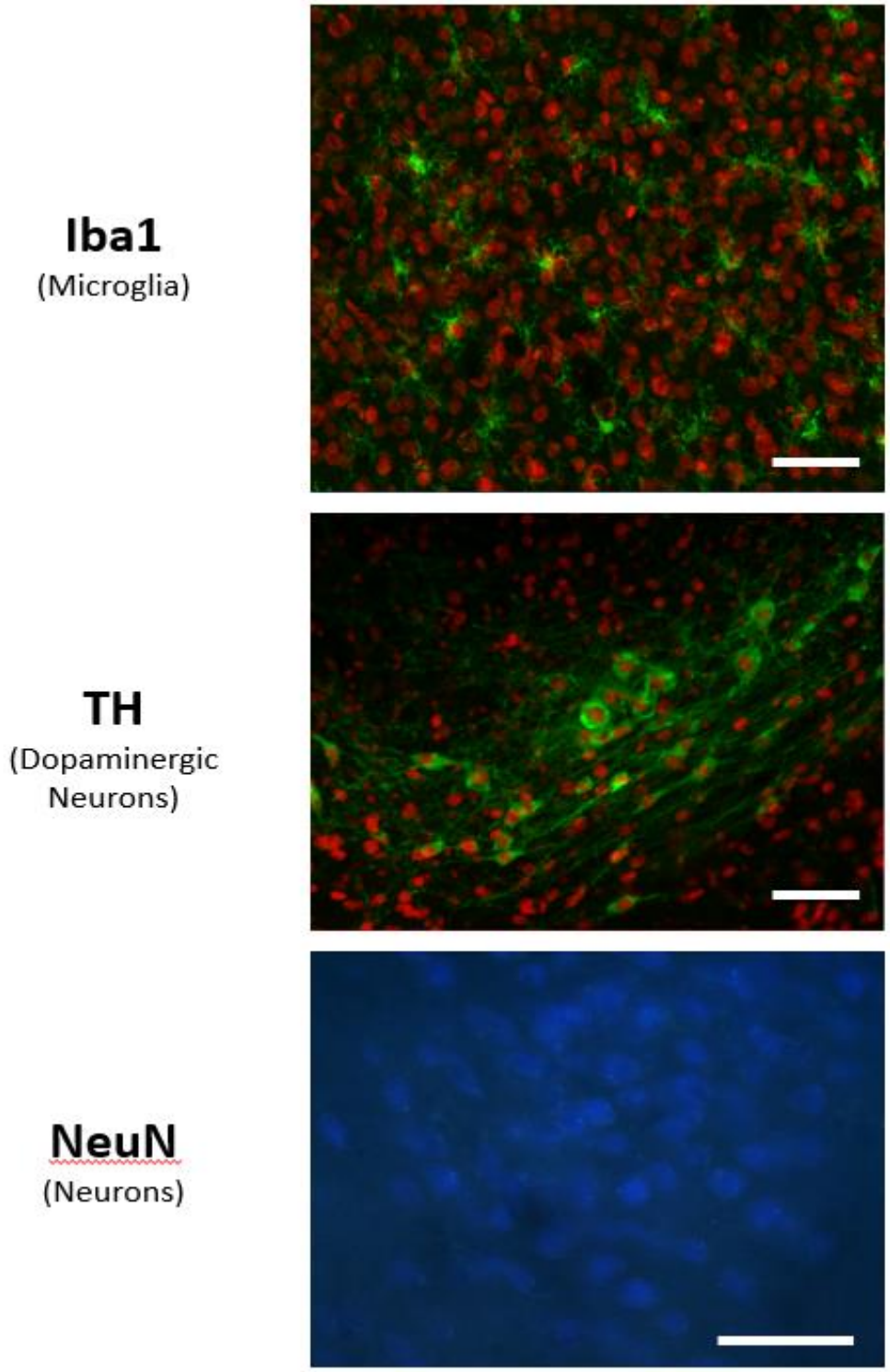


Figure 2.4: Staining of various cell types
Antibodies targeting Iba1, TH and NeuN were used to stain for microglia, dopaminergic neurons and NeuN+ neurons, respectively, in mouse brain tissue. *Top*: Microglia were positively stained for Iba1 (green), though no microglia were also positively stained for 5hmC (red). *Middle*: Dopaminergic neurons were positively stained for TH (green), with TH+ cells also positively stained for 5hmC (red). *Bottom*: Cells were stained with antibodies targeting NeuN, though fluorescent intensity of positively stained cells (blue) was low in comparison to background. Scale bar = 50µm in each image.

2.3.2: Post-stroke 5hmC levels in the cortex

Brains of mice that were euthanised at different time points following MCAO surgery were stained for 5hmC using immunohistochemistry and analysed for fluorescent intensity as an indirect measure of 5hmC levels. Infarct borders were determined by analysis of NeuN staining on adjacent brain sections and infarcted and non-infarcted areas were analysed separately (Figure 2.5) (*NB: As the NeuN antibody used for this infarct delineation is separate from that which was shown to fail in Figure 2.4, this NeuN staining was successful and deemed of high enough quality to delineate infarct borders*).

In infarcted tissue, there was no significant difference in 5hmC levels between all time points (Figure 2.6A; Kruskal-Wallis=2.63; p=0.62). In non-infarcted tissue, there was a significant increase in 5hmC levels between groups (Figure 2.6B; Kruskal Wallis=14.57; p=0.006). Post hoc analysis reveals that this significant difference is due to a significant increase in 5hmC levels at 48h post-stroke in comparison to controls (p=0.002).

2.3.3: Post-stroke 5hmC levels in the striatum

In the striatum, a significant difference in 5hmC levels between groups was found only in the non-infarcted tissue (Figure 2.7; infarcted: Kruskal-Wallis=9.37; p=0.053; non-infarcted: Kruskal-Wallis=19.48; p<0.001), driven by a significant increase in 5hmC levels at 7 days post-stroke in comparison to controls (p=0.002).

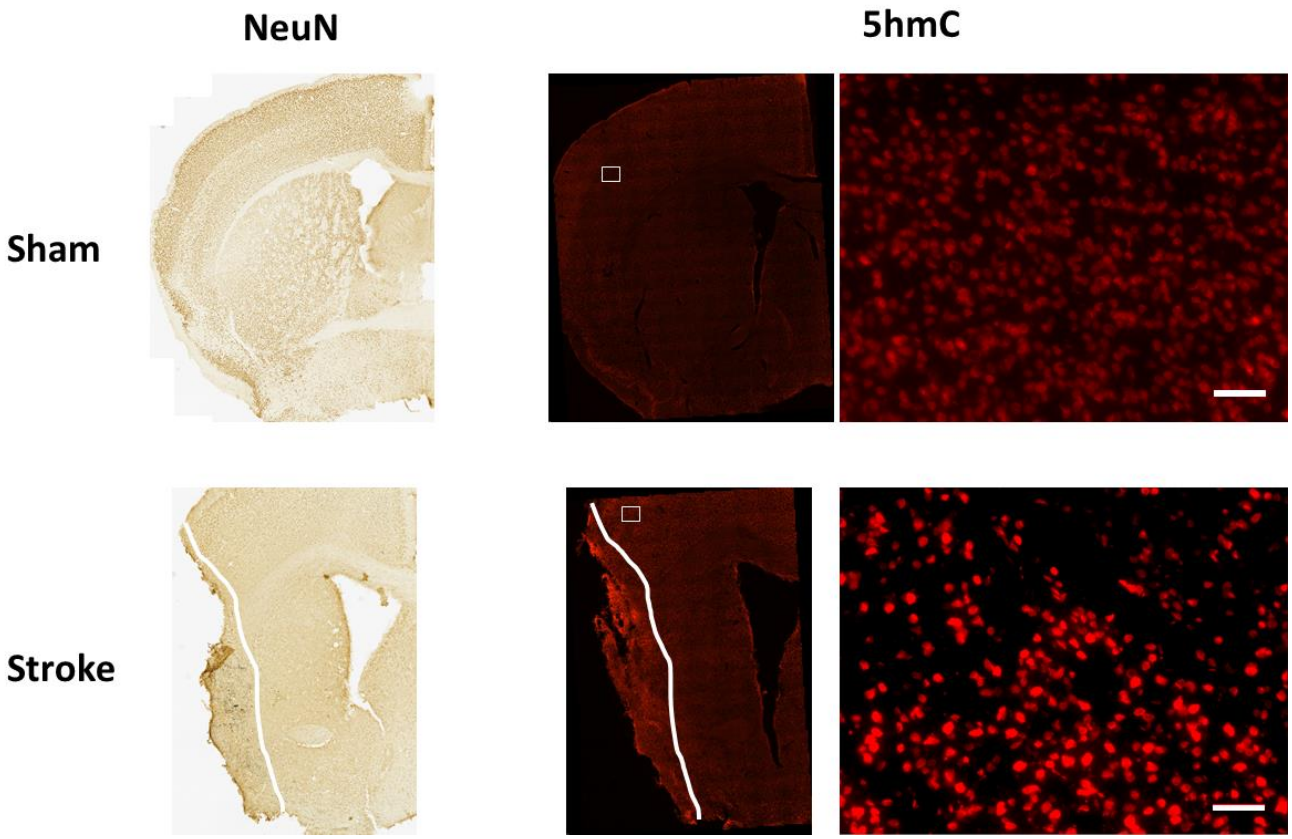


Figure 2.5: Immunohistochemical staining for NeuN + 5hmC in mouse tissue
The brains of mice that underwent transient MCAO (*bottom*) or control mice that underwent sham surgery or no surgery at all (*top*) were sectioned and then stained for 5hmC using immunohistochemistry. Adjacent sections were stained for NeuN (*left*) in order to determine infarct borders (*infarct border shown in white*). Sections stained for 5hmC were imaged at x20 magnification and images were stitched together to form a view of the entire infarcted hemisphere. From these images, the intensity of 5hmC staining in the infarcted cortex & striatum and non-infarcted cortex & striatum were analysed. Scale bar = 50µm in each image.

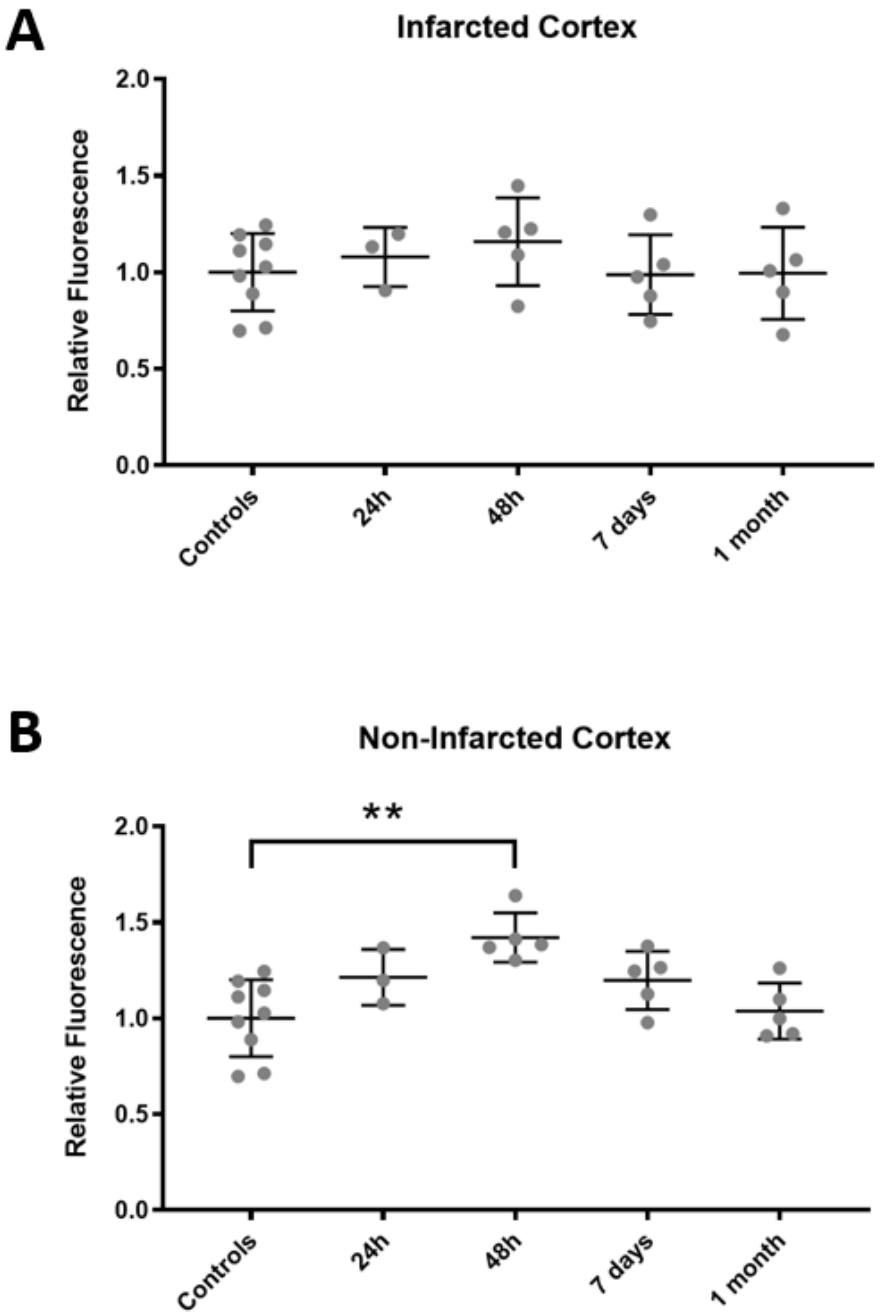


Figure 2.6: Timeline of post-stroke cortical 5hmC levels
Male C57BL/6 mice underwent 30 minutes MCAO and were euthanised 24h (n=4), 48h (n=5), 7 days (n=5) or 1 month (n=5) later. Controls included mice that underwent a sham surgery (n=4) or no surgery (n=5). Relative levels of 5hmC were analysed in the infarcted (**A**) and non-infarcted (**B**) cortex of the infarcted hemisphere. **A**: In infarcted cortical tissue, there was no significant difference in 5hmC levels between groups (p=0.62). **B**: In non-infarcted cortical tissue, there was a significant increase in 5hmC levels post-stroke, with a peak at 48 hours post-stroke (p=0.002). Data presented as mean ± SD. ** represents a significant difference (p<0.01) in post-hoc analysis.

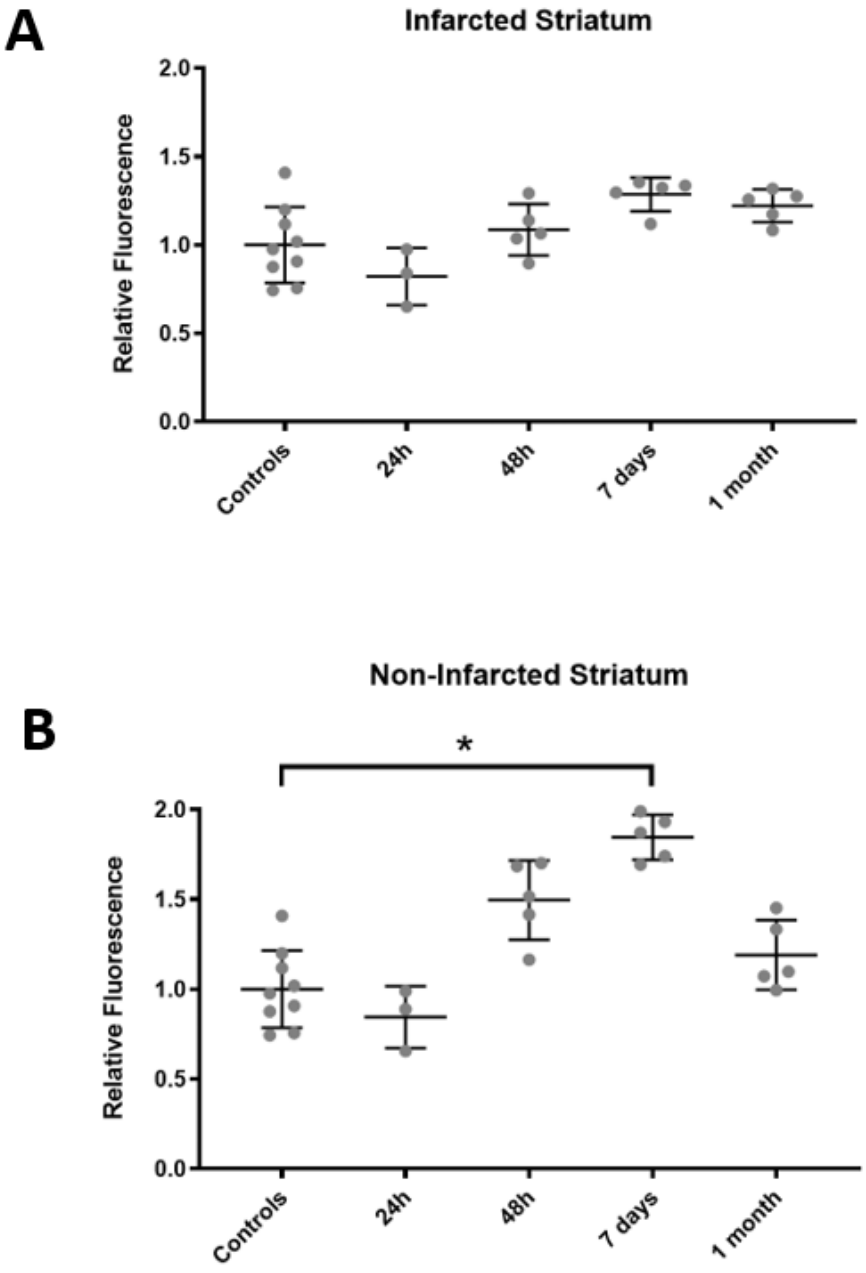


Figure 2.7: Timeline of post-stroke striatal 5hmC levels
Male C57BL/6 mice underwent 30 minutes MCAO and were euthanised 24h (n=4), 48h (n=5), 7 days (n=5) or 1 month (n=5) later. Controls included mice that underwent a sham surgery (n=4) or no surgery (n=5). Relative levels of 5hmC were analysed in the infarcted and non-infarcted striatum of the infarcted hemisphere. **A**: In infarcted striatal tissue, there was no significant difference in 5hmC levels between groups (p=0.053). **B**: In non-infarcted striatal tissue, there was a significant increase in post-stroke 5hmC levels, with a peak at 7 days post-stroke (p=0.002). Data presented as mean ± SD. * represents a significant difference (p<0.05) in post-hoc analysis.

2.3.4: Post-stroke 5hmC levels in the substantia nigra pars compacta

The brains of mice that underwent transient MCAO were immunohistochemically co-stained for tyrosine hydroxylase and 5hmC. The intensity of 5hmC staining in TH+ (dopaminergic) cells of the substantia nigra was analysed as an indirect measure of 5hmC levels. In these cells, there was a significant difference in the relative 5hmC levels between groups (Figure 2.8; Kruskal-Wallis=10.0; p=0.04). Post-hoc analysis reveals that this significant difference is driven by a significant increase in 5hmC levels at 7 days post-stroke (p=0.01). Representative images of each group are shown in Figure 2.9.

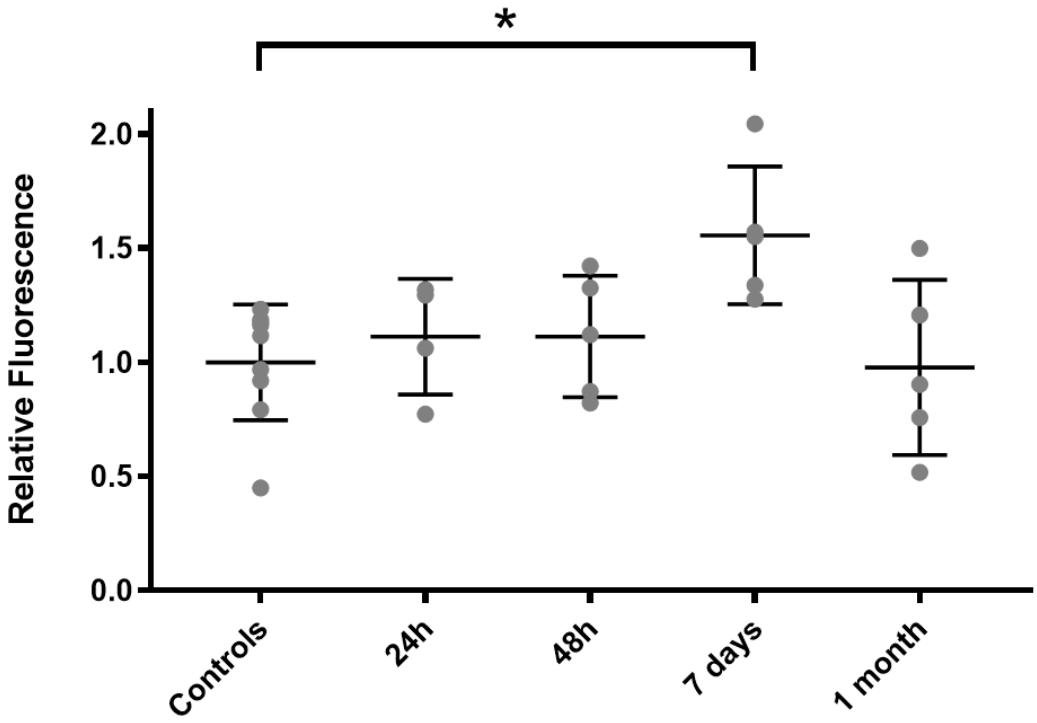


Figure 2.8: Post-stroke 5hmC levels of dopaminergic cells in the substantia nigra pars compacta
Male C57BL/6 mice underwent 30 minutes MCAO and were euthanised 24h (n=4), 48h (n=5), 7 days (n=5) or 1 month (n=5) later. Controls included mice that underwent a sham surgery (n=4) or no surgery (n=5). Relative levels of 5hmC were analysed in dopaminergic (TH+) cells of the substantia nigra pars compacta. In these cells, there was a significant increase in 5hmC levels post-stroke, with a peak at 7 days post-stroke (p=0.01). Data presented as mean ± SD. * represents a significant difference (p<0.05) in post-hoc analysis.

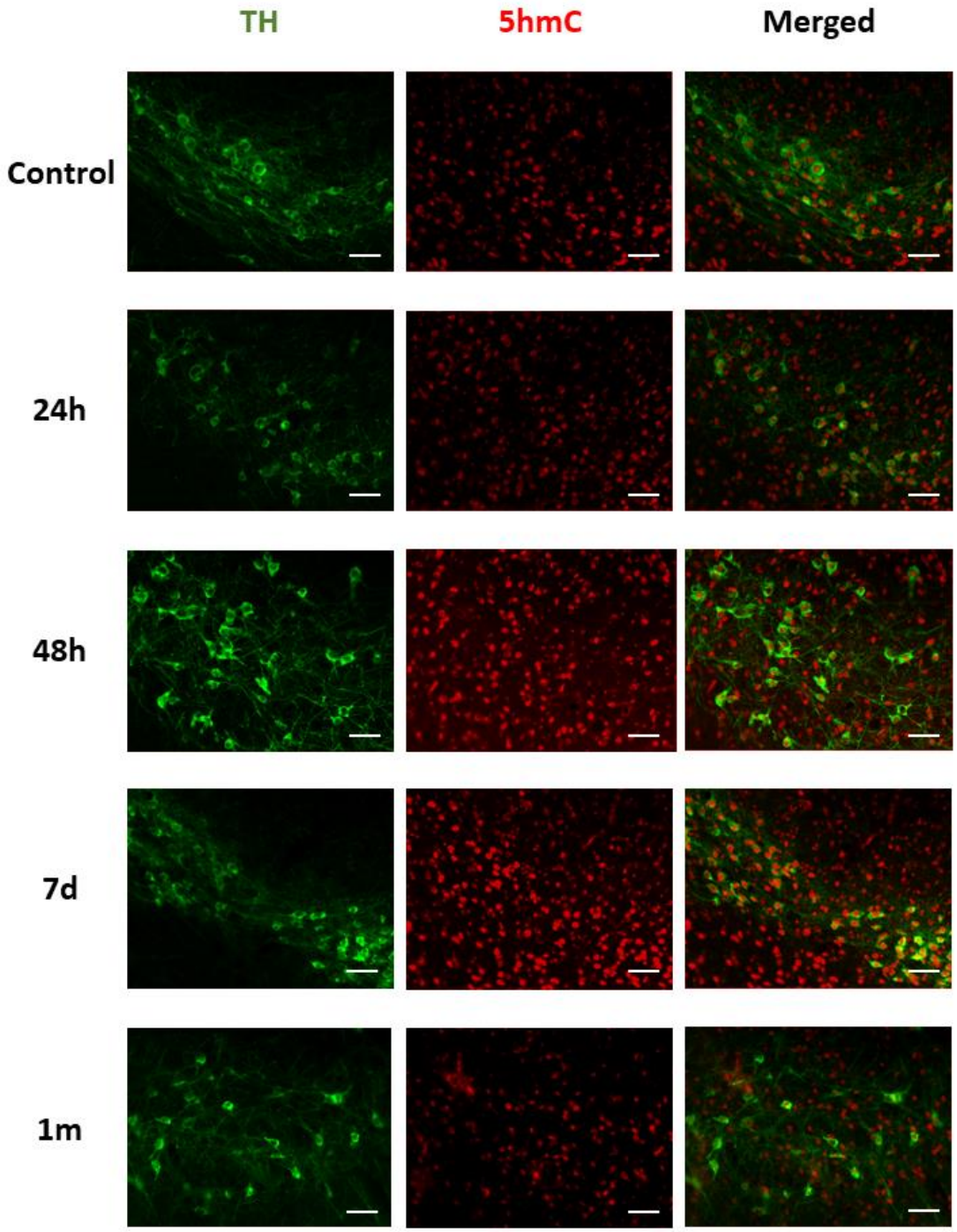


Figure 2.9: Immunohistochemical detection of TH and 5hmC
Brain sections from mice that underwent MCAO surgery and were culled at various timepoints post-surgery (24 hours, 48 hours, 7 days and 1 month) were immunohistochemically stained with antibodies to detect tyrosine hydroxylase (green) or 5hmC (red). Control animals that underwent either a sham surgery or no surgery were also included (this figure represents a sham surgery animal) . From these images, the intensity of 5hmC staining within TH+ cells was analysed, as well as total number of TH+ cells. Scale bar = 50µm in each image.

2.3.5: Loss of dopaminergic cells in substantia nigra

The number of TH+ cells in the substantia nigra pars compacta of mice that were euthanised at various time points following MCAO was counted following immunohistochemical staining of brain sections. Statistical analysis revealed that there were differences in cell count between groups (Figure 2.10; Kruskal-Wallis =10.5; p=0.03), with post-hoc analysis revealing that this difference is driven by a significant decrease in cell count at 1 month post-stroke in comparison to controls (p=0.03). Representative images of each group are shown in Figure 2.9.

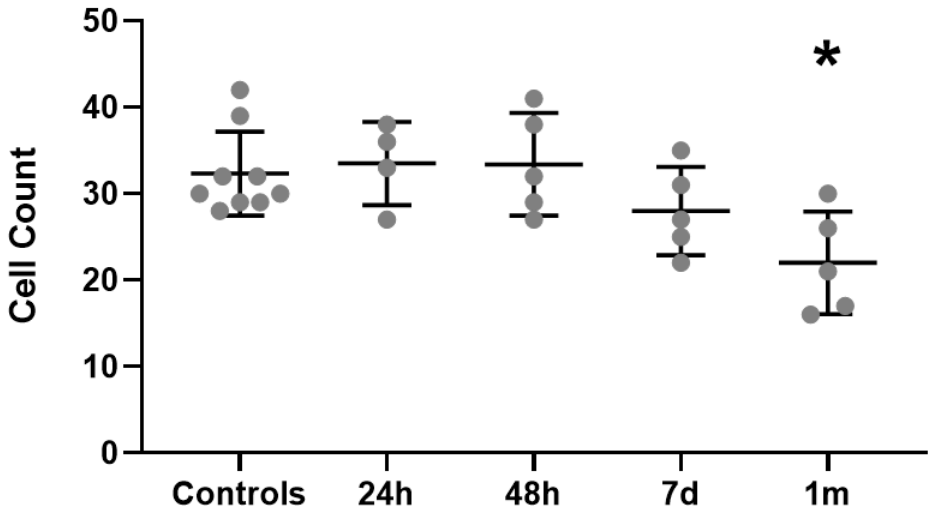


Figure 2.10: Count of TH+ cells of substantia nigra pars compacta following MCAO
Male C57BL/6 mice underwent 30 minutes MCAO and were euthanised 24h (n=4), 48h (n=5), 7 days (n=5) or 1 month (n=5) later. Controls included mice that underwent a sham surgery (n=4) or no surgery (n=5). The number of cells that positively stained for TH were counted in the substantia nigra pars compacta of these brains at bregma point ~-3.08. In the substantia nigra pars compacta, there was a significant decrease in the number of TH+ cells at 1 month following MCAO (p=0.03). Data presented as mean ± SD. * represents a significant difference ($p<0.05$) in comparison to controls in post-hoc analysis.

2.3.6: Correlations between infarct size and 5hmC levels

The infarct volumes of brain sections obtained from mice that were euthanised following 30 minute MCAO were calculated as a percentage volume of the contralateral hemisphere. These volumes were correlated with the relative 5hmC levels of non-infarcted cortical and striatal tissue of the ipsilateral hemisphere. No significant correlational relationship was found between infarct volume and 5hmC levels of the striatum (Figure 2.11; Spearman's r=0.07; p=0.77) or substantia nigra (Figure 2.11; Spearman's r=0.02; p=0.95). Although a slight correlation between infarct volume and cortical 5hmC levels appears to be present, this was not found to be significant (Figure 2.11; Spearman's r=0.50; p=0.06).

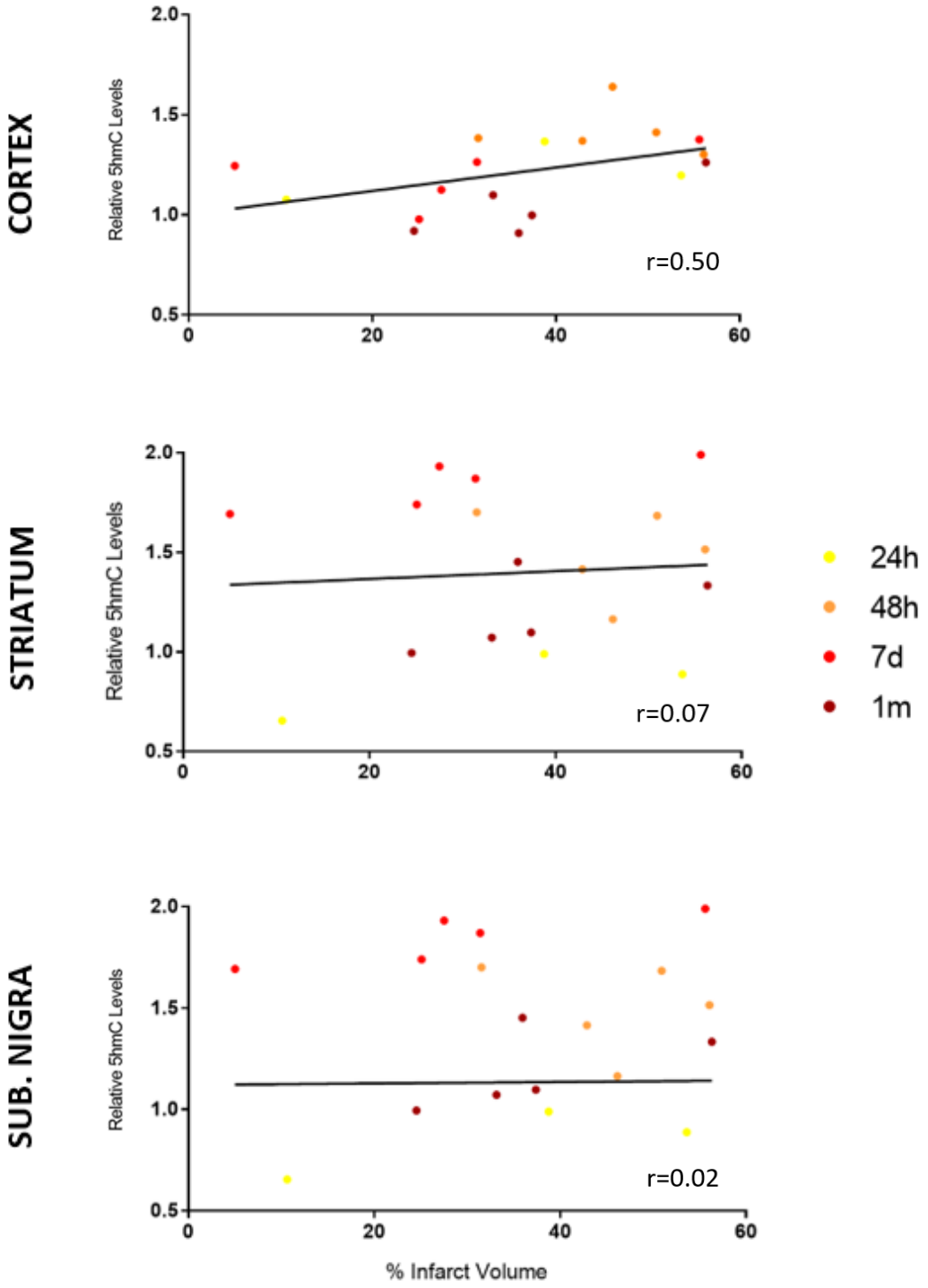


Figure 2.11: Correlation between infarct volume and 5hmC level in various brain areas
Infarct volumes of brains obtained from mice that underwent transient MCAO were calculated as % volume of contralateral hemisphere. These volumes were then correlated with relative 5hmC levels in non-infarcted cortical and striatal tissue. No significant correlation was found between infarct volume and striatal (Spearman's r=0.07; p=0.77), cortical (Spearman's r=0.50; p=0.06) or nigral (Spearman's r=0.02; p=0.95) 5hmC levels.

2.3.7: 5hmC levels in the medial geniculate nucleus

Using immunohistochemistry, relative 5hmC levels within the medial geniculate nucleus (MGN; a brain area not known to be directly or indirectly affected by MCAO) of mice that underwent transient MCAO was analysed at various time points post-stroke. In the MGN, no significant differences in 5hmC levels were observed between groups (Figure 2.12; Kruskal-Wallis=3.33; p=0.50). Representative images of each timepoint are shown in Figure 2.13.

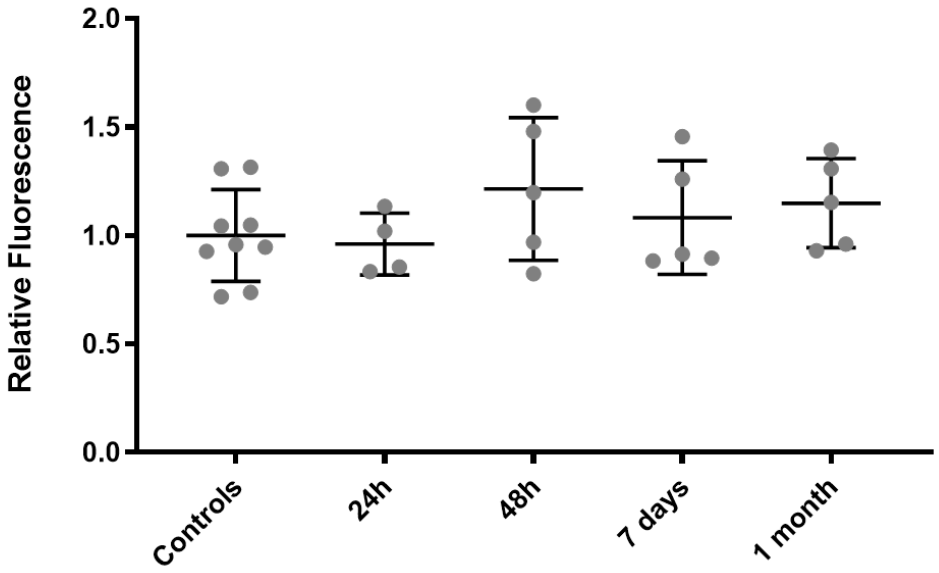


Figure 2.12: Post-stroke 5hmC levels of the medial geniculate nucleus
Male C57BL/6 mice underwent 30 minutes MCAO and were euthanised 24h (n=4), 48h (n=5), 7 days (n=5) or 1 month (n=5) later. Controls included mice that underwent a sham surgery (n=4) or no surgery (n=5). Relative levels of 5hmC were analysed in the medial geniculate nucleus (MGN). No significant difference in relative 5hmC levels was found between groups (p=0.50). Data presented as mean ± SD.

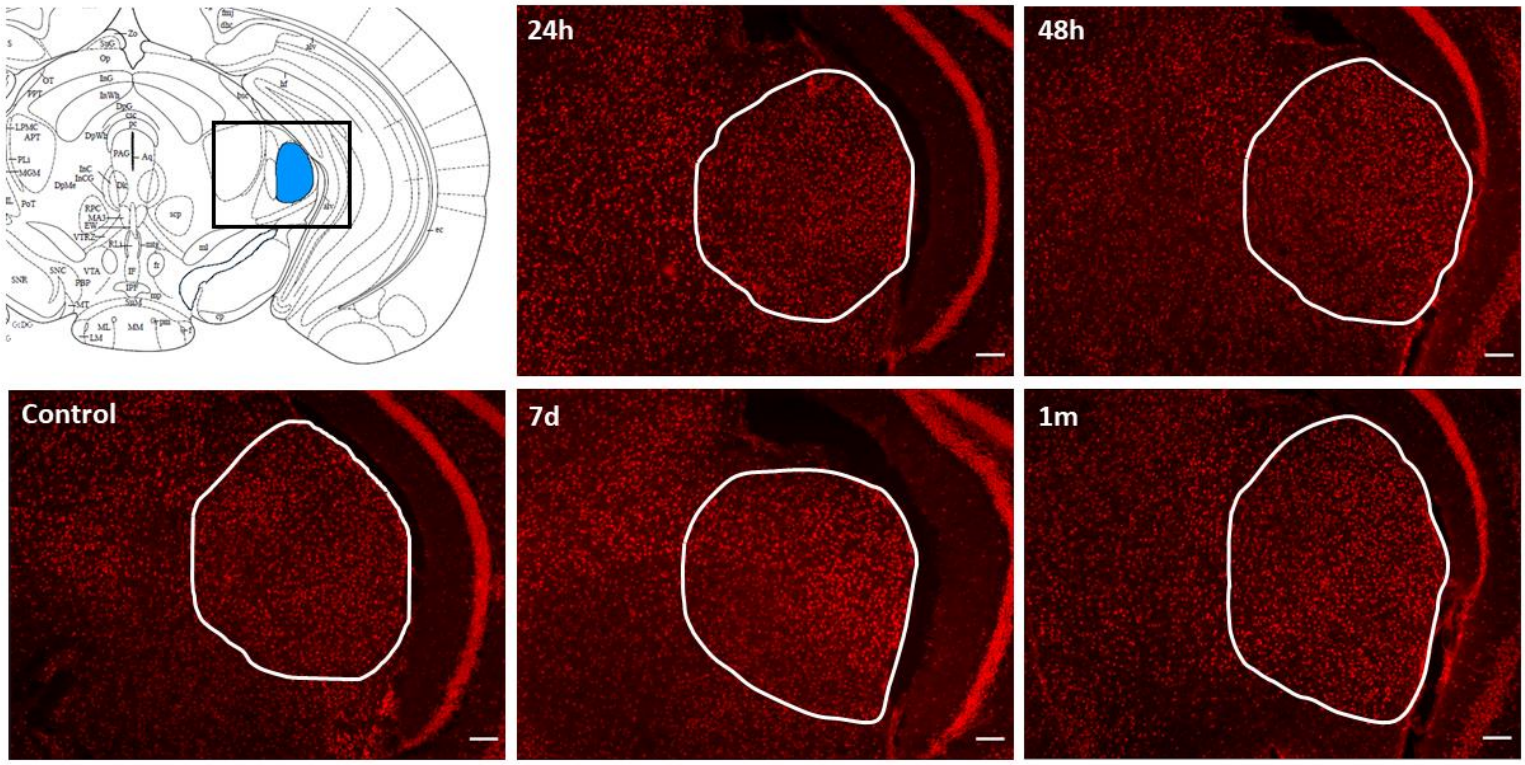


Figure 2.13: Immunohistochemical detection of 5hmC in MGN

Mice that underwent MCAO surgery, or control mice that underwent sham surgery or no surgery, were culled at various time points post-surgery (24 hours, 48 hours, 7 days or 1 month) and their brains sections and immunohistochemically stained for 5hmC. These images were used to analyse intensity of 5hmC staining in the medial geniculate nucleus (MGN); outlined in white. Sections from bregma point ~3.08 were stained; atlas image shows field of view in black box, and medial geniculate nucleus in blue. Scale bar = 200µm in each image. Atlas image adapted from Paxinos & Franklin (2001).

2.4: Discussion

The aim of this chapter was to determine the timeline of changes in global (hydroxy)methylation levels in the brain following ischemic stroke, and to determine if these changes vary between different brain regions that are affected by ischemic stroke. Through use of immunohistochemistry to determine relative 5hmC levels, it was determined that 5hmC levels appear to increase in areas of the brain that are affected by ischemic stroke either directly or indirectly.

Previous research focusing on the role of 5hmC in the pathophysiology of ischemic stroke is extremely limited. Miao et al. (2015) were the first to determine that global 5hmC levels are increased in brain tissue following ischemic stroke, although these changes were determined by analysing the infarcted hemisphere as a whole and did not consider differences between brain regions or infarcted and non-infarcted tissue. This study also failed to assess long term changes in post-stroke 5hmC expression as the latest post-stroke time point analysed was 7 days. Similarly, Morris-Blanco et al. (2019) determined significantly increased 5hmC levels post-stroke, peaking at 12-24h, but were limited by not investigating beyond the 24h timepoint. Using immunohistochemistry, this chapter has analysed post-stroke 5hmC levels in distinct brain areas directly (cortex and striatum) and indirectly (substantia nigra pars compacta) affected by stroke up to 1 month following the ischemic event.

In the cortex, a significant increase in post-stroke 5hmC levels was found in non-infarcted tissue, but not in infarcted tissue (Figure 2.6). In the non-infarcted cortex, there appears to be a slight increase in global 5hmC at 24h and 7 days post-stroke, although the only significant increase is found at 48h post-stroke, when the global 5hmC level peaks. Similarly, changes to global 5hmC levels in the striatum were found only in the non-infarcted tissue (Figure 2.7). However, in this brain region, global 5hmC levels peaked at 7 days post-stroke. In both brain

regions, the global levels of 5hmC appear to have returned to the baseline levels of the controls by 1 month post-stroke. These timelines of post-stroke 5hmC levels match the only available comparable data that is available in the literature (Miao et al., 2015; Morris-Blanco et al., 2019), in which it was determined that global 5hmC levels in the entire infarcted hemisphere significantly increase post-stroke, with a peak at 12-48 hours post-stroke.

In addition to analysing post-stroke 5hmC levels, Miao et al. (2015) also determined a timeline in the levels of post-stroke 5mC, with increased levels found following MCAO with a peak at 24-36 hours post-stroke. Given that this peak in 5mC levels occurs slightly before the observed peak in global 5hmC, this seems to elucidate a timeline of post-stroke methylome changes in which global 5mC is increased in response to the ischemic event, followed by global demethylation, presenting as an increase in global 5hmC. By 7 days – 1 month post-stroke, 5hmC levels return to baseline, suggesting that the methylome has returned to normal. This suggested timeline is further evidenced by research carried out by Lindner et al. (2014) which determined that global methylation is significantly increased at 24 hours following sciatic nerve ligation, but is then significantly decreased at 7 days post-injury. Whilst this research does not consider 5hmC levels, and attempts at determining levels of 5mC in this study failed (Figure 2.3), this timeline of post-injury methylome changes would appear to fit in with the changes in 5hmC levels observed in this current study. Although the study carried out by Lindner et al. (2014) focused on peripheral nerve injury and not ischemic stroke, taken together with data from this study it would seem to suggest an endogenous response of the nervous system to axonal injury that involves immediate global hypermethylation followed by 5hmC-mediated demethylation, perhaps as a means of priming axon-growth related genes for expression.

Further evidence for the theory that increased 5hmC levels are indicative of demethylation leading to increased gene expression comes from the fact that the significant increase in 5hmC levels in the cortex slightly precedes previously determined peak expression of axon-growth related genes in the peri-infarct cortex (Carmichael et al., 2005). The occurrence of peak 5hmC expression in the peri-infarct cortex (at 48h) slightly prior to peak axon-growth related gene expression (at 3-28 days post-stroke) could suggest that the peak in global 5hmC levels is indicative of mass genomic demethylation that leads to the observed increase in axon-growth related genes in the following days. These altered patterns of gene expression lead to increased neuronal excitability, which facilitates axonal growth and rewiring of injured tissue (Carmichael & Chesselet, 2002), thereby suggesting that global demethylation via oxidisation of 5mC may play a role in the control of post-stroke neuronal plasticity. This evidence cannot, however, be used to conclude that a causal relationship exists; further research is needed to determine if global demethylation influences post-stroke neuronal plasticity.

In addition to assessing changes in global 5hmC in brain areas directly affected by ischemic stroke, this study also analysed the timeline of post-stroke 5hmC levels in dopaminergic cells of the substantia nigra pars compacta; cells which project directly to the striatum as part of the nigrostriatal pathway and have been shown to undergo retrograde degeneration following ischemic damage to the striatum (Tamura et al., 1990). By identifying dopaminergic cells as those that were positively stained for tyrosine hydroxylase (Figure 2.4), the intensity of 5hmC staining in these cells was measured as an indirect measure of global 5hmC levels. It was determined that following ischemic stroke, there is a significant increase in global 5hmC with a peak at 7 days post-stroke (Figure 2.8). Similarly to the cortex and striatum, 5hmC levels appear to have returned to baseline 1 month after the ischemic event.

It is, however, once again not possible to determine the cause of these changes in 5hmC levels in the SNc. It is possible that hypoxic damage to the axon terminals in the striatum triggers an axonal regrowth/repair response, which is thereby reflected by an increase in 5hmC levels as axon-growth related genes undergo demethylation. Alternatively, given that the peak in 5hmC levels coincides with the delayed onset of cell death in the SNc that has been demonstrated in both previous research (Nakajima et al., 2010; Tamura et al., 1990) and this current study (Figure 2.10), it is therefore also possible that the observed increase in 5hmC levels at 7 days post-stroke is secondary to cell death signals occurring. It is important to note that the TH+ cells that are being observed in this study are almost exclusively those which have survived the phenomenon of exfocal post-ischemic neurodegeneration, particularly at the 1 month post-stroke timepoint. Seeing as the surviving cells at this point did not exhibit significantly increased levels of 5hmC (Figure 2.8), this would seem to suggest that the observed increase in 5hmC levels at 7 days may not be related to the regrowth of axons that these cells would be undergoing at this timepoint. Determining the cause of the observed increase in SNc 5hmC levels should be a focus of future research as elucidating this cause could provide a potential therapeutic target for the treatment of exfocal post-ischemic neurodegeneration.

When considering the observed changes in 5hmC levels in dopaminergic neurons of the SNc, it is also important to consider that staining for TH alone does not allow for the absolute distinction of cells that belong to the SNc and the VTA, especially since these two brain areas are situated alongside one another (Figure 2.2). Therefore, it is possible that a number of the TH+ cells analysed in this study were dopaminergic cells of the VTA, and not necessarily nigral cells. However, it is also worth considering that the infarcted areas of striatum more closely align with the projections of the SNc (dorsolateral striatum) as opposed to the VTA (ventromedial striatum) (Figures 2.2 and 2.5). It is therefore likely that the observed results

are due to changes in dopaminergic cells of the SNc, though this cannot be determined for certain until dopaminergic cells of the SNc and VTA are identified absolutely.

Whilst ischemic stroke-induced increases in 5hmC have been determined in three distinct brain areas (cortex, striatum and SNc), with peak levels occurring at similar times, it is important to note that these changes do not appear to be global, as evidenced by the lack of changes to post-stroke 5hmC levels in the MGN (Figure 2.12). The MGN is a brain area that is not directly or indirectly affected by stroke (as it is not directly supplied by the MCA nor does it connect directly to the infarcted cortex or striatum), therefore suggesting that changes to 5hmC levels occur only in brain areas that are affected by the stroke. It can also be concluded that the observed global changes in 5hmC in response to ischemic stroke are not influenced by the severity of the stroke, as evidenced by the fact that there is no correlation between relative global 5hmC levels and infarct size in the cortex, striatum, or substantia nigra (Figure 2.11). It may be of note, however, that correlation between cortical 5hmC levels and infarct volume were close to significance ($p=0.06$) and that post-hoc power analysis indicated that this particular experiment was underpowered (see Appendix A6), therefore suggesting that increasing the number of animals in this experiment may have revealed a significant correlation.

2.4.1: Limitations

Most of the limitations of this study come from the inherent limitations of IHC as a method of determining global 5hmC levels (as discussed in section 2.1.3). For example, the quality and reproducibility of staining using IHC is highly dependent on the preparation of the sample, and this is incredibly important to consider especially when using IHC in a quantitative analysis, as was done in this study. Factors that can affect the staining of tissue, such as

incubation time and amount of fixative used, were accounted for as much as possible in this chapter (eg. all sections were stained at the same time with the same amount of antibody and fixative used for every section).

A further limitation of this study came from the failure to accurately stain for 5mC, 5caC and NeuN. Whilst attempts were made to improve the quality of the staining with each of these antibodies (including attempts at antigen retrieval and changes to antibody dilution & incubation times), high quality staining was not achieved. It is also possible that a lack of sufficient tissue fixation caused the loss of specific staining; in this study, a formulation of 1.5% PFA was used as a fixative, as opposed to the commonly used 4% PFA. This was done in order to minimise the risk of over-fixation. However, it is possible that this created a opposite issue wherein the tissue was underfixed, allowing for the proteolytic degradation of the target antigens and potentially explaining the lack of specific staining. Although it would be extremely informative to determine post-stroke changes in 5mC and 5caC expression and analyse NeuN+ cells specifically, this analysis was not possible using IHC and an alternative method needs to be implemented. Determining these changes through use of an alternative method is an aim of a subsequent chapter of this thesis.

Whilst the limitations of this study are mostly due to the use of IHC, there are several aspects of the experimental design that could be improved also. For example, the experimental design could be improved by analysing more time points post-stroke. This study assessed 5hmC levels at 24h, 28h, 7 days and 1 month post-stroke. Each of the brain areas analysed that showed increased 5hmC levels had peak 5hmC levels at 48h or 7 days post-stroke, with levels returning to baseline after 1 month. Due to the large amount of time between the 48h + 7 day and 7 day + 1 month timepoints, it could be possible that peak 5hmC levels actually occur at a time somewhere between these points, such as 72 hours or 2 weeks. Whilst the addition

of more experimental groups would help further elucidate the timeline of post-stroke 5hmC expression, this would involve the use of more animals, which brings its own monetary and ethical considerations.

2.4.2: Summary

Having used IHC to analyse relative levels of global 5hmC in the brains of mice that have undergone transient MCAO, it has been determined that significant increases in 5hmC levels are observed in the cortex, striatum and SNc following ischemic stroke. These changes in response to ischemic stroke are found only in the non-infarcted tissue and not in the infarct itself, and the temporal profile of these changes is varied between distinct brain regions. Whilst changes in brain areas directly or indirectly affected by stroke were determined, it can be concluded that this change does not occur throughout the entire brain due to the fact that no changes to 5hmC levels were observed in the MGN, a brain area not (in)directly affected by stroke. Although these timelines of post-stroke 5hmC levels in various brain regions may be indicative of potential global demethylation and subsequent neuronal plasticity, more research is needed to determine a causal effect. Also, inefficient staining of cell type markers means that changes in 5hmC content of specific cell types was not determined. Determining cell type-specific changes in 5hmC and a direct causal relationship with axon growth are aims of subsequent chapters in this thesis.

Chapter 3: Developing a method of isolating neurons & microglia from ischemic rat brain

3.1: Introduction

Chapter 2 of this thesis has identified an intrinsic response of the central nervous system to ischemic stroke that involves a delayed but significant increase in 5hmC levels in various brain areas affected. However, it has also identified the importance of analysing this effect in different cell types, as data gathered in Chapter 2 assessed 5hmC levels across all cells of the brain with no consideration of cell type. Determining if this epigenetic response to ischemic stroke is varied across different cell types is important as it will not only further elucidate the role that oxidative demethylation plays in the pathophysiology of ischemic stroke but could also help to identify a therapeutic target for possible post-stroke treatment. Determining these differences between cell types is an aim of Chapter 4 of this thesis, with the current chapter covering the stages of development of a method for isolating various cell types from the post-ischemic rat brain for use in Chapter 4.

3.1.1: Methods of cell isolation

When planning to isolate various cell types from a culture of cells or a tissue sample, there are a number of available methods which can be considered. The most common and widely used methods of cell isolation are density gradient centrifugation, magnetic cell isolation and fluorescence-activated cell sorting (FACS). Each of these protocols requires the input of a heterogeneous single cell suspension but differ in their methods of isolating specific cell types.

Density gradient centrifugation involves layering the heterogenous suspension atop a density gradient medium and centrifuging at a specific speed for a set amount of time. Following centrifugation, cells will have settled at their isopycnic point, which is the point at which the density of the cell and the density of the medium are equal. With more elaborate density gradient setups, various different cell types can be isolated from one heterogeneous sample as long as their densities are not too similar. Whilst density gradient centrifugation is relatively simple and inexpensive, the method has limited specificity which results in low purity and is unable to separate cell types of similar densities.

An alternative method of cell type isolation from a heterogeneous suspension is magnetic cell isolation. This process involves adding antibodies to the cell suspension which are conjugated to magnetic particles. The cells to which the antibody has attached are then separated from the rest of the suspension by passing the solution through a magnetic column. This column captures the cells attached to the magnetic particles, which can then be flushed out of the column (Miltenyi et al., 1990). Given that this process involves the use of antibodies that target specific antigens, this method is highly specific and gives much higher purity populations in comparison to density gradient centrifugation. The speed and specificity of magnetic cell separation makes it a widely used method of cell isolation, however limitations of the method include being unable to sort multiple cell types simultaneously; being unable to sort complex cells with multiple markers; and also being unable to sort cells based on their relative levels of expression of a single marker. A method of cell isolation that addresses the limitations of magnetic cell isolation is FACS, which utilises the process of flow cytometry.

3.1.2: Flow cytometry & FACS

Flow cytometry is a widely used laser-based technology that can analyse the characteristics of a population of cells on a cell-by-cell basis. When the cell population has been probed with fluorescent antibodies, or otherwise fluorescently stained, it is possible to use flow cytometry to separate these cells into distinct populations based on their fluorescent profile. This process is known as fluorescence-activated cell sorting (FACS) and was first developed in the early 1970s (Herzenberg et al., 1976).

The process of FACS begins much like density gradient centrifugation and magnetic cell sorting, with the production of a heterogeneous single-cell suspension. Similarly to magnetic cell isolation, cells are then probed with antibodies, although in FACS the antibodies are conjugated to a fluorophore as opposed to a magnetic particle. Additionally, fluorescent cellular dyes such as propidium iodide or Hoechst 33342 can be utilised. Following fluorescent labelling, the cell suspension is then loaded into a flow cytometer. Once in the flow cytometer, the cell suspension is hydrodynamically focused using sheath fluid, such that the cells pass through a small nozzle in a 'single file' stream. Once focused into this stream, the cells pass one-by-one through an excitation laser that excites the cell-bound fluorophores, thereby causing light-scattering and fluorescent emissions. Numerous detectors record these signals, including forward- and side-scatter of the light as well as the fluorescent intensity of the cell across various wavelengths. Once passed through the laser, the stream passes through a vibrating mechanism that breaks it into individual droplets. The equipment is set up so that there is a low probability of more than one cell being present in each droplet. Based on the wavelengths of the emitted light signals, the droplet that is formed around the individual cell is assigned a charge. The droplets then pass through charged deflector plates, which cause the droplets to be deflected into a designated collection tube or into a waste chamber. A schematic detailing the process of FACS is shown in Figure 3.1.

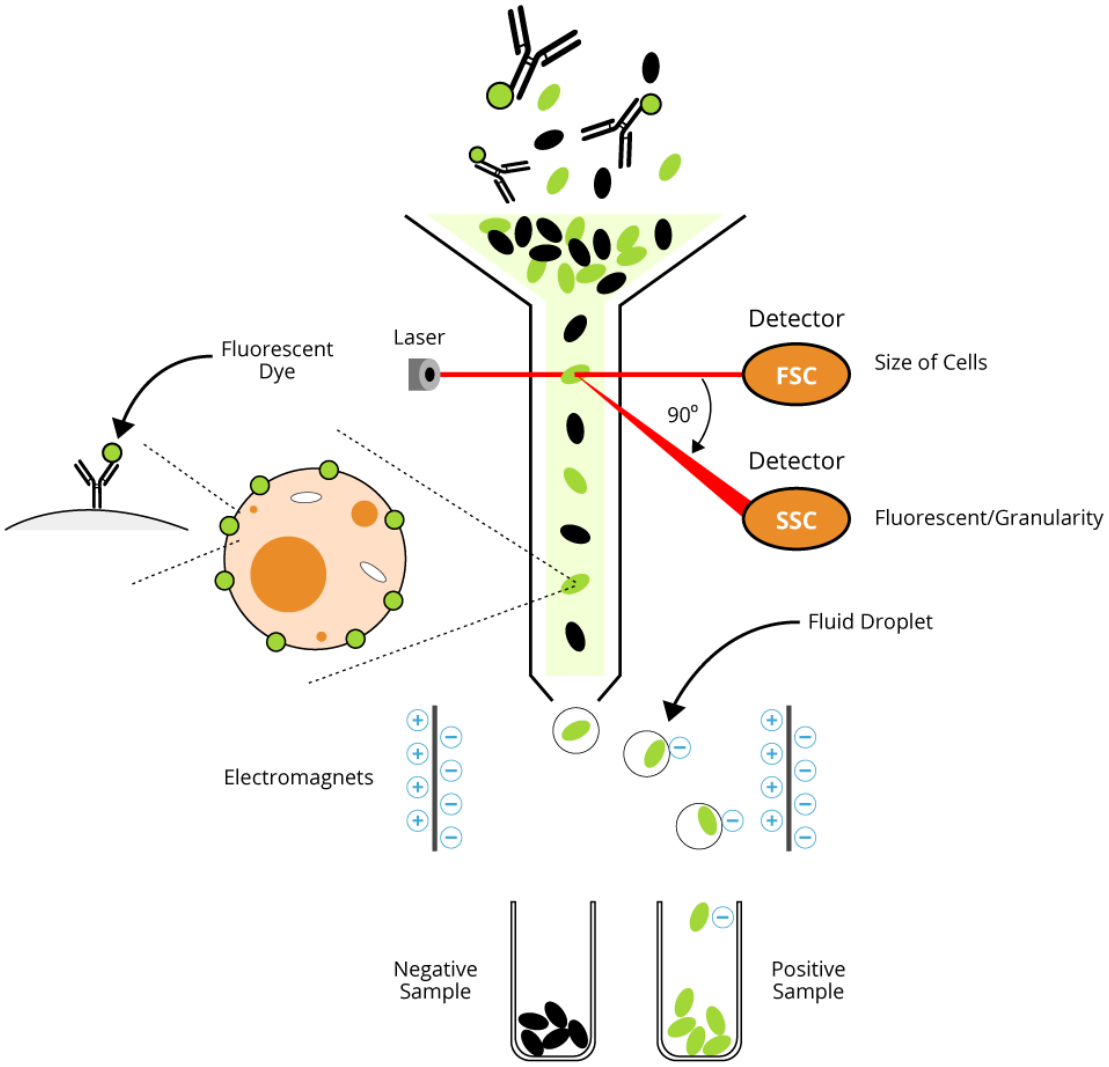


Figure 3.1: Fluorescence-activated cell sorting (FACS)
A schematic showing the process of FACS in a flow cytometer. A heterogeneous cell suspension that has been probed with fluorescent antibodies targeting specific antigens is loaded into the flow cytometer. The suspension is then focused through a small nozzle before cells pass through an excitatory laser. The fluorescent intensity of each cell, as well as their forward (FSC) and side scatter (SSC) of light, are detected. Depending on the intensity of these signals in relation to gates set by the user, the droplets containing individual cells are assigned a charge. The droplets then pass through charged plates which deflect the charged droplets into specific collection tubes based on their fluorescent profile. *(Image adapted from BosterBio, 2019 [https://www.bosterbio.com/protocol-and-troubleshooting/flow-cytometry-principle])*

When using FACS to isolate cell types based on expression of specific antigens, a control sample of unstained cells is run first and using the information from this control, gates are set such that cells with higher levels of fluorescence are considered 'positive'. As well as analysing the fluorescent intensity of cells, FACS is also able to analyse and sort cells based on their forward and side scatter of light, which indicates further physiological properties that may be of interest. When illuminated by the laser, cells scatter the light in all directions. The flow cytometer measures the light scatters in the forward direction (forward scatter), which is directly proportional to cell size, as well as light scattered at a 90° angle (side scatter), which is directly proportional to cell granularity. By analysing these properties together, cell populations can be identified based on differences in their size, shape and complexity, independently of their fluorescence (Figure 3.2).

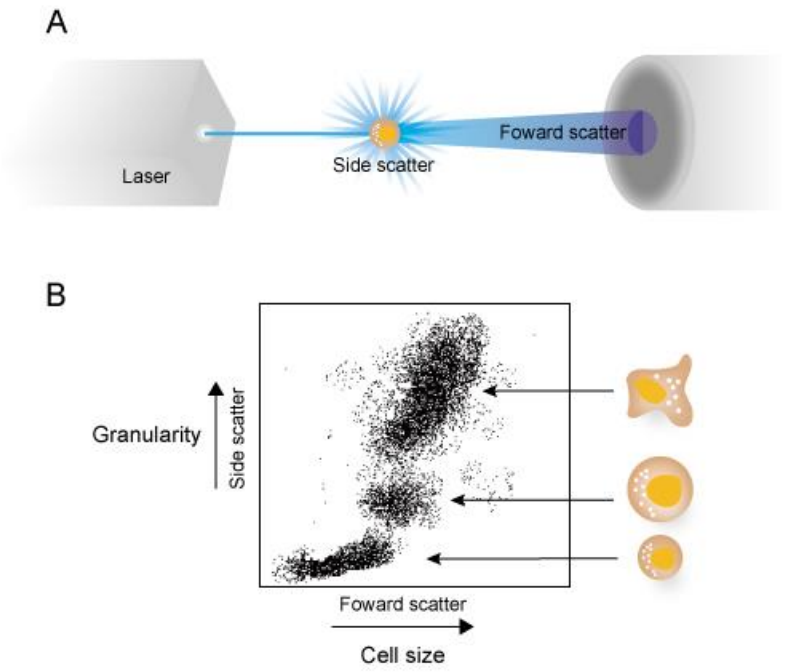


Figure 3.2: Detection of forward and side scatter in flow cytometry
(A) - When passing through the laser of a flow cytometer, cells scatter light in all directions. The forward scatter and side scatter at 90° are detected. (B) - These properties can then identify various cell populations based on their size (Forward scatter, x axis) and granularity (Side scatter, y axis). *(Image adapted from Creative Diagnostics, 2019 [https://www.creative-diagnostics.com/flow-cytometry-guide.htm]).*

Although FACS is more expensive and time consuming than density gradient centrifugation, the added benefits of being able to isolate multiple cell types at once; sort cells based on the expression of multiple antigens; and the ability to analyse information such as cell size and complexity make it an ideal method of cell isolation for this present study.

3.1.3: Consideration & requirements of planned experiment

The overall aim of the experiment to be carried out in Chapter 4 is to isolate neurons and microglia from the brains of adult rats that have undergone MCAO or sham surgery; ideally from the cortex and striatum separately. These cells will then be used to extract DNA, from which levels of 5mC and 5hmC can be analysed. Determining 5mC and 5hmC content of neurons and microglia specifically will help to further elucidate the methylomic response to ischemic stroke, as previously discussed.

Given this general experiment plan, there are a number of considerations that must be made when designing a method of cell isolation via FACS. A list of these considerations and any steps designed to account for them are listed below:

- The brain contains a lot of fatty tissue and white matter
    - This can cause the production of a large amount of cellular debris during homogenisation. Also, myelin can produce autofluorescence and increase background fluorescence signals. To remedy this, cells will be stained with the DNA stain Hoechst 33342. During analysis, only Hoechst+ cells will be analysed, ensuring that all analysed events are whole cells/nuclei and not cellular debris or myelin

- A sufficient amount of DNA and RNA will be required for subsequent assays
    - To maximise the amount of DNA and RNA collected, the number of collected cells will need to be maximised. To accomplish this, the cell suspension will undergo one round of sorting and will forego a second round of purification; whilst this may result in a slightly less pure cell population, it will prevent a loss of a large number of cells during a second round of purification.

- The process of tissue homogenisation and staining will take a number of hours, during which changes to 5hmC levels and microglial phenotype can occur
    - In order to prevent cells from significantly changing 5hmC levels or microglial activation status during the protocol, cells will need to be fixed at the earliest possible timepoint

- RNA is relatively unstable and will degrade throughout the process of staining and FACS
    - To minimise RNA degradation, all reagents used will be cleared of nucleases. Steps that don't require a set temperature will be performed at 4^{o}C, and to minimise the length of the protocol, all antibodies used will be primary antibodies conjugated to a fluorophore. This will negate the need for secondary antibodies and cut out the time required for a second antibody incubation. Additionally, RNA stabilisation solutions such as RNAlater can be added to compatible solutions.

- During the experiment, a large number of repeats will be performed across several days/weeks
    - This therefore means the protocol will need to be reliable and reproducible. During the development of the protocol, multiple tests will be performed to ensure reliability. Fresh controls of unstained cells will also be produced each day.

3.1.4: Previous research performing FACS on brain tissue

The first step in developing a FACS protocol for isolating neurons and microglia from adult rat brains was to search the literature for publications that have already performed the same, or similar, protocols. Whilst there were a number of papers published that have isolated neurons or microglia from adult rodent brain tissue, there was no published protocol for isolating both cell types from a single sample at the time. The reason for this appears to be that following the production of a heterogenous single-cell suspension from adult brain tissue, a clearance of debris is required as the brain is a tissue that contains a lot of white matter and myelin. The large amount of debris can interfere with the antibody staining, with antibodies binding to cellular debris in a non-specific manner, meaning that it must be cleared prior to staining. As a result, previously published protocols that isolate cell types from adult brain tissue using FACS include a debris clearance step that involves the use of density gradient centrifugation to collect the cells of interest whilst eliminating debris. However, there does not appear to be a usable density gradient setup that collects both neurons and microglia whilst eliminating debris. For example, Lobo et al. (2006) used a discontinuous gradient of albumin ovomucoid inhibitor to isolate neuronal progenitor cells of the striatum prior to FACS, whereas Jiang et al. (2008) and Kozlenkov et al. (2013) isolated neuronal nuclei through use of sucrose

gradients. Conversely, protocols that have isolated glial cells from adult brain tissue via FACS have used alternative density gradients designed specifically for glial isolation. Grabert et al. (2016) used the density gradient medium Percoll at a concentration of 35% in order to isolate glial cells before subsequently identifying various phenotypes via flow cytometry. Interestingly, a very similar gradient (utilising 25% Percoll) was used by Pösel et al. (2016) in order to isolate glial cells from mouse brains following MCAO.

As each of the aforementioned papers utilised a method of debris exclusion that favours either neuronal or glial isolation, none of them successfully isolated both cell types from a single sample. However, Guez-Barber et al. (2012) claim to have isolated neurons and glial cells from single samples by performing debris exclusion via filtration through cell strainers. The resulting cell population was then probed with NeuN antibodies and sorted into NeuN+ and NeuN- populations via FACS. Through analysis of mRNA expression, it was determined that the NeuN+ population had significantly higher expression of neuron-specific genes (encoding ion channels and synaptic proteins) compared to the NeuN- population, whereas the NeuN- population had significantly higher mRNA levels of glial-specific genes (encoding immune system proteins). Though the NeuN- population demonstrated this increased expression of glial-specific genes, the cells themselves were not probed with antibodies for microglia-specific markers and therefore cannot be confidently identified as microglia. It therefore cannot be concluded that this protocol has successfully isolated both neurons and microglia from single samples. A subsequent experiment performed by Liu et al. (2014) further developed this protocol, excluding debris only by serial filtration through cell strainers from 100µm to 40µm and still managing to isolate NeuN+ cells. Though neither of these papers demonstrated clear isolation of both neurons and microglia simultaneously, they do provide a protocol to begin testing in the development of a method that can isolate both cell types from a single sample.

3.1.5: Objectives

The objectives of this chapter are as follows:

- To develop a protocol that allows for the homogenisation of rat brain tissue and the reliable isolation of neuronal and microglial cells
- To extract DNA and RNA from isolated populations of cells that is of sufficient quantity and quality for downstream applications (namely RT-qPCR and DNA ELISAs)

3.2: Developing FACS protocol

3.2.1: Methods of cell homogenisation

As previously described, the first step in performing FACS is the homogenisation of the tissue sample to produce a single cell suspension. For adult rodent brains, there are various homogenisation methods used in previous research; namely mechanical homogenisation through use of a device such as a Dounce homogeniser (Jiang et al., 2008) or enzymatic digestion through use of enzymes such as Accutase (Guez-Barber et al., 2012; Liu et al., 2014) or a combination of various enzymes such as Collagenase and Dispase (Grabert et al., 2016). In the first stage of development of a FACS protocol, these 3 methods were tested on the striatum of an adult rat. The details of each method are as follows:

Mechanical homogenisation

The striatum of an adult rat (tissue was obtained from animals which were due to be culled) was extracted and placed onto a sterile, ice-cold petri dish. Using a razor blade, the tissue was chopped 25 times in each orthogonal direction and then transferred to a 15ml glass Dounce homogeniser containing 10ml of 1X Hank's Buffered Salt Solution (HBSS; Sigma-Aldrich, UK). The tissue was then homogenised with 40 passes of a large clearance glass pestle. Following

this, the cell suspension was filtered into a 50ml Falcon tube through a pre-wetted 40µm filter. The suspension was then centrifuged at 500 x g for 5 minutes at 4°C and the cell pellet was resuspended in 1ml of HBSS.

Accutase digestion

The striatum of an adult rat was extracted and placed onto a sterile, ice-cold petri dish. The tissue was then finely diced using a clean razor blade before being transferred to a 1.5ml Eppendorf tube containing 1ml of Accutase (Sigma-Aldrich, UK). The tissue was then incubated in the Accutase solution for 30 minutes at 4°C with constant end-over-end rotation. The resulting cell suspension was then centrifuged at 500 x g for 5 minutes at 4°C and the cell pellet was resuspended in 1ml of HBSS.

"Enzyme cocktail" digestion

An "enzyme cocktail" of various digestive enzymes was created by measuring 10ml of 1X HBSS and adding Collagenase Type IV (ThermoFisher, UK) to a final concentration of 50U/ml; Dispase II (ThermoFisher, UK) to a final concentration of 0.5U/ml; DNase I (Roche, Switzerland) to a final concentration of 200U/ml; and N-Tosyl-L-lysine chloromethyl ketone hydrochloride (TLCK; Sigma-Aldrich, UK) to a final concentration of 10µM. The striatum of an adult rat was then placed onto a sterile, ice-cold petri dish before being diced using a clean razor blade. The diced tissue was then transferred to a 15ml Falcon tube containing 10ml of the enzyme cocktail. The tissue was then incubated at 37°C for 1 hour with constant end-over-end rotation. 1ml of foetal bovine calf serum (Sigma-Aldrich, UK) was then added to the solution to deactivate the enzymes. The cell suspension was then centrifuged at 500 x g for 5 minutes at 4°C and the cell pellet was resuspended in 1ml of HBSS.

Once homogenised, cell counts were performed on each cell suspension using a haemocytometer and Trypan Blue dye (ThermoFisher, UK). Cell counts and proportion of live cells in each suspension are given in Table 3.1.

Method of homogenisation	Total number of cells (x10^6)	% live cells
Mechanical	1.21	91
Accutase	0.94	94
Enzyme cocktail	1.38	78

Table 3.1: Testing various methods of tissue homogenisation on adult rat striatum
Different methods of homogenisation were tested on adult rat brain striatum to produce heterogenous single-cell suspension. Total number of cells and the proportion of live cells were then measured using a haemocytometer.

As seen in Table 3.1, each method of homogenisation gave a similar number of cells, the variability in which could be due to differences in the size of the starting tissue, as each striatum was taken from a different rat. However, the enzyme cocktail method of homogenisation gave a lower yield of live cells. Given that the mechanical and Accutase methods produced a similar yield of live cells, the decision on which method to implement into the FACS protocol could be based on practicality. Therefore, the chosen method of homogenisation was mechanical homogenisation through use of a Dounce homogeniser, as this was both cheaper and less time consuming than either of the enzymatic digestion protocols. As previously described in section 3.1.3, minimising the time needed to perform the protocol is important as this will minimise RNA degradation and any changes to 5hmC levels or microglial activation.

3.2.2: Methods of cell fixation

As previously explained in section 3.1.3, a step taken in order to prevent changes in 5hmC levels and microglial activation status occurring during the process of antibody staining and FACS was to fix the cells prior to staining. Additionally, cells required permeabilisation due to the use of antibodies that target intracellular epitopes. Fixation and subsequent permeabilisation of cells is a common feature of many FACS experiments and the protocols are standard and widely used. The most commonly used methods of cell fixation and permeabilisation in FACS are ethanol fixation and paraformaldehyde (PFA) fixation followed by permeabilisation with Triton X-100. Each of these methods of fixation were tested on a suspension of cells from an adult rat striatum. The details of each method are as follows:

Ethanol fixation

Ice-cold ethanol (stored at -20^{o}C) was added in equal volume to the cell suspension such that the final concentration of ethanol is 50%. The suspension was then incubated at -20^{o}C for 10 minutes before being centrifuged at 500 x g for 5 minutes at 4^{o}C. The supernatant was removed, and the cell pellet resuspended in 1ml of 1X HBSS.

PFA + Triton X-100

A solution of 4% PFA in phosphate buffered saline (PBS) was produced. The cell suspension was centrifuged at 500 x g for 5 minutes at 4^{o}C, and the pellet resuspended in 1ml of the 4% PFA solution. This suspension was then incubated at room temperature for 15 minutes before centrifugation at 500 x g for 5 minutes at 4^{o}C. The pellet was then resuspended in 1ml of PBS containing 0.1% Triton X-100 (Sigma-Aldrich, UK) and incubated at room temperature for 10 minutes. The suspension was then centrifuged again at 500 x g for 5 minutes at 4^{o}C, and the pellet resuspended in 1ml of 1X HBSS.

Following fixation and permeabilisation, each of the cell suspensions were stained with the nuclear dye Hoechst 33342 (Sigma-Aldrich, UK). This was done by adding a stock solution of Hoechst 33342 to the cell suspension to a final concentration of 1µg/ml. The suspensions were then incubated at 4°C in the dark for 15 minutes before being centrifuged at 500 x g for 5 minutes at 4°C. Pellets were then resuspended in 1ml of 1X HBSS. The number of Hoechst+ cells in each suspension was then analysed via flow cytometry using the Beckman Coulter Astrios EQ. As Hoechst 33342 is a nuclear dye, detecting Hoechst+ cells allows for the analysis of whole cells/cell bodies, excluding cellular debris that would not be stained by Hoechst 33342. The number of Hoechst+ cells and the forward scatter/Hoechst plots produced by each fixation method are shown in Figure 3.3.

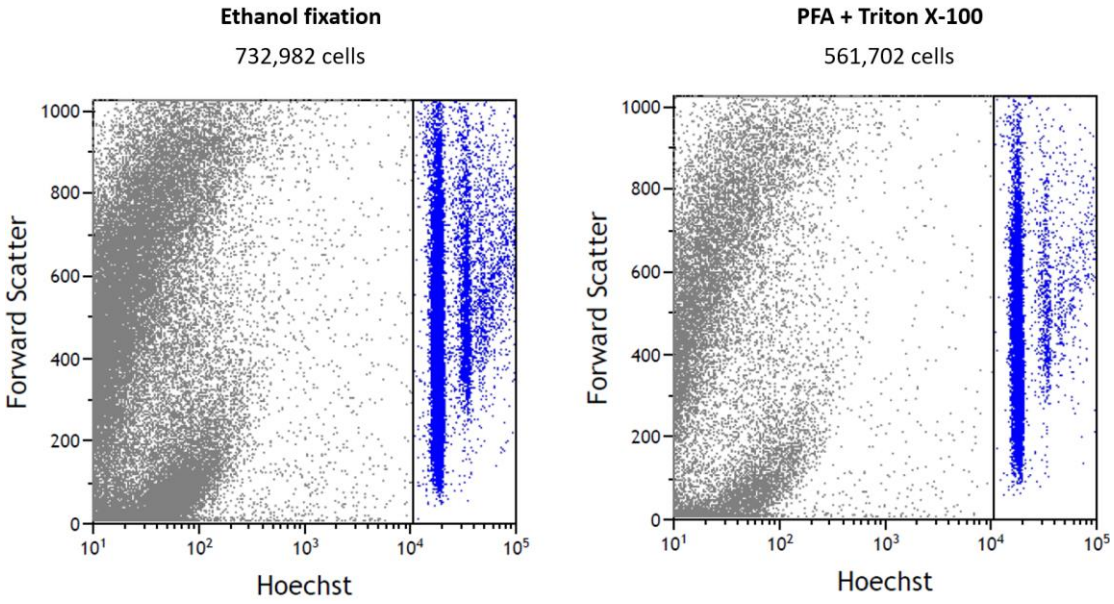


Figure 3.3: Testing methods of fixation & permeabilisation for FACS
Two methods of cell fixation and permeabilisation were performed on cell suspensions – ethanol fixation and PFA fixation followed by Triton X-100 permeabilisation. Each suspension was then stained with Hoechst 33342 dye and analysed via flow cytometry. Dot plots are shown as forward scatter (y-axis) v. fluorescent intensity at Hoechst 33342 wavelength (x-axis).

It can be seen in Figure 3.3 that both fixation methods produced a cell suspension that contained a similar number of Hoechst+ cells. The ethanol fixation procedure did appear to produce slightly more cells, and this could be due to the multiple rounds of centrifugations that were required in the PFA + Triton X-100 protocol, during which cells can be lost. Considering these results, the chosen method of cell fixation and permeabilisation for the development of this FACS protocol was ethanol fixation, as it is less time consuming than PFA fixation and required fewer rounds of centrifugation, thereby minimising cell loss. Furthermore, previous research has determined that fixation of tissue with ethanol produces RNA yields of greater quantity and quality than fixation with formalin-based solutions (Cox et al., 2006).

3.2.3: Developing panel of antibodies

Having determined suitable methods of tissue homogenisation and cell fixation, the next step in the development of a FACS protocol was determining which antibodies to use in order to isolate the desired cell types. As previously described, the aim of this study was to isolate neurons and microglia from adult rat brain tissue.

NeuN is a nuclear antigen that is expressed exclusively by neurons, with the vast majority of neurons being NeuN-positive. For this reason, it is a widely used biomarker for identification of neuronal cells and an ideal target for use in isolating neurons in this study. As previously described, the antibodies used in this study will be primary antibodies directly conjugated to fluorophores in order to eliminate the need for secondary antibodies and further antibody incubations. For this reason, the chosen NeuN antibody for testing in this protocol was a NeuN antibody directly conjugated to phycoerythrin (PE) that was used by Rubio et al. (2016) to

isolate neurons from adult rat brain tissue via FACS (Milli-Mark Anti-NeuN-PE, Clone A60 [mouse monoclonal] antibody; EMD Millipore, USA).

When determining target antigens for the isolation of microglia, the options are far more varied as microglia are an extremely reactive cell type and constantly change the antigens on their cell surface based upon their environment. There are therefore many possible antigens that can be targeted depending on the activation state and phenotype of the microglia. For the purposes of this study, isolation of microglia in all states of activation (active and inactive) was desired, though analysing active v. inactive microglia may also be of interest if these subtypes can be successfully separated.

For the identification of total microglia regardless of activation state, previous research indicates that microglia possess the phenotype $CD11b^{+}/CD45^{low/int}$, which makes them distinguishable from peripheral monocytes/macrophages, which possess the phenotype $CD11b^{+}/CD45^{high}$ (Becher & Antel, 1996). Therefore, antibodies targeting the CD11b and CD45 antigens have been used in flow cytometry experiments to isolate microglia from adult rodent brain tissue (Bedi et al., 2013; Cardona et al., 2006). For use in this FACS protocol, primary antibodies targeting CD11b and CD45 were chosen; CD11b-FITC (Miltenyi Biotec, Germany) and CD45-APC (Miltenyi Biotec, Germany). Though an Iba1 antibody was used to identify microglia in Chapter 2 of this thesis, targeting this antigen would not be ideal for flow cytometry. This is because Iba1 is a cytoplasmic protein, which makes it problematic when attempting to reliably stain fixed & permeabilised cells in suspension. Cytoplasmic antigens are suitable for staining fixed sections of tissue, but when staining cells in suspension for flow cytometry, nuclear or membrane-bound antigens are ideal, hence the decision to stain for CD11b and CD45. This is also why other known M1 and M2 phenotype markers, such as IL-6 and IL-4, respectively, were not chosen for use in this flow cytometry protocol.

In an attempt to further subdivide the microglial population into 'active' and 'inactive' subpopulations, further antigens can be targeted that are preferentially expressed in either of the activation states. Previous research has found that CD68 is an antigen localised primarily to the lysosome, and is therefore more highly expressed in activated microglia, whereas quiescent ramified microglia express lower levels of this antigen (Slepko & Levi, 1996). More recent research has suggested that defining microglia as existing in either an 'activated' or 'inactivated' state is arbitrary, as microglial activation occurs across a spectrum, with varying degrees of 'activation' and levels of antigen expression (Town et al., 2005). However, the use of CD68 as a target antigen in FACS can still aid in identifying microglia in varying stages of activation post-stroke and would elucidate more information than using CD11b and CD45 alone. It is for this reason that a CD68 primary antibody was chosen for testing in the development of this FACS protocol; CD68-PEVio770 (Miltenyi Biotec, Germany).

Having considered the cell types to be isolated and possible target antigens to identify them, the panel of antibodies chosen to start testing the FACS staining are shown in Table 3.2. The flow cytometer used for this study was the Beckman Coulter MoFlo XDP; the antibodies listed in Table 3.2 have been chosen such that each fluorophore is detected by a different fluorescent channel of the machine, meaning that all 4 fluorophores can be detected simultaneously, alongside Hoechst 33342.

Target Antigen	Fluorophore	Supplier	Catalogue No.	Target cell type
NeuN	PE	EMD Millipore	FCMAB317PE	Neurons
CD11b	FITC	Miltenyi Biotec	130-105-273	Microglia
CD45	APC	Miltenyi Biotec	130-107-843	Microglia/Macrophages
CD68	PE-Vio770	Miltenyi Biotec	130-103-365	"Activated" microglia

Table 3.2: Panel of antibodies chosen for development of protocol
Details of the antibodies chosen to test in the development of a protocol to isolate neurons and microglia from ischemic rat brains

3.2.4: Development of final protocol

Having developed protocols for tissue homogenisation & cell fixation and developed a panel of antibodies for identification of desired cell types, the next step in development of the FACS protocol was to stain the cells with the antibodies and determine if neurons and microglia can be reliably isolated. The development of a reliable final protocol required multiple rounds of testing over several months, with this section describing each round and the changes made after each attempt in an effort to improve the protocol.

3.2.4.1: First round

The method used for the first round of testing is given below. The results of this test are shown in Figure 3.4.

The striatum of an adult rat was extracted and placed onto a sterile, ice-cold petri dish. Using a razor blade, the tissue was chopped 25 times in each orthogonal direction and then

transferred to a 15ml glass Dounce homogeniser containing 10ml of 1X HBSS. The tissue was then homogenised with 40 passes of a large clearance glass pestle. Following this, the cell suspension was filtered into a 50ml Falcon tube through a pre-wetted 40µm filter. The suspension was then centrifuged at 500 x g for 5 minutes at 4^{o}C and the cell pellet was resuspended in 1ml of HBSS. To this, an equal volume (1ml) of ice-cold ethanol was added and the suspension was incubated at -20^{o}C for 10 minutes before being centrifuged again at 500 x g for 5 minutes at 4^{o}C. The cell pellet was then resuspended in 550µl of FACS buffer (PBS w/ 0.5% Bovine Serum Albumin + 5% RNAlater) and transferred to a 1.5ml Eppendorf tube. From this, 50µl was placed into a separate Eppendorf tube and topped up to 500µl with FACS buffer to act as an unstained negative control. Stock solution of Hoechst 33342 was added to both the positive and negative samples to a final concentration of 1µg/ml. To the positive sample, 1µl of NeuN-PE, CD45-APC and CD11b-FITC antibodies were added. Samples were then incubated at 4^{o}C for 30 minutes with constant end-over-end rotation. Following this, samples were centrifuged at 500 x g for 5 minutes at 4^{o}C and pellets resuspended in 500µl of FACS buffer. Samples were then loaded into a Beckman Coulter MoFlo XDP flow cytometer for analysis.

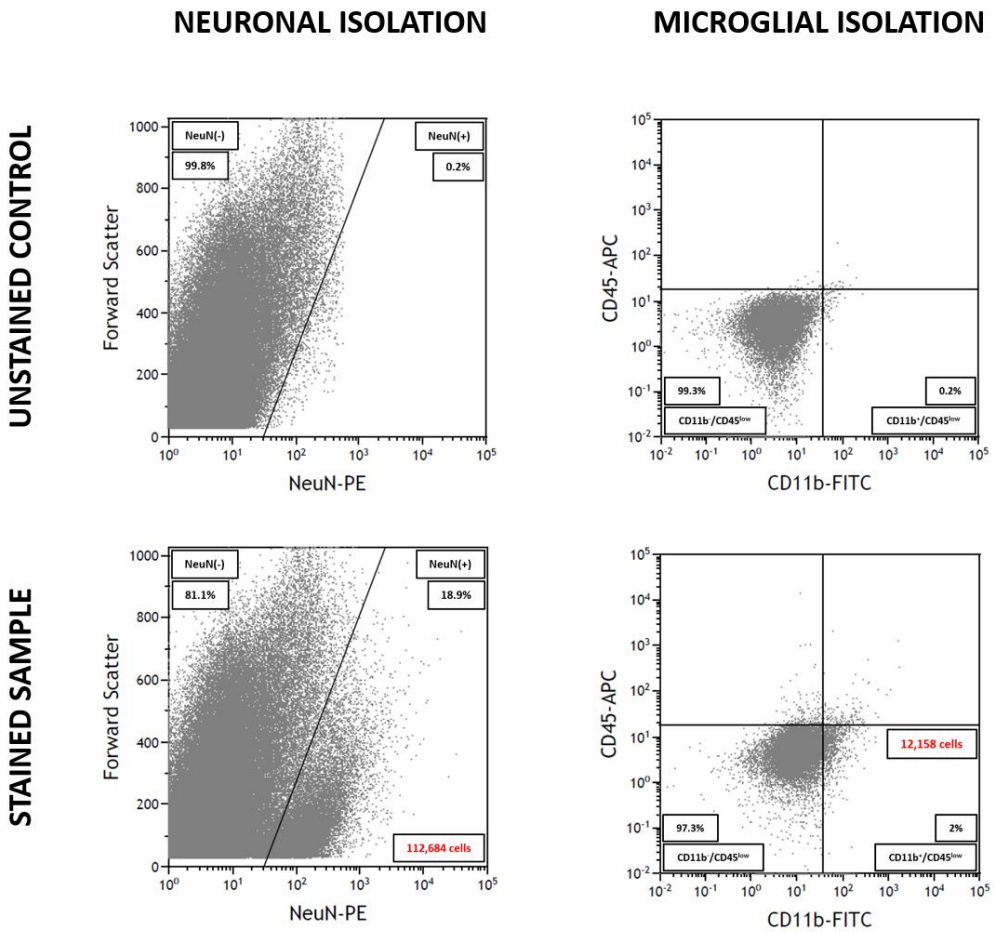


Figure 3.4: Outcome of first round of FACS protocol testing
Flow cytometry dot plots of cells taken from adult rat striatum and processed in order to isolate neuronal (NeuN+) and microglial ($CD11b^+/CD45^{low}$) cells. All cells were first gated for Hoechst 33342 fluorescence. Gates for positively stained cells were then set using unstained controls. For neuronal cell isolation, 18.9% of Hoechst+ cells were NeuN+ (112,684 cells). For microglial isolation, 2% of Hoechst+ cells were of the $CD11b^+/CD45^{low}$ phenotype (12,158 cells).

As seen in Figure 3.4, the first round of testing did not result in desirable staining or cell isolation. Although a percentage of cells were detected as NeuN+, there are not 2 distinct populations of cells that allow for absolute neuronal isolation. Microglial isolation is even less clear, with only 2% of all Hoechst+ cells detected as the $CD11b^+/CD45^{low}$ phenotype. As with NeuN+ cells, there is no clear population of $CD11b^+/CD45^{low}$ cells.

3.2.4.2: Second round

Having considered the undesirable results of the first round of FACS testing, changes were made to the protocol in an attempt to improve the quality of staining. Namely, the volume of FACS buffer in which samples were resuspended during antibody staining was increased from 500µl to 1ml, and 4µl of each of the NeuN-PE, CD45-APC and CD11b-FITC antibodies were added to the positive sample, thereby decreasing dilution from 1:500 to 1:250. The rest of the protocol was carried out exactly as described previously. The results of this second round of testing are shown in Figure 3.5.

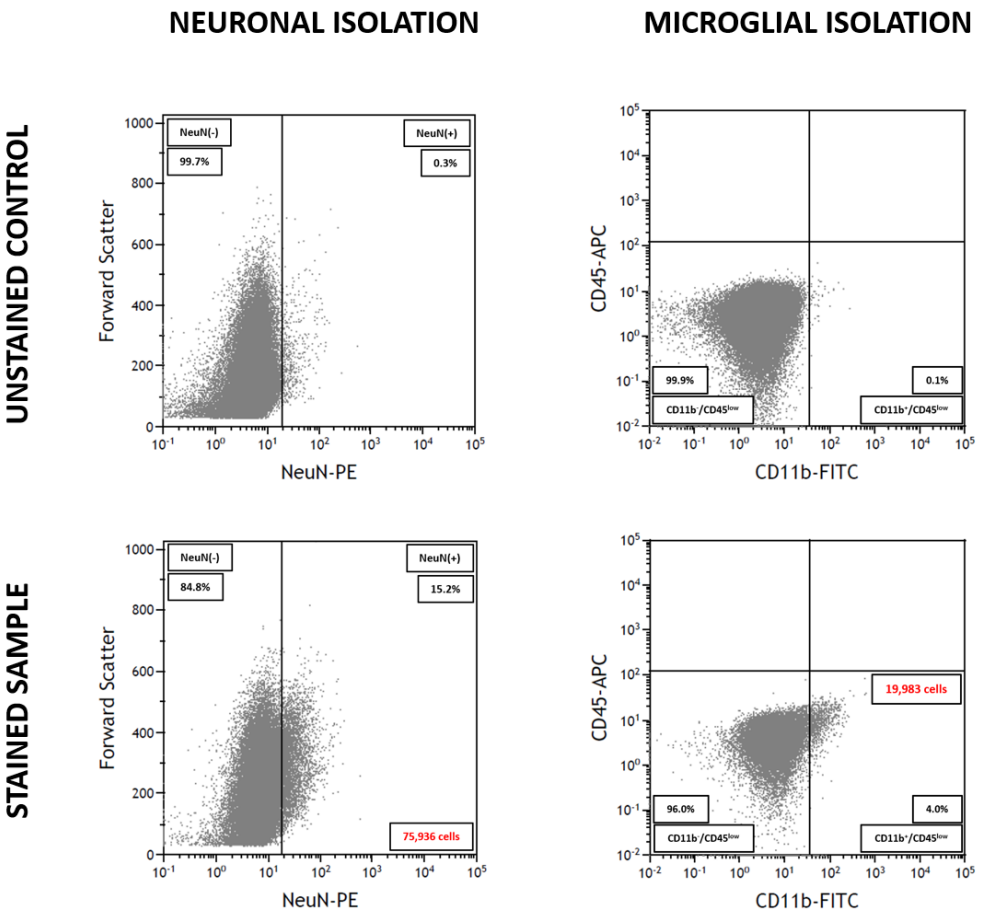


Figure 3.5: Outcome of second round of FACS protocol testing
Flow cytometry dot plots of cells taken from adult rat striatum and processed in order to isolate neuronal (NeuN+) and microglial ($CD11b^+/CD45^{low}$) cells. All cells were first gated for Hoechst 33342 fluorescence. Gates for positively stained cells were then set using unstained controls. For neuronal cell isolation, 15.2% of Hoechst+ cells were NeuN+ (75,936 cells). For microglial cell isolation, 4% of Hoechst+ cells were of the $CD11b^+/CD45^{low}$ phenotype (19,983 cells).

As can be seen in Figure 3.5, the increase in antibody concentration did not improve quality of staining for neuronal or microglial isolation. The percentage of Hoechst+ cells that were also NeuN+ (15.2%) was lower than in the first round of testing (18.9%). For microglial isolation, although the percentage of Hoechst+ cells that were of the $CD11b^{+}/CD45^{low}$ phenotype (4%) was higher than in the first round of testing (2%), there was still no clear population of positively stained cells that allows for accurate isolation of microglia.

3.2.4.3: Third Round

Following homogenisation and fixation of cells in the first two rounds of testing, the cell suspension appeared 'cloudy', suggesting that there was still a significant amount of debris present in the solution despite the filtration through a 40µm cell filter. It is possible that the presence of this debris impedes the ability of the antibodies to effectively bind to their target antigen. Therefore, the third round of testing involved utilising density gradients to eliminate debris with the aim of improving staining. However, as previously discussed in section 3.1.4, density gradients that remove debris can isolate either neuronal cells or microglial cells, but not both. Therefore, in this round of testing, the sample of homogenised striatal tissue was split into two, with one half undergoing a Percoll gradient centrifugation to eliminate debris and isolate microglial cells, whereas the other half underwent a sucrose density gradient centrifugation in order to eliminate debris and isolate neuronal nuclei. Performing the protocol in this way meant that neurons and microglia could no longer be isolated simultaneously from the same cell suspension; and halving the suspension prior to staining meant that a lower number of cells is collected after FACS. However, these were necessary changes that needed to be made in order to attain high quality and reliable staining for FACS.

In this round of testing, the adult rat striatum was extracted, homogenised and filtered just as in the previous 2 tests. Once homogenised, the cell suspension was split into two 5ml

halves and processed for neuronal and microglial staining. Unstained controls, one from each method of staining, were also processed. The outcomes of these staining protocols are shown in Figure 3.6. The protocol for each process is as follows:

Neuronal staining

1ml of 1.1M sucrose was placed at the bottom of a 15ml falcon tube. The 5ml of cell suspension was carefully layered on top of the sucrose using a P1000 pipette and then centrifuged at 1300 x g for 15 minutes at room temperature. Following this, a cell pellet was visible at the bottom of the tube whereas myelin and other debris settled at the cell suspension/sucrose interface. Debris and supernatant were removed, and the cell pellet was resuspended in 500µl of 1X HBSS. To this, an equal volume of ice-cold ethanol was added. The cell suspension was incubated for 10 minutes at -20^{o}C and then centrifuged at 500 x g for 5 minutes at 4^{o}C. The cell pellet was resuspended in 1ml of FACS buffer containing 1µg/ml of Hoechst 33342 and a 1:250 dilution of NeuN-PE antibody. The suspension was incubated for 30 minutes at 4^{o}C with constant end-over-end rotation and then centrifuged at 500 x g for 5 minutes at 4^{o}C. The cell pellet was resuspended in 500µl of FACS buffer and then loaded into the Beckman Coulter MoFlo XDP for analysis.

Microglial staining

A solution of stock isotonic Percoll (SIP) was made by combining 90ml of Percoll (Sigma-Aldrich, UK) with 10ml of 10X HBSS (ThermoFisher, UK). From this SIP stock, a 35% SIP solution was made by combining 35ml of SIP with 65ml of 1X HBSS.

Following homogenisation and filtration, the 5ml of cell suspension was centrifuged at 500 x g for 5 minutes at 4^{o}C. The cell pellet was then resuspended in 8ml of 35% SIP solution and transferred to a 15ml falcon tube. 5ml of 1X HBSS was then carefully layered atop the

cell suspension using a P1000 pipette. The solution was then centrifuged at 800 x g for 30 minutes at room temperature. Following centrifugation, microglial cells pelleted at the bottom of the tube whereas myelin and other debris settled at the interface between the 35% SIP solution and 1X HBSS. Debris and supernatant were removed, and the pellet was resuspended in 1ml of 1X HBSS. To this, an equal volume of ice-cold ethanol was added. The cell suspension was incubated for 10 minutes at -20^{o}C and then centrifuged at 500 x g for 5 minutes at 4^{o}C. The cell pellet was resuspended in 1ml of FACS buffer containing 1µg/ml of Hoechst 33342 and a 1:250 dilution of CD11b-FITC and CD45-APC antibody. The suspension was incubated for 30 minutes at 4^{o}C with constant end-over-end rotation and then centrifuged at 500 x g for 5 minutes at 4^{o}C. The cell pellet was resuspended in 500µl of FACS buffer and then loaded into the Beckman Coulter MoFlo XDP for analysis.

As demonstrated in Figure 3.6, performing debris exclusion through the use of density gradients greatly improved the quality of staining. With regards to NeuN staining, there was a clear and separate population of NeuN+ cells (53.6% of total Hoechst+ cells); and with regards to microglial staining, there was a clear population of CD11b^{+}/CD45^{low} cells (51.2% of total Hoechst+ cells). However, as expected, the number of total cells collected had also been reduced (from 75,936 to 11,906 for NeuN+ cells, and from 19,983 to 9,329 for CD11b^{+}/CD45^{low} cells). This reduction in the number of collected cells was likely due not only to halving the cell suspension prior to staining, but possibly also due to the density gradients not being 100% efficient and losing some target cells along with debris and myelin. Despite this, the quality of staining was much improved in comparison to previous runs, and this protocol could be adapted in an attempt to increase the cell number.

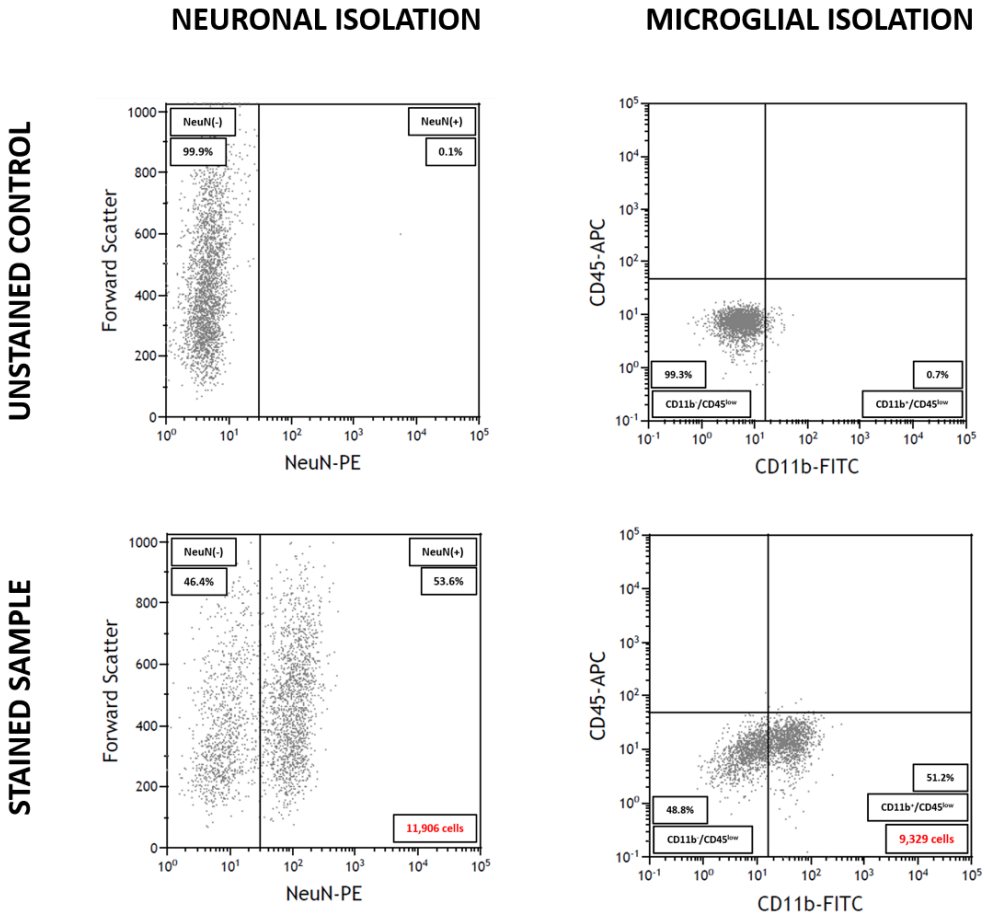


Figure 3.6: Outcome of third round of FACS protocol testing
Flow cytometry dot plots of cells taken from adult rat striatum and processed in order to isolate neuronal (NeuN+) and microglial ($CD11b^{+}/CD45^{low}$) cells. All cells were first gated for Hoechst 33342 fluorescence. Gates for positively stained cells were then set using unstained controls. For neuronal cell isolation, 53.6% of Hoechst+ cells were NeuN+ (11,906 cells). For microglial cell isolation, 51.2% of Hoechst+ cells were of the $CD11b^{+}/CD45^{low}$ phenotype (9,329 cells).

3.2.4.4: Fourth round

With the third round of testing having produced high quality staining, albeit with low cell numbers, the fourth round of testing was aimed at increasing the number of collected cells whilst maintaining the quality of staining. In order to do this, the protocol carried out was the exact same as in the third round of testing, however the amount of starting tissue was increased. Although the original aim of the experiment was to process the cortex and striatum

of each animal separately, the previous FACS test demonstrated that doing so was likely to result in a low yield of cells. In order to ensure that a high number of cells are collected, thereby meaning enough DNA and RNA can be collected from each sample for use in further downstream applications, the fourth round of testing involved processing the cortex and striatum of an adult rat together. This is preferable to pooling the same tissue/brain areas of multiple animals together as this keeps the number of required animals to a minimum. Homogenisation of cortex and striatum and subsequent cell fixation and staining were carried out as previously described (section 3.2.4.3). The outcomes of this round of FACS testing are shown in Figure 3.7.

As demonstrated in the dot plots in Figure 3.7, increasing the amount of starting tissue by processing cortex and striatum simultaneously successfully increased cell numbers whilst maintaining high quality staining. In both neuronal and microglial isolation, there were clearly defined populations of positively stained cells. Moreover, the number of collected cells greatly increased in comparison to the third round of testing that processed only striatal tissue: the number of collected NeuN+ cells increased from 11,906 to 37,021; whilst the number of $CD11b^{+}/CD45^{low}$ cells collected increased from 9,329 to 28,104. Though a 100% recovery rate of microglial cells would be in the range of 100,000+ cells, the changes to this protocol have increased the number of isolated cells such that enough DNA & RNA can be collected for downstream applications. The protocol used in this round of testing therefore appeared to produce high quality staining that allows for the isolation of a relatively high number of neuronal and microglial cells from the adult rat brain.

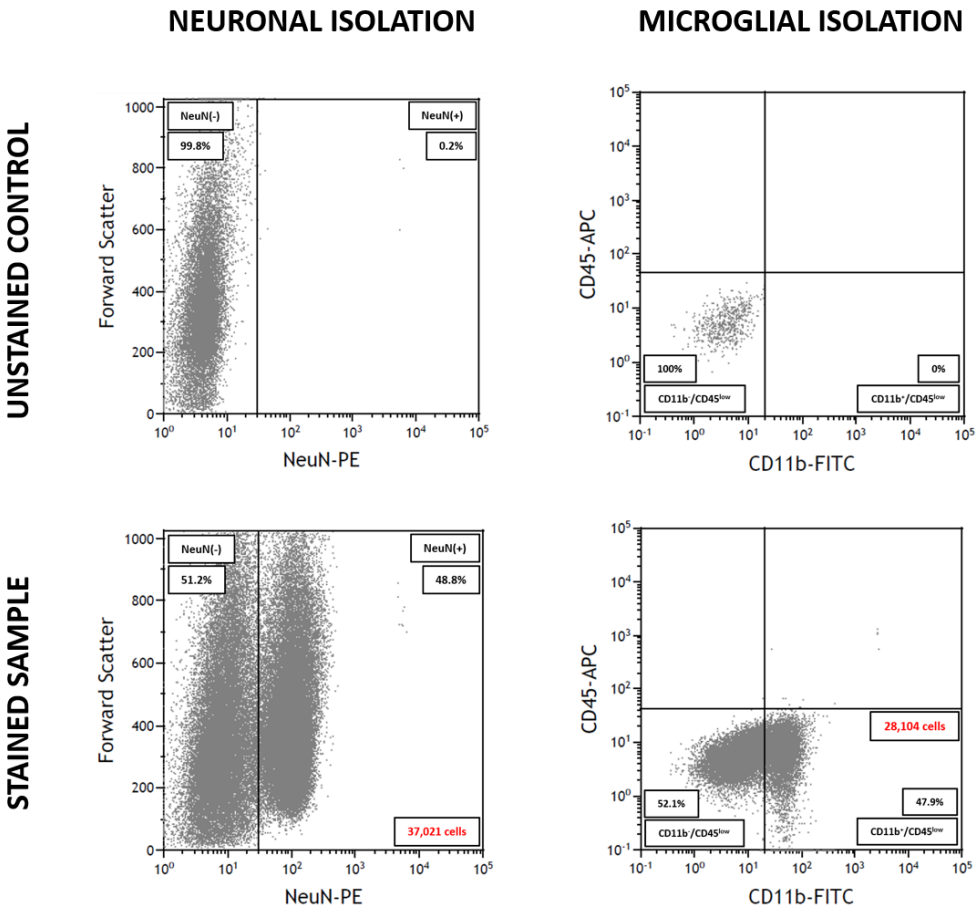


Figure 3.7: Outcome of fourth round of FACS protocol testing
Flow cytometry dot plots of cells taken from adult rat cortex & striatum and processed in order to isolate neuronal (NeuN+) and microglial ($CD11b^{+}/CD45^{low}$) cells. All cells were first gated for Hoechst 33342 fluorescence. Gates for positively stained cells were then set using unstained controls. For neuronal cell isolation, 48.8% of Hoechst+ cells were NeuN+ (37,021 cells). For microglial cell isolation, 47.9% of Hoechst+ cells were of the $CD11b^{+}/CD45^{low}$ phenotype (28,104 cells).

3.2.4.5: Fifth round

As previously explained, the final FACS protocol utilised in the full experiment needs to be reliable as it is carried out a number of times across many days. This therefore means that although the protocol used in the fourth round of testing produced high quality staining, it needed to be tested for reliability. To do this, the exact same protocol was repeated in order to ensure that similar results are obtained. The outcomes of this repeated protocol are shown in Figure 3.8

The dot plots shown in Figure 3.8 demonstrate that the quality of staining and number of collected cells from this fifth round of testing were very similar to that of the fourth round of testing. Once again, clear populations of NeuN+ and CD11b^{+}/CD45^{low} cells can be seen, and similar numbers of neurons and microglia were collected. This therefore signifies that the protocol used in each round was reliable.

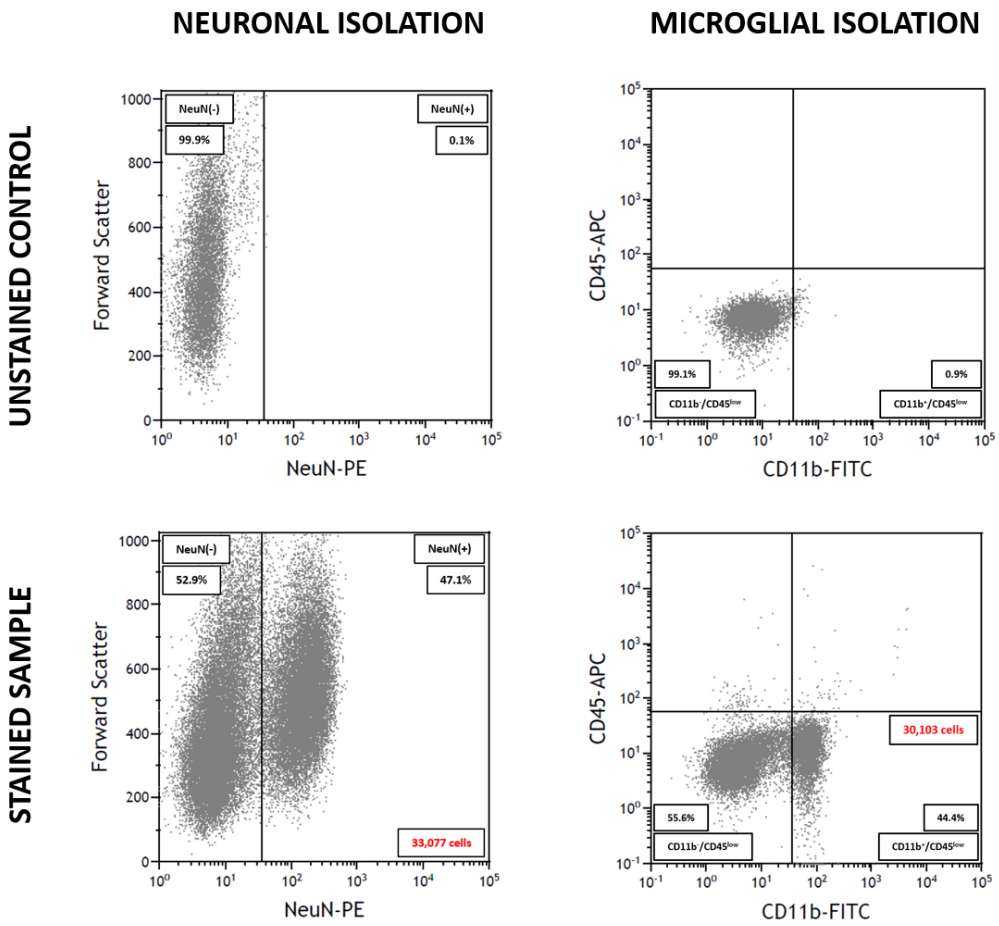


Figure 3.8: Outcome of fifth round of FACS protocol testing
Flow cytometry dot plots of cells taken from adult rat cortex & striatum and processed in order to isolate neuronal (NeuN+) and microglial (CD11b^{+}/CD45^{low}) cells. All cells were first gated for Hoechst 33342 fluorescence. Gates for positively stained cells were then set using unstained controls. For neuronal cell isolation, 47.1% of Hoechst+ cells were NeuN+ (33,077 cells). For microglial cell isolation, 44.4% of Hoechst+ cells were of the CD11b^{+}/CD45^{low} phenotype (30,103 cells).

3.2.4.6: Sixth round

Although the fourth and fifth rounds of testing appeared to have identified a reliable protocol for producing high quality staining of neuronal and microglial cells for FACS sorting, as previously explained, the full experiment involves sorting these cells from the brains of rats that have undergone ischemic stroke. It is possible that the process of ischemic stroke causes changes to the cortex and striatum that negatively affect the outcome of this FACS protocol. For this reason, the sixth round of testing involved repeating the procedure from the fourth and fifth rounds on the cortex and striatum of a rat that had undergone ischemic stroke. This is more representative of what occurs in the full experiment and will highlight any issues that may occur when applying this protocol to ischemic tissue. It is also in this run that the CD68-PEVio770 antibody was used, as it should highlight any 'activated' microglia or invading peripheral macrophages (as described in section 3.2.3) that may be present as a result of ischemic stroke.

24 hours prior to the commencement of the FACS protocol, and adult male Wistar rat underwent MCAO surgery (details of surgery protocol can be found in Chapter 4; section 4.2.2). The following day, the rat was euthanised and the cortex and striatum of the infarcted hemisphere were extracted. From this point, the exact same FACS protocol was carried out as in the fourth and fifth runs, with the exception that microglial cells were stained with CD68-PEVio770 antibody as well as the CD11b-FITC and CD45-APC antibodies. The outcomes of this round of testing are shown in Figure 3.9.

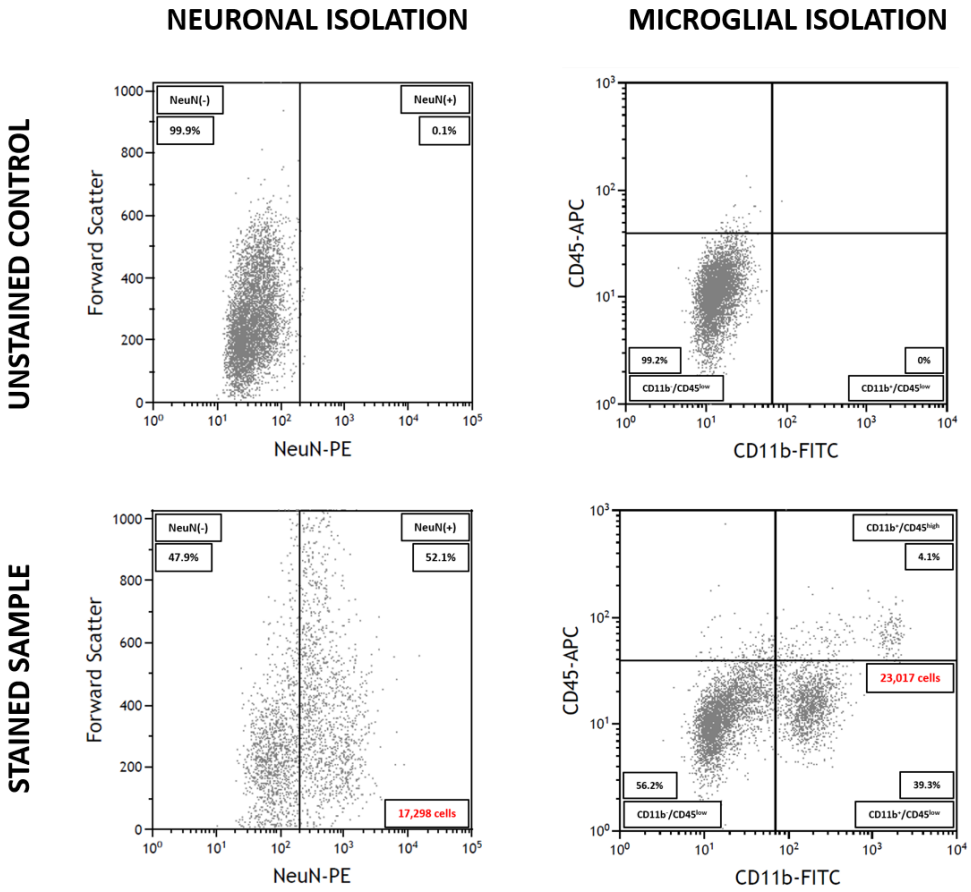


Figure 3.9: Outcome of sixth round of FACS protocol testing
Flow cytometry dot plots of cells taken from ischemic adult rat cortex & striatum and processed in order to isolate neuronal (NeuN+) and microglial ($CD11b^{+}/CD45^{low}$) cells. All cells were first gated for Hoechst 33342 fluorescence. Gates for positively stained cells were then set using unstained controls. For neuronal cell isolation, 52.1% of Hoechst+ cells were NeuN+ (17,298 cells). For microglial cell isolation, 39.3% of Hoechst+ cells were of the $CD11b^{+}/CD45^{low}$ phenotype (23,017 cells). Additionally, 4.1% of Hoechst+ cells were of the $CD11b^{+}/CD45^{high}$ phenotype.

The flow cytometry plots displayed in Figure 3.9 demonstrate that the FACS protocol produced high quality staining of neuronal (NeuN+) and microglial ($CD11b^{+}/CD45^{low}$) cells from ischemic tissue, as it did from healthy tissue in previous test runs. However, with regards to isolation of neuronal cells, less total cells were collected than in previous runs (17,298 NeuN+ cells as opposed to ~35,000 cells in previous runs). This is not unexpected, as the tissue that was processed included an ischemic infarct that would have led to the death and degradation of a large number of neuronal cells. This is something to be wary of, however, as

collecting a very low number of cells in the full experiment produces the risk that not enough DNA and RNA can be extracted for downstream applications.

With regards to microglial isolation from ischemic cortex and striatum, there was once again a clear population of $CD11b^{+}/CD45^{low}$ cells as in previous runs. Interestingly, there was also a small population of $CD11b^{+}/CD45^{high}$ cells that can be identified. As these were not present in any of the runs performed on healthy tissue, it can be deduced that this population of cells appeared due to ischemic stroke. However, the exact origin of these cells cannot be determined by their expression of these antigens alone. Previous research has determined that CNS-derived microglial cells express intermediate levels of CD45 in their 'activated' state, whereas invading peripheral macrophages exhibit relatively high levels of CD45 (Renno et al., 1995). Although the population of $CD11b^{+}/CD45^{high}$ cells seen in Figure 3.9 exhibit higher levels of CD45 expression than quiescent ramified microglia ($CD11b^{+}/CD45^{low}$), there is no available threshold to determine if these levels of CD45 expression are 'intermediate' or 'high'. It is therefore not possible to determine if these cells are 'activated' microglia or invading peripheral macrophages. Further investigation of activated microglia and invading macrophages is the reason that the CD68-PEVio770 antibody was included in the chosen panel of antibodies (as described in section 3.2.3). CD68 is an antigen that is localised primarily to lysosomes and is therefore more highly expressed in lysosomal 'activated' microglia and invading macrophages. However, when analysing only the $CD11b^{+}/CD45^{high}$ population of cells, it was found that none were also positively stained for CD68 (Figure 3.10). This is unexpected because as previously mentioned, it is assumed that the $CD11b^{+}/CD45^{high}$ population of cells are lysosomal and would therefore stain positively for CD68. The lack of positive staining therefore suggests that the antibody may not have been working correctly, though this cannot be determined for certain without use of a positive control.

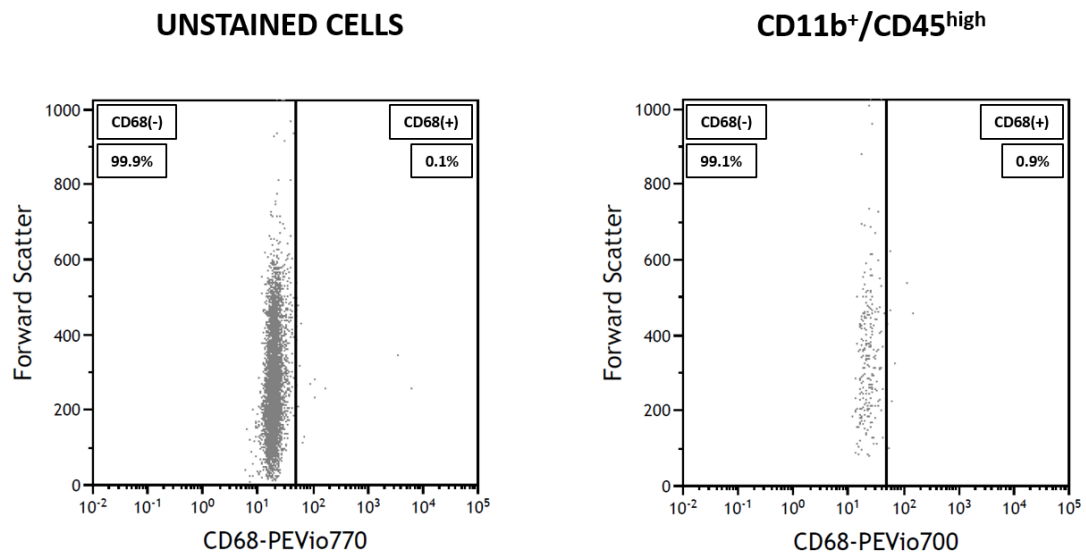


Figure 3.10: Analysis of CD11b^{+}/CD45^{high} population
Flow cytometry dot plots of cells taken from ischemic adult rat cortex & striatum. A population of CD11b^{+}/CD45^{high} cells was identified following FACS analysis; very few of these cells (0.9%) were also positive for CD68, similarly to the negative control of unstained cells (0.1%). All cells displayed were first gated for Hoechst 33342 fluorescence.

3.2.4.7: Testing purity of sorted samples

The FACS protocol used in the fourth, fifth and sixth runs in this chapter have reliably produced high quality staining to allow for the isolation of neuronal (NeuN+) and microglial (CD11b^{+}/CD45^{low}) cells. However, one aspect of the protocol required testing is the purity of the sorted samples. As explained in section 3.1.3, the samples undergo only one round of cell sorting and forego a second round of purification in order to minimise cell loss and maximise cell number. Despite this, it is still important to assess the purity of the samples that the protocol is producing. It is for this reason that the NeuN+ and CD11b^{+}/CD45^{low} populations of cells that were sorted during the sixth run were reanalysed to test their purity. The results of this analysis are shown in Figure 3.11.

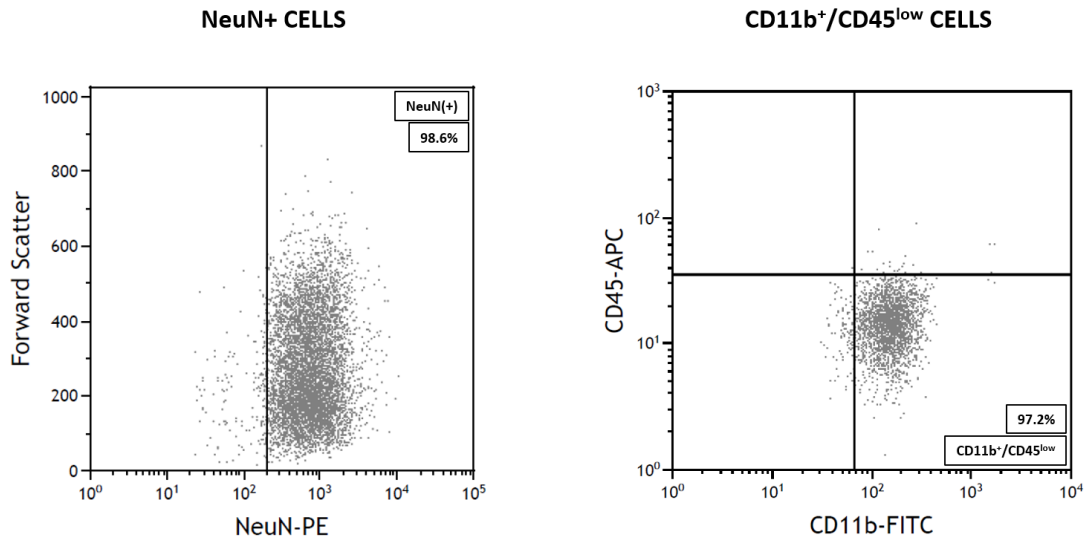


Figure 3.11: Testing purity of FACS-sorted cells
Flow cytometry dot plots of cells taken from ischemic adult rat cortex & striatum that had been previously sorted via FACS to isolate neuronal (NeuN+) and microglial ($CD11b^+/CD45^{low}$) cells. Cells were reanalysed after sorting to test for purity; the NeuN+ population was found to have a purity of 98.6% (left) and the $CD11b^+/CD45^{low}$ population was found to have a purity of 97.2% (right).

As demonstrated in Figure 3.11, both the sorted populations of neuronal and microglial cells demonstrated high purity at 98.6% and 97.2%, respectively. Whilst another round of sorting with stricter parameters/gates would likely have resulted in populations of higher purity, this would also lower cell numbers. Considering the high level of purity already seen after one round of sorting and the need to maximise the number of collected cells, a second round of sorting is unnecessary.

3.2.5: DNA & RNA quality check

The overall aim of this experiment is to extract DNA and RNA from the isolated cell types and analyse 5mC and 5hmC levels as well as mRNA expression levels of the Tet enzymes. In order to ensure that the isolated cell populations provide enough DNA and RNA for these

downstream applications, the quantity and quality of DNA and RNA was analysed from the neuronal and microglial populations obtained from the fourth and fifth runs from this chapter (section 3.2.4). Additionally, in each of these runs 500µl of cell suspension was taken just after homogenisation to act as a 'backup' of total cell population – in the event that cell numbers are too low, DNA and RNA could be extracted from these unsorted cells and analysed instead. DNA & RNA quantity & quality from these total cell population were also analysed.

In order to extract DNA and RNA, cells were sorted directly from the flow cytometer into 1ml of Trizol reagent (Invitrogen, USA) in a 1.5ml Eppendorf tube. For backups, 500µl cell suspension was centrifuged at 500 x g for 5 minutes at 4^{o}C and the pellet resuspended in 1ml of Trizol. To this Trizol reagent, 200µl of chloroform was added and samples were shaken vigorously for 15 seconds before being left to incubate at room temperature for 15 minutes. Samples were then centrifuged at 12,000 x g for 15 minutes at 4^{o}C, producing 3 distinct phases; an upper clear aqueous phase, a cloudy interphase, and a lower red organic phase.

For RNA extraction, the upper aqueous phase was removed and transferred to a new 1.5ml Eppendorf tube. To this, 500µl of isopropanol and 1µl of glycogen were added and the samples were then mixed and left to incubate at room temperature for 10 minutes. Samples were then centrifuged at 12,000 x g for 10 minutes at 4^{o}C, producing a pellet of RNA. Supernatant was removed and the pellet was washed by adding 1ml of 75% ethanol and mixing. Samples were then centrifuged again at 12,000 x g for 5 minutes at 4^{o}C before the supernatant was removed and the pellet left to air dry in a clean fume hood for 5 minutes. RNA pellets were then resuspended in 20µl of nuclease-free water and stored at -80^{o}C until quantification.

For DNA extraction, a back-extraction buffer was made by measuring 150ml of nuclease-free water and dissolving 118g of Guanidine Thiocyanate (4M), 3.7g of sodium citrate (50mM) and 30.3g of Tris base (1M). 500µl of back-extraction buffer was added to the remainder of the Trizol solution (interphase and red organic phase) and mixed thoroughly for 3 minutes. Samples were then centrifuged at 12,000 x g for 30 minutes at room temperature, forming a clear upper layer and red lower layer. The clear upper layer was discarded and 400µl of isopropanol and 1µl of glycogen were added to the lower layer. Samples were then mixed and incubated at -20°C for 15 minutes. Samples were then centrifuged at 12,000 x g for 15 minutes at 4°C, forming a pellet of DNA. Supernatant was removed and the pellet was washed by adding 1ml of 75% ethanol and mixing. Samples were then centrifuged at 12,000 x g for 5 minutes at 4°C and the pellets then left to air dry in a clean fume hood for 5 minutes. After drying, pellets were resuspended in 50µl of TE buffer and incubated at 60°C for 5-10 minutes, until the pellet had fully dissolved. Samples were then stored at -20°C until quantification.

For quantification of DNA and RNA, samples were run on a Qubit 4 Fluorometer using DNA BR Assay and RNA BR Assay kits, following manufacturer's instructions. For analysis of RNA quality, samples were run on an Agilent 4200 TapeStation System using Agilent High Sensitivity RNA Screentape, following manufacturer's instructions. This system outputs an RNA Integrity Number (RIN): a score of RNA degradation on a scale of 1 to 10, in which 1 indicates complete degradation and 10 indicates no degradation. The DNA and RNA quantity and quality of each sample and backup are given in Table 3.3.

Sample ID	Number of cells	Total DNA (ng)	DNA 260/280 value	Total RNA (ng)	RIN
Run 4 - Neurons	37021	601	1.62	940	7.2
Run 4 - Microglia	28104	427	1.69	791	7.9
Run 4 - Backup	-	3760	1.76	5510	9.1
Run 5 - Neurons	33077	503	1.66	897	6.9
Run 5 - Microglia	30103	412	1.70	631	8.1
Run 5 - Backup	-	4103	1.84	4755	9.0

Table 3.3: DNA & RNA analysis from test samples
DNA & RNA were extracted from neurons and microglia isolated via FACS, as well as backups of unsorted cell suspension. DNA & RNA quantity of each sample was measured using a Qubit 4 Fluorometer. DNA quality was analysed using a NanoDrop 2000 Spectrophotometer and RNA quality was analysed using an Agilent 4200 TapeStation System.

3.3: Discussion

This chapter has covered the development of a protocol to isolate neurons and microglia from ischemic rat brain, beginning by analysing the widely available methods of cell isolation; then setting out the aims and requirements/considerations of the full study; and finally covering each stage of development of a robust protocol for the FACS sorting of rat brain tissue.

Considering the original aims of the study, some compromises have had to be made in order to produce reliable FACS isolation of neurons and microglia. Namely, the aim of analysing cortical and striatal tissue separately has been forsaken, since it was found that increasing the amount of starting tissue by analysing both brain areas together was required to produce a sufficient number of cells. Whilst this is unfortunate, these brain areas were previously analysed separately in Chapter 2 of this thesis with regards to post-stroke 5hmC expression, which previous research has not considered.

The potential aim of separating 'active' and 'inactive' microglia has also been discarded, as it cannot be determined whether the CD68-PEVio770 antibody is staining cells effectively. In either case, separating the already small number of microglia into 'active' and 'inactive' groups is likely to mean that not enough DNA and RNA will be extracted from the resulting populations. It is for these reasons that the CD68-PEVio770 antibody will not be included in the full experiment.

All other requirements and considerations of the study previously listed in section 3.1.3 have been accounted for in the final protocol: a process of debris elimination has been incorporated into the protocol in order to remove the high amount of myelin and fatty tissue found in the brain; many steps have been taken to maintain RNA integrity through to the end of the experiment; changes have been made to the protocol in order to maximise the final cell numbers (and therefore subsequent DNA & RNA yields); and the protocol has been tested multiple times and performed reliably.

As seen from the values in Table 3.3, the populations of cells sorted by FACS produce measurable amounts of DNA in the range of 400-600ng. For the planned downstream applications (quantification of 5mC and 5hmC through use of ELISA plates), the absolute minimum amount of DNA required is 200ng, though 400ng is ideal. Evidently, acquiring around 30,000 cells produces just enough DNA for this requirement. This means that if there are samples in the full experiment from which less than around 30,000 cells can be collected, there is a chance that not enough DNA can be extracted from that sample. Fortunately, the backups taken from the unsorted cell suspension provide much more DNA, in the range of around 4μg. In the case that cell numbers are low, and samples do not provide enough DNA, then backups taken from cell suspension could possibly be used instead. This is not ideal, as

it would mean that DNA is not from a specific cell type, though it may still be of interest to analyse.

With regards to RNA, cells sorted via FACS produce measurable RNA quantities in the range of 600-1000ng. As expected, backup samples taken from unsorted cell suspension produce much more RNA, in the range of 4-5µg. Also, RNA samples taken from the backup samples appear to be of high quality, with little degradation as evidenced by RINs around 9. The RNA samples extracted from FACS-sorted cells appear to exhibit slightly more degradation, with RINs in the range of 6.5-8. Although, this is to be expected, as the FACS protocol takes a number of hours to carry out during which time the RNA in the cells is undergoing degradation. However, the many precautions taken to preserve RNA quality (including clearing all solutions of nucleases, working in a nuclease-free environment, adding RNAlater to buffers where possible, and sorting cells directly into Trizol solution) appear to have helped retain some RNA integrity as the samples are not completely degraded, and are still suitable for downstream applications such as RT-qPCR and possible RNA sequencing.

Analysis of DNA and RNA samples extracted from sorted cells revealed that collecting less than 30,000 cells means that there is a chance that not enough DNA will be collected at the end of the experiment. This scenario seems most likely in animals that have undergone ischemic stroke, as the test run performed on an ischemic brain in this chapter (Figure 3.9) produced less neurons than the test runs performed on healthy brains (Figures 3.7 + 3.8). Therefore, a contingency plan has been implemented in which backup DNA and RNA is extracted from cell suspension that is taken prior to staining, with analysis showing that these backups produce large quantities of high quality DNA and RNA that can be used in the case of low cell numbers after FACS (Table 3.3). Although this cell suspension to heterogenous and does not allow for the downstream analysis of neurons and microglia in isolation, the results

will still be relevant as despite the fact that data from whole tissue was obtained in Chapter 2 of this thesis, the timepoint studied in this chapter (2 weeks post-stroke) was not tested in Chapter 2. Furthermore, the use of a commercially available ELISA kit for the analysis of 5mC content will allow for the quantitative measurement of global 5mC levels, which was not possible in Chapter 2.

The many rounds of testing and development have led to the formation of a FACS protocol that accurately and reliably stains and isolates neuronal (NeuN+) and microglial/macrophage ($CD11b^{+}/CD45^{low}$) cells, producing cell populations with high purity (Figure 3.11).

Chapter 4: Methylomic response to stroke in specific cell types

4.1: Introduction

In Chapter 2 of this thesis, immunohistochemistry was used in order to elucidate an intrinsic epigenetic response of the CNS to ischemic stroke. This response involved a delayed increase in global hydroxymethylation in various brain areas affected by stroke as part of an apparent demethylation event. Whilst the use of immunohistochemistry successfully identified differences in this epigenetic response between brain areas, elucidating differences between specific cell types was not successful, due to poor staining of cell type markers (in the case of neurons; NeuN) or a lack of observed 5hmC co-staining (in the case of microglia; Iba1). As a result of this, 5hmC levels in all cell types were analysed simultaneously. Analysis of the epigenetic response to ischemic stroke in these specific cell types is of great interest as it may allow for the development of a targeted post-stroke therapeutic treatment to promote axonal regeneration and aid recovery. To this end, a method of isolating neurons and microglia from post-ischemic adult rat brains was developed in Chapter 3 of this thesis.

4.1.1: Importance of isolating and analysing neurons

The working theory developed from the results displayed in Chapter 2 is that neuronal cells exhibit increased 5hmC levels following ischemic stroke as genes promoting axon growth/regeneration and synaptogenesis undergo demethylation and become primed for expression. Although neuronal cells exhibit around 10x higher 5hmC levels than other cell types of the CNS (Kriaucionis & Heintz, 2009; Szulwach et al., 2011) and it is therefore likely

that the majority of positive 5hmC staining observed in those experiments was due to neuronal cells, it cannot be determined for certain that this effect is specific to neuronal cells as all cell types were analysed together in Chapter 2. Analysis of (hydroxy)methylation in neuronal cells collected via the method developed in Chapter 3 will help to investigate the working theory by ascertaining whether this effect is observed specifically in neuronal cells.

Additionally, another limitation of the experiments performed in Chapter 2 was that only analysis of 5hmC levels was possible, as staining of 5mC and 5caC was not of high enough quality for quantitative analysis. By collecting specific cell types and utilising the immuno dot-blot method of quantification adapted to an ELISA format (section 2.1.4), both 5mC and 5hmC levels can be analysed. This will also help to further investigate the working theory that the observed post-stroke increases in 5hmC levels lead to a decrease in genome-wide 5mC levels.

Furthermore, by extracting RNA from isolated neurons, it is possible to analyse mRNA expression levels of not only Tet enzymes, but also neurotrophic factors and axon growth-related genes such as BDNF and Ttll7. Ttll7 is a neuron-specific protein that promotes neurite growth and is shown the be upregulated following ischemic stroke in the sprouting neurons of young adult mice (Li et al., 2010). Analysing the expression of these genes of interest in neuronal cells will help to further elucidate a mechanism by which altered 5hmC levels influence the expression of axon growth-related genes.

4.1.2: Importance of isolating and analysing microglia

Although the lack of 5hmC staining in microglial (Iba1+) cells in Chapter 2 suggests that the observed increase in post-stroke 5hmC levels does not involve microglia, investigating the epigenome in these cells post-stroke may reveal a potential role of DNA (hydroxy)methylation

in the control of post-stroke microglial activity. The absence of visible 5hmC staining in Iba1+ cells may be due to the fact that microglial cells have far lower levels of 5hmC present than neurons, as previously mentioned. However, utilisation of a more sensitive ELISA format of immuno-dot blot quantification of 5hmC in this chapter may elucidate an epigenetic response to ischemic stroke that is specific to microglia/macrophages.

As previously described in the introductory chapter of this thesis (section 1.1.2), ischemic stroke leads to the initiation of an immune response which involves the 'activation' of resident microglia (into either pro- or anti-inflammatory phenotypes) as well as the infiltration of peripheral macrophages due to deterioration of the blood-brain barrier (Iadecola & Anrather, 2011). Some previous research has demonstrated that these activated microglia and macrophages can be detrimental to axon growth and neurogenesis. For example, the pro-inflammatory M1 phenotype microglia have been shown to inhibit neurite outgrowth *in vitro* and cause axonal dieback *in vivo* (Kitayama et al., 2011). However, investigations into the anti-inflammatory M2 phenotype have suggested that M2 microglia/macrophages promote axon growth and neurogenesis following CNS injury through release of neurotrophic factors such as BDNF and GDNF (glial cell-derived neurotrophic factor) (Batchelor et al., 2002). Furthermore, research has also found that phagocytic microglia and macrophages actively clear cellular debris following CNS injury, which is considered an obstacle for post-injury axonal outgrowth. Tanaka et al. (2009) found that LPS- (lipopolysaccharide) activated microglia clear axonal debris and allow co-cultured cortical neurons to regrow following mechanical axotomy. A similar effect was determined *in vivo* when it was found that following spinal cord injury in mice, microglia containing phagocytic material make contact with injured neurons 24h after injury, followed by contact with phagocytic peripheral macrophages that persists up to 42 days post-injury (Greenhalgh & David, 2014). These findings demonstrate a varied response of microglia & macrophages to CNS injury that can be either beneficial or

detrimental to axonal regrowth, seemingly dependent on the polarisation of the immune cells towards the pro-inflammatory M1 phenotype or the anti-inflammatory M2 phenotype.

In the context of ischemic stroke, treatment with minocycline, a selective inhibitor of M1 microglia, has been found to promote neurogenesis when administered as a delayed treatment (4-6 days post-stroke), but suppresses neurogenesis when given immediately following stroke and administered chronically (Kim et al., 2009; Liu et al., 2007). Additionally, it has been found that following transient MCAO in rats, M2 microglia/macrophages enhance axon growth and neurogenesis by releasing trophic factors such as galectin-3 (Yan et al., 2009). Taken together, these findings hint at a dynamic role of microglia and macrophages in the promotion and suppression of post-stroke axon growth and neurogenesis. Identifying changes in microglia/macrophage activation state and any epigenetic changes that occur alongside them is one of the aims of this chapter and may reveal an intrinsic immune response to stroke that is mediated by DNA (hydroxy)methylation and could therefore indirectly affect axon growth.

4.1.3: Objectives & Hypotheses

The objectives of this chapter are as follows:

- Determine changes in post-stroke global 5mC levels in neurons and microglia independently
- Determine changes in post-stroke global 5hmC levels in neurons and microglia independently
- Assess mRNA levels of BDNF, Ttll7, Tet1, Tet2 and Tet3 in neurons following MCAO

Based on previous research carried out in this area, the hypotheses for the findings of this chapter are as follows:

- Levels of global 5mC will be significantly decreased in neurons following MCAO
- Levels of global 5hmC will be significantly increased in neurons following MCAO
- Global levels of 5mC and 5hmC in microglia will not be significantly different following MCAO
- mRNA levels of BDNF, Ttll7, Tet1, Tet2 and Tet3 in neurons will be significantly increased following MCAO

4.2: Methods

4.2.1: Experimental design

Note: The animals included in the experiment detailed in this chapter were a subset of animals from a larger study that also assessed post-stroke infection. This following section will only detail the procedures carried out on the animals that were used to assess post-stroke DNA methylation changes.

All experiments were performed according to the UK Animals (Scientific Procedures) Act 1986 under a project license from the UK Home Office. All surgical procedures (section 4.2.2) were carried out by Rebecca Trueman and Clare Spicer. MRI scanning was performed by Malcolm Prior and David Watson. LPS/saline injections were carried out by Rebecca Trueman.

Male Wistar rats weighing 350-450g (Charles River, UK) were used for this study. Animals were housed in groups of four, in IVC cages under standard conditions (see section 2.2.1) and had unlimited access to food and water throughout the study. Supplementary softened food was provided once prior to surgery and daily post-surgery. Animals were weighed and health monitored weekly prior to surgery and 4 times a day in the first 48 hrs, and daily subsequently (at a minimum, following the IMPROVE guidelines (Percie du Sert et al., 2017)).

Animals underwent 1 hour middle cerebral artery occlusion (MCAO) or an equivalent sham surgery. 24 hours post-surgery, animals underwent MRI scanning to determine infarct volume. These infarct volumes were then used to perform stratified randomisation in order to allocate animals to saline or LPS groups. Fourteen days following surgery, animals were euthanised and perfused with saline. Brains were collected and the cortex and striatum of the

infarcted hemisphere dissected for subsequent homogenisation and FACS. The number of animals used for each experimental group is shown in Table 4.1.

Group	Initial Number of Animals	Animals Excluded	Animals taken for alternative study	Final Number of Animals
Sham	16	2	7	7
MCAO	28	12	8	8

Table 4.1: The number of rats used to assess cell-specific post-stroke 5mC/5hmC levels
Rats underwent 1 hour middle cerebral artery occlusion (n=28) or an equivalent sham surgery (n=16). Sham surgery animals were excluded due to anaesthetic related death (n=2). MCAO animals were excluded due to severity of stroke (n=10), abnormal brain structure (abnormally large ventricles seen in MRI; n=1) or lack of stroke (no stroke symptoms during occlusion or infarct < 500mm^3; n=1). From the remaining rats, some were taken for use in an alternative study focused on post-stroke infection, and the rest were used in the current study.

4.2.2: Surgical procedures

4.2.2.1: Middle cerebral artery occlusion

Surgery to occlude the right MCA was performed as described in Chapter 2 (section 2.2.2), with the following differences:

- Prior to first incision, Lidocaine (0.5%, (stock solution 2%; Hameln Pharmaceuticals, UK) was administered as a local anaesthetic (line block via subcutaneous injection, 7mg/kg maximum dose)
- The MCAO was occluded for 1 hour using a silicone coated filament with a diameter of ~0.39mm (Doccol, US).

- A laser doppler was used to confirm occlusion of the MCA (details provided below). Both MCAO and Sham animals underwent the surgical procedures necessary for the placement of the laser doppler probe.

4.2.2.2: Laser Doppler Placement and Monitoring

Before surgery to induce the stroke began, a laser doppler probe was placed against the skull (moorVMS-LDF1; Moor Instruments, UK). To allow placement of the laser doppler probe, an incision was made between the eye and ear on the right side of the head. A hole was then made in the temporal muscle so that the probe could rest against the skull. Blood flow was then monitored as the filament was being moved through the ICA, with a drop in blood flow indicating occlusion of the MCA. Once the occlusion was confirmed, the laser doppler was removed and incision closed so that the animals could recover from the anaesthetic during the occlusion period.

4.2.3: MRI scanning & infarct volume analysis

24 hours post-surgery, animals were once again anaesthetised using 5% isoflurane (100% w/w, 250ml; Abbott, US), and during scanning were maintained using 1-2.0% isoflurane in 0.6 NLt/min O_2 and 0.8NLt/min N_2O. Animals were placed into a 7 Tesla Biospec with rat head surface coil (Bruker BioSpo, Ettlingen, Germany) to carry out T_2 mapping. A spin echo T_2 weighted sequence was then performed (TR/TE = 5000/8 ms, 16 echoes; field of view: 32 x 32mm; matrix: 128 x 128; thirteen 1mm thick contiguous coronal slices; acquisition time = 10 minutes). These echoes were then collated to create T_2 maps using ITK-SNAP software (Yushkevich et al., 2006).

Infarct volumes were measured using ImageJ software. As previously described in Chapter 2 (section 2.2.5.3), infarct volume was calculated as a percentage of the volume of the contralateral hemisphere in order to account for oedema. Only sections that correspond to the dissected tissue were measured.

4.2.4: Tissue collection

Animals were euthanised using intraperitoneal injection of Euthatal (200mg, Merial Animal Health Ltd, UK). After injection, animals were left in a transport cage until they had no toe or corneal reflexes and breathing had just ceased. At this point animals were perfused via the left ventricle with PBS containing 5% RNAlater until the solution ran clear. Brains were then removed and placed onto sterile petri dishes. The cortex and striatum of the infarcted hemisphere (or hemisphere of sham surgery in sham animals) were then dissected from the rest of the brain and taken for homogenisation.

4.2.5: Staining & FACS

The development of this protocol is detailed in Chapter 3 of this thesis. The details of the final protocol are as follows:

The cortex and striatum were placed onto a sterile petri dish and were finely minced using a clean razor blade, performing 25 chops in each orthogonal direction. Tissue was then transferred to a 15ml glass Dounce homogeniser containing 10ml of 1X HBSS. Tissue was homogenised by 40x passes with a glass large clearance pestle. The resulting homogenate was then transferred into a sterile 50ml Falcon tube through a 40µm cell filter.

From this 10ml of tissue homogenate, a 'total cell population' source of DNA and RNA was produced by aliquoting 500µl into a sterile 1.5ml Eppendorf tube. This was then centrifuged at 500 x g for 5 minutes at 4^{o}C. The resulting cell pellet was resuspended in 500µl of Trizol solution and stored at -20^{o}C until DNA and RNA extraction was performed later the same day. Additionally, a further 500µl of homogenate was aliquoted into a sterile 1.5ml Eppendorf tube and snap frozen in isopentane for future use in an alternative experiment.

The remaining 9ml of tissue homogenate was divided into two 4.5ml aliquots in 15ml Falcon tubes. Each aliquot then underwent a different method of debris exclusion for the isolation of neuronal nuclei and microglial cells:

Debris exclusion for neuronal cells:

1ml of 1.1M sucrose was placed at the bottom of a 15ml falcon tube. The 4.5ml of tissue homogenate was carefully layered on top of the sucrose using a P1000 pipette and then centrifuged at 1300 x g for 15 minutes at room temperature. Following this, a cell pellet was visible at the bottom of the tube whereas myelin and other debris settled at the cell suspension/sucrose interface. Debris and supernatant were removed, and the cell pellet was resuspended in 500µl of 1X HBSS.

Debris exclusion for microglial cells:

A solution of stock isotonic Percoll (SIP) is made by combining 90ml of Percoll with 10ml of 10X HBSS. From this SIP stock, a 35% SIP solution was made by combining 35ml of SIP with 65ml of 1X HBSS.

The 4.5ml of tissue homogenate was centrifuged at 500 x g for 5 minutes at 4^{o}C. The cell pellet was then resuspended in 8ml of 35% SIP solution and transferred to a 15ml falcon tube. 5ml of 1X HBSS was carefully layered atop the cell suspension using a P1000 pipette.

The solution was then centrifuged at 800 x g for 30 minutes at room temperature. Following centrifugation, microglial cells pelleted at the bottom of the tube whereas myelin and other debris settled at the interface between the 35% SIP solution and 1X HBSS. Debris and supernatant were removed, and the pellet was resuspended in 500µl of 1X HBSS.

Following debris exclusion, an equal volume (500µl) of ice-cold ethanol was added to each aliquot of cells and these were then left to incubate at -20^{o}C for 10 minutes. Following this, samples were centrifuged at 500 x g for 5 minutes at 4^{o}C and the resulting cell pellets were resuspended in 1ml of FACS buffer (PBS w/ 0.5% Bovine Serum Albumin + 5% RNAlater) containing 1µg/ml Hoechst 33342. To the samples containing neuronal nuclei, 4µl of NeuN-PE antibody was added. To samples containing microglial cells, 4µl of CD11b-FITC and CD45-APC antibodies were added. Samples were then left to incubate in the dark at 4^{o}C for 30 minutes with constant end-over-end rotation. Samples were then centrifuged at 500 x g for 5 minutes at 4^{o}C, resuspended in 500µl of FACS buffer and taken for FACS.

A total of between 3 and 7 animals were processed each day over the course of two weeks. All flow cytometry and cell sorting was performed on the Beckman Coulter MoFlo XDP. Cells were sorted directly into Eppendorf tubes containing 1ml of Trizol solution.

4.2.6: Issue with neuronal cell isolation

As previously described in Chapter 3 of this thesis (section 3.2.5), a minimum of around 30,000 cells was needed from each sample in order to produce a sufficient amount of DNA and RNA for downstream applications. Unfortunately, when isolating neurons in this experiment, this

cell number was not reached. Though a clear population of NeuN+ cells was visible, the number of cells in this population did not meet the minimum requirement.

Ten animals were processed across the first three days of the experiment. From these ten animals, the number of NeuN+ cells collected from these animals ranged from 3,000 to 20,000 cells; far below the previously set threshold. The issue appeared to be due to the sucrose density gradient, as the resulting cell pellet appeared smaller than in test runs performed in the development of the method. Despite failed attempts to rectify this issue on days 2 and 3 of the experiment (including increasing centrifugation speed and changing the temperature of the sucrose), the decision was made that from day 4 onwards, no neuronal isolation would be carried out on subsequent animals in the interest of saving on time, costs and tissue. Instead, for the remaining 20 animals, 5ml of tissue homogenate would be collected and used as a source of backup DNA and RNA, accounting for the 4.5ml of tissue homogenate that was originally designated for neuronal isolation. For downstream applications, these backup sources of DNA and RNA would be tested in place of DNA and RNA from neuronal populations.

4.2.7: DNA & RNA extraction

Immediately following FACS, extraction of DNA and RNA from sorted cells and backup samples was performed exactly as described in Chapter 3 of this thesis (section 3.2.5). For quantification of DNA and RNA, samples were run on a Qubit 4 Fluorometer using DNA BR Assay and RNA BR Assay kits, following manufacturer's instructions.

4.2.8: 5mC & 5hmC quantification

Total 5mC and 5hmC content of DNA samples were measured using the Quest 5mC DNA ELISA Kit and Quest 5hmC DNA ELISA Kit (Zymo Research, USA) following the manufacturer's instructions. In short, polyclonal antibodies targeting 5mC or 5hmC were immobilised to the well surface. Single stranded DNA was then added, which binds to these antibodies. This DNA was then probed by anti-DNA HRP antibodies, and subsequent addition of HRP developer produced a green-blue colour in wells containing 5mC- or 5hmC-DNA. Following the final step of colour development, the absorbance at 405nm was measured using a SpectraMax M2e Microplate Reader (Molecular Devices, USA). 100ng (for 5mC ELISA) or 50ng (for 5hmC ELISA) from each sample were tested. For microglial cells, the low amount of DNA collected meant that samples could not be run in duplicate. All other samples were run in duplicate. Standard curves for 5mC and 5hmC kits produced R^2 values of 0.96 and 0.95, respectively (curves shown in Appendix A2).

4.2.9: Reverse transcription & qPCR

500ng of RNA from each sample was used to perform reverse transcription and synthesise cDNA using ReadyScript cDNA Synthesis Mix (Sigma Aldrich, UK). In short, 4µl of ReadyScript was added to 500ng of RNA in 16µl of nuclease-free water, producing a total reaction volume of 20µl. Samples were then heated to 25^{o}C and incubated for 5 minutes, before being heated to 42^{o}C and incubated for a further 30 minutes. The reaction was then inactivated by heating samples to 85^{o}C and incubating for 5 minutes. The resulting samples of cDNA were then kept at 4^{o}C until real-time polymerase chain reaction (RT-PCR). Prior to qPCR, cDNA samples were quantified using a Qubit 4 Fluorometer and DNA BR Assay kits, following manufacturer's instructions.

cDNA samples were then used to perform RT-PCR to determine mRNA expression levels of genes of interest. TaqMan Gene Expression Assays were purchased from ThermoFisher Scientific (UK) that target Tet1 (Assay ID: Rn01428192_m1), Tet2 (Assay ID: Rn01522037_m1), Tet3 (Assay ID: Rn01425643_m1), brain-derived neurotrophic factor (BDNF) (Assay ID: Rn02531967_s1) and Tubulin tyrosine ligase like 7 (Tubulin polyglutamylase; Ttll7) (Assay ID: Rn01522232_m1).

In short, 50ng of cDNA was added to 0.5µl of TaqMan Assay Mix and 5µl of TaqMan Fast Advanced Master Mix (ThermoFisher, UK). The reaction volume was then made up to 20µl using nuclease free water. A StepOnePlus Real-Time PCR System (Applied Biosystems, USA) was then used to perform the following RT-PCR protocol: hold at 50^{o}C for 2 minutes; hold at 95^{o}C for 2 minutes; then 40 PCR cycles of 95^{o}C for 1 second and 60^{o}C for 20 seconds. All samples were run in triplicate. As RNA extracted from sorted microglia was required for an alternative experiment, only RNA samples extracted from total cell population were analysed.

In order to calculate relative expression levels of genes of interest, an endogenous reference (housekeeping) gene was also analysed: HPRT1 (Assay ID: Rn01527840_m1). HPRT1 expression was found to not be significantly different between sham and MCAO groups (see Appendix A3). C_T values of HPRT1 and genes of interest were then used to determine relative expression of genes of interest (expressed as fold difference) using the Pfaffl method (Pfaffl, 2001).

4.2.9: Statistical analysis

Data is presented as mean ± standard deviation (SD). Statistical analysis was performed using GraphPad Prism 7. Normality of all data was confirmed using the D'Agostino normality test. CD11b expression data and 5mC & 5hmC content data were analysed using unpaired t-tests. For correlational analysis, Pearson correlation coefficient was utilised. For qPCR data, unpaired t tests were used to compare relative expression levels between groups. Differences were considered significant if $p \leq 0.05$.

4.3: Results

4.3.1: Infarct volumes

Figure 4.1 shows the infarct volumes of MCAO animals, expressed as percentage of the volume of the contralateral hemisphere. Infarct volumes range from between 5-35%; though variable, these volumes are comparable to those seen in previous publications that have utilised this same model of ischemic stroke (Trueman et al., 2017). T_2 weighted images of infarcted brains are shown in Figure 4.2.

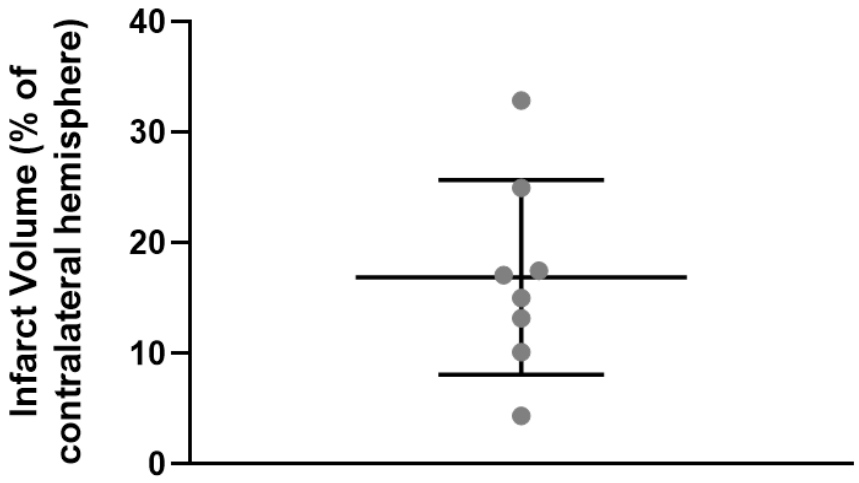


Figure 4.1: Infarct volumes of rats that have undergone MCAO surgery
Male Wistar rats (n=8) underwent transient (1 hour) MCAO and were later subjected to MRI scanning to calculate infarct volume. Infarct volume was calculated as % of volume of contralateral hemisphere. Data is presented as mean ± SD.

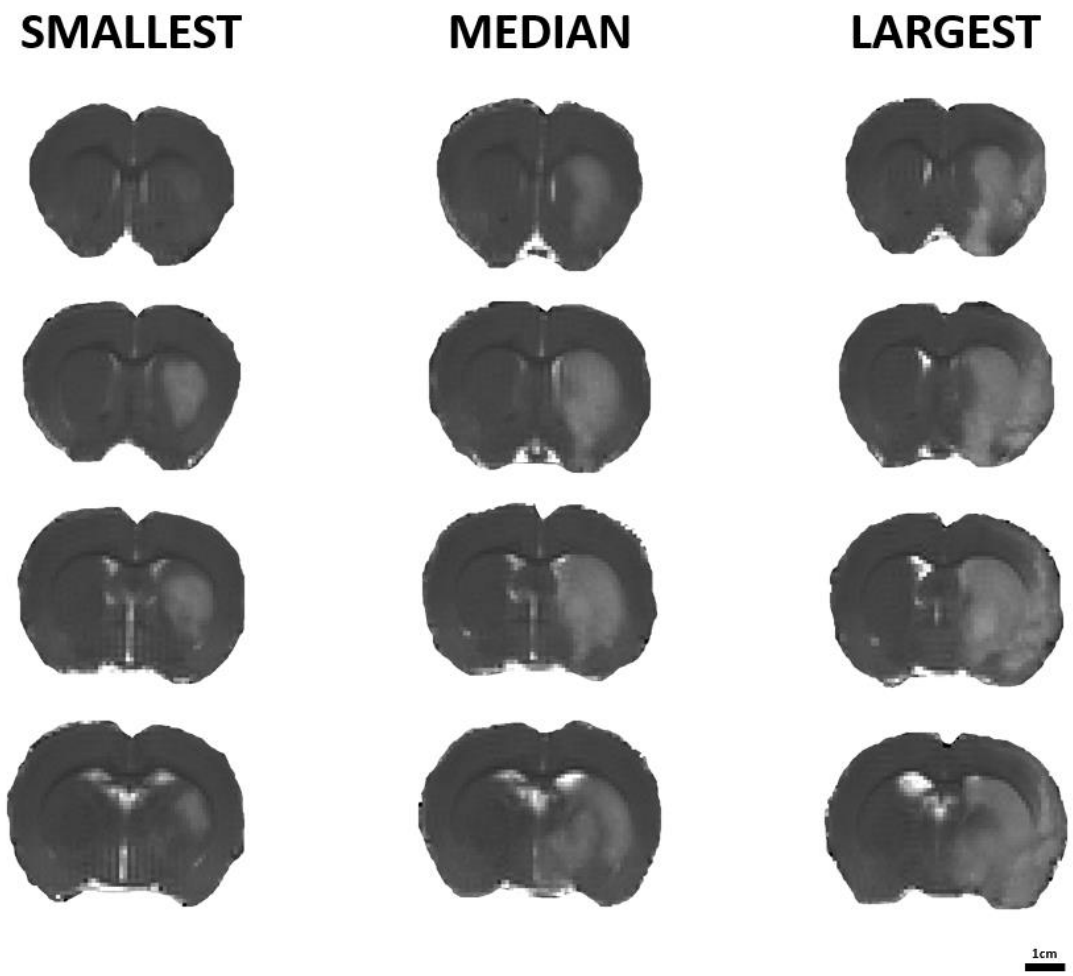


Figure 4.2: T_2 weighted images of rats that have undergone MCAO surgery
Male Wistar rats underwent surgery to transiently occlude the MCA (1 hour). 24 hours post-surgery, rats underwent MRI scanning to produce T_2 maps for use in assessing infarct volume. In these images, infarcted tissue appears as lighter in colour than non-infarcted tissue. Above shows the smallest sized infarct (*left*), median infarct (*centre*) and the largest infarct (*right*) from animals used in the study. Scale bar = 1cm.

4.3.2: Microglial staining & sorting

Figure 4.3 shows examples of microglial staining in an unstained control, sham animal and an MCAO animal. In some MCAO animals, two distinct populations of CD11b+ cells could be seen, categorised as CD11b-int and CD11b-high. Though existing as two distinct populations, CD11b-int and CD11b-high populations were sorted and collected together in order to maximise cell number and subsequent DNA and RNA quantity.

Of the 30 animals from which microglial cells were isolated, 5 were excluded from downstream analysis due to insufficient number of cells collected. Of these 7 animals, 4 were from the sham group and 1 was from the MCAO group.

4.3.3: Microglial CD11b expression

The populations of CD11b-high microglia (Figure 4.3) were quantified as a percentage of total Hoechst+ cells. There was a significantly higher proportion of CD11b-high cells in the MCAO group in comparison to the sham group (Figure 4.4; $t_8=5.11$, $p<0.001$).

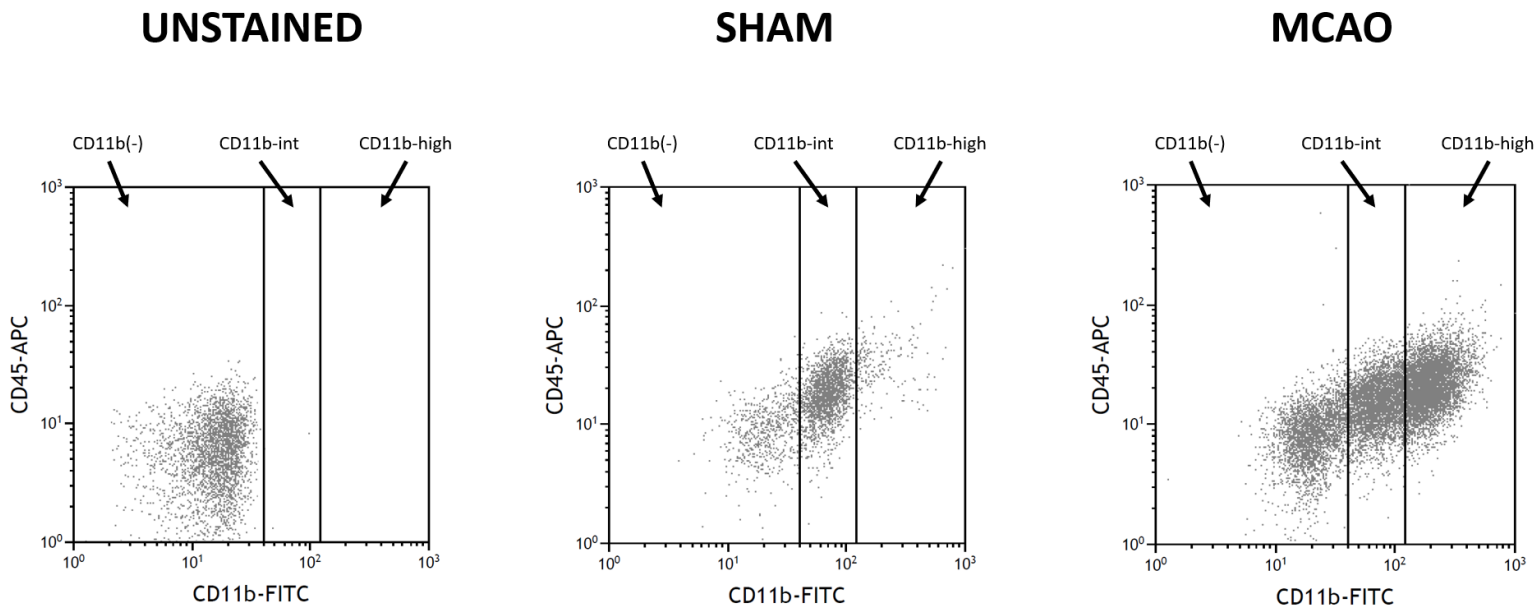


Figure 4.3: Phenotypic profile of microglia analysed by flow cytometry
Flow cytometry dot plots of cells taken from the cortex and striatum of rats that underwent MCAO or equivalent sham surgery. Each image represents one sample taken from each of the experimental groups. *Left:* Hoechst+ cells that were not probed with any antibodies are used to set gates for positively stained cells in subsequent analyses. Gates are set such that almost all unstained cells fall within the CD11b-negative (CD11b(-)) gate. *Centre:* Microglia/macrophage cells ($CD11b^{+}/CD45^{low}$) isolated from the cortex and striatum of a rat that underwent sham surgery exhibit mostly intermediate levels of CD11b expression (CD11b-int), with a small subset of CD11b+ cells exhibiting high levels (Cd11b-high). *Right*: Microglia/macrophage cells isolated from the ipsilateral cortex and striatum of a rat that underwent MCAO surgery exhibit higher levels of CD11b. Around 50% of CD11b+ cells in this sample are designated as CD11b-int, and the remaining 50% are designated as CD11b-high.

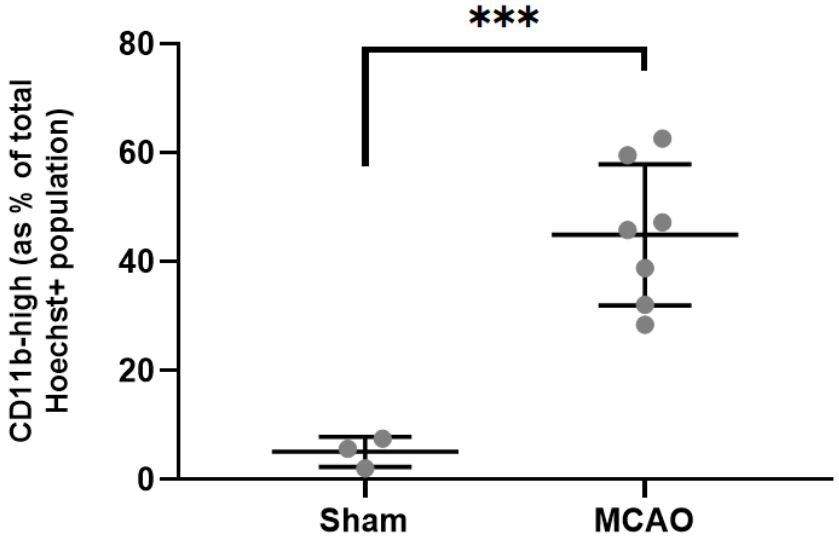


Figure 4.4: Proportions of CD11b-high populations
Microglial cells were isolated from the ipsilateral cortex and striatum of rats that underwent MCAO or sham surgery. Of these microglial cells, CD11b-int and CD11b-high populations were identified. The proportion of CD11b-high cells was significantly higher in MCAO animals (n=7) than sham animals (n=3) ($p<0.001$). Data is presented as mean ± SD. *** represents a highly significant difference ($p<0.001$).

4.3.4: 5mC and 5hmC levels in total cell populations

Though the original aim of this study was to analyse 5mC and 5hmC content of DNA extracted from neurons, issues with collecting low numbers of cells (described in section 4.2.7) meant that backup samples comprising of DNA isolated from the total cell population were analysed instead.

Commercial ELISA kits were used to quantify 5mC and 5hmC content of DNA. There was no significant difference in 5mC content between sham and MCAO groups (Figure 4.5A; $t_{13}=1.4$, $p=0.19$), although 5hmC content was significantly increased in MCAO animals compared to sham animals (Figure 4.5B; $t_{13}=3.37$, $p=0.003$).

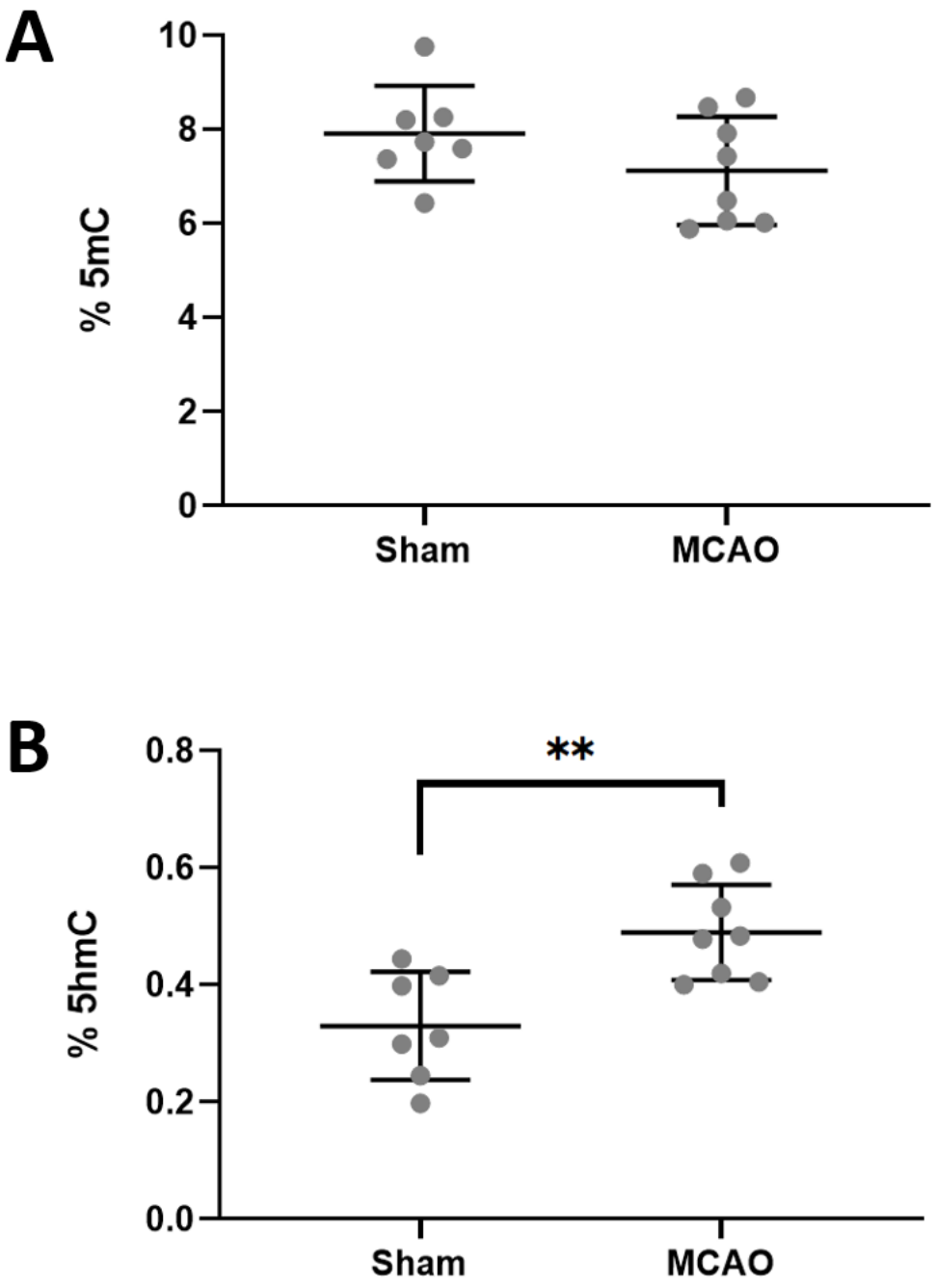


Figure 4.5: 5mC and 5hmC content of DNA from total cell population
DNA was extracted from ipsilateral cortex and striatum of rats that underwent MCAO (n=8) or sham surgery (n=7). 5mC and 5hmC content of these DNA samples was then quantified using ELISA kits. **A**: There was no significant difference in DNA 5mC content between sham and MCAO animals (p=0.19). **B**: There was significantly higher 5hmC content in the DNA of MCAO animals in comparison to sham animals (p=0.003). Data is presented as mean ± SD. ** represents a significant difference (p<0.005).

When correlating 5mC and 5hmC content of total cell population with infarct volume, Pearson correlation coefficient revealed that there is no significant correlation between infarct volume and 5mC content (r=0.07; p=0.87) (Figure 4.6A) or 5hmC content (r=0.31; p=0.45) (Figure 4.6B).

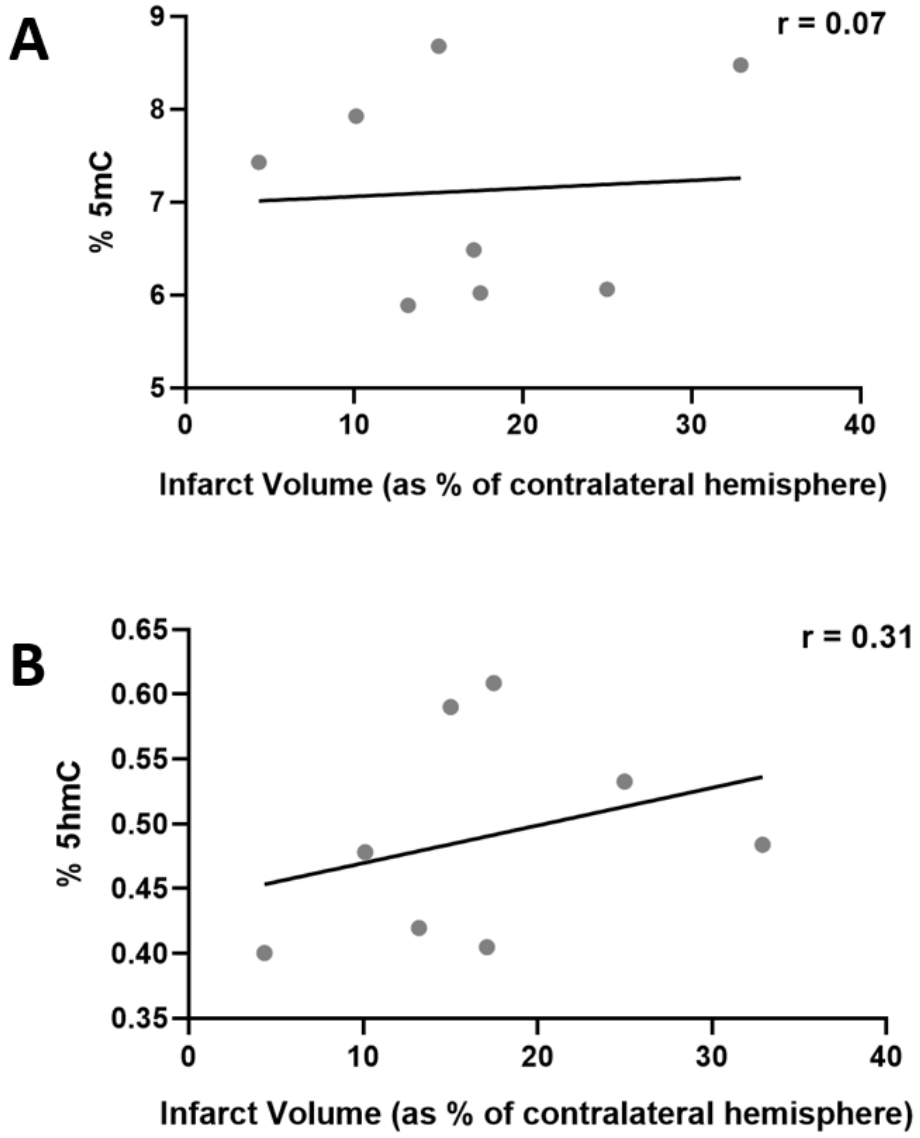


Figure 4.6: Correlation between infarct volume and 5mC and 5hmC content in total cell population

Infarct volumes of rats that underwent transient MCAO were calculated as % volume of contralateral hemisphere. These volumes were then correlated with 5mC and 5hmC levels of DNA obtained from total cell population. No significant correlation was found between infarct volume and 5mC content (**A**; r=0.07; p=0.87) or 5hmC content (**B**; r=0.31; p=0.45).

4.3.5: 5mC and 5hmC levels in microglia/macrophage cells

Microglia/macrophage cells ($CD11b^{+}/CD45^{low}$) were isolated from the ipsilateral cortex & striatum of rats that underwent MCAO or sham surgery. DNA was extracted from these sorted microglia and the 5mC and 5hmC content of these DNA samples was quantified through use of commercial ELISA kits.

As previously mentioned (section 4.3.2), 4 sham animals and 1 MCAO animal were removed from downstream microglial analysis following FACS due to an insufficient number of microglia/macrophage cells being collected. Due to this, the number of sham animals in these analyses was reduced to 3. In an attempt to remedy this, DNA taken from microglial cells of two pilot animals (as part of experiments performed in Chapter 3) was analysed alongside samples from the current experiment. As these test animals received no surgery, they can be considered somewhat analogous to sham animals. They are, however, not part of the current study and as such, their data points are highlighted in results figures, and statistical analysis is reported both with and without the inclusion of these data points.

There was no significant difference in 5mC content between sham and MCAO animals (Figure 4.7A; *with test animals:* $t_{10}=1.98$, $p=0.08$; *without test animals:* $t_{8}=1.21$, $p=0.26$). There was, however, significantly higher 5hmC content in microglial cells of MCAO animals compared to sham animals (only when the test animals are included) (Figure 7.7B; *with test animals:* $t_{10}=2.43$, $p=0.03$; *without test animals:* $t_{8}=1.56$, $p=0.15$).

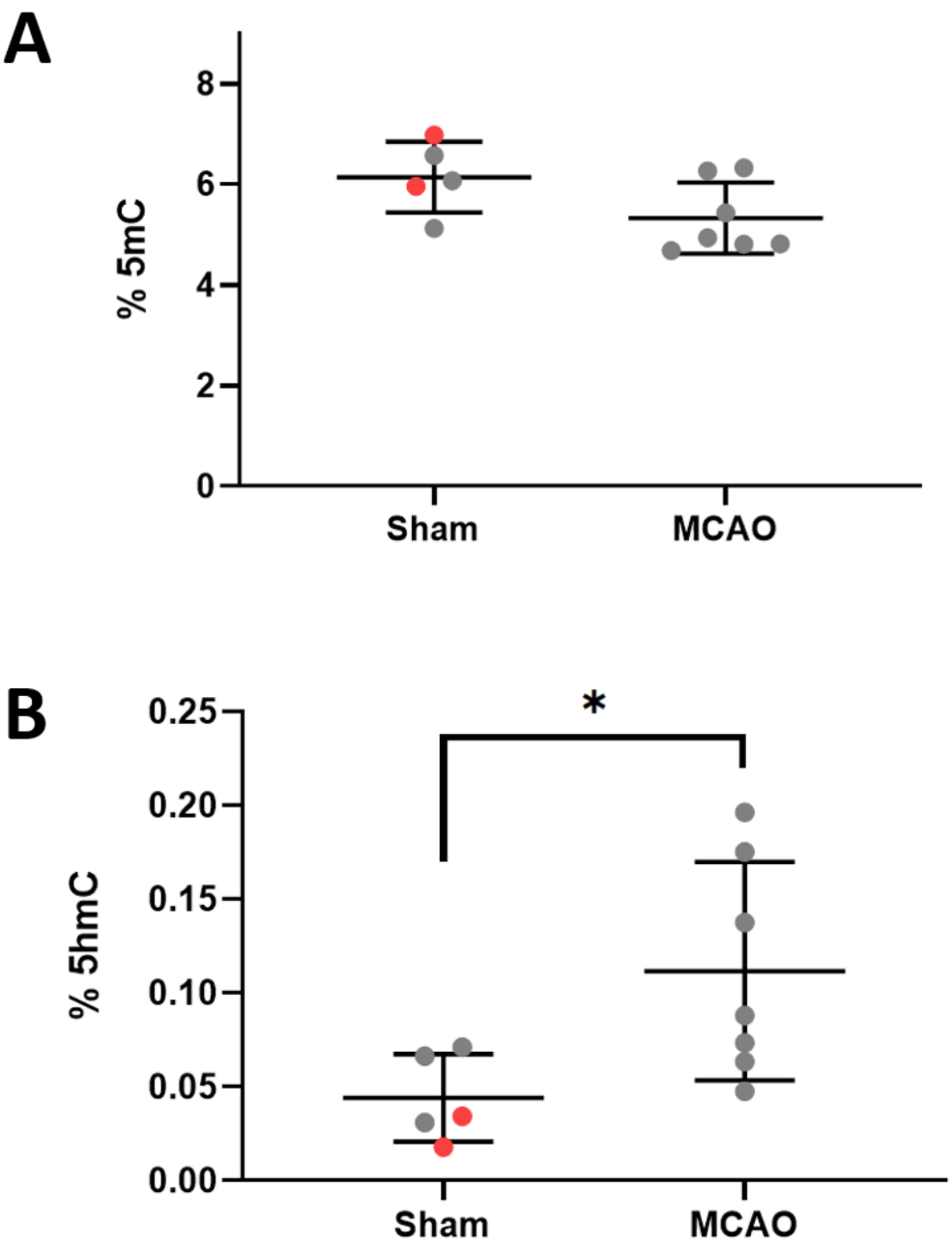


Figure 4.7: 5mC and 5hmC content of DNA from microglia
DNA was collected from microglia/macrophage cells ($CD11b^{+}/CD45^{low}$) that were isolated from the ipsilateral cortex and striatum of rats that had undergone sham (n=3) or MCAO (n=7) surgery. **A**: no significant difference in 5mC content of microglial DNA was found between sham and MCAO groups (p=0.08). **B**: 5hmC content of microglial DNA was found to be significantly increased in MCAO animals (p=0.03). Data is presented as mean ± SD. * represents a significant difference (p<0.05). Red data points represent samples obtained from animals that were not part of the present study (n=2).

When correlating 5mC and 5hmC content of microglia/macrophage cells with proportion of CD11b-high cells, Pearson correlation coefficient revealed that there is no significant correlation between proportion of CD11b-high cells and 5mC content (r=-0.39; p=0.26) (Figure 4.8A) or 5hmC content of microglia/macrophage cells (r=0.43; p=0.21) (Figure 4.8B).

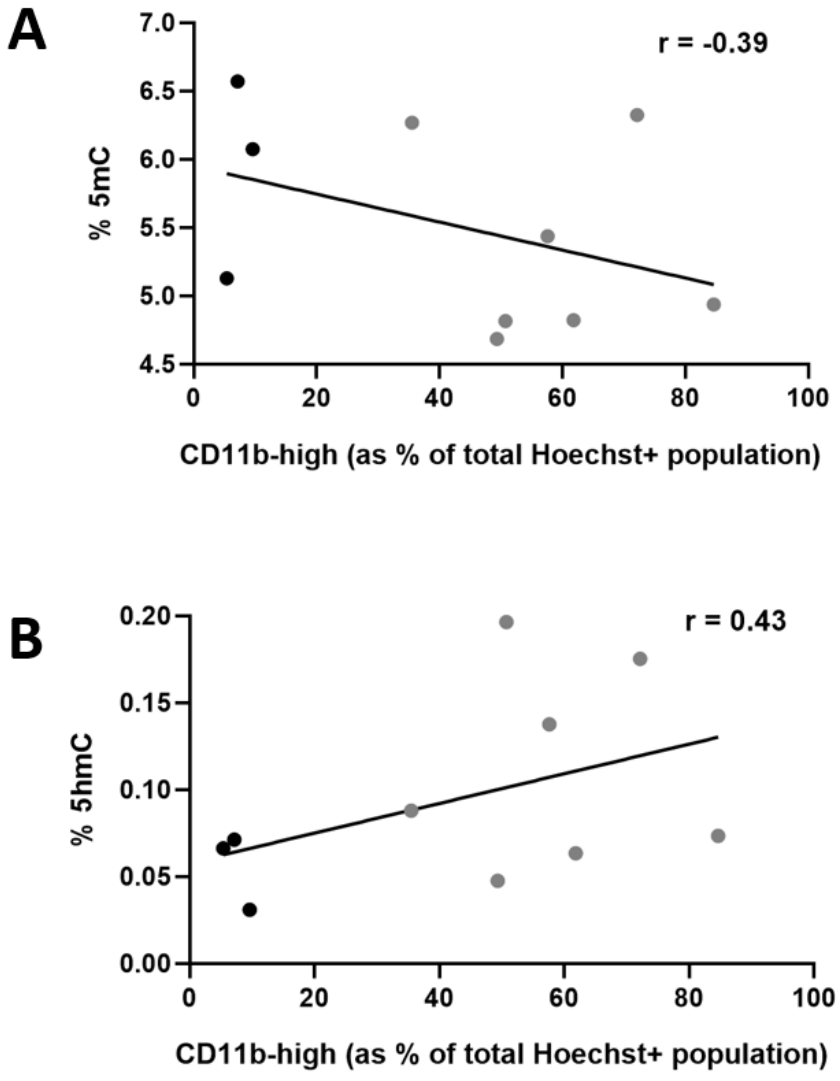


Figure 4.8: Correlation between 5mC & 5hmC content of microglia/macrophage cells and proportion of CD11b-high cells

Proportions of CD11b-high cells from brains of rats that underwent sham (n=3; black) or MCAO (n=7; grey) were calculated as % of total Hoechst+ population. These values were then correlated with 5mC and 5hmC levels of DNA obtained from microglia/macrophage cells. No significant correlation was found between proportions of CD11b-high cells and 5mC content (**A**; r=-0.39; p=0.26) or 5hmC content (**B**; r=0.43; p=0.21).

4.3.6: mRNA expression levels of BDNF, Ttll7 and Tet enzymes

The use of reverse transcription followed by qPCR determined that there was no significant difference between Sham and MCAO animals in expression levels of Ttll7 (t_{13}=1.69, p=0.113), Tet1 (t_{13}=0.04, p=0.968) or Tet2 (t_{13}=1.13, p=0.286) (see Figure 4.9). There appeared to be a slight increase in BDNF expression in the MCAO group, although this was not found to be significant (t_{13}=2.1, p=0.054). There was, however, found to be a significantly increased Tet3 expression in MCAO animals in comparison to Sham animals (t_{13}=3.31, p=0.006).

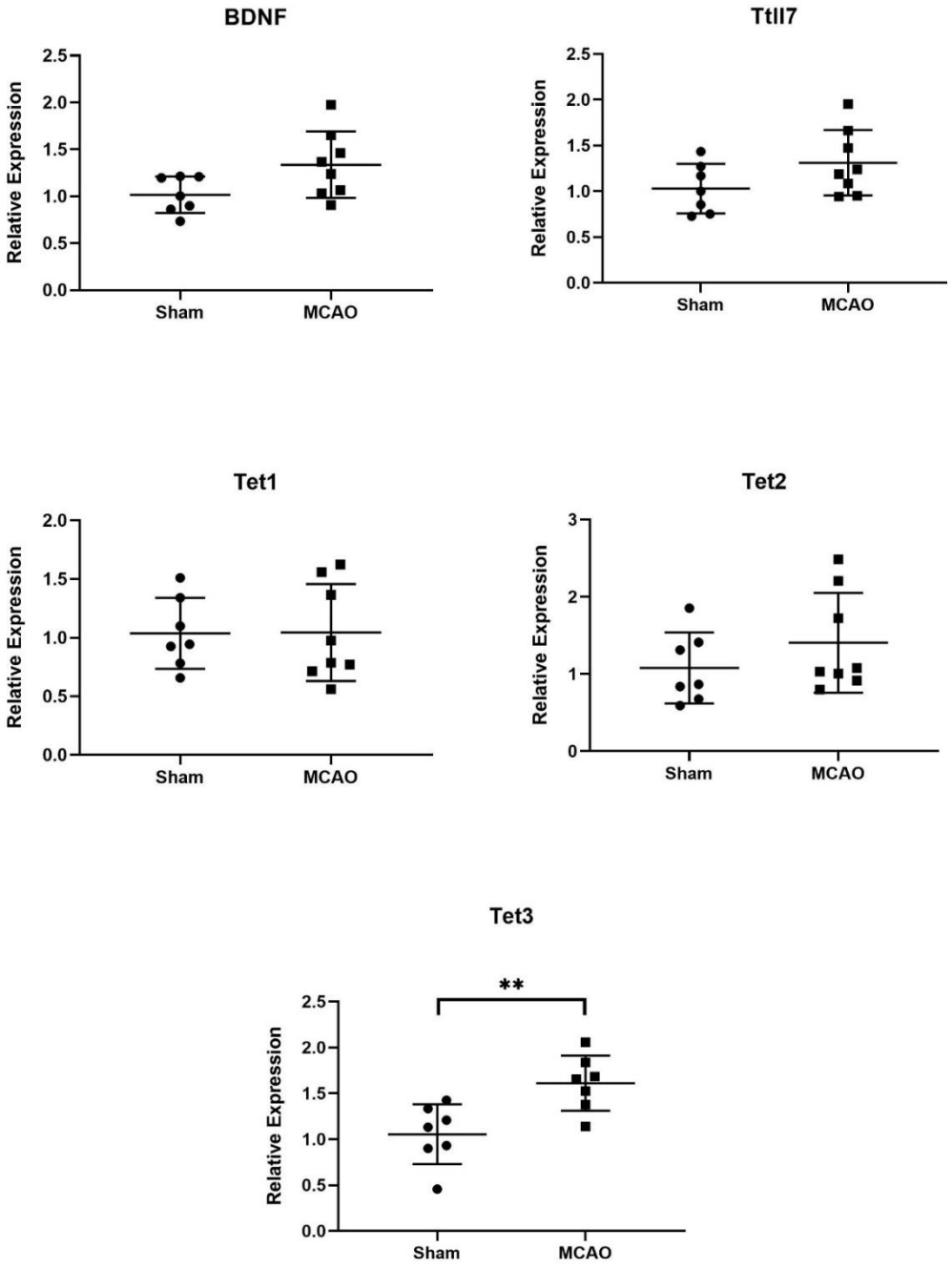


Figure 4.9: Relative expression levels of genes of interest

RNA was extracted from total cell populations obtained from the cortex and striatum of mice that had undergone MCAO surgery (n=8) or an equivalent sham surgery (n=7). Reverse transcription and subsequent qPCR of these RNA samples revealed that there was no significant difference in expression of Tet1 ($p=0.968$), Tet2 ($p=0.286$), Ttll7 ($p=0.113$) or BDNF ($p=0.054$) between groups. There was, however, a significant increase in Tet3 expression in the MCAO group ($p=0.006$). Data is presented as mean ± SD. ** represents a significant difference ($p<0.01$).

4.4: Discussion

4.4.1: Post-stroke (hydroxy)methylation in total cell population

One of the original aims of this chapter was to isolate neuronal (NeuN+) cells in order to extract DNA and RNA and identify post-stroke changes in the methylome that are specific to neurons. However, as described in section 4.2.6, this aim was not met as the number of neuronal cells being collected did not meet the minimum requirement for downstream applications. Therefore, DNA and RNA samples extracted from a backup source of tissue homogenate, consisting of the total cell population, were analysed instead. Whilst this does not help to discover any neuronal-specific effects, analysing this tissue does support the data presented in Chapter 2 of this thesis. Namely, a significant increase in 5hmC content was observed at 2 weeks post-stroke (Figure 4.5B), which aligns with the findings in Chapter 2 that there is an increase in global 5hmC following MCAO in mice. This increase in 5hmC content was also accompanied by a significant increase in mRNA expression of Tet3 (Figure 4.9), although no significant differences in Tet1 or Tet2 expression levels were found.

This significant increase in 5hmC is not, however, accompanied by any changes in 5mC content in total cell population; though there was a small decrease in 5mC content of MCAO animals, this was not found to be significant (Figure 4.5A). This does not support previous research, with Miao et al. (2015) determining that there was a significant decrease in 5mC levels at 7 days post-stroke. In the current experiment, 5mC content was analysed at 14 days post-stroke, and as such it is therefore plausible that there was a significant decrease in 5mC content following MCAO, but these levels had returned to baseline by the 2 week timepoint.

Alternatively, it is possible that the small, albeit insignificant, decrease in 5mC content reflects demethylation of a small number of specific genes. Previous research has identified a small

number of axon growth- and neuroplasticity-related genes that are up-regulated in sprouting neurons following ischemic stroke (Li et al., 2010), including Neuropilin-1 and Tubulin tyrosine ligase like 7 (Ttll7). This chapter has identified a similar effect, having utilised qPCR to determine that levels of BDNF and Ttll7 are slightly increased following ischemic stroke (Figure 4.9). Although neither of these increases were deemed statistically significant, these experiments were deemed underpowered in post-hoc power analyses (see Appendix A6), suggesting that slightly increasing the number of animals may have revealed a significant effect. It is therefore possible that the increased expression of these axon-growth related genes is caused by the observed increase in 5hmC levels; and any resulting changes in gene-specific 5mC levels are masked by analysing 5mC content of the whole genome. However, further research into this area is required in order to determine if such an effect exists. This research would need to focus on post-stroke DNA (hydroxy)methylation at a gene-specific level, utilising techniques such as methylated DNA immunoprecipitation (MeDIP) or bisulphite sequencing. Though not looking at a gene-specific level, determining a direct causal relationship between Tet enzyme expression/DNA (hydroxy)methylation and axon growth is the main aim of the next chapter in this thesis.

When correlating post-stroke 5mC and 5hmC levels in total cell population with infarct volume (Figure 4.6), it was found that no significant correlation exists between infarct volume and levels of either modified cytosine base. Although this does not help to elucidate any kind of effect stroke severity has on the methylome, this data does support the similar findings in Chapter 2 that global 5hmC levels do not correlate with infarct volume.

4.4.2: Post-stroke (hydroxy)methylation in microglia/macrophage cells

By using flow cytometry to investigate the phenotype of microglia/macrophage cells following ischemic stroke, it was found that MCAO causes a large significant increase in CD11b expression, such that an entirely separate population of CD11b-high cells can be visualised in the post-stroke brain (Figures 4.3 + 4.4). This is indicative of microglia/macrophage activation and also supports previous findings that this cell type significantly increases CD11b expression following MCAO and reperfusion in rodents (Morrison & Filosa, 2013; Perego et al., 2011). This increase in CD11b expression is accompanied by a significant increase in the 5hmC content of DNA isolated from microglia/macrophage cells (Figure 4.7B), meaning it is possible that the measured increase in CD11b could be controlled by DNA demethylation via oxidisation of 5mC. However, there are no significant changes in 5mC content in microglia/macrophage cells observed (Figure 4.7A). Also, when correlating proportions of CD11b-high cells with levels of 5mC and 5hmC, no significant correlational relationships were determined (Figure 4.8). This would therefore suggest that demethylation via production of 5hmC is not influencing CD11b expression, as if this were the case then a positive correlation between 5hmC levels and CD11b expression would be expected.

Once again, however, it is possible that activity of the Tet enzymes and resulting DNA demethylation is causing phenotypic changes to microglia/macrophage cells at a gene specific level, and that analysing global 5mC and 5hmC content is masking this effect. As previously explained, determining such an effect would require research that focuses at a gene-specific level. Potential candidates for such research include galectin-3, which previous research has shown is required for microglial recruitment and activation in response to ischemic stroke (Lalancette-Hébert et al., 2012; Yan et al., 2009). Alternatively, research has also identified a protein that is directly involved in the inhibition of axonal growth by M1 phenotype microglia. Kitayama et al. (2011) found that by using siRNAs to knock down expression of repulsive

guidance molecule a (RGMa) in a mouse model of spinal cord injury, the inhibitory effect of M1 phenotype microglia/macrophages on axonal growth was attenuated. This therefore highlights RGMa as a particular gene of interest for future studies. Further research in this area could present a new epigenetic target for future therapeutic treatments aimed at promoting post-stroke axon growth via modulation of the CNS immune response.

4.4.3: Limitations

The main limitation of this study came from the inability to reliably isolate required amounts of DNA and RNA from neuronal cells due to low cell numbers. Because this was identified as a potential issue in the development of the FACS protocol (Chapter 3, section 3.2.5), a contingency plan was put into place and DNA and RNA samples from total cell populations could instead be analysed. Despite this, the inability to isolate neuronal DNA and RNA means that one of the main aims of this chapter was not met.

Changes that could be made in any future experiments of this nature that could remedy this problem include sorting only neuronal cells and not microglia/macrophage cells. As was detailed in Chapter 3, isolation of both of these cell types required the tissue homogenate to be split in two in order to undergo debris clearance. This effectively halved cell yield, so foregoing microglia/macrophage isolation would be one way to increase the number of neuronal cells that can be isolated. As another option, it may have been possible to switch to sorting astrocytes instead of neurons when neuronal sorting became problematic, thereby investigating the potential role of the astrocytic cell type in the pathophysiology of ischemic stroke. However, as the neuronal isolation became an issue at a very late stage of the experiment, there were no readily available methods or reagents for the isolation of astrocytes. Alternative methods of remedying the issue of neuronal isolation include

increasing the amount of starting tissue, or utilising another method of cell type isolation, such as magnetic cell isolation or density gradient isolation, at the expense of specificity. Furthermore, it is possible that the administration of RNAlater during perfusion, and as an additive in various solutions used in the protocol, could have affected tissue integrity and protein quality. It has been previously shown that preservation of brain tissue in RNAlater can lead to dehydration and increased protein degradation (Wang et al., 2018), which could then affect tissue homogenisation and NeuN staining. As such, removing the RNAlater perfusion steps in subsequent studies may increase the yield of NeuN+ cells.

A further limitation of the study performed in this chapter comes from the fact that the microglial/macrophage cells could not be further subdivided into phenotypic groups. The CD68 antibody tested in Chapter 3 did not effectively isolate peripheral macrophages, and no distinction between M1 and M2 phenotype microglia/macrophage cells was available. Analysing these immune cell subtypes would likely have garnered more information on the role of (hydroxy)methylation in the control of the post-stroke immune response that could then better inform future studies. Similarly, other cell types, such as astrocytes, were not considered as part of this study. Studying astrocytes in particular would be of great interest as previous research has shown that this cell type is involved in the formation of glial scars following ischemic stroke, which act as physical and biochemical barriers to axon growth (Choudhury & Ding, 2016).

4.4.4: Summary

By utilising FACS to isolate microglial/macrophage cells, the experimental work carried out in this chapter has helped to identify an epigenetic response to stroke that appears to not only be observed across all cell types but is also observed specifically in immune cells of the CNS.

The observed post-stroke increase in 5hmC content in $CD11b^{+}/CD45^{low}$ cells, whilst not accompanied by any changes in 5mC levels, coincides with a large increase in CD11b expression that may hint at a possible epigenetic mechanism in the control of post-stroke microglial activation. The exact implications of this epigenetic response are unknown, but future research focusing on gene-specific post-stroke methylation levels may further elucidate this relationship and present new therapeutic targets. A similar epigenetic response is also seen in the total cell population, further confirming the response that was observed in Chapter 2 of this thesis. Having now gathered evidence that ischemic stroke causes changes to the epigenome in the CNS, the next chapter of this thesis will focus on determining a direct causal relationship between Tet enzyme activity/DNA (hydroxy)methylation and axon growth.

Chapter 5: Determining role of Tet enzymes in control of axon growth *in vitro*

5.1: Introduction

Previous chapters in this thesis have determined changes in global 5mC and 5hmC levels in the post-stroke brain that may indicate a potential role of the modified cytosine bases, and the enzymes that catalyse their formation, in the sprouting of new axons following stroke. However, a direct causal effect of modified 5hmC levels and Tet enzyme activity on axon growth is yet to be determined, which is the overall aim of this chapter.

5.1.1: The role of DNA methylation in axon growth

Although previous research focusing on the role of methylated cytosine residues in the pathophysiology of ischemic stroke has hinted at a potential role in the control of post-stroke axon growth (Endres et al., 2001; Endres et al., 2000), the direct role of DNA methylation in axon growth is scarcely studied. Experiments on the neuroblastic cell line PC12 has determined that DNMT3b positively regulates neurite growth by decreasing expression of the growth-suppressing gene T-cadherin (Fredette et al., 1996). However, it was later found that this effect occurs due to DNMT3b recruiting the histone deacetylase (HDAC) family of enzymes, which subsequently silence the T-cadherin gene, as opposed to direct DNA methylation itself (Bai et al., 2006). Subsequent research determined that whilst a double knockout of DNMT1 and DNMT3a in post-mitotic forebrain mice neurons did not impair axonal development, it did impair synaptic plasticity (Feng et al., 2010).

Whilst this early research did not elucidate a clear role of DNA methylation in the control of axon growth, later investigations into a known positive regulator of post-axotomy axon regeneration, folic acid, did highlight a potential DNA methylation-dependent mechanism. Iskandar et al. (2010) found that following spinal cord injury in rats, expression of a folic acid receptor (folate surface receptor 1; FLR1) is significantly increased in DRG neurons. FLR1 was also found to be required for neurite outgrowth of DRG neurons in vitro, as neurite outgrowth was significantly decreased in $Flr1^{+/-}$ cells. Folate supplementation was then found to promote axonal regrowth in the same injury model, although this effect was attenuated in $Flr1^{+/-}$ mice. Spinal cord injury was accompanied by a significant decrease in DNMT3a/b expression and global DNA methylation levels, with these decreases counteracted by folate supplementation. This therefore suggests that the mechanism through which folic acid promotes axon growth involves DNA methylation. Interestingly, folic acid is directly involved in the synthesis of SAM (Bottiglieri, 2013), the primary source of methyl group donors utilised by DNMTs, although whether this is the mechanism through which folic acid increases DNA methylation is yet to be investigated.

Although the study by Iskandar et al. began to clarify that DNA methylation plays a potential role in the control of axon growth, the major limitation of the study came from the methodology, in which assessments were made on bulk spinal cord tissue. This therefore means that it cannot be determined whether the observed effects are due to changes in neuronal or glial cells. As glial cells play a vital role in the injured CNS (Trakhtenberg & Goldberg, 2011), it is possible that changes to DNA methylation in these cells alters post-injury neuroimmune modulation and has an effect on axon regeneration. A later study by Pollema-Mays et al. (2014) attempted to address this by analysing cell-specific post-injury DNMT levels via immunohistochemistry. They found that although DNMT1 was expressed by both neurons and microglia, DNMT3a was preferentially expressed by microglia whereas DNMT3b was

preferentially expressed by neurons following sciatic nerve ligation. The same study also found that following sciatic nerve ligation, DNMT3a expression peaked 1 week post-injury, whereas the increase in DNMT3b expression was lower and sustained for a number of weeks post-injury. As these enzymes are responsible for *de* novo DNA methylation, this indicates that changes in DNA methylation in response to axotomy differs between these 2 cell types, meaning each could potentially have differing effects on the control of axon regeneration. In either case, taken together with the data obtained by Iskandar et al., this indicates that DNA methylation plays a key role in the regrowth of axons following CNS injury.

It is important to note that the conclusions of the aforementioned studies aimed at determining a direct role of DNA methylation in axon regeneration appear to contradict those which aimed to determine a role of DNA methylation in stroke recovery. Namely, studies such as those carried out by Iskandar et al. and Pollema-Mays et al. indicate that increased expression of DNMTs and subsequent increases in DNA methylation are positive regulators of axon growth, whereas studies focused on ischemic stroke find that knockdown of DNMTs and decreasing methylation leads to smaller infarcts and improved functional recovery (Endres et al., 2001; Endres et al., 2000). This seems counterintuitive, as it would be assumed that providing an intervention that negatively regulates axon growth would lead to worse ischemic injury. The apparent contradictions between these studies could be due to the differences in the ischemic stroke and spinal cord injury models, with ischemic stroke not involving mechanical disruption of the axon but instead involving hypoxia and an altered immune response. Alternatively, these contradictory findings could reflect a highly dynamic role of DNA methylation in ischemic stroke. Axonal regeneration and sprouting are not the only cellular mechanisms involved in ischemic stroke pathophysiology, with processes such as apoptosis, excitotoxicity, diaschisis and immune cell activation all occurring simultaneously (Dirnagl et al., 1999). It is therefore likely that any observed effects of altering DNA

methylation post-stroke are due to the involvement of a number of these processes and not axonal growth alone. This therefore highlights the need to determine a specific role of DNA methylation in the regrowth of axons following ischemic stroke independently of other cellular processes.

5.1.2: The role of Tet enzymes in axon growth

Whilst a potential role of DNMTs and 5mC in the control of axon growth has been somewhat identified by previous research, the role of the oxidised forms of 5mC and the Tet enzymes that form them is even less widely studied. Using sciatic nerve ligation in adult mice as a model of axotomy, it was found that 5hmC and Tet3, but not Tet1 or Tet2, were significantly increased in DRG neurons (Weng et al., 2017). The same study also found that knockdown of Tet3 via short hairpin RNA (shRNA) reduced the number of DRG neurites in vitro and decreased the number of regenerating axons in vivo. A further study also found that the injury-dependent increase in Tet3 and 5hmC was counteracted by the administration of Ca^{2+} chelators (Loh et al., 2017), thereby suggesting that an increase in intracellular calcium may be responsible for the increase in Tet3 and 5hmC. Together, these recent studies indicate a clear potential role for Tet3 and 5hmC in the control of axon growth following injury. Whilst Tet1 and Tet2 were not found to have an effect on axon regeneration in these studies, they may still play a role in the control of post-stroke axon growth given the vastly different pathophysiology of stroke and peripheral nerve injury, as previously described.

5.1.3: The role of hypoxia in axon growth

A major aspect of ischemic stroke pathophysiology is the involvement of hypoxia, which is an aspect that has not been considered in previous research focused on DNA methylation and axon growth. Hypoxia itself has been shown to positively influence axon growth in sensory neurons, with the process being mediated by hypoxia-inducible factor 1α (HIF1α), as evidenced by the fact that knockdown of HIF1α attenuates hypoxia-induced increases in axon regeneration (Cho et al., 2015). More recent research has linked this HIF1α activity to Tet enzyme expression. Lin et al. (2017) used the hepatoblastoma HepG2 cell line to demonstrate that hypoxia leads to significant increases in not only HIF1α, but also Tet1, Tet2 and Tet3. Administration of cobalt-II-chloride ($CoCl_2$), a chemical inducer of HIF1α, also significantly increased expression of HIF1α and all three Tet enzymes. Knockdown of HIF1α completely attenuated the hypoxia and $CoCl_2$-induced increases in Tet enzyme expression, thereby indicating that hypoxia could have an effect on DNA methylation by HIF1α-mediated changes in Tet enzyme expression. This would therefore suggest that any potential mechanism of axon regeneration control involving Tet enzymes could differ when following ischemic stroke due to the hypoxia and increased expression of HIF1α. However, the studies that have determined these relationships between HIF1α and axon growth/Tet enzyme expression have not been performed on neurons of the CNS, therefore the conclusions cannot be applied to ischemic stroke. Determining what roles hypoxia and the Tet family of enzymes play in the control of axon growth in the CNS is one of the aims of this chapter.

5.1.4: Objectives & Hypotheses

The objectives of this chapter are as follows:

- To determine the effects of increasing and decreasing Tet enzyme expression on axon and dendrite growth in both normoxic and hypoxic conditions
- To determine the effect of hypoxia on HIF1α and Tet enzyme expression in CNS neuronal cells
- To determine the effect of hypoxia on 5mC and 5hmC levels in CNS neuronal cells

Based on previous research carried out in this area, the hypotheses for the findings of this chapter are as follows:

- Increasing Tet enzyme expression will lead to increased axonal and dendritic growth
- Decreasing Tet enzyme expression will lead to decreased axonal and dendritic growth
- Hypoxia will induce increased expression of HIF1α and Tet enzymes
- Hypoxia will induce increased expression of 5hmC and decreased expression of 5mC

5.2: Methods

Most preparations of cortical neuronal cultures (section 5.2.2) were performed by Raquel Ribeiro.

5.2.1: Experimental design

In order to study the role of Tet enzymes and hypoxia in the process of neuronal growth, cultures of primary cortical neurons from neonatal mice were used in three separate experiments. In the first experiment (**A**), cultures were subjected to an oxygen-glucose deprivation (OGD), a commonly used method of modelling ischemic stroke *in vitro*, followed immediately by fixation and processing to determine cell viability and protein expression levels of Tet1-3 and HIF1α. In the second experiment (**B**), cultures were again subjected to OGD followed by reoxygenation and DNA was extracted 48 hours later for processing to determine global levels of 5mC and 5hmC. In the third and final experiment (**C**), cultures were transfected with either siRNA targeting Tet1, Tet2 or Tet3, or plasmid constructs for Tet1, Tet2 or Tet3. In each case, cells were also co-transfected with a plasmid construct of green fluorescent protein (GFP). Following transfection, cultures underwent OGD and reoxygenation and were fixed 48 hours later for processing to determine neuronal growth. The timeline of each of these experiments can be seen in Figure 5.1.

In each experiment, 5 experimental repeats were performed. For transfection experiments, cultures transfected with GFP only or GFP plus a non-targeting (NT) siRNA were used as controls. Allocation of siRNA/plasmid to each well was randomised, and all analysis was performed with the experimenters blinded to group allocation.

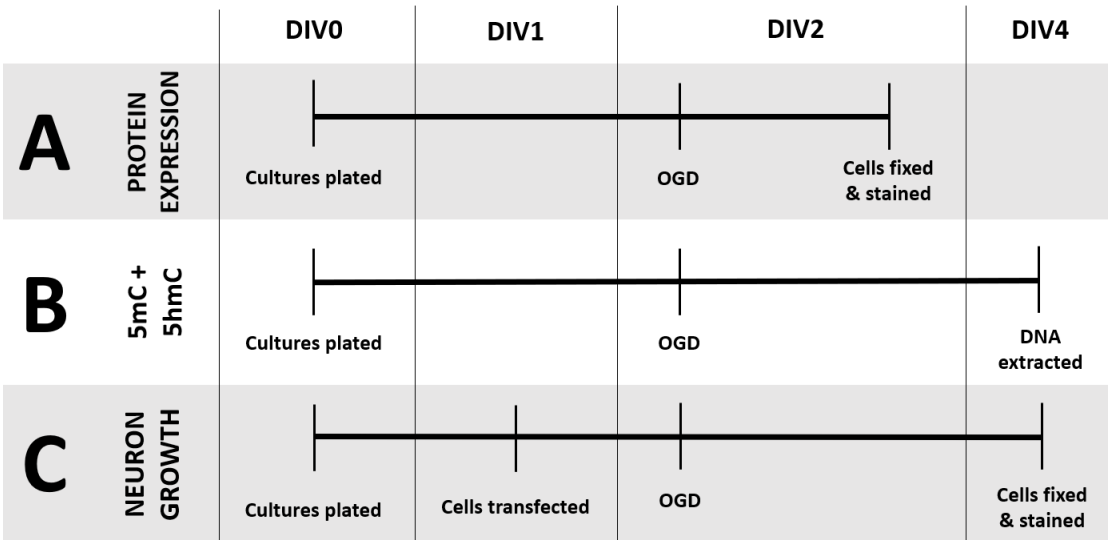


Figure 5.1: Timeline of cell culture experiments
Experimental work carried out in this chapter can be defined as three separate experiments: one to assess protein expression following hypoxia (**A**), one to assess 5mC and 5hmC content following hypoxia (**B**), and one to assess neuronal growth (**C**). DIV = Days *in vitro*. For all experiments, cultures were plated at DIV0. For neuronal growth experiments, cells were transfected with plasmids and/or siRNA at DIV1. Cultures in all experiments underwent 2.5 hour OGD at DIV2. For protein expression experiments, cultures were fixed and stained immediately following OGD. At DIV4, cultures used for neuron growth analysis were fixed and stained; and DNA was extracted from cultures used to assess 5mC and 5hmC content.

5.2.2: Culture preparation

For experiments A, B and C, C57BL/6 mouse embryos (embryonic day 15) were collected from pregnant mice that were euthanized humanely via cervical dislocation. The uterus was surgically removed and transferred to a 90mm petri dish with neurobasal media (Thermo Fisher, UK). The embryos were then removed from the uterus and cortices dissected from their brains. A maximum of 10 cortices were then placed into a new petri dish containing 2ml of Hanks buffer (Thermo Fisher, UK).

The mouse cortices were then subjected to enzymatic dissociation via addition of 200µl of trypsin (Sigma-Aldrich, UK) and 20µl of DNAse (Sigma-Aldrich, UK). Tissue and solution were then mixed and incubated at 37^{o}C for 30 mins. Following this, 100µl of trypsin inhibitor

(Thermo Fisher, UK) was added, and the mixture was transferred to a falcon tube. Once the tissue had settled at the bottom of the falcon tube, the medium was removed and replaced with 1.5ml of fresh neurobasal media. The tissue and medium were then triturated using a 2ml pipette approximately 10 times, or until no clumps of tissue were visible.

The tubes were then topped up to 10ml with additional neurobasal media and centrifuged at a speed of 250 xG for 5 minutes. The supernatant was removed, and the dissociated cells were resuspended in 2ml of neurobasal media. The cell density of the sample solution was determined using a haemocytometer, and an appropriate volume of neurobasal media was then added to dilute the cells to 10 x 10^6 per ml of solution. Glass coverslips (22x22mm) were initially soaked in 70% ethanol, left to dry, and coated with poly-L-lysine solution (Sigma-Aldrich, UK). One coverslip was then placed into each well of a 6-well plate and 1.75ml of cell suspension was added to each well. Cells were then placed in an incubator set to 37^{o}C with 5% CO_2.

5.2.3: Plasmid preparation

For experiment C, plasmid constructs for the expression of Tet1, Tet2 and Tet3 in mammalian cells were gifted by Yi Zhang (Wang & Zhang, 2014) via Addgene (Addgene plasmids #60938 (Tet1); #60939 (Tet2); #60940 (Tet3)). Each Tet plasmid construct comprised of a pcDNA3 backbone and coded for the entire Tet protein with an included an N-terminal FLAG tag. GFP plasmid (pmaxFP^{TM}-Green-C vector) was obtained from Lonza (Cologne, Germany). Plasmids were received in the form of a bacterial stab with ampicillin resistance.

In order to culture the bacterial stocks and isolate plasmid DNA, the bacterial stabs were streaked onto LB-Agar plates containing 100µg/ml Ampicillin (Sigma-Aldrich, UK) and

incubated at 37°C for 24 hours. From each of these plates, a single bacterial colony was picked using a sterile pipette tip and the tip was dropped into a 15ml Falcon tube containing 2ml of LB broth with 100µg/ml Ampicillin. These inoculated liquid cultures were then incubated at 37°C for 24 hours. The tubes were then centrifuged to pellet the bacteria and plasmid DNA was then isolated from the cultures using the QIAprep Spin Miniprep Kit (Qiagen, Germany), following manufacturers instructions. Once isolated, plasmid DNA was quantified using a NanoDrop 2000 Spectrophotometer (Thermo Fisher, UK) and stored at -20°C until cell transfection.

5.2.4: Cell transfection

For experiment C, cultures underwent transfection approximately 24 hours following plating. A working stock of transfection reagent (Lipofectamine 2000; LF2000) was made by mixing 5µl LF2000 (Sigma-Aldrich, UK) with 125µl of Opti-MEM (Thermo Fisher, UK) per well and incubating at room temperature for 15 minutes.

Stocks of siRNA (GE Healthcare Dharmacon, USA) or plasmid were then mixed in 125µl Opti-MEM, producing working stocks that give a final in-well concentration of 50nM of siRNA or 0.75µg of total plasmid DNA. To these working stocks, 0.75µg of solubilised GFP plasmid stock (Sigma-Aldrich, UK) was added. For control cultures that received no siRNA or Tet-coding plasmid, only GFP plasmid was added to this solution. In order to match the total amount of plasmid DNA in each well, control wells received 1.5µg of GFP plasmid. The lipofectamine solution (125µl per well) and siRNA/plasmid stock solution (125µl per well) were then mixed and incubated at room temperature for 30 minutes. Following this, the solutions were then added to the cells – 250µl per well, giving a final volume of 2ml in each well. The cultures were then returned to the incubator.

Specificity of the Tet-targeting siRNAs was determined by immunocytochemically staining for Tet1-3 in cultures transfected with each of the siRNAs. It was determined that the siRNAs were specific as each siRNA knocked down only its target Tet enzyme and did not affect expression of others. Data can be found in Appendix A3. Cell density of each transfected culture was 1.75 x 10^5 cells/cm^2, with an observed transfection rate of around 3% (determined by counting number of GFP+ cells).

5.2.5: Oxygen-glucose deprivation (OGD)

For all 3 experiments, cultures that underwent OGD were taken from the incubator at DIV2. The hypoxic chamber was initially prepared by setting the O_2 concentration to 0.5%, CO_2 concentration to 5% and the temperature at 37°C. A falcon tube containing 10ml of glucose-free DMEM media (Thermo Fisher, UK) was then placed in the chamber to deoxygenate for at least 2 hours.

The cells were moved into the chamber, and the media was removed from the wells and stored in 2ml Eppendorf tubes at 37°C. 1.5ml of the deoxygenated glucose-free DMEM was then added to each well and cells were then incubated for 2.5 hours. After 2.5 hours had elapsed, cultures were either processed immediately (see sections 3.2.6 + 3.2.7), or the deoxygenated media was replaced with the previous oxygenated media. These plates were then removed from the hypoxic chamber and returned to the incubator (set to 37°C, 5% CO_2 and atmospheric O_2).

Cultures that did not undergo OGD (normoxic controls) had their media removed 48 hours after plating and stored at 37°C whilst 1.5ml of fresh OptiMEM was added to each well. Once 2.5h had elapsed, the fresh OptiMEM was removed and the original media was replaced.

5.2.6: MTT reduction assay

For experiment A, the MTT reduction assay was performed on cultures immediately following OGD in order to quantify cell viability and validate the model of OGD. Deoxygenated glucose-free DMEM was removed from the wells and replaced by 2ml of Opti-MEM media. 200µl of PBS containing 5mg/ml MTT (Methylthiazolyldiphenyl-tetrazolium bromide; Sigma-Aldrich, UK) was added to each well and cells were then removed from the hypoxic chamber and left to incubate at 37^{o}C for 30 minutes. Following this incubation, media was removed from the wells and replaced with 1ml of DMSO (Dimethyl sulfoxide; Sigma-Aldrich, UK). DMSO was mixed by pipetting several times in order to dissolve the crystals on the bottom of the well. The DMSO was then transferred to a 96-well plate and absorbance at 570nm was read using a SpectraMax M2e Microplate Reader (Molecular Devices, USA).

Control samples were performed by performing the assay on cultures that had not undergone OGD (normoxic controls) and fresh DMSO was also analysed as a blank. Percentage cell viability was calculated by subtracting the absorbance reading value of the blank from each sample and then calculating the absorbance readings of each sample as a percentage of the normoxic controls.

5.2.7: Fixation & staining

For all 3 experiments, fixation of cells was performed by removing the media and adding 1.5ml of 4% paraformaldehyde (PFA) in phosphate-buffered saline (PBS). For cultures processed immediately following OGD, this step was performed in the hypoxic chamber and the plates were then removed from the chamber. For remaining cultures, this step was performed 96 hours after the cultures had been plated (Figure 5.1). Cells were incubated at room

temperature for 10 mins, the PFA solution was removed, and cells were washed three times with PBS containing 0.3M glycine.

Cells were permeabilised by adding 1.5ml of PBS containing 0.5% Triton X-100 and incubating at room temperature for 30 minutes. PBS was removed before adding a blocking buffer (PBS w/ 0.3M glycine, 0.5% Triton X-100 and 0.5% bovine serum albumin) containing a 1 in 500 dilution of primary antibody targeting either: Tet1 (Abcam, UK); Tet2 (Abcam, UK); Tet3 (Abcam, UK); or Hif1α (Bio-Rad Labs, USA). Cells were left to incubate with the primary antibody overnight at 4^{o}C. Following this, cells were washed three times with PBS before incubation with AlexaFluor-647-conjugated secondary antibody (Sigma-Aldrich, UK) at a dilution of 1 in 400 in blocking buffer. Cells were incubated for 2 hours in the dark at room temperature. Following this, cells were washed three times in PBS.

Coverslips were then removed from the wells and 2 drops of Hard-Set Vectashield Mounting Medium with DAPI (Vector Labs, UK) was added to each coverslip. The coverslips were then placed face-down onto a microscope slide and gently pressed to remove air bubbles. The slides were placed in the fridge to set for a minimum of two hours and were re-labelled by an independent researcher to maintain blinding.

5.2.8: Image analysis

For experiments A and C, cultures were imaged at x20 magnification using a Zeiss 200M microscope. From each culture, 5 neurons were imaged at random (one from each corner of the coverslip and one from the centre, determined using x/y co-ordinates on the stage of the microscope). Using the Simple Neurite Tracer plugin for ImageJ (Ferreira et al., 2014), every neurite for each imaged cell was traced. These tracings were then used to calculate several

parameters: axon length (defined as longest neurite), number of neurites, and total neurite length. The measurements of the five imaged neurons were then averaged to produce one data point. This process was repeated on 5 different cultures to give n=5 for each experimental group. Measurements of average axon length and average total neurite length were normalised to normoxic controls.

Relative levels of Tet enzyme and Hif1α expression were calculated by measuring intensity of fluorescent staining. This was done by calculating CTF, as described in Chapter 2 (section 2.1.5.1). This same method was also used to determine the specificity of each of the Tet-targeting siRNAs (see Appendix A4).

5.2.9: DNA extraction and 5mC + 5hmC quantification

For experiment B, 48 hours after OGD, media was removed from wells and replaced with 1ml of Trizol solution. This solution was then pipetted up and down several times in order to disrupt cells. DNA was then extracted using this Trizol solution as previously described in Chapter 3 (section 3.2.5). Use of this method precluded the use of commercially available kits (such as the Qiagen AllPrep DNA/RNA Micro Kit) as assessments of DNA quantity and quality using a NanoDrop 2000 Spectrophotometer (Thermo Fisher, UK) deemed that samples derived using Trizol were sufficient for downstream applications. 5mC and 5hmC content of these DNA samples was then measured using commercial ELISA kits as described in Chapter 4 (section 4.2.8). All samples were run in duplicate.

5.2.10: Statistical analysis

Data is presented as mean ± standard deviation (SD). Statistical analysis was performed using GraphPad Prism 7. Normality of all data was confirmed using D'Agostino & Pearson normality test. For analysis of relative expression of proteins in normoxic & hypoxic cultures, and 5mC and 5hmC content, unpaired t-tests were performed. For analysis of average axon length, average number of neurites, and average total neurite length, two-way ANOVA was performed followed by Tukey's multiple comparisons test in post-hoc analysis. For analysis of siRNA-transfected cultures, GFP-only and GFP + non-targeting siRNA control groups were combined due to there being no significant difference between these groups (see Appendix A5). Differences were considered significant if $p \leq 0.05$.

Power calculations to determine sample size were performed using preliminary axon length data from siRNA transfection experiments. Using an online sample size calculator (HyLown, USA) it was determined that a sample size of 3 per group was needed to reach sufficient power (using the following values: Group A mean = 100; Group B mean = 67.4; standard deviation = 11.8; power = 0.8; Type I error rate = 5%). In order to maximise power, 5 experimental repeats were performed per group.

5.3: Results

5.3.1: The effect of hypoxia on cell viability

The MTT assay performed in experiment A revealed that following 2.5h of OGD, cell viability is reduced by around 40% (Figure 5.2), which is comparable to previous publications that have used the same or similar OGD protocol on neuronal cultures as an *in vitro* model of ischemic stroke (Scorziello et al., 2001; Wu et al., 2008).

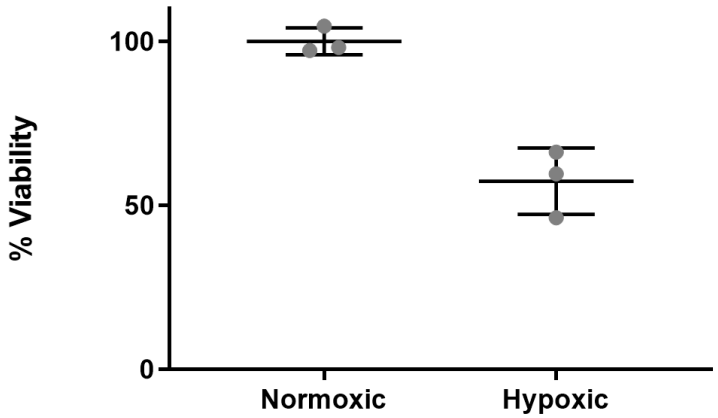


Figure 5.2: Viability of mouse cortical neurons following 2.5h of OGD
Cultures of cortical neurons derived from embryonic mice underwent either 2.5h of oxygen-glucose deprivation (OGD; Hypoxic, n=3) or no OGD (Normoxic, n=3). Cell viability was then assessed using the MTT assay. Data presented as mean ± SD.

5.3.2: The effect of hypoxia on Hif1α and Tet protein expression

In experiment A, immunocytochemistry was used to determine changes in protein expression levels of Tet1, Tet2, Tet3 and Hif1α in normoxic (no OGD) and hypoxic (2.5h OGD) cultures immediately following hypoxic insult. Representative images are shown in Figure 5.3. There were no significant changes in Tet1 (t_8=2.23, p=0.06) or Tet2 (t_8=1.00, p=0.35) expression, although both Tet3 (t_8=2.73, p=0.03) and Hif1α (t_8=3.77, p=0.005) were significantly increased following OGD (Figure 5.4).

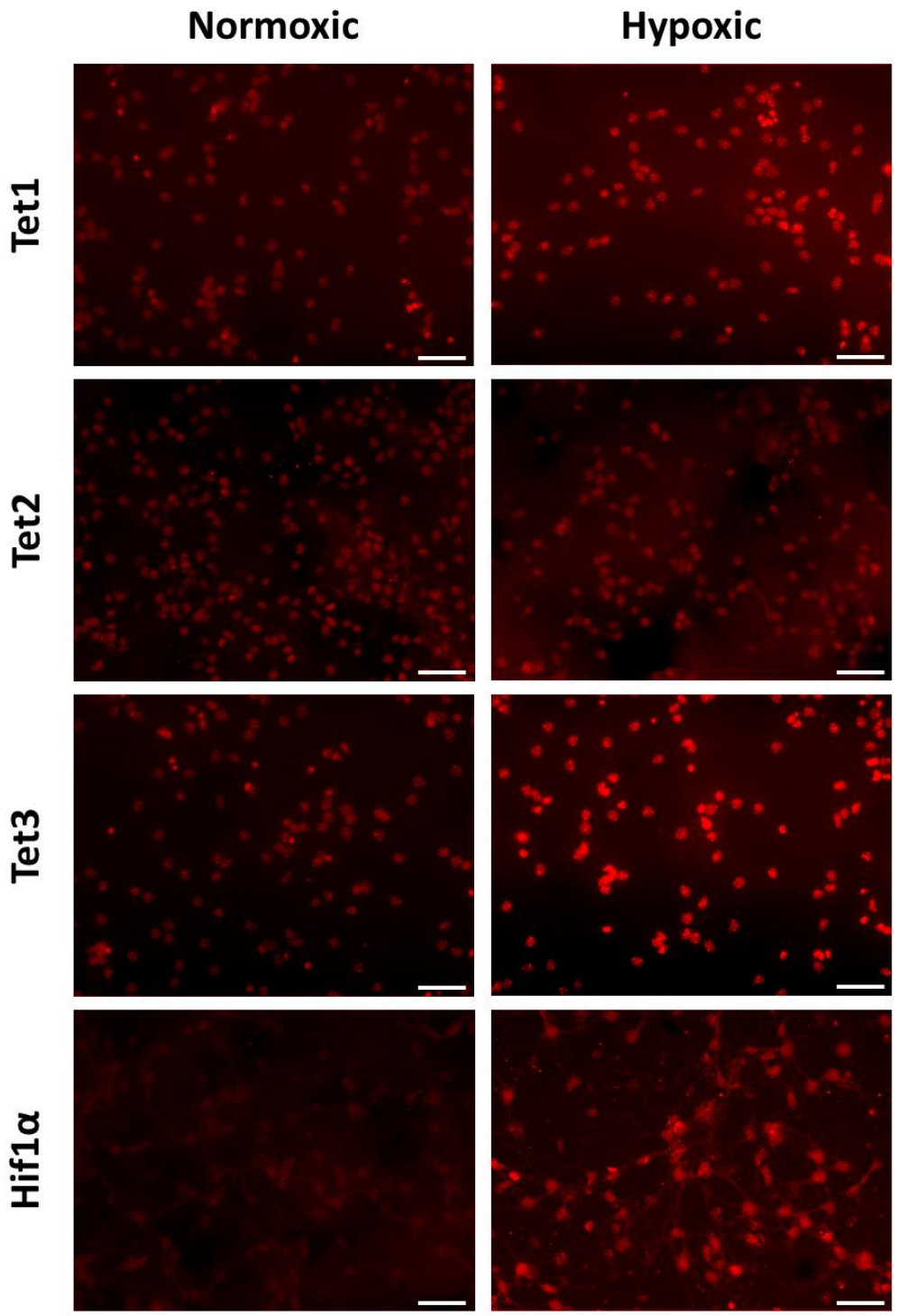


Figure 5.3: Images of normoxic and hypoxic cultures stained for Tet and Hif1α proteins
Cultures of primary cortical neurons were subjected to no OGD (normoxic, *left*) or 2.5h OGD (hypoxic, *right*). Immediately following OGD treatment, cultures were fixed and immunocytochemically stained for Tet1, Tet2, Tet3 and Hif1α. Scale bars = 50µm.

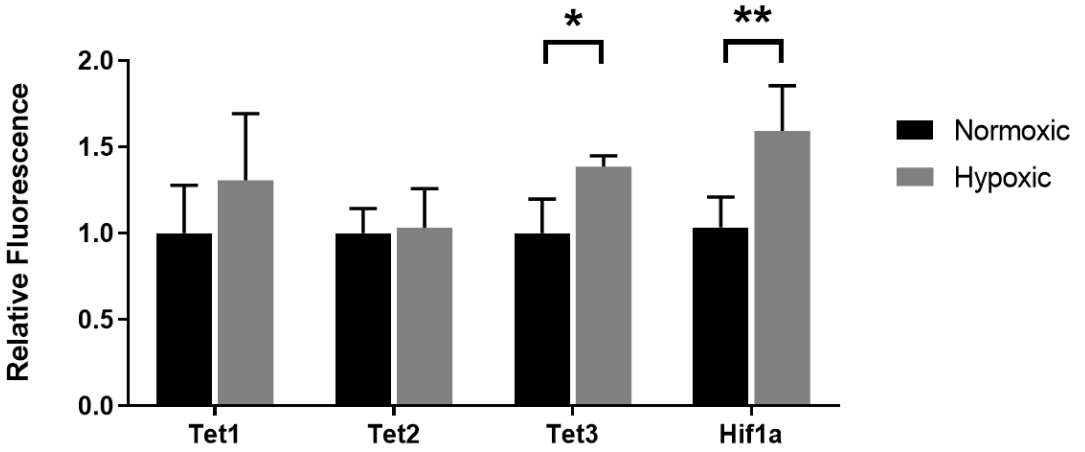


Figure 5.4: The effect of hypoxia on expression of Tet enzymes and Hif1α
Cultures of cortical neurons underwent 2.5h OGD (hypoxic) or no OGD (normoxic) and Immunocytochemistry was used to assess protein expression levels immediately following OGD. There was no significant difference in relative intensity of staining for Tet1 (p=0.06) or Tet2 (0.35) following OGD, although there were significant increases found in the intensity of staining for Tet3 (p=0.03) and Hif1α (p=0.005). n=5 in each group. Data is presented as mean ± SD. * represents p≤0.05; ** represents p≤0.01.

5.3.3: The effect of hypoxia on 5mC and 5hmC levels

In experiment B, cultures of cortical neurons underwent no OGD (normoxic) or 2.5h OGD (hypoxic) and DNA was extracted from the cultures 48h after hypoxic insult. Commercial ELISA plates were then used to determine 5mC and 5hmC content of DNA. There was no significant difference in 5mC content between normoxic and hypoxic groups (t_8=1.33, p=0.29), although there was a significant increase in 5hmC content in the hypoxic group (t_8=2.58, p=0.03) (Figure 5.5).

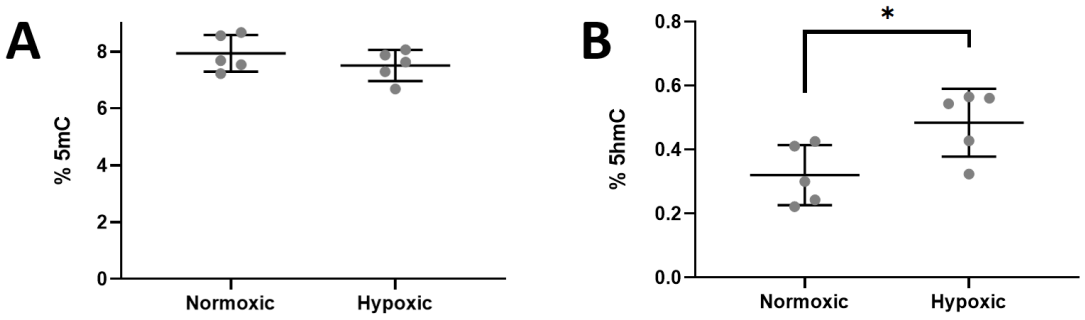


Figure 5.5: The effect of hypoxia on 5mC and 5hmC content
5mC (A) and 5hmC (B) content of DNA that was extracted from neuronal cultures that underwent no OGD (normoxic) or 2.5h OGD (hypoxic) was analysed. No differences in 5mC content were found between groups (p=0.29), although 5hmC content was found to be significantly increased following OGD p=0.03). Data is presented as mean ± SD. * represents p≤0.05.

5.3.4: Effects of decreased Tet enzyme expression

Figure 5.6 shows representative images, from experiment C, of cortical neurons that have been transfected with a plasmid construct for expression of GFP along with a non-targeting siRNA or siRNA targeting Tet1, Tet2 or Tet3, demonstrating differences in axon/dendrite length and Tet enzyme expression.

Figure 5.7 demonstrates changes in axon length as a result of using siRNAs to knock down expression of each of the Tet enzymes in both normoxic and hypoxic conditions. There was a significant difference in axon length between normoxic and hypoxic groups ($F_{1,42}$=12.54; p=0.001) and between different transfection status groups ($F_{3,42}$=6.04; p=0.002). Tet1 knockdown was not significantly different to controls (p=0.10), although neurons with Tet2 and Tet3 knockdown showed significantly shorter axon lengths than controls (p=0.005 and p=0.01, respectively). There was no significant interaction between hypoxia and Tet knockdown ($F_{3,42}$=1.52; p=0.24).

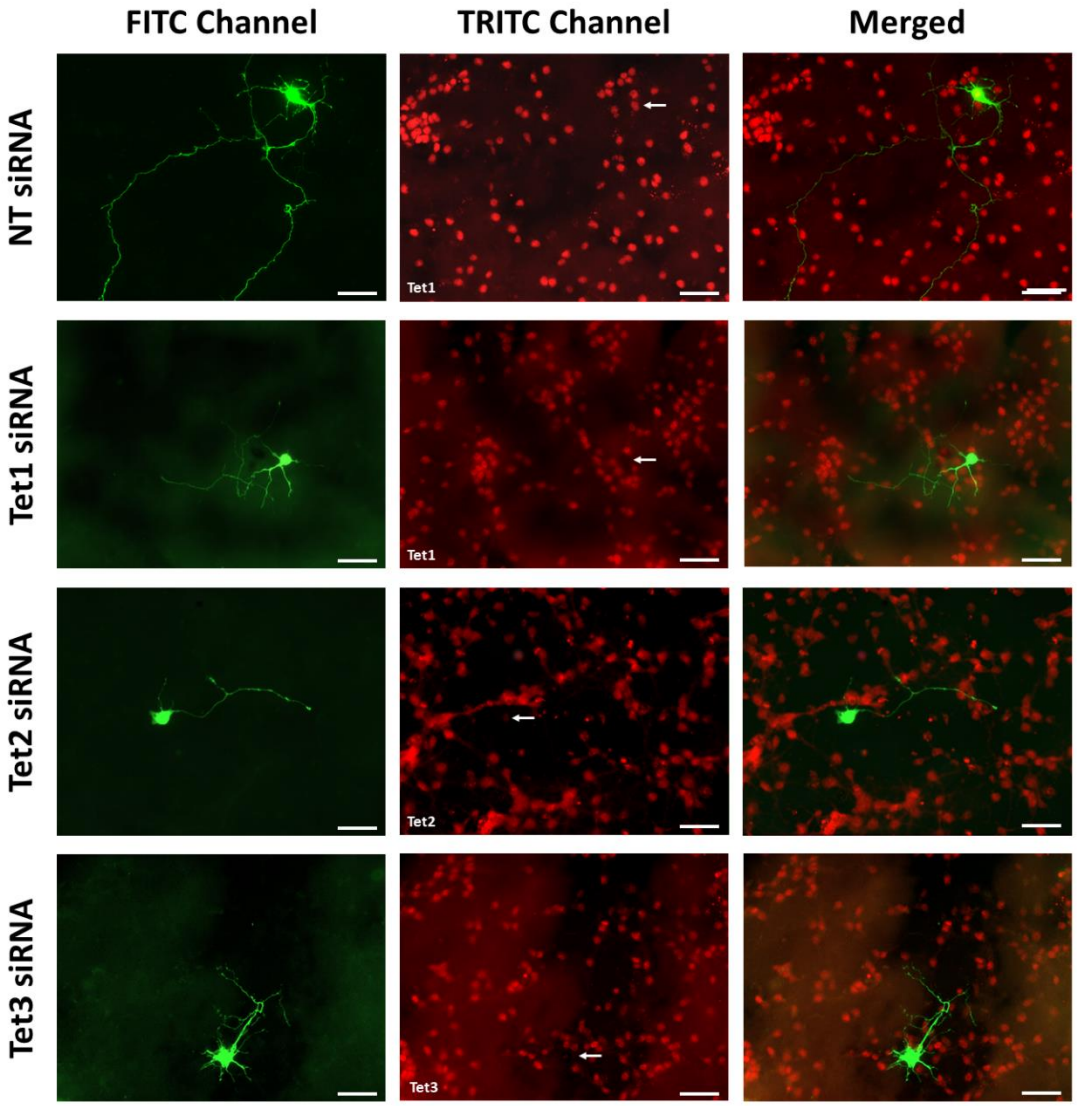


Figure 5.6: Images of neuronal cultures transfected with siRNAs targeting Tet1-3
Cultures of cortical neuronal cells derived from neonatal mice were transfected with a plasmid construct for expression of GFP along with a non-targeting control siRNA or siRNA targeting Tet1, Tet2 or Tet3. 3 days after transfection, cells were fixed and stained with antibodies for Tet1-3 and a subsequent fluorescent secondary antibody. Arrows indicate positively transfected cells. Scale bars = 50µm.

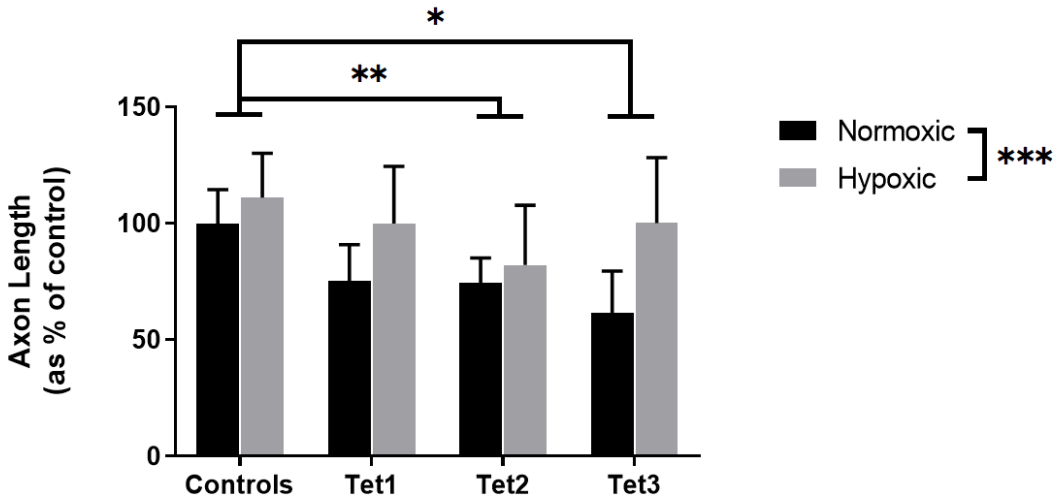


Figure 5.7: The effects of hypoxia and knocking down Tet enzymes on axon length
Cultures of mouse cortical neurons were transfected with a plasmid construct of GFP alongside a non-targeting siRNA or siRNAs targeting Tet1, Tet2 or Tet3, and were subjected to 2.5h of OGD (hypoxic), or no OGD (normoxic). Cultures were stained and imaged in order to assess axon length. Axon lengths were normalised to normoxic controls. A significant effect of hypoxia (p=0.001) and transfection status (p=0.002) were observed; the latter being driven by significantly decreased axon length in Tet2 (p=0.005) and Tet3 (p=0.01) targeting siRNA groups. No significant interaction between factors was determined (p=0.24). For controls, n=10 in each group. For Tet-knockdown groups, n=5 in each group. Data is presented as mean ± SD. * represents p≤0.05; ** represents p≤0.01; *** represents p≤0.001.

There were no significant differences in the number of neurites between normoxic and hypoxic groups (Figure 5.8; $F_{1,42}$=0.54; p=0.47) or between transfection status groups ($F_{3,42}$=2.36; p=0.09). There was also no significant interaction between these factors ($F_{3,42}$=1.00; p=0.40).

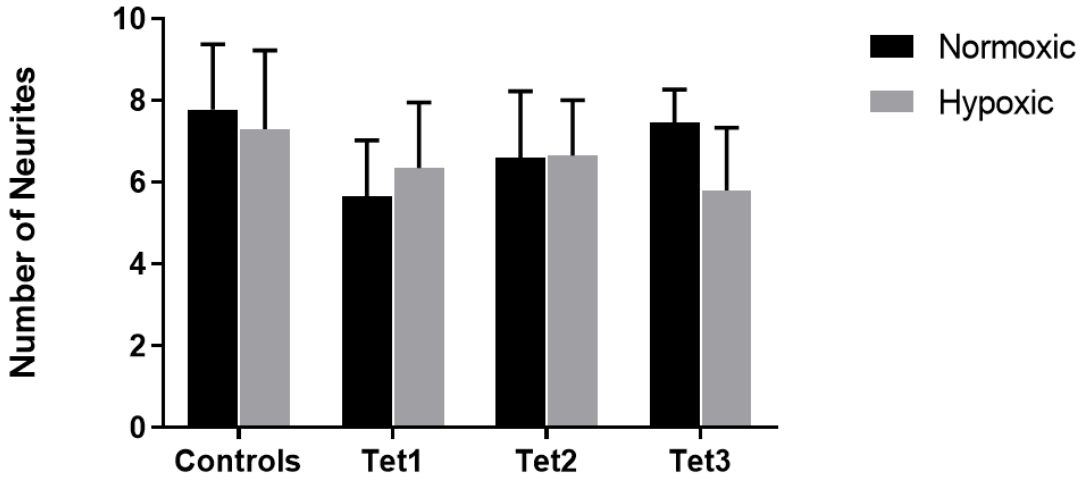


Figure 5.8: The effects of hypoxia and knocking down Tet enzymes on number of neurites Cultures of mouse cortical neurons were transfected with a plasmid construct of GFP alongside a non-targeting siRNA or siRNAs targeting Tet1, Tet2 or Tet3, and were subjected to 2.5h of OGD (hypoxic), or no OGD (normoxic). Cultures were stained and imaged in order to assess number of neurites. No significant effects of hypoxic status (p=0.47) or transfection status (p=0.09) were determined, and there was no significant interaction between these factors (p=0.40). For controls, n=10 in each group. For Tet-knockdown groups, n=5 in each group. Data is presented as mean ± SD.

Figure 5.9 shows changes in total neurite length as a result of knocking down Tet enzyme expression and subjecting cultures to 2.5h of OGD. Overall, total neurite length was significantly increased in the hypoxic groups compared to normoxic groups ($F_{1,42}$=4.57; p=0.04). Knockdown of Tet enzyme expression significantly reduced total neurite length ($F_{3,42}$=4.74; p=0.008), with post-hoc analysis revealing that Tet2 (p=0.05) and Tet3 (p=0.03) knockdown produced significantly shorter total neurite lengths than controls, whereas knockdown of Tet1 does not (p=0.08). There was no significant interaction between hypoxia and Tet expression ($F_{3,42}$=0.34; p=0.79).

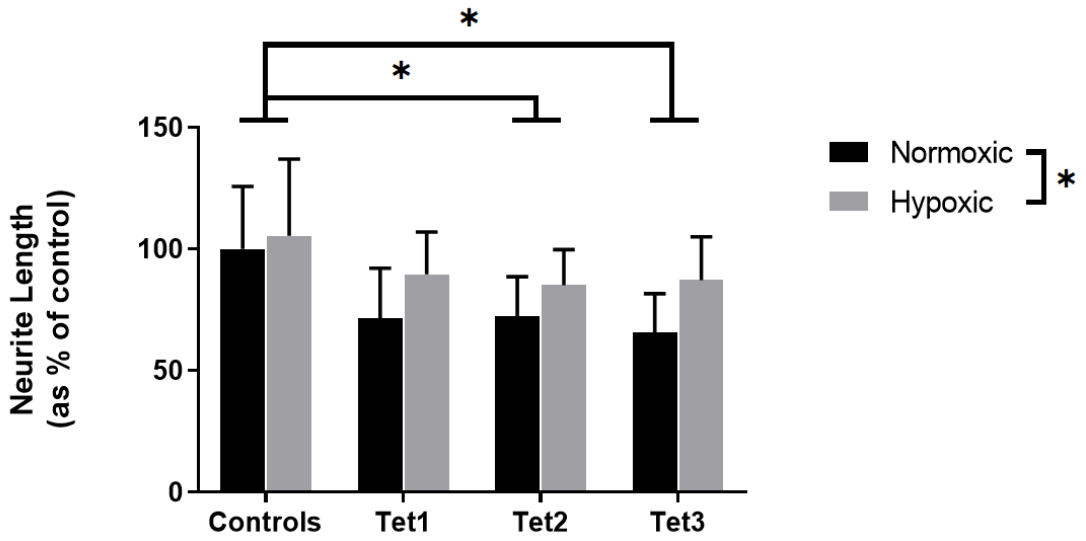


Figure 5.9: The effects of hypoxia and knocking down Tet enzymes on total neurite length Cultures of mouse cortical neurons were transfected with a plasmid construct of GFP alongside a non-targeting siRNA or siRNAs targeting Tet1, Tet2 or Tet3, and were subjected to 2.5h of OGD (hypoxic), or no OGD (normoxic). Cultures were stained and imaged in order to assess total neurite length. Total neurite length was normalised to normoxic controls. A significant effect of hypoxia ($p=0.04$) and transfection status ($p=0.008$) were observed; the latter being driven by significantly decreased neurite length in Tet2 ($p=0.05$) and Tet3 ($p=0.03$) targeting siRNA groups. No significant interaction between factors was determined ($p=0.79$). For controls, n=10 in each group. For Tet-knockdown groups, n=5 in each group. Data is presented as mean ± SD. * represents $p \leq 0.05$.

5.3.5: Effects of increased Tet enzyme expression

Figure 5.10 shows representative images of cortical neurons that have been transfected with a plasmid construct for expression of GFP along with a plasmid constructs for expression of Tet1, Tet2 or Tet3, demonstrating differences in axon/dendrite length and Tet enzyme expression.

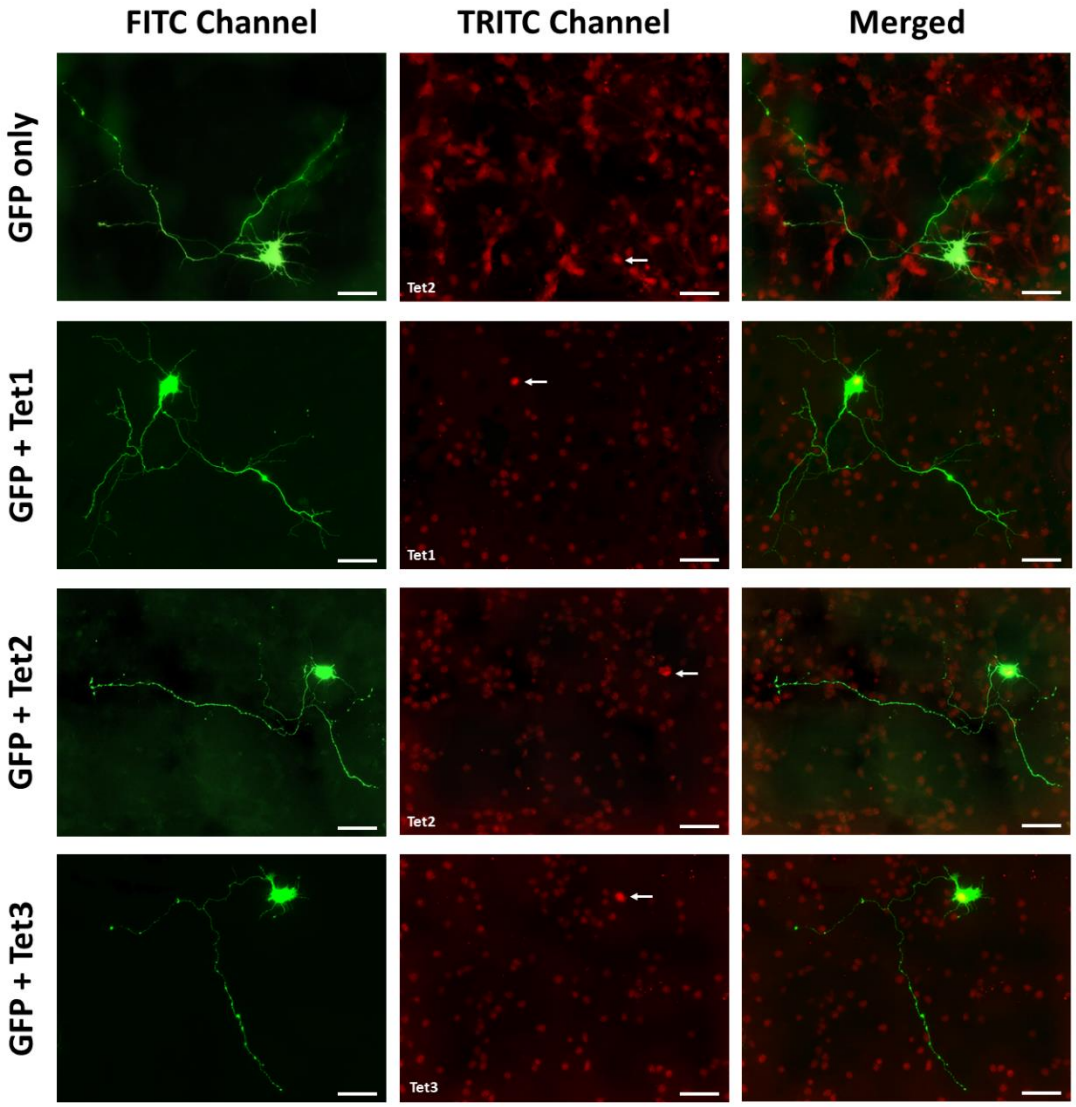


Figure 5.10: Images of neuronal cultures transfected with plasmid constructs of Tet1-3
Cultures of cortical neuronal cells derived from neonatal mice were transfected with either a plasmid construct for expression of GFP, or GFP plasmid along with a plasmid construct for expression of Tet1, Tet2 or Tet3. 3 days after transfection, cells were fixed and stained with antibodies for Tet1-3 and a subsequent fluorescent secondary antibody. Arrows indicate positively transfected cells. Scale bars = 50µm.

Figure 5.11 demonstrates changes in axon length as a result of using plasmid constructs to increase expression of Tet enzymes in both normoxic and hypoxic conditions. There was no significant difference in axon length between normoxic and hypoxic groups ($F_{1,32}$<0.01; p=0.97), although there was a significant difference between transfection status groups ($F_{3,32}$=3.13; p=0.04). Axon length in neurons transfected with plasmid constructs for expression of Tet1 and Tet2 did not differ from controls (p=0.82 and p=0.79, respectively), however those transfected with a plasmid construct for expression of Tet3 showed significantly increased axon length (p=0.03). There was no significant interaction between hypoxia and expression of Tet enzymes ($F_{3,32}$=0.13; p=0.94).

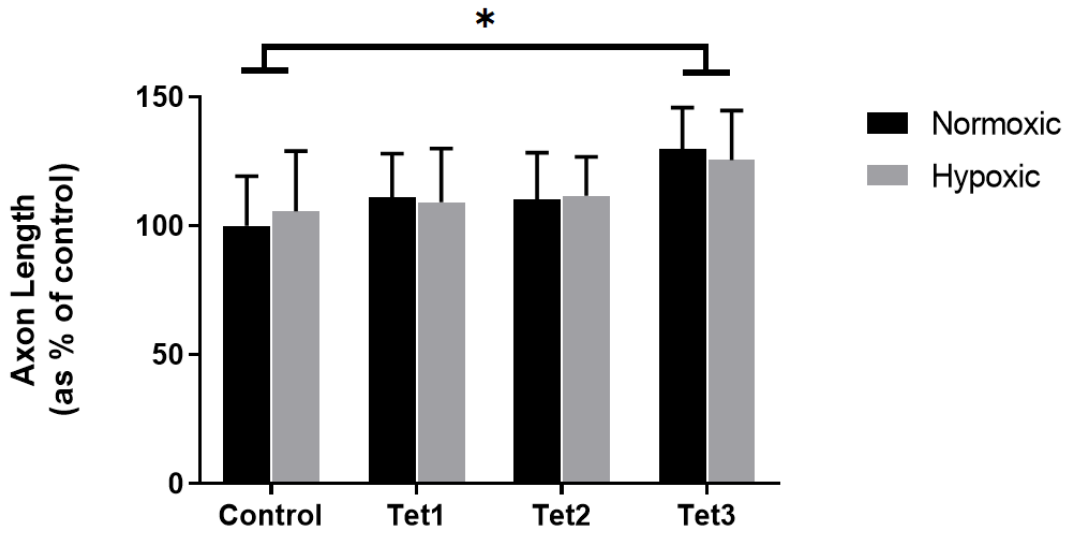


Figure 5.11: The effects of hypoxia and increasing Tet enzyme expression on axon length
Cultures of mouse cortical neurons were transfected with only a plasmid construct of GFP plasmid (control), or GFP plasmid alongside plasmid constructs for expression of Tet1, Tet2 or Tet3, and were subjected to 2.5h of OGD (hypoxic), or no OGD (normoxic). Cultures were stained and imaged in order to assess axon length. Axon length is normalised to normoxic controls. No significant effect of hypoxia was determined (p=0.97), though a significant effect of transfection status (p=0.04) was observed; the latter being driven by significantly increased axon length in Tet3 (p=0.03) plasmid groups. No significant interaction between factors was determined (p=0.94). n=5 in each group. Data is presented as mean ± SD. * represents p≤0.05.

There were also no significant differences in the number of neurites between normoxic and hypoxic groups (Figure 5.12; $F_{1,32}$=1.07; p=0.31), and no significant difference in number of neurites between transfection status groups ($F_{3,32}$=0.60; p=0.62). There was, however, a significant interaction between these factors ($F_{3,32}$=2.90; p=0.05), although Tukey's multiple comparisons test failed to reach significance between any pairs of groups.

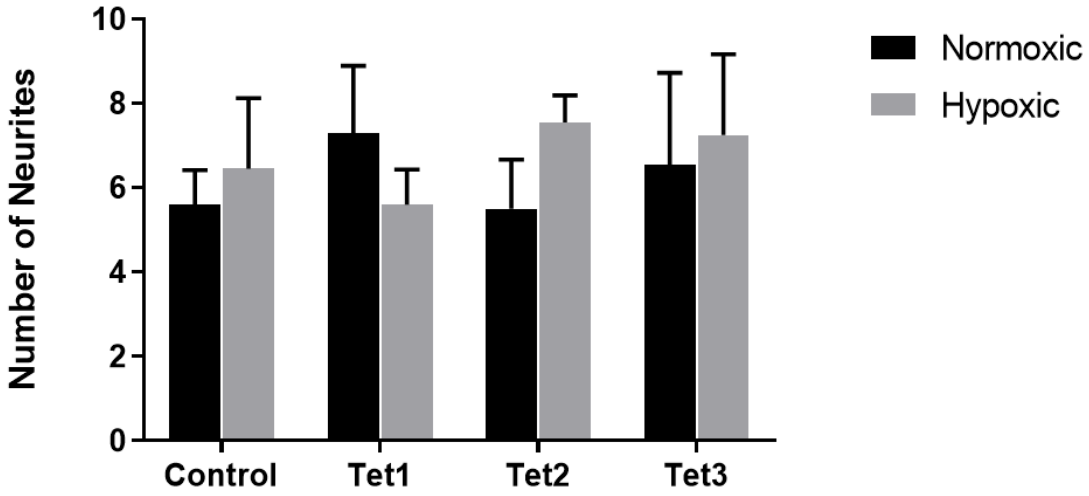


Figure 5.12: The effects of hypoxia and increasing Tet enzyme expression on number of neurites
Cultures of mouse cortical neurons were transfected with only a plasmid construct of GFP plasmid (control), or GFP plasmid alongside plasmid constructs for expression of Tet1, Tet2 or Tet3, and were subjected to 2.5h of OGD (hypoxic), or no OGD (normoxic). Cultures were stained and imaged in order to assess number of neurites. No significant effects of hypoxic status (p=0.31) or transfection status (p=0.062) were determined, although there was a significant interaction between these factors (p=0.05). However, post-hoc analysis did not reveal any significant differences between any pairs of groups. n=5 in each group. Data is presented as mean ± SD.

Figure 5.13 shows changes in total neurite length as a result of increasing Tet enzyme expression and subjecting cultures to 2.5h of OGD. There was no significant difference between normoxic and hypoxic groups ($F_{1,32}$=0.31; p=0.58), no significant difference between transfection status groups ($F_{3,32}$=1.78; p=0.17), and no significant interaction between these factors ($F_{3,32}$=0.47; p=0.71).

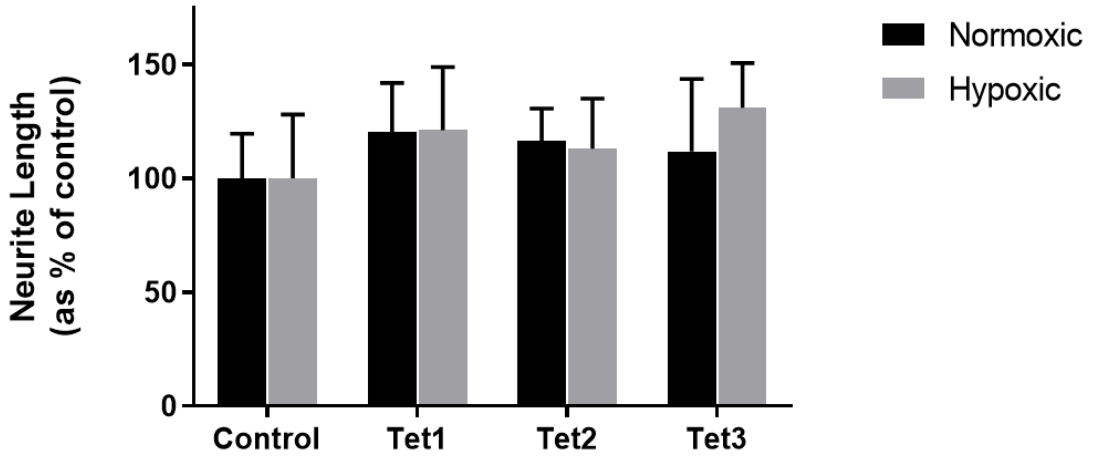


Figure 5.13: The effects of hypoxia and increasing Tet enzyme expression on total neurite length

Cultures of mouse cortical neurons were transfected with only a plasmid construct of GFP plasmid (control), or GFP plasmid alongside plasmid constructs for expression of Tet1, Tet2 or Tet3, and were subjected to 2.5h of OGD (hypoxic), or no OGD (normoxic). Cultures were stained and imaged in order to assess total neurite length. Neurite length is normalised to normoxic controls. No significant effects of hypoxic status ($p=0.58$) or transfection status ($p=0.17$) were determined, and there was no significant interaction between these factors ($p=0.71$). $n=5$ in each group. Data is presented as mean ± SD.

5.4: Discussion

Previous chapters in this thesis have used various methods to elucidate an intrinsic epigenetic response to stroke that involves increased expression of 5hmC in various cell types. The timing of these changes coincides with previously determined increases in neuronal plasticity and changes in expression of axon growth related genes (Li et al., 2010), therefore suggesting a potential role of 5hmC, and the family of Tet enzymes that catalyse its formation, in the control of post-stroke axon growth. The overall aim of this chapter was to determine a direct effect of Tet enzyme activity and axonal growth, and through the use of an *in vitro* model of ischemic stroke, the experimental work performed in this chapter has helped to determine such an effect.

5.4.1: Hypoxia and cell viability

In experiment A, performing the MTT reduction assay on cultures that had undergone 2.5h of OGD revealed that cell viability had reduced by around 40% in comparison to normoxic cultures (Figure 5.2). Though these levels of cell viability are in line with previous research using the same model of OGD (Scorziello et al., 2001; Wu et al., 2008), it is important to consider how this loss of viable cells may have affected subsequent observations. The cultures used in this experiment are classed as cortical neuronal cultures, as the lack of serum in neurobasal media prevents the growth of glial cells and thereby selects for the growth of neurons. However, around 5-10% of the cells in culture are astrocytes, with this proportion increasing over time as the astrocytes proliferate whereas the neurons do not. It is therefore important to consider that one of these cell types may be more resistant to hypoxic damage than the other, and therefore that any differences observed in the hypoxic groups in this chapter may be due to changes in the proportions of these cells. An alternative experimental

design that may remedy this is the purification of a neuronal cell population using a method such as magnetic cell separation or FACS. However, it could then be argued that a purely neuronal cell population is not representative of the *in vivo* environment and as such, results would not be translatable.

5.4.2: The effects of Tet enzyme expression on neuronal growth

The transfection of cortical neuronal cells with siRNAs to elicit a knockdown in protein expression of Tet2 and Tet3 each caused a significant reduction in both axon length (Figure 5.7) and total neurite length (Figure 5.9). Furthermore, overexpression of Tet3 protein via transfection with mammalian plasmid construct caused significantly increased axon length (Figure 5.11). This supports previous research that has determined that Tet3 knockdown causes significantly reduced axon growth in the CNS (Weng et al., 2017), although this research focused on a model of sciatic nerve injury whereas the present work has determined a similar effect in cortical neurons.

Though neuronal cells with decreased expression of Tet3 exhibit significantly shorter axon and neurite lengths, the magnitude of this effect appears to be larger in normoxic conditions (although this cannot be consolidated as the interaction between these factors was not significant) (Figures 5.7 + 5.11). However, in cells transfected with Tet2-targeting siRNA, there is a trend towards axon and neurite lengths being similar in both normoxic and hypoxic conditions. This phenomenon could potentially be explained by the finding that Tet3, but not Tet2, protein expression levels are increased following hypoxic insult (Figure 5.4). This suggests that perhaps in hypoxic conditions, the hypoxia-induced increase in Tet3 mRNA means that the deleterious effects of the Tet3-targeting siRNA are being lessened, thereby attenuating the detrimental effects of the siRNA. The finding that Tet3 and Hif1α protein expression levels are both increased following hypoxic insult support previous findings that

hypoxia increases Tet3 expression via increased expression of Hif1α (Lin et al., 2017). It may also be important to note that although the increase in Tet1 expression with hypoxia came close to statistical significance without passing the threshold for significance, post-hoc power analysis deemed this experiment slightly underpowered (see Appendix A6), suggesting that slightly increasing the number of repeats in this experiment may have revealed a significant effect.

Extraction of DNA from neuronal cells in normoxic and hypoxic conditions and subsequent analysis of 5mC and 5hmC content revealed that neuronal cells that suffered a hypoxic insult exhibited significantly higher levels of 5hmC than cells in normoxic conditions 2 days post-OGD (Figure 5.5), although this is not reflected by a significant difference in 5mC levels. This supports the findings in Chapter 2 (that ischemic stroke leads to increased 5hmC levels in the cortex and striatum) and Chapter 4 (that ischemic stroke leads to significantly increased expression of 5hmC in the total cell population). As in Chapter 4, the lack of observed changes to global 5mC levels indicate that the significant increases in 5hmC levels are not indicative of global demethylation, but may instead indicate that demethylation is occurring at a gene-specific level, with Tet-mediated demethylation causing increased expression of axon- and neurite-growth related genes, causing the observed changes in axon and neurite lengths. This 5hmC quantification data, taken together with the neuronal growth data obtained in this chapter, supports pervious research and strengthens the theory that Tet enzymes, particularly Tet3, control axon and neurite growth, with this mechanism perhaps being altered in ischemia/hypoxia via Hif1α.

Not all experimental data obtained in this chapter, however, supports previous research. For example, neither knockdown or overexpression of Tet enzymes caused significant differences in neurite numbers (Figures 5.8 + 5.12), whereas Weng et al. (2017) determined that

knockdown of Tet3 expression caused decreased numbers of DRG neurites *in vivo*. Given a lack of research in this particular area, it is difficult to determine why this effect was not observed in the current experiments, although it can most likely be attributed to the difference in experimental models (use of DRG neurons *in vivo* v. cortical neurons *in vitro*).

5.4.3: The effects of hypoxia on neuronal growth

When assessing only control (GFP-only or NT siRNA-transfected cells) groups, there appears to be no differences in axon length between normoxic and hypoxic cells (Figures 5.7 + 5.11), suggesting that hypoxia alone does not affect axon growth. Previous research has determined that hypoxia can affect axon growth, but there are conflicting statements as to whether hypoxia is beneficial or detrimental to axon growth. For example, Cho et al. (2015) determined that 4 hours of hypoxia either before or immediately following mechanical axotomy increased axonal growth by ~2-fold, whereas no differences in axon growth were determined when hypoxia treatment was delayed by any longer than 4 hours. However, in the same experiments, it was determined that both knockdown of Hif1α and overexpression of Hif1α significantly reduce DRG axon length following axotomy. Additionally, Zhang et al. (2017) cultured rat hippocampal neurons and administered OGD for 1 hour at DIV7 and found that hypoxia had significantly reduced axon length at DIV11.

The conflicting results of these experiments and the experimental work carried out in this chapter may be due to differences in experimental model & design. Cho et al. tested axon growth following mechanical axotomy, whereas Zhang et al. and the experiments performed in this chapter assessed axon growth in uninjured primary neurons. Also, the timepoints of hypoxic treatment differ, with Zheng et al. performing OGD at DIV7 and allowing 4 days of growth before measuring, whereas the experiments performed in this chapter involved

administering OGD at DIV2 and allowing 2 days of growth before measuring (Figure 5.1). This suggests that the effect of hypoxia on axon growth may be delayed, with no observable differences occurring for several days. Moreover, the differences in hypoxic insult intensity (1h of OGD performed by Zheng et al. v. 2.5h OGD performed in this chapter) may have led to the differences in resulting axon lengths, especially given the findings by Cho et al. that both over- and under-expression of Hif1α negatively affect axon length *in vitro*.

5.4.4: Potential role of ascorbate

Considering that knockdown of Tet2 and Tet3 caused significant decreases in axon and neurite length, it could be expected that increasing expression of these proteins by transfecting with plasmid constructs would therefore have the opposite effect and increase axon and neurite length. However, it was seen that only increased expression of Tet3, not Tet2, caused any significant increases in axon length (Figure 5.8). Furthermore, increased expression of Tet enzymes did not have any effect on total neurite length (Figure 5.13). The reason for the lack of any observed effects may indicate that increased expression of Tet proteins does not directly relate to increased enzymatic activity of these proteins. One way to determine this would be to assess 5hmC content within positively transfected cells.

Increased expression of Tet enzymes may not necessarily lead to increased 5mC oxidation perhaps due to a limiting factor preventing increased rates of reaction. As explained in the general introduction of this thesis (Chapter 1; section 1.2.4), the catalytic activity of Tet enzymes is positively regulated by the presence of Vitamin C, otherwise known as ascorbate. Ascorbate is vital to normal CNS function, acting as an antioxidant molecule to prevent damage by reactive oxygen species and also acting as an important cofactor in many other vital enzymatic reactions, such as the synthesis of catelcholamines and amino acids (Harrison

& May, 2009). Given its important functions, it is unsurprising that ascorbate is abundantly present in CNS extracellular fluid; around 200-400µM in rodents (Miele & Fillenz, 1996; Schenk et al., 1982). In the present study, however, the concentration of ascorbate in the cell culture media (Opti-MEM; Thermo Fisher, UK) is 0.00025mg/ml, or around 1.5nM. This is far lower than endogenous levels *in vivo*, and as such it is possible that despite increased expression of Tet enzymes in plasmid-transfected cells, the oxidation of 5mC to 5hmC was limited by this absence of enzymatic cofactor. Given that the Opti-MEM cell culture media is specifically designed for use in lipid transfection, and the current experiment was used as a proof of concept, extra ascorbate was not added to the cultures. This is, however, a possibility for future experiments; if increasing extracellular ascorbate concentrations to match endogenous levels reveals a positive effect of increased Tet enzyme expression on axon growth, this could therefore possibly lead to potential therapeutic interventions aimed at increasing Tet enzyme levels post-stroke.

5.4.5: Limitations & future research

Although the use of OGD in primary neuronal cultures has been well established as an *in vitro* model of ischemic stroke and reperfusion (Holloway & Gavins, 2016), there are limitations of the model utilised in this chapter that may prevent the observed results from being translated to ischemic stroke *in vivo*. Namely, measurements were made based on the growth of newly sprouting axons and neurites in developing neurons derived from E15 neonatal mice, which is not representative of the majority of ischemic stroke cases which occur in aged individuals. E15 cortical neurons and mature cortical neurons may vary in their resistance to hypoxic damage and in their response to changes in Tet enzyme expression, and as such it could be argued that using E15 cortical neurons is not representative of stroke. Alternatively, neonatal cortices could still be used to set up cultures in future research, but the cultures could then

be allowed to mature before administering OGD and/or Tet-targeting siRNAs in order to make a more representative *in vitro* model of ischemic stroke.

Although the plasticity of brain regions following ischemic stroke is largely due to sprouting of new axons, the regeneration of damaged axons also occurs (Carmichael, 2003; Li et al., 2010; Q. Zhang et al., 2013), which was not assessed in this study. It may therefore be of interest to study how this regrowth of damaged axons is affected by Tet enzyme expression and hypoxia. A potential method of assessing this would be through the use of microfluidic devices (Figure 5.14). Microfluidic devices designed for axonal growth analysis consist of two compartments (one somal and one axonal, each connected to two reservoirs) that are connected by microgrooves. Neurons are added to the somal reservoir and are drawn into the somal compartment via capillary action. Over several days, axonal growth is guided through the microgrooves, meaning that axons are aligned in parallel and can be axotomised reliably (Tong et al., 2015). Although using such a device would allow for the investigation of the role of Tet enzyme expression on axonal regeneration, this model is still not fully representative of ischemic stroke as mechanical axotomy is not akin to axonal damage due to hypoxia.

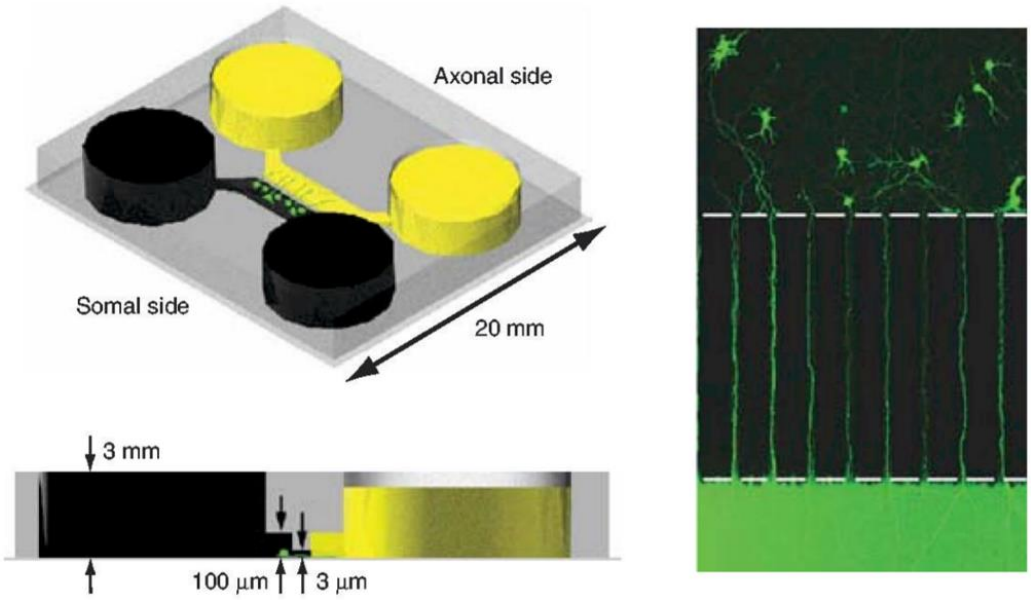


Figure 5.14: Microfluidic device culture platform for assessment of axonal growth
Left: The microfluidic chamber consists of two sets of reservoirs connected by a chamber; one somal and one axonal. These chambers are connected to one another by microgrooves (10µm wide, 3µm high). These microgrooves direct the growth of axons from the somal chamber to the axonal chamber, effectively isolating cell bodies from axons. *Right:* A volume difference between chambers, and the fluidic resistance of the microgrooves, allows for the isolation of microenvironments to the axonal chamber. Shown in the image is isolation of CellTracker Green dye to the axonal chamber; this dye has backtracked neurons from their isolated axons. (*Image adapted from Taylor et al., 2005*).

Alternatively, a microfluidic device could be set up in order to create a specialised *in vitro* model of ischemic stroke in which cell bodies remain in a normoxic environment, whereas axon terminals are subjected to hypoxia. As shown in Figure 5.14, a volume difference between the somal and axonal chambers allows for chemical microenvironments to be isolated to axons, owing to the high fluidic resistance of the microgrooves. This feature could be utilised to set up specialised microfluidic devices in which cell bodies are cultured in normoxic conditions whereas axons are subjected to hypoxia. OGD would not be possible in this setup as the entire device would need to be incubated in a hypoxic chamber, meaning that cell bodies would also be subjected to hypoxia. However, a chemical inductor of hypoxia such as cobalt (II) chloride ($CoCl_2$) (Wu & Yotnda, 2011) could be introduced to the axonal

chamber. Setup of such a device would allow for the assessment of axonal damage due to hypoxia, and how this affects Tet enzyme activity and/or 5hmC levels. The addition of dopaminergic nigral neurons to this setup would also allow for the modelling of nigrostriatal projections, as was observed in Chapter 2 of this thesis. In Chapter 2, it was observed that dopaminergic neurons of the substantia nigra, which project directly to the infarcted striatum, exhibited increased levels of 5hmC following ischemic stroke. By utilising the described microfluidic device setup, this effect could be modelled *in vitro*.

It is also important to note that the use of the GFP plasmid in control cultures could have introduced unintentional bias – in experiment C, cultures that did not receive Tet plasmid instead received twice the amount of GFP plasmid, in order to match the amount of DNA loaded into each culture. This could have therefore have made it more likely that smaller, thinner axonal/dendritic process fluoresce brighter and show up in images that may not have done if the GFP plasmid content was lowered, thereby leading to increases in measured axon length. In future studies, it is important to instead utilise a non-sensical plasmid that does not code for a fluorescent protein as a loading control, in order to account for this limitation.

Aside from the utilisation of microfluidic devices, there are further potential follow-up experiments that can be performed to further elucidate the effects of Tet enzyme expression and activity on post-stroke axon growth. For example, knocking down multiple Tet enzymes at once and assessing neuronal growth may reveal further detrimental effects. Similarly, overexpressing multiple Tet enzymes may reveal a synergistic effect in the positive regulation of axonal growth. Determining such effects would help to further inform any future potential Tet-mediated therapeutic interventions.

5.4.6: Summary

Previous chapters in this thesis have hinted at a potential role of Tet enzymes in the control of post-stroke axon growth by demonstrating changes in 5hmC levels at a global and cell-specific level following ischemic stroke, the timing of which coincides with peak post-stroke expression of axon-growth related genes. However, a direct relationship between Tet enzyme expression/activity and post-stroke axon growth had not been determined. Having utilised an *in vitro* model of ischemic stroke and altering Tet enzyme expression through use of siRNAs and plasmids, the experimental work performed in this chapter has determined that some members of the Tet family of enzymes appear to play a direct role in the control of axon growth. Namely, knockdown of Tet2 and Tet3 significantly decreased axon and neurite length in normoxic conditions, although when increasing expression of these enzymes only Tet3 demonstrated a positive effect on axon length. Furthermore, the detrimental effect of Tet3 knockdown appeared to be attenuated following hypoxic insult, although this is likely due to the observed increase in Tet3 protein expression in post-hypoxic neurons. The observed increase in Tet3 expression following hypoxic insult is also accompanied by a significant increase in global 5hmC levels, which supports findings in previous chapters of this thesis. Although modifications in order to more accurately replicate ischemic stroke, the data obtained in this chapter appears to define a role of Tet enzymes, particularly Tet3, in the control of neuronal growth that could potentially translate to post-stroke axon growth.

Chapter 6: General Discussion

6.1: Summary and overall relevance

This thesis has aimed to determine a potential role of the oxidised 5mC residue 5hmC, and the Tet family of enzymes that catalyse its formation, in the control of post-stroke axon growth. Through various *in vivo* methods, an intrinsic methylomic response of the brain to ischemic stroke was determined. This response involves significantly increased levels of 5hmC in brain areas (in)directly affected by stroke and is observed in the total cell population as well as microglial cells specifically. Alongside this, the use of an *in vitro* model of ischemic stroke and reperfusion has helped to determine a direct effect of Tet enzyme expression, particularly Tet3, on axon growth. Taken together, these findings suggest that the observed post-stroke increase in 5hmC levels are potentially involved in the positive regulation of post-stroke axon growth.

6.1.1: Methylomic response to ischemic stroke

Previous research has established that 5mC levels in the brain are significantly increased following ischemic stroke, which has a detrimental effect given that reductions in 5mC lead to decreased infarct size, increased axonal sprouting and improved functional recovery (Choi et al., 2018; Dock et al., 2015; Endres et al., 2001; Endres et al., 2000). Whilst the role of this 'classical' form of DNA methylation in the pathophysiology of ischemic stroke is relatively well characterised, the potential roles of 5hmC and other oxidised 5mC residues are comparatively understudied.

One of the first papers that determined a potential role was published by Miao et al. (2015), in which it was discovered that following MCAO, both 5mC and 5hmC levels are significantly increased in the ischemic hemisphere. However, 5mC levels peak sooner than 5hmC levels (at 36 hours and 48 hours, respectively), and both having returned to baseline levels by 7 days. A very recent study carried out by Morris-Blanco et al. (2019) also determined a similar effect, with 5mC levels increasing significantly post-stroke and peaking at 12 hours, and 5hmC also being significantly increased, sustained for 6-24 hours. Although having determined an acute timeline of changes to the methylome following ischemic stroke, neither of these studies assessed 5hmC levels in the long term. This assessment was performed in Chapter 2 of this thesis, in which it was determined that 5hmC levels are significantly increased post-stroke in both the non-infarcted cortex and striatum, peaking at 48 hours and 7 days post-stroke, respectively. Assessment at 1 month post-stroke determined that 5hmC levels had returned to baseline levels by this timepoint. Similarly, in Chapter 4, assessment of 5hmC content of DNA extracted from total cell population at 2 weeks post-stroke revealed significantly higher 5hmC content in stroke animals. Although this experiment used a slightly different animal model of ischemic stroke than that utilised in Chapter 2, these findings indicate that 5hmC levels are still significantly increased at 2 weeks post-stroke. Furthermore, the significant increase in 5hmC levels were also observed in the substantia nigra pars compacta, in cells that project directly to the infarcted striatum, however it is possible that the measured increases in 5hmC may be secondary to cell death signals occurring. Taken together, these observations not only concur with the previous research carried out in this area, they also elucidate an extended timeline of post-stroke hydroxymethylation changes that appears to differ between distinct brain regions, which had not been previously determined.

It should be noted that although the data obtained in Chapter 2 determines a similar timeline of post-stroke 5hmC changes to those observed by Miao et al. and Morris-Blanco et al., the

magnitude of these changes appears to be smaller. In Chapter 2, maximum 5hmC levels reached around a 1.75-fold increase over control animals, whereas in the aforementioned studies, 5hmC was found to peak at around a 4-fold increase over controls. This could be explained by the differences in stroke severity, as in Chapter 2, the MCA of mice was occluded for 30 minutes, whereas in the previously published studies the MCA was occluded for 45-75 minutes. Although 5hmC levels did not correlate with infarct size in Chapters 2 or 4, it is possible that the increased severity of stroke in the previously published studies may have induced more drastic changes in 5hmC levels.

The observed timeline of post-stroke methylome changes appears to be characterised by an initial increase in global 5mC, followed by significant increases in 5hmC in the following hours/days that may be indicative of a global demethylation event. The peak in post-stroke 5hmC levels also coincides with increased expression of recovery- and axon growth-related genes at 7 days (Li et al., 2010). This therefore suggests that the observed increase in hydroxymethylation may be working towards demethylation of these particular genes, priming them for expression as part of the endogenous post-stroke recovery response.

Through the use of FACS, Chapter 4 of this thesis determined that the post-stroke increase in 5hmC was observed not only in the total cell population, but also in microglial/macrophage cells ($CD11b^{+}/CD45^{low}$) specifically. This increase in microglial/macrophage cell hydroxymethylation was also accompanied by a significant increase in CD11b expression, which is indicative of microglial activation. This therefore suggests that the observed increase in 5hmC levels following ischemic stroke may be involved not only in the increased expression of axon growth-related genes, but also in microglial activation. However, neither global levels of 5mC or 5hmC significantly correlated with CD11b expression, suggesting that increased expression of this antigen is not directly caused by hydroxymethylation. Alternatively, the

marked increase in 5hmC content in microglial cells post-stroke could be indicative of increased expression of any number of microglial activation markers, such as TNF-α, IL-6 or IL-1β. Further determination of the role of Tet enzymes and hydroxymethylation in the control of post-stroke microglial activation via investigation of these markers is a possible aim of future studies.

Until further research elucidates a direct role of DNA (hydroxymethylation) in the control of post-stroke microglial activation, however, such relationships are speculative. Despite previous research finding increased 5hmC immunoreactivity in microglial cells in an animal model of hypoperfusion (Tsenkina et al., 2014), and global hypomethylation of activated microglia following traumatic brain injury (Zhang et al., 2007), no such effects have been previously observed within the specific context of ischemic stroke. If the currently observed post-stroke increase in 5hmC levels in microglia is involved in the control of microglial activation, this could present a possible target for therapeutic treatments that target microglial cells in order to indirectly promote axon growth and functional recovery.

6.1.2: Tet-mediated regulation of axon growth

With previous chapters in this thesis having established a methylomic response of the brain to ischemia that presents as marked increases in 5hmC levels, Chapter 5 used an *in vitro* model of ischemia and reperfusion to determine a direct effect of Tet enzyme expression on axon growth, further establishing a potential role of 5hmC in the control of post-stroke axon growth.

Transfection with siRNAs to knock down the expression of Tet2 and Tet3 each caused significantly decreased axon length, which is in concurrence with previous research having

determined that knocking down Tet3 causes significant decreases in axonal regeneration and functional recovery following sciatic nerve ligation in mice (Weng et al., 2017). Furthermore, within the context of ischemic stroke, Morris-Blanco et al. (2019) discovered that administering siRNAs targeting Tet3 to the infarct region produced significantly reduced infarct sizes, whilst Miao et al. (2015) found that administration of Pluripotin, an inhibitor of Tet2, had similar effects. These two studies, however, do not demonstrate a direct effect of Tet knockdown on axon growth but instead demonstrate a neuroprotective effect of the enzymes. This thesis, however, has determined an effect of Tet enzyme expression on the growth of axons that could be targeted post-stroke in a form of delayed therapeutic treatment.

Although decreased expression of Tet2 and Tet3 caused significantly decreased axon growth in normoxic conditions, hypoxic insult appeared to somewhat ameliorate this effect, with siRNA transfection in hypoxic cultures leading to a smaller decreases in axon length. This is likely because following hypoxia, it was observed that 5hmC levels and Tet3 expression are significantly increased, which has also been determined in previous research (Lin et al., 2017). The method by which hypoxia induces Tet enzyme expression is believed to be through increased expression of Hif1α, given that knockout of Hif1α completely attenuates hypoxia induced increases in Tet enzyme expression (Lin et al., 2017). Furthermore, Loh et al. (2017) determined, through use of transcription factor motif enrichment analysis, that Hif1α plays a central role in the regulation of 5hmC dynamics following axonal injury. Alternatively, Weng et al. (2017) found that the increase in Tet3 expression that is observed following axonal injury is dependent on an influx of calcium ions, propagating from injured axons back to cell bodies. Given that the pathophysiology of ischemic stroke involves both the induction of hypoxia (and subsequent increase in Hif1α) and an excitotoxic response that leads to increased intracellular

calcium levels (Dirnagl et al., 1999), it is likely that both of these mechanisms contribute to increased Tet enzyme expression following ischemia.

The mechanism through which Tet enzymes influence axonal growth is believed to be through altered expression of axon growth-related genes via demethylation. When studying changes in mRNA expression levels in total cell populations in Chapter 4 of this thesis, it was determined that significant increases in 5hmC and Tet3 expression were accompanied by slightly increased (albeit not statistically significant) increases in BDNF and Ttll7 expression. These findings are in concurrence with previous research, such as Weng et al. (2017) finding that sciatic nerve ligation caused significant increases in mRNA levels of the axon growth-related genes ATF3, Smad1, STAT3 and Myc, with these increases attenuated when Tet3 expression was knocked down. Alongside this, they determined that knockout of TDG (the enzyme responsible for the removal of oxidised 5mC residues and complete DNA demethylation) also attenuated these post-injury gene expression increases and impaired axonal regeneration. This therefore suggests that increased 5hmC levels alone are not sufficient for the promotion of axon growth, but rather complete DNA demethylation must occur. Furthermore, genomic mapping of hydroxymethylation in dorsal root ganglion cells following axotomy has revealed that the most differentially hydroxymethylated regions were found on genes associated with axon growth, namely ATF3, Smad1 and BDNF (Loh et al., 2017). Interestingly, only 0.5% of these differentially hydroxymethylated regions were located on CpG islands, with most (55%) found on the gene bodies of axon growth-related genes.

The importance of hydroxymethylation changes in gene bodies vs. CpG islands, particularly in the context of axon growth, is relatively unknown. Tet2, unlike Tet1 and Tet3, does not possess the CXXC domain, which has been shown to be non-essential for enzymatic activity but responsible for binding to CpG islands (Tan & Shi, 2012). It is therefore plausible that

increased Tet2 activity is responsible for increased 5hmC occurrence at gene bodies, as it is unable to bind to CpG islands. Whilst increased 5hmC levels at gene bodies is unlikely to be responsible for increased gene expression, previous research has begun to elucidate a potential role for this loci-specific change in hydroxymethylation. When analysing genomic distribution of 5hmC in developing neurons, Hahn et al. (2013) discovered that increased levels of 5hmC did not correlate with demethylation, but were instead associated with loss of the histone methylation marker H3K27me3, an epigenetic marker strongly associated with gene inactivation. Considering this, it is therefore possible that the currently observed changes in post-stroke 5hmC levels, and effects of Tet enzyme knockdown on axon growth, are a result of 5hmC acting not only as an intermediate of demethylation, but also as a stable epigenetic marker in conjunction with other epigenetic mechanisms.

6.2: Areas for future research

Determining a role of hydroxymethylation in the control of axon growth, particularly within the context of ischemic stroke, is a novel venture. Although this thesis has worked towards determining such a role, there are certain aspects of the process that need to be fully elucidated before any attempts can be made at developing therapeutic interventions.

Namely, it has not been determined that the observed increases in 5hmC levels and Tet enzyme expression following ischemic stroke/hypoxia directly lead to demethylation and/or subsequent increased expression of axon growth related genes. Although 5hmC peaks coincide with peak expression of axon growth related genes, and Tet knockdown causes decreased axon growth, there has been little to no research to determine that this is due to direct changes to hydroxymethylation of these genes. Morris-Blanco et al. (2019) profiled antioxidant and DNA repair genes to determine significant changes in the 5hmC content of

these genes following MCAO, which were attenuated by knockdown of Tet3, however they did not profile any axon growth related genes. Miao et al. (2015) determined that the promoter region of BDNF is contains significantly higher 5hmC content following ischemic stroke, although no other axon growth genes were assessed. Determination of hydroxymethylation of particular genes of interest following ischemic stroke would help inform any future therapeutic treatments, and there are a number of available methods that could determine such changes. For example, DNA extracted from post-ischemic brains could undergo methylated DNA immunoprecipitation (commonly referred to as MeDIP) and subsequent qPCR in order to quantify relative levels of 5mC or 5hmC on particular genes. Alternatively, determination of methylation at a base-specific level can be performed via bisulphite sequencing, in which DNA is treated with bisulphite, converting cytosine residues to uracil but leaving methylated cytosine residues unaffected. Though original methods of bisulphite sequencing are unable to differentiate between 5mC and 5hmC residues, more recent methods such as Tet-mediated bisulphite sequencing (Yu et al., 2012) and oxidative bisulphite sequencing (Booth et al., 2013) can be utilised to asses 5hmC content specifically.

As previously mentioned, it is possible that Tet enzymes and 5hmC work to influence post-stroke axon growth via a mechanism other than direct demethylation of axon growth-related genes, as evidenced by its higher abundance at gene bodies than CpG islands/promoter regions (Loh et al., 2017). Previous research has shown than 5hmC is recognised and bound to by methyl-CpG binding proteins such as MECP2 and MBD3, with an affinity similar to that of 5mC (Mellen et al., 2012; Yildirim et al., 2011). These binding interactions can regulate changes to histone acetylation and chromatin structure, further evidencing that 5hmC can act as a stable epigenetic marker in conjunction with other epigenetic mechanisms. Numerous studies have evidenced that alternative epigenetic mechanisms such as histone modifications and RNA interference play vital roles in the control of axon growth (Palmisano & Di Giovanni,

2018), with these same mechanisms also being affected by ischemic stroke (Hu et al., 2017). It is therefore important for future research to consider the importance of these alternative epigenetic mechanisms and how they interplay with hydroxymethylation in the control of post-stroke axon growth as this will also help to inform future therapeutic targets.

The ultimate aim of this venture into determining how hydroxymethylation regulates post-stroke axon growth is to develop some form of therapeutic intervention that targets the methylomic response of the brain in order to promote axon growth and functional recovery. The benefit of targeting hydroxymethylation is that, as this thesis has shown, the observed increases in 5hmC and their potential effects on axon growth occur in the days/weeks following the ischemic event, meaning that any therapeutic intervention aimed at targeting this response could likely be administered at a delayed timepoint from the onset of stroke. The only licensed drug for use in stroke patients, tPA, works by breaking down the offending blood clot via thrombolysis, meaning it is most effective in the few hours following the onset of stroke symptoms and therefore its main disadvantage is a narrow therapeutic window (Hacke et al., 1999). Developing a therapeutic treatment for ischemic stroke that aims to enhance axon growth via changes to hydroxymethylation could present a treatment with a much wider therapeutic window, thereby addressing the main disadvantages of currently used treatments.

Development of such a treatment would require testing on animal models of ischemic stroke. Investigations of this manner have already been attempted, with Morris-Blanco et al. (2019) determining that administration of ascorbate following MCAO in mice significantly increased global 5hmC levels whilst decreasing infarct size and improving functional recovery. However, ascorbate was administered 3-6h following MCAO, meaning that its viability as a delayed treatment (in the order of days post-stroke) has not been assessed. Furthermore, whilst

determining an effect on infarct size, no effects on axon growth/sprouting or neuroplasticity were assessed. This could be performed in future studies through the use of tracer dyes such as cholera toxin B in order to quantify the number of newly sprouting axons, as has been done previously (Li et al., 2010). Other than administration of substances that affect Tet enzyme activity, it could be possible in future studies to target specific axon-growth related genes following ischemic stroke in order to up- or down-regulate gene expression (Liu et al. (2016)). have demonstrated that fusion of DNMT1 or Tet1 with a catalytically inactive form of recombinant Cas9 allows for targeted methylation or demethylation of promoter regions, causing activation or silencing of endogenous reporters. They showed that use of Tet1-Cas9 can elicit increased BDNF expression in post-mitotic neurons and have also demonstrated that the system can also be used to alter DNA methylation in the brains of adult mice. Use of this system in post-ischemic animals could therefore plausibly induce increased expression of axon growth related genes and thereby improve functional recovery.

6.3: Conclusion

In conclusion, this thesis has shown through use of *in vivo* models that the brain exhibits an endogenous methylomic response to ischemic stroke that is characterised by transient significant increases in global 5hmC levels, although the temporal profile of this response differs between distinct brain areas. Furthermore, FACS sorting of post-ischemic brains has helped to demonstrate that this response is seen not only in the total cell population, but in microglial/macrophage cells in particular. This therefore suggests that hydroxymethylation may play a role in the control of the post-stroke immune response, and thereby indirectly affect axon growth. The use of an *in vitro* model of ischemia and reperfusion has demonstrated that Tet enzyme expression directly affects axon growth, with hypoxia altering

these effects. Further research is needed in order to determine which specific genes are being affected by changes to the methylome, or perhaps determine alternative processes by which changes in 5hmC content regulate post-stroke axon growth. It is hoped that the novel findings presented in this thesis can provide a basis for the development of a new therapeutic treatment for ischemic stroke that targets hydroxymethylation to promote axon growth and functional recovery.

APPENDIX

A1: Comparing sham & naïve animal data from Chapter 2

As the sham equivalent of MCAO surgery does not induce ischemic stroke, these animals should have no differences in relative 5hmC expression levels or numbers of dopaminergic cells in the substantia nigra pars compacta in comparison to naïve animals. To confirm that this is true, the relative fluorescence of cells in various areas of brain sections immunohistochemically stained for 5hmC were analysed. The D'Agostino and Pearson omnibus normality test determined that all data was not normally distributed, therefore the Mann-Whitney U test was used to determine differences between naïve and sham groups in each brain area. This revealed no differences in relative fluorescence between sham and naïve animals in the cortex ($p=0.73$), striatum ($p=0.90$), substantia nigra pars compacta (TH+ cells only; $p=0.91$) or medial geniculate nucleus ($p=0.41$). As naïve and sham animals do not suffer ischemic stroke, no distinction between infarcted and non-infarcted tissue can be made. The numbers of TH+ cells in the substantia nigra pars compacta of naïve and sham animals were also analysed, and no differences were found between sham and naïve animals ($p=0.59$).

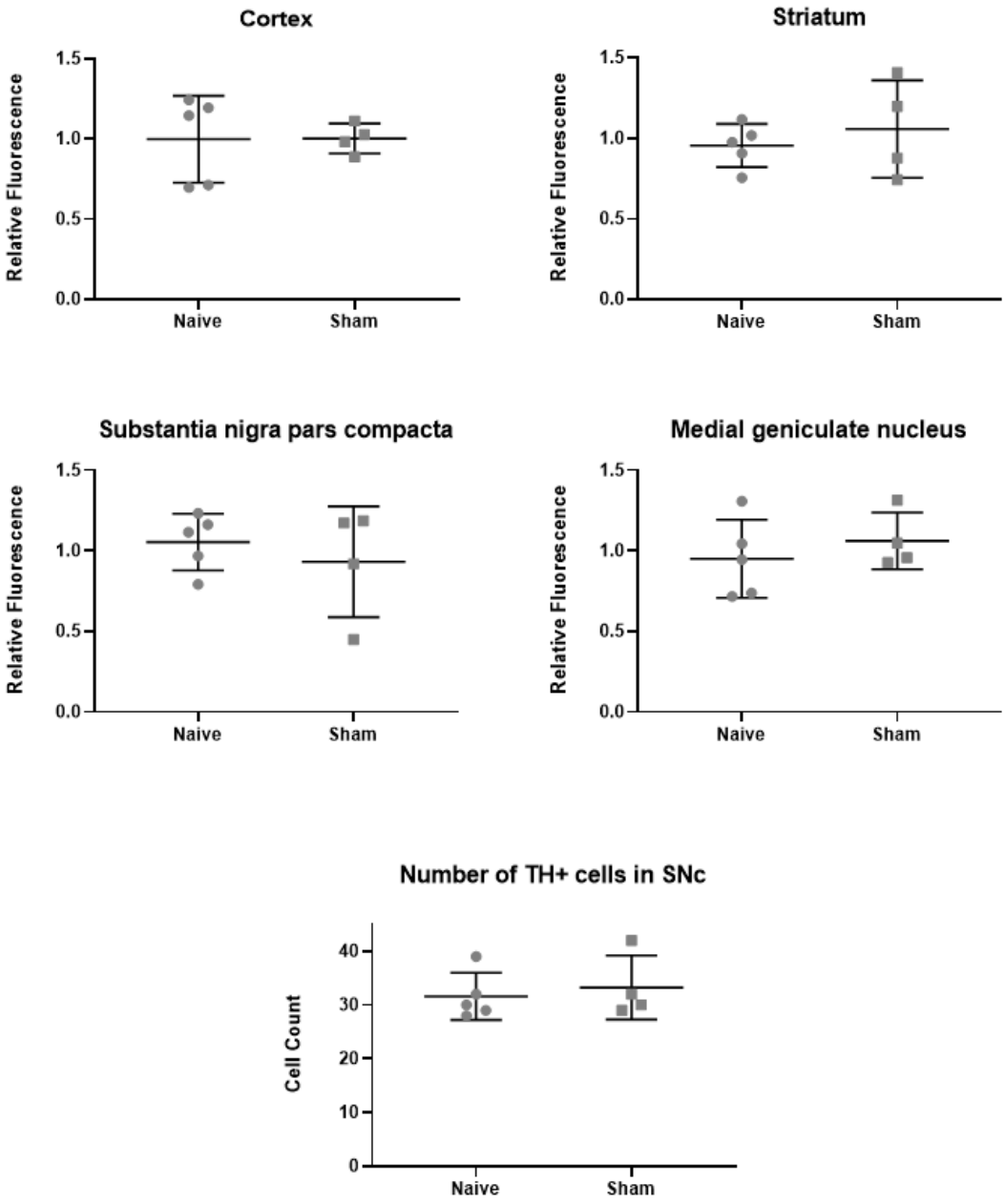


Figure A1: Comparing sham and naïve animal data from Chapter 2
Analysis of 5hmC staining intensity in the cortex (p=0.73), striatum (p=0.90), substantia nigra pars compacta (p=0.91) and medial geniculate nucleus (p=0.41) revealed no differences between sham and naïve animals. No differences were found between these two groups when analysing the number of TH+ cells present in the substantia nigra pars compacta (p=0.59). Data is presented as mean ± SD.

A2: Standard curves for 5mC and 5hmC ELISAs

In order to quantify 5mC and 5hmC content of DNA collected from rat brains, commercial ELISA kits were used (Zymo Research USA). As part of the manufacturer's protocol, control samples of known concentrations were run in duplicate and plotted as standard curves (Figure A2). The slopes of these curves were then used to quantify the samples obtained as part of the studies carried out in Chapter 4 and Chapter 5.

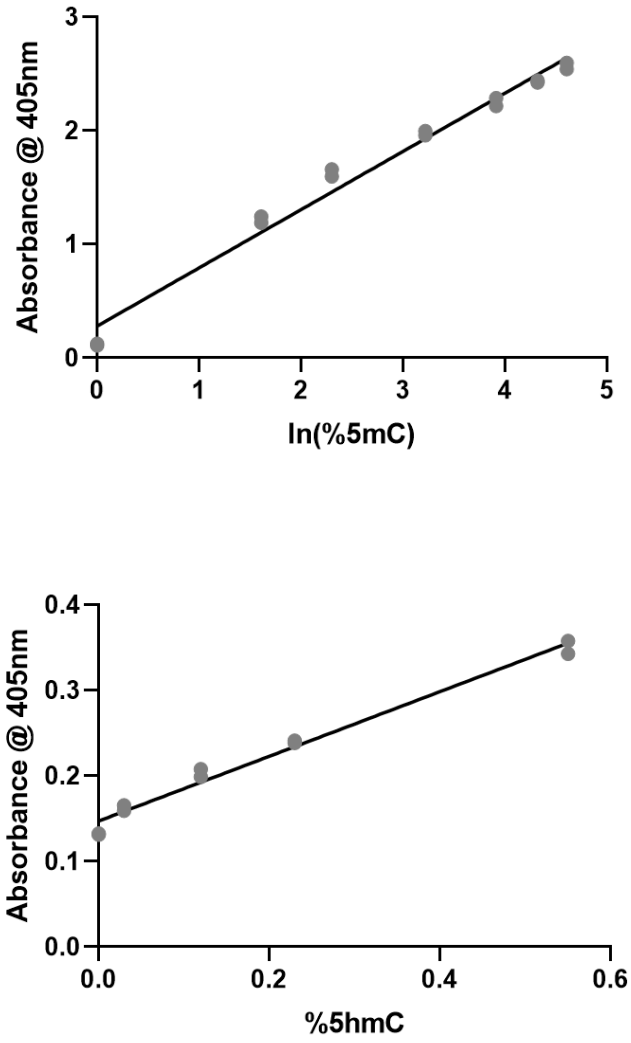


Figure A2: Standard curves for 5mC and 5hmC ELISA kits
ELISA kits were used to quantify 5mC and 5hmC content of DNA samples from rat brain. Control samples of known concentrations were run in order to produce standard curves. *Top*: 5mC standard curve; $R^2 = 0.96$. *Bottom*: 5hmC standard curve; $R^2 = 0.95$.

A3: qPCR Housekeeping Gene

In Chapter 4, RNA was extracted from total cell population of rats that underwent sham or MCAO surgery. This RNA was then used to perform qPCR, with the results analysed using the Pfaffl method (Pfaffl, 2001). As part of this analysis, expression levels of the genes of interest are normalised to that of an endogenous housekeeping gene; in this case, HPRT1. For a valid analysis, it is important that expression levels of the housekeeping gene do not differ between experimental groups. By analysing the relative expression of HPRT1 in sham and MCAO animals, it was found that expression levels were not significantly different between groups (t_{13}=0.52, p=0.70), and HPRT1 was therefore determined as a valid housekeeping gene to use for normalisation.

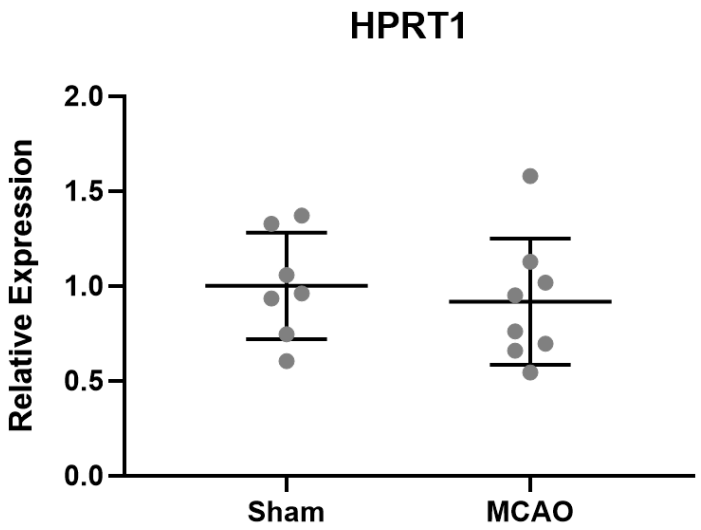


Figure A3: Expression of HPRT1
RNA was extracted from total cell populations obtained from the cortex and striatum of mice that had undergone MCAO surgery (n=8) or an equivalent sham surgery (n=7). Reverse transcription and subsequent qPCR of these RNA samples revealed that there was no significant difference in expression of HPRT1 (p=0.70) between groups. Data is presented as mean ± SD.

A4: Specificity of Tet-targeting siRNAs

In Chapter 5, siRNAs were used to knock down Tet1-3 in cortical neuronal cultures. To assess the specificity of these siRNAs, cultures were transfected with the siRNAs and immunocytochemically stained for each of the Tet enzymes to ensure that siRNAs only knocked down protein expression of their target protein. The intensity of this staining in positively transfected (GFP+) cells was measured using the CTF method (as described in section 2.1.5.1) and normalising all fluorescence data to that of non-transfected cells. Using unpaired t tests, it was determined that NT siRNA did not reduce expression of any Tet enzyme vs. non-transfected controls (Tet1 $p=0.91$; Tet2 $p=0.99$; Tet3 $p=0.81$). Tet1 siRNA only reduced expression of Tet1 protein (Tet1 $p<0.001$; Tet2 $p=0.93$; Tet3 $p=0.51$). Tet2 siRNA only reduced expression of Tet2 protein (Tet1 $p=0.65$; Tet2 $p<0.01$; Tet3 $p=0.85$). Tet3 siRNA only reduced expression of Tet3 protein (Tet1 $p=0.97$; Tet2 $p=0.33$; Tet3 $p<0.001$). Each of the Tet1-3 targeting siRNAs only decreased expression of their target protein, demonstrating that the siRNAs are specific.

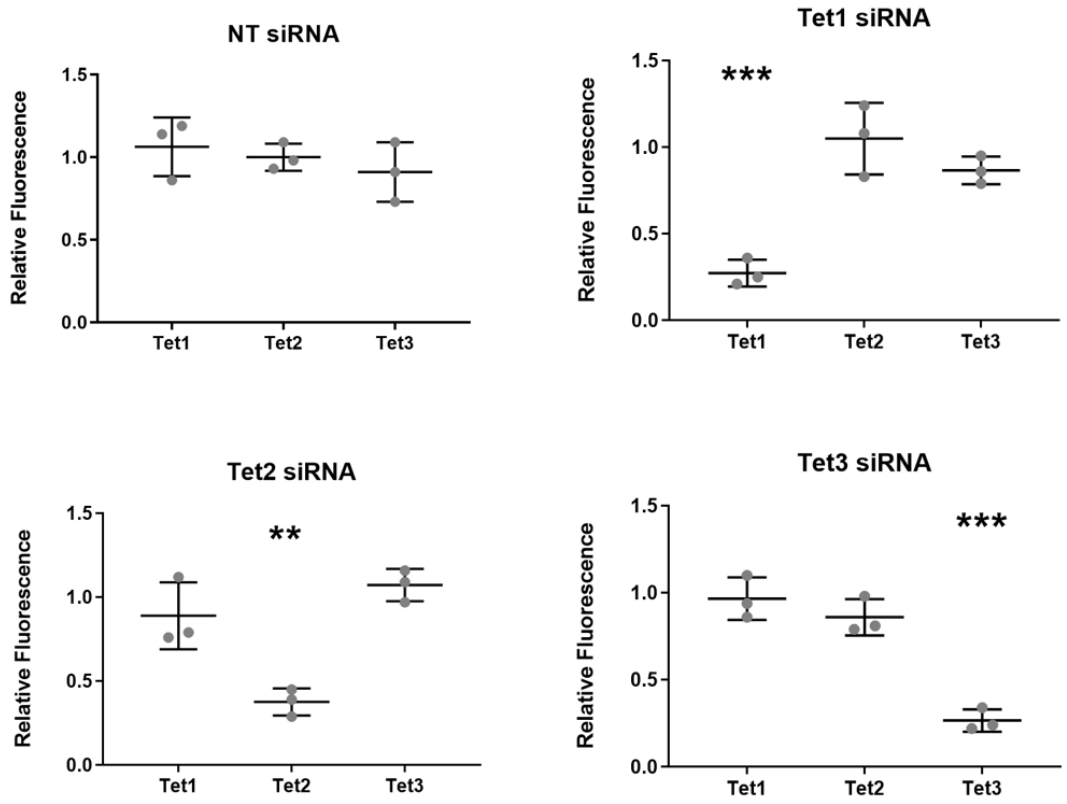


Figure A4: Analysing specificity of Tet-targeting siRNAs
Specificity of Tet-targeting siRNAs was analysed by measuring intensity of Tet protein staining in transfected cells. NT siRNA did not reduce expression of any enzyme compared to non-transfected controls (Tet1 $p=0.91$; Tet2 $p=0.99$; Tet3 $p=0.81$). Tet1 siRNA only reduced Tet1 expression ($p<0.001$); Tet2 siRNA only reduced expression of Tet2 protein ($p<0.01$); Tet3 siRNA only reduced expression of Tet3 protein ($p<0.001$). Data is presented as mean ± SD. ** represents $p<0.01$. *** represents $p<0.001$.

A5: Comparing GFP only and NT siRNA data from Chapter 5

In Chapter 5, siRNAs were used to knock down protein expression of Tet1-3 in neuronal cultures. As controls, cultures transfected with only GFP plasmid were cultivated, as were cultures transfected with GFP plasmid and a non-targeting (NT) siRNA. As the NT siRNA does not target any particular gene, it should not affect expression of any protein and should therefore not have any effect on the parameters tested in the experiment (axon length, number of neurites, and total neurite length). These parameters were compared between GFP only and NT siRNA groups using unpaired t tests. There were no differences in average axon length between GFP only and NT siRNA groups in normoxic ($p=0.51$) or hypoxic conditions (0.95). There were no differences in average neurite length between GFP only and NT siRNA groups in normoxic ($p=0.87$) or hypoxic conditions (0.50). There were no differences in average neurite number between GFP only and NT siRNA groups in normoxic ($p=0.55$) or hypoxic conditions (0.45). Therefore, there were no differences found between the two groups and as such, they were combined to form one "Controls" group for subsequent analysis in Chapter 5.

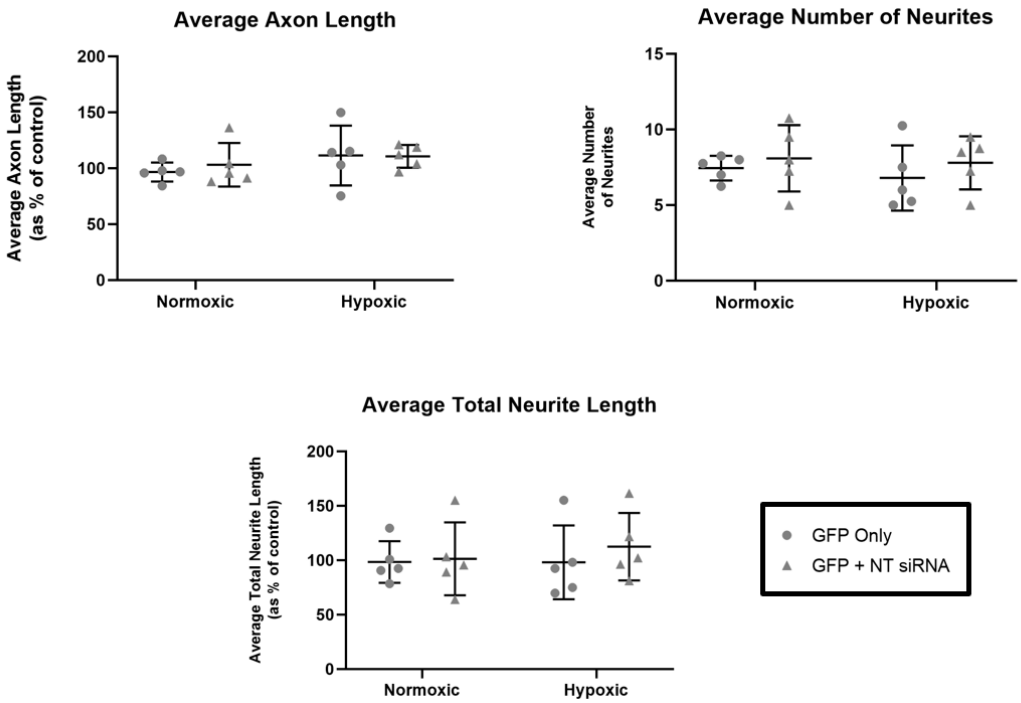


Figure A5: Comparing GFP only and NT siRNA data from Chapter 5
Data from two control groups – GFP only and GFP + NT siRNA – were compared to allow for formation of a singular control group for subsequent analysis. There were no differences in average axon length in normoxic (p=0.51) or hypoxic conditions (0.95). There were no differences in average neurite length in normoxic (p=0.87) or hypoxic conditions (0.50). There were no differences in average neurite number in normoxic (p=0.55) or hypoxic conditions (0.45). Data is presented as mean ± SD.

A6: Post-hoc power analyses

Post-hoc power analyses were performed for all statistical analyses from Chapters 2, 4 and 5. The power calculator G*Power (Faul et al., 2007) was used to perform post-hoc determination of power (given as %) by inputting the following parameters: mean and SD of each group (in order to determine effect size, d, and degrees of freedom, df); α error = 0.05; total sample size; number of groups; and n number of each group. For experiments that were deemed underpowered (power < 80%), "*a priori*" calculations were performed, using the same input parameters and setting power to 80%, in order to determine what the required sample size would have been in order to reach 80% power. These power analyses are summarised in Table A1.

Chapter	Measured Parameter	Figure	Groups being compared	Sample size	Power (%)	Sample size for 80% power
2	5hmC levels in infarcted cortex	2.6	Controls, 24h, 48h, 7d, 1m	28	40	42
2	5hmC levels in healthy cortex	2.6	Controls, 24h, 48h, 7d, 1m	28	100	-
2	5hmC levels in infarcted striatum	2.7	Controls, 24h, 48h, 7d, 1m	28	56	40
2	5hmC levels in healthy striatum	2.7	Controls, 24h, 48h, 7d, 1m	28	100	-
2	5hmC levels in TH+ cells	2.8	Controls, 24h, 48h, 7d, 1m	28	89	-
2	TH+ cell count	2.10	Controls, 24h, 48h, 7d, 1m	28	93	-
2	Correlation of infarct volume v. cortical 5hmC	2.11	Cortical 5hmC, infarct volume	18	75	21
2	Correlation of infarct volume v. striatal 5hmC	2.11	Cortical 5hmC, infarct volume	18	9	309
2	Correlation of infarct volume v. SNc 5hmC	2.11	Cortical 5hmC, infarct volume	18	6	423
2	5hmC levels in MGN	2.12	Controls, 24h, 48h, 7d, 1m	28	68	35
4	Proportions of CD11b+ cells	4.4	Sham, MCAO	10	99	-
4	%5mC in total cell population	4.5	Sham, MCAO	15	38	48
4	%5hmC in total cell population	4.5	Sham, MCAO	15	96	-
4	Correlation of infarct volume v. %5mC	4.6	Infarct volume, %5mC	8	7	386
4	Correlation of infarct volume v. %5hmC	4.6	Infarct volume, %5hmC	8	20	259
4	%5mC in microglia (with test runs)	4.7	Sham, MCAO	12	95	-
4	%5mC in microglia (without test runs)	4.7	Sham, MCAO	10	30	38
4	%5hmC in microglia (with test runs)	4.7	Sham, MCAO	12	79	14
4	%5hmC in microglia (without test runs)	4.7	Sham, MCAO	10	50	18
4	Correlation of CD11b proportion v. %5mC	4.8	CD11b proportion, %5mC	10	33	36
4	Correlation of CD11b proportion v. %5hmC	4.8	CD11b proportion, %5mC	10	39	29
4	mRNA levels of BDNF	4.9	Sham, MCAO	15	65	22
4	mRNA levels of Ttll7	4.9	Sham, MCAO	15	49	34
4	mRNA levels of Tet1	4.9	Sham, MCAO	15	5	213
4	mRNA levels of Tet2	4.9	Sham, MCAO	15	28	76
4	mRNA levels of Tet3	4.9	Sham, MCAO	15	94	-
5	Relative fluorescence of Tet1 staining	5.4	Normoxic, Hypoxic	10	67	14
5	Relative fluorescence of Tet2 staining	5.4	Normoxic, Hypoxic	10	23	64
5	Relative fluorescence of Tet3 staining	5.4	Normoxic, Hypoxic	10	80	-
5	Relative fluorescence of Hif1a staining	5.4	Normoxic, Hypoxic	10	90	-
5	%5mC of cell cultures	5.5	Normoxic, Hypoxic	10	27	50
5	%5hmC of cell cultures	5.5	Normoxic, Hypoxic	10	84	-
5	Axon length of Tet siRNA cultures	5.7	Normoxic, Hypoxic	50	88	-
5	Axon length of Tet siRNA cultures	5.7	Controls, Tet1, Tet2, Tet3	50	98	-
5	Neurite number of Tet siRNA cultures	5.8	Normoxic, Hypoxic	50	19	248
5	Neurite number of Tet siRNA cultures	5.8	Controls, Tet1, Tet2, Tet3	50	66	68
5	Neurite length of Tet siRNA cultures	5.9	Normoxic, Hypoxic	50	57	92
5	Neurite length of Tet siRNA cultures	5.9	Controls, Tet1, Tet2, Tet3	50	98	-
5	Axon length of Tet plasmid cultures	5.11	Normoxic, Hypoxic	40	5	387
5	Axon length of Tet plasmid cultures	5.11	Controls, Tet1, Tet2, Tet3	40	83	-
5	Neurite number of Tet plasmid cultures	5.12	Normoxic, Hypoxic	40	12	204
5	Neurite number of Tet plasmid cultures	5.12	Controls, Tet1, Tet2, Tet3	40	20	196
5	Neurite length of Tet plasmid cultures	5.13	Normoxic, Hypoxic	40	8	342
5	Neurite length of Tet plasmid cultures	5.13	Controls, Tet1, Tet2, Tet3	40	70	52

Table A1: Post-hoc analyses of experiments from Chapters 2, 4 and 5

A7: PIP Reflection

Note to examiners:
This statement is included as an appendix to the thesis in order that the thesis accurately captures the PhD training experienced by the candidate as a BBSRC Doctoral Training Partnership student.

The Professional Internship for PhD Students (PIP) is a compulsory 3-month placement which must be undertaken by DTP students. It is usually centred on a specific project and must not be related to the PhD project. This reflective statement is designed to capture the skills development which has taken place during the student's placement and the impact on their career plans it has had.

PIP Reflective Statement

My PIP took place from September to December of 2018 at Sygnature Discovery, a contract research organisation (CRO) that specialises in drug discovery.

My project was focused on developing a high-throughput fragment screen assay using microscale thermophoresis (MST). MST is a biophysical assay technique that was brand new to the company at the time, and my capability build project involved using the new MST equipment to screen a library of chemical fragments against a protein that had already been well characterised by the company. The project was designed such that myself and others would become familiar with the new technique and equipment, troubleshooting any issues that should arise. The project went extremely well, and a full fragment screen was performed. Following this screen, I had the opportunity to consolidate the fragment hits by performing other biophysical and biochemical assays such as surface plasmon resonance (SPR) and fluorescent thermal shift assays (FTSA). After completing the project, I spent my final week writing a case study to be published on the company's website, briefly summarising the project in order to advertise the company's MST capabilities to potential clients.

Whilst at Sygnature Discovery, I gained a working knowledge and appreciation of many biophysical and biochemical assay techniques. As well as learning many new laboratory techniques, I gained experience in public speaking (by presenting my work on a bi-weekly basis at company meetings) and scientific writing for various audiences (by writing case studies and various lab reports). I was also fascinated to learn about the inner workings of a CRO and about the differences between a post-doctoral career in industry v. a post-doctoral career in academia.

Overall, I thoroughly enjoyed my PIP placement at Sygnature Discovery. I was very appreciative of the opportunity to spend time working on science that was completely unrelated to my PhD and was grateful to learn about employment opportunities outside of academia.

REFERENCES

Abakir, A., Wheldon, L., Johnson, A. D., Laurent, P., & Ruzov, A. (2016). Detection of modified forms of cytosine using sensitive immunohistochemistry. *JoVE (Journal of Visualized Experiments)*(114), e54416.

Abe, O., Nakane, M., Aoki, S., Hayashi, N., Masumoto, T., Kunimatsu, A., Mori, H., Tamura, A., & Ohtomo, K. (2003). MR imaging of postischemic neuronal death in the substantia nigra and thalamus following middle cerebral artery occlusion in rats. *NMR in Biomedicine: An International Journal Devoted to the Development and Application of Magnetic Resonance In Vivo, 16*(3), 152-159.

Abràmoff, M. D., Magalhães, P. J., & Ram, S. J. (2004). Image processing with ImageJ. *Biophotonics international, 11*(7), 36-42.

Akintola, A., & Parrish, A. (2010). Gene-Specific Hypermethylation in Aging. In T. Tollefsbol (Ed.), *Epigenetics of Aging* (pp. 29-39). New York: Springer.

Bai, S., Ghoshal, K., & Jacob, S. T. (2006). Identification of T-cadherin as a novel target of DNA methyltransferase 3B and its role in the suppression of nerve growth factor-mediated neurite outgrowth in PC12 cells. *Journal of Biological Chemistry, 281*(19), 13604-13611.

Barreto, G., Schäfer, A., Marhold, J., Stach, D., Swaminathan, S. K., Handa, V., Döderlein, G., Maltry, N., Wu, W., & Lyko, F. (2007). Gadd45a promotes epigenetic gene activation by repair-mediated DNA demethylation. *Nature, 445*(7128), 671.

Batchelor, P. E., Porritt, M. J., Martinello, P., Parish, C., Liberatore, G., Donnan, G. A., & Howells, D. W. (2002). Macrophages and microglia produce local trophic gradients that stimulate axonal sprouting toward but not beyond the wound edge. *Molecular and Cellular Neuroscience, 21*(3), 436-453.

Becher, B., & Antel, J. P. (1996). Comparison of phenotypic and functional properties of immediately ex vivo and cultured human adult microglia. *Glia, 18*(1), 1-10.

Bederson, J. B., Pitts, L. H., Tsuji, M., Nishimura, M., Davis, R., & Bartkowski, H. (1986). Rat middle cerebral artery occlusion: evaluation of the model and development of a neurologic examination. *Stroke, 17*(3), 472-476.

Bedi, S. S., Smith, P., Hetz, R. A., Xue, H., & Cox, C. S. (2013). Immunomagnetic enrichment and flow cytometric characterization of mouse microglia. *J Neurosci Methods, 219*(1), 176-182.

Bestor, T. H. (1992). Activation of mammalian DNA methyltransferase by cleavage of a Zn binding regulatory domain. *The EMBO Journal, 11*(7), 2611.

Bhutani, N., Burns, David M., & Blau, Helen M. (2011). DNA Demethylation Dynamics. *Cell, 146*(6), 866-872. doi: http://dx.doi.org/10.1016/j.cell.2011.08.042

Blaschke, K., Ebata, K. T., Karimi, M. M., Zepeda-Martínez, J. A., Goyal, P., Mahapatra, S., Tam, A., Laird, D. J., Hirst, M., Rao, A., Lorincz, M. C., & Ramalho-Santos, M. (2013). Vitamin C induces Tet-dependent DNA demethylation in ESCs to promote a blastocyst-like state. *Nature, 500*(7461), 222-226. doi: 10.1038/nature12362

Bogousslavsky, J., Van Melle, G., & Regli, F. (1988). The Lausanne Stroke Registry: analysis of 1,000 consecutive patients with first stroke. *Stroke, 19*(9), 1083-1092.

Booth, M. J., Ost, T. W., Beraldi, D., Bell, N. M., Branco, M. R., Reik, W., & Balasubramanian, S. (2013). Oxidative bisulfite sequencing of 5-methylcytosine and 5-hydroxymethylcytosine. *Nature Protocols, 8*(10), 1841.

Bottiglieri, T. (2013). Folate, vitamin B12, and S-adenosylmethionine. *Psychiatric Clinics, 36*(1), 1-13.

Bradley-Whitman, M., & Lovell, M. (2013). Epigenetic changes in the progression of Alzheimer's disease. *Mechanisms of ageing and development, 134*(10), 486-495.

Brait, V. H., Jackman, K. A., Walduck, A. K., Selemidis, S., Diep, H., Mast, A. E., Guida, E., Broughton, B. R., Drummond, G. R., & Sobey, C. G. (2010). Mechanisms contributing to cerebral infarct size after stroke: gender, reperfusion, T lymphocytes, and Nox2-derived superoxide. *Journal of Cerebral Blood Flow & Metabolism, 30*(7), 1306-1317.

Brown, C. E., Aminoltejari, K., Erb, H., Winship, I. R., & Murphy, T. H. (2009). In vivo voltage-sensitive dye imaging in adult mice reveals that somatosensory maps lost to stroke are replaced over weeks by new structural and functional circuits with prolonged modes of activation within both the peri-infarct zone and distant sites. *The Journal of Neuroscience, 29*(6), 1719-1734.

Buchan, A. M., Xue, D., & Slivka, A. (1992). A new model of temporary focal neocortical ischemia in the rat. *Stroke, 23*(2), 273-279.

Bushnell, C. D., Lee, J., Duncan, P. W., Newby, L. K., & Goldstein, L. B. (2008). Impact of comorbidities on ischemic stroke outcomes in women. *Stroke, 39*(7), 2138-2140.

Cameron, J. S., Alexopoulou, L., Sloane, J. A., DiBernardo, A. B., Ma, Y., Kosaras, B., Flavell, R., Strittmatter, S. M., Volpe, J., & Sidman, R. (2007). Toll-like receptor 3 is a potent negative regulator of axonal growth in mammals. *The Journal of Neuroscience, 27*(47), 13033-13041.

Cardona, A. E., Huang, D., Sasse, M. E., & Ransohoff, R. M. (2006). Isolation of murine microglial cells for RNA analysis or flow cytometry. *Nature Protocols, 1*(4), 1947-1951. doi: 10.1038/nprot.2006.327

Carmichael, S. T. (2003). Plasticity of Cortical Projections after Stroke. *The Neuroscientist, 9*(1), 64-75. doi: 10.1177/1073858402239592

Carmichael, S. T. (2005). Rodent models of focal stroke: size, mechanism, and purpose. *NeuroRx : the journal of the American Society for Experimental NeuroTherapeutics, 2*(3), 396-409. doi: 10.1602/neurorx.2.3.396

Carmichael, S. T., Archibeque, I., Luke, L., Nolan, T., Momiy, J., & Li, S. (2005). Growth-associated gene expression after stroke: evidence for a growth-promoting region in peri-infarct cortex. *Experimental Neurology, 193*(2), 291-311.

Carmichael, S. T., & Chesselet, M.-F. (2002). Synchronous neuronal activity is a signal for axonal sprouting after cortical lesions in the adult. *Journal of Neuroscience, 22*(14), 6062-6070.

Centonze, D., Rossi, S., Tortiglione, A., Picconi, B., Prosperetti, C., De Chiara, V., Bernardi, G., & Calabresi, P. (2007). Synaptic plasticity during recovery from permanent occlusion of the middle cerebral artery. *Neurobiology of disease, 27*(1), 44-53.

Cheng, X., & Blumenthal, R. M. (2008). Mammalian DNA methyltransferases: a structural perspective. *Structure, 16*(3), 341-350.

Cherry, J. D., Olschowka, J. A., & O'Banion, M. K. (2014). Neuroinflammation and M2 microglia: the good, the bad, and the inflamed. *Journal of neuroinflammation, 11*(1), 98.

Cho, Y., Shin, J. E., Ewan, E. E., Oh, Y. M., Pita-Thomas, W., & Cavalli, V. (2015). Activating injury-responsive genes with hypoxia enhances axon regeneration through neuronal HIF-1α. *Neuron, 88*(4), 720-734.

Choi, I., Lee, C., Kim, H., Choi, D.-H., & Lee, J. (2018). Effect of inhibition of DNA methylation combined with Task-Specific Training on chronic stroke recovery. *International journal of molecular sciences, 19*(7), 2019.

Choudhury, G. R., & Ding, S. (2016). Reactive astrocytes and therapeutic potential in focal ischemic stroke. *Neurobiology of disease, 85*, 234-244. doi: https://doi.org/10.1016/j.nbd.2015.05.003

Clarkson, A. N., Overman, J. J., Zhong, S., Mueller, R., Lynch, G., & Carmichael, S. T. (2011). AMPA receptor-induced local brain-derived neurotrophic factor signaling mediates motor recovery after stroke. *The Journal of Neuroscience, 31*(10), 3766-3775.

Connolly, E. S., Winfree, C. J., Stern, D. M., Stern, D. M., Solomon, R. A., & Pinsky, D. J. (1996). Procedural and strain-related variables significantly affect outcome in a murine model of focal cerebral ischemia. *Neurosurgery, 38*(3), 523-532.

Coppieters, N., Dieriks, B. V., Lill, C., Faull, R. L. M., Curtis, M. A., & Dragunow, M. (2014). Global changes in DNA methylation and hydroxymethylation in Alzheimer's disease human brain. *Neurobiology of Aging, 35*(6), 1334-1344. doi: http://dx.doi.org/10.1016/j.neurobiolaging.2013.11.031

Cortázar, D., Kunz, C., Selfridge, J., Lettieri, T., Saito, Y., MacDougall, E., Wirz, A., Schuermann, D., Jacobs, A. L., & Siegrist, F. (2011). Embryonic lethal phenotype reveals a function of TDG in maintaining epigenetic stability. *Nature, 470*(7334), 419-423.

Coulondre, C., Miller, J. H., Farabaugh, P. J., & Gilbert, W. (1978). Molecular basis of base substitution hotspots in Escherichia coli. *Nature, 274*(5673), 775.

Cox, M. L., Schray, C. L., Luster, C. N., Stewart, Z. S., Korytko, P. J., Khan, K. N. M., Paulauskis, J. D., & Dunstan, R. W. (2006). Assessment of fixatives, fixation, and tissue processing on morphology and RNA integrity. *Experimental and molecular pathology, 80*(2), 183-191.

Dawlaty, M. M., Breiling, A., Le, T., Raddatz, G., Barrasa, M. I., Cheng, A. W., Gao, Q., Powell, B. E., Li, Z., & Xu, M. (2013). Combined deficiency of Tet1 and Tet2 causes epigenetic abnormalities but is compatible with postnatal development. *Developmental cell, 24*(3), 310-323.

Dawlaty, M. M., Ganz, K., Powell, B. E., Hu, Y.-C., Markoulaki, S., Cheng, A. W., Gao, Q., Kim, J., Choi, S.-W., & Page, D. C. (2011). Tet1 is dispensable for maintaining pluripotency and its loss is compatible with embryonic and postnatal development. *Cell stem cell, 9*(2), 166-175.

Dirnagl, U., Iadecola, C., & Moskowitz, M. A. (1999). Pathobiology of ischaemic stroke: an integrated view. *Trends in neurosciences, 22*(9), 391-397.

Dock, H., Theodorsson, A., & Theodorsson, E. (2015). DNA Methylation Inhibitor Zebularine Confers Stroke Protection in Ischemic Rats. *Translational Stroke Research, 6*(4), 296-300. doi: 10.1007/s12975-015-0397-7

Donzelli, R., Marinkovic, S., Brigante, L., de Divitiis, O., Nikodijevic, I., Schonauer, C., & Maiuri, F. (1998). Territories of the perforating (lenticulostriate) branches of the middle cerebral artery. *Surg Radiol Anat, 20*(6), 393-398.

Endres, M., Fan, G., Meisel, A., Dirnagl, U., & Jaenisch, R. (2001). Effects of cerebral ischemia in mice lacking DNA methyltransferase 1 in post-mitotic neurons. *Neuroreport, 12*(17), 3763-3766.

Endres, M., Meisel, A., Biniszkiewicz, D., Namura, S., Prass, K., Ruscher, K., Lipski, A., Jaenisch, R., Moskowitz, M. A., & Dirnagl, U. (2000). DNA methyltransferase contributes to delayed ischemic brain injury. *The Journal of Neuroscience, 20*(9), 3175-3181.

Faul, F., Erdfelder, E., Lang, A.-G., & Buchner, A. (2007). G* Power 3: A flexible statistical power analysis program for the social, behavioral, and biomedical sciences. *Behavior research methods, 39*(2), 175-191.

Feng, J., Zhou, Y., Campbell, S. L., Le, T., Li, E., Sweatt, J. D., Silva, A. J., & Fan, G. (2010). Dnmt1 and Dnmt3a maintain DNA methylation and regulate synaptic function in adult forebrain neurons. *Nat Neurosci, 13*(4), 423.

Ferreira, T. A., Blackman, A. V., Oyrer, J., Jayabal, S., Chung, A. J., Watt, A. J., Sjöström, P. J., & Van Meyel, D. J. (2014). Neuronal morphometry directly from bitmap images. *Nature methods, 11*(10), 982.

Ficz, G., Branco, M. R., Seisenberger, S., Santos, F., Krueger, F., Hore, T. A., Marques, C. J., Andrews, S., & Reik, W. (2011). Dynamic regulation of 5-hydroxymethylcytosine in mouse ES cells and during differentiation. *Nature, 473*(7347), 398.

Finger, S., Koehler, P. J., & Jagella, C. (2004). The Monakow concept of diaschisis: origins and perspectives. *Archives of neurology, 61*(2), 283-288.

Franklin, K. B., & Paxinos, G. (2008). *The mouse brain in stereotaxic coordinates* (Vol. 3): Academic press New York:.

Frauer, C., Rottach, A., Meilinger, D., Bultmann, S., Fellinger, K., Hasenöder, S., Wang, M., Qin, W., Söding, J., & Spada, F. (2011). Different binding properties and function of CXXC zinc finger domains in Dnmt1 and Tet1. *PLoS ONE, 6*(2), e16627.

Fredette, B. J., Miller, J., & Ranscht, B. (1996). Inhibition of motor axon growth by T-cadherin substrata. *Development, 122*(10), 3163-3171.

Fujie, W., Kirino, T., Tomukai, N., Iwasawa, T., & Tamura, A. (1990). Progressive shrinkage of the thalamus following middle cerebral artery occlusion in rats. *Stroke, 21*(10), 1485-1488.

Garrido, C., Galluzzi, L., Brunet, M., Puig, P., Didelot, C., & Kroemer, G. (2006). Mechanisms of cytochrome c release from mitochondria. *Cell Death & Differentiation, 13*(9), 1423-1433.

Gelderblom, M., Leypoldt, F., Steinbach, K., Behrens, D., Choe, C.-U., Siler, D. A., Arumugam, T. V., Orthey, E., Gerloff, C., Tolosa, E., & Magnus, T. (2009). Temporal and Spatial Dynamics of Cerebral Immune Cell Accumulation in Stroke. *Stroke, 40*(5), 1849-1857. doi: 10.1161/strokeaha.108.534503

Gold, M., & Hurwitz, J. (1963). *The enzymatic methylation of the nucleic acids.* Paper presented at the Cold Spring Harbor Symposia on Quantitative Biology.

Grabert, K., Michoel, T., Karavolos, M. H., Clohisey, S., Baillie, J. K., Stevens, M. P., Freeman, T. C., Summers, K. M., & McColl, B. W. (2016). Microglial brain region−dependent diversity and selective regional sensitivities to aging. *Nat Neurosci, 19*, 504.

Greenhalgh, A. D., & David, S. (2014). Differences in the Phagocytic Response of Microglia and Peripheral Macrophages after Spinal Cord Injury and Its Effects on Cell Death. *The Journal of Neuroscience, 34*(18), 6316-6322. doi: 10.1523/jneurosci.4912-13.2014

Guez-Barber, D., Fanous, S., Harvey, B. K., Zhang, Y., Lehrmann, E., Becker, K. G., Picciotto, M. R., & Hope, B. T. (2012). FACS purification of immunolabeled cell types from adult rat brain. *J Neurosci Methods, 203*(1), 10-18. doi: https://doi.org/10.1016/j.jneumeth.2011.08.045

Guo, Junjie U., Su, Y., Zhong, C., Ming, G.-l., & Song, H. (2011). Hydroxylation of 5-Methylcytosine by TET1 Promotes Active DNA Demethylation in the Adult Brain. *Cell, 145*(3), 423-434. doi: http://dx.doi.org/10.1016/j.cell.2011.03.022

Haber, S. N. (2016). Corticostriatal circuitry. *Dialogues in clinical neuroscience, 18*(1), 7-21.

Hacke, W., Brott, T., Caplan, L., Meier, D., Fieschi, C., Donnan, G., Heiss, W., Wahlgren, N., Spranger, M., & Boysen, G. (1999). Thrombolysis in acute ischemic stroke: controlled trials and clinical experience. *Neurology, 53*(7 Suppl 4), S3-14.

Haffner, M. C., Chaux, A., Meeker, A. K., Esopi, D. M., Gerber, J., Pellakuru, L. G., Toubaji, A., Argani, P., Iacobuzio-Donahue, C., & Nelson, W. G. (2011). Global 5-hydroxymethylcytosine content is significantly reduced in tissue stem/progenitor cell compartments and in human cancers. *Oncotarget, 2*(8), 627.

Hahn, M. A., Qiu, R., Wu, X., Li, A. X., Zhang, H., Wang, J., Jui, J., Jin, S.-G., Jiang, Y., & Pfeifer, G. P. (2013). Dynamics of 5-hydroxymethylcytosine and chromatin marks in Mammalian neurogenesis. *Cell reports, 3*(2), 291-300.

Harrison, F. E., & May, J. M. (2009). Vitamin C function in the brain: vital role of the ascorbate transporter SVCT2. *Free Radical Biology and Medicine, 46*(6), 719-730.

He, Y.-F., Li, B.-Z., Li, Z., Liu, P., Wang, Y., Tang, Q., Ding, J., Jia, Y., Chen, Z., & Li, L. (2011). Tet-mediated formation of 5-carboxylcytosine and its excision by TDG in mammalian DNA. *Science, 333*(6047), 1303-1307.

Herzenberg, L. A., Sweet, R. G., & Herzenberg, L. A. (1976). Fluorescence-activated cell sorting. *Scientific American, 234*(3), 108-118.

Holloway, P. M., & Gavins, F. N. (2016). Modeling ischemic stroke in vitro: status quo and future perspectives. *Stroke, 47*(2), 561-569.

Hossmann, K. A. (1994). Viability thresholds and the penumbra of focal ischemia. *Ann Neurol, 36*(4), 557-565. doi: 10.1002/ana.410360404

Hotchkiss, R. D. (1948). The quantitative separation of purines, pyrimidines, and nucleosides by paper chromatography. *Journal of Biological Chemistry, 175*(1), 315-332.

Howells, D. W., Porritt, M. J., Rewell, S. S., O'collins, V., Sena, E. S., Van Der Worp, H. B., Traystman, R. J., & Macleod, M. R. (2010). Different strokes for different folks: the rich diversity of animal models of focal cerebral ischemia. *Journal of Cerebral Blood Flow & Metabolism, 30*(8), 1412-1431.

Hu, Z., Zhong, B., Tan, J., Chen, C., Lei, Q., & Zeng, L. (2017). The Emerging Role of Epigenetics in Cerebral Ischemia. *Molecular neurobiology, 54*(3), 1887-1905. doi: 10.1007/s12035-016-9788-3

Huang, Y., & Rao, A. (2014). Connections between TET proteins and aberrant DNA modification in cancer. *Trends in Genetics, 30*(10), 464-474.

Huff, J. T., & Zilberman, D. (2014). Dnmt1-independent CG methylation contributes to nucleosome positioning in diverse eukaryotes. *Cell, 156*(6), 1286-1297.

Hurn, P. D., Subramanian, S., Parker, S. M., Afentoulis, M. E., Kaler, L. J., Vandenbark, A. A., & Offner, H. (2007). T-and B-cell-deficient mice with experimental stroke have reduced lesion size and inflammation. *Journal of Cerebral Blood Flow & Metabolism, 27*(11), 1798-1805.

Iadecola, C., & Anrather, J. (2011). The immunology of stroke: from mechanisms to translation. *Nature medicine, 17*(7), 796-808.

Ishikawa, H., Tajiri, N., Shinozuka, K., Vasconcellos, J., Kaneko, Y., Lee, H. J., Mimura, O., Dezawa, M., Kim, S. U., & Borlongan, C. V. (2013). Vasculogenesis in experimental stroke after human cerebral endothelial cell transplantation. *Stroke, 44*(12), 3473-3481.

Iskandar, B. J., Rizk, E., Meier, B., Hariharan, N., Bottiglieri, T., Finnell, R. H., Jarrard, D. F., Banerjee, R. V., Skene, J. P., & Nelson, A. (2010). Folate regulation of axonal regeneration in the rodent central nervous system through DNA methylation. *The Journal of clinical investigation, 120*(5), 1603-1616.

Ito, S., D'Alessio, A. C., Taranova, O. V., Hong, K., Sowers, L. C., & Zhang, Y. (2010). Role of Tet proteins in 5mC to 5hmC conversion, ES-cell self-renewal and inner cell mass specification. *Nature, 466*(7310), 1129-1133.

Ito, S., Shen, L., Dai, Q., Wu, S. C., Collins, L. B., Swenberg, J. A., He, C., & Zhang, Y. (2011). Tet proteins can convert 5-methylcytosine to 5-formylcytosine and 5-carboxylcytosine. *Science, 333*(6047), 1300-1303.

Jeltsch, A., Nellen, W., & Lyko, F. (2006). Two substrates are better than one: dual specificities for Dnmt2 methyltransferases. *Trends in Biochemical Sciences, 31*(6), 306-308.

Jiang, Q., Ewing, J. R., Ding, G. L., Zhang, L., Zhang, Z. G., Li, L., Whitton, P., Lu, M., Hu, J., & Li, Q. J. (2005). Quantitative evaluation of BBB permeability after embolic stroke in rat using MRI. *Journal of Cerebral Blood Flow & Metabolism, 25*(5), 583-592.

Jiang, Y., Matevossian, A., Huang, H.-S., Straubhaar, J., & Akbarian, S. (2008). Isolation of neuronal chromatin from brain tissue. *BMC Neuroscience, 9*(1), 42. doi: 10.1186/1471-2202-9-42

Jost, J.-P., Siegmann, M., Sun, L., & Leung, R. (1995). Mechanisms of DNA demethylation in chicken embryos purification and properties of a 5-methylcytosine-DNA glycosylase. *Journal of Biological Chemistry, 270*(17), 9734-9739.

Kannan, V., Brouwer, N., Hanisch, U. K., Regen, T., Eggen, B. J., & Boddeke, H. W. (2013). Histone deacetylase inhibitors suppress immune activation in primary mouse microglia. *Journal of neuroscience research, 91*(9), 1133-1142.

Kilic, E., Hermann, D. M., & Hossmann, K.-A. (1998). A reproducible model of thromboembolic stroke in mice. *Neuroreport, 9*(13), 2967-2970.

Kim, B. J., Kim, M.-J., Park, J.-M., Lee, S.-H., Kim, Y.-J., Ryu, S., Kim, Y. H., & Yoon, B.-W. (2009). Reduced neurogenesis after suppressed inflammation by minocycline in transient cerebral ischemia in rat. *Journal of the neurological sciences, 279*(1-2), 70-75.

Kim, C. C., Nakamura, M. C., & Hsieh, C. L. (2016). Brain trauma elicits non-canonical macrophage activation states. *Journal of neuroinflammation, 13*(1), 117.

Kitayama, M., Ueno, M., Itakura, T., & Yamashita, T. (2011). Activated microglia inhibit axonal growth through RGMa. *PLoS ONE, 6*(9), e25234.

Koizumi, J., Yoshida, Y., Nakazawa, T., & Ooneda, G. (1986). Experimental studies of ischemic brain edema. 1. A new experimental model of cerebral embolism in rats in which recirculation can be introduced in the ischemic area. *Jpn J stroke, 8*, 1-8.

Kozlenkov, A., Roussos, P., Timashpolsky, A., Barbu, M., Rudchenko, S., Bibikova, M., Klotzle, B., Byne, W., Lyddon, R., & Di Narzo, A. F. (2013). Differences in DNA methylation between human neuronal and glial cells are concentrated in enhancers and non-CpG sites. *Nucleic acids research, 42*(1), 109-127.

Kriaucionis, S., & Heintz, N. (2009). The nuclear DNA base 5-hydroxymethylcytosine is present in Purkinje neurons and the brain. *Science, 324*(5929), 929-930.

Kudo, M., Aoyama, A., Ichimori, S., & Fukunaga, N. (1982). An animal model of cerebral infarction. Homologous blood clot emboli in rats. *Stroke, 13*(4), 505-508.

Lalancette-Hébert, M., Swarup, V., Beaulieu, J. M., Bohacek, I., Abdelhamid, E., Weng, Y. C., Sato, S., & Kriz, J. (2012). Galectin-3 is required for resident microglia activation and proliferation in response to ischemic injury. *Journal of Neuroscience, 32*(30), 10383-10395.

Li, E., Bestor, T. H., & Jaenisch, R. (1992). Targeted mutation of the DNA methyltransferase gene results in embryonic lethality. *Cell, 69*(6), 915-926.

Li, F., Omae, T., & Fisher, M. (1999). Spontaneous hyperthermia and its mechanism in the intraluminal suture middle cerebral artery occlusion model of rats. *Stroke, 30*, 2464-2469.

Li, S., Overman, J. J., Katsman, D., Kozlov, S. V., Donnelly, C. J., Twiss, J. L., Giger, R. J., Coppola, G., Geschwind, D. H., & Carmichael, S. T. (2010). An age-related sprouting transcriptome provides molecular control of axonal sprouting after stroke. *Nat Neurosci, 13*(12), 1496-1504. doi: 10.1038/nn.2674

Li, X., Wei, W., Zhao, Q.-Y., Widagdo, J., Baker-Andresen, D., Flavell, C. R., D'Alessio, A., Zhang, Y., & Bredy, T. W. (2014). Neocortical Tet3-mediated accumulation of 5-hydroxymethylcytosine promotes rapid behavioral adaptation. *Proceedings of the national academy of sciences, 111*(19), 7120-7125.

Li, Z., Cai, X., Cai, C.-L., Wang, J., Zhang, W., Petersen, B. E., Yang, F.-C., & Xu, M. (2011). Deletion of Tet2 in mice leads to dysregulated hematopoietic stem cells and subsequent development of myeloid malignancies. *Blood, 118*(17), 4509-4518.

Li, Z., Gu, T.-P., Weber, A. R., Shen, J.-Z., Li, B.-Z., Xie, Z.-G., Yin, R., Guo, F., Liu, X., & Tang, F. (2015). Gadd45a promotes DNA demethylation through TDG. *Nucleic acids research, 43*(8), 3986-3997.

Liesz, A., Suri-Payer, E., Veltkamp, C., Doerr, H., Sommer, C., Rivest, S., Giese, T., & Veltkamp, R. (2009). Regulatory T cells are key cerebroprotective immunomodulators in acute experimental stroke. *Nature medicine, 15*(2), 192-199.

Lin, G., Sun, W., Yang, Z., Guo, J., Liu, H., & Liang, J. (2017). Hypoxia induces the expression of TET enzymes in HepG2 cells. *Oncology letters, 14*(6), 6457-6462.

Lindner, R., Puttagunta, R., Nguyen, T., & Di Giovanni, S. (2014). DNA methylation temporal profiling following peripheral versus central nervous system axotomy. *Scientific data, 1*, 140038.

Lister, R., Mukamel, E. A., Nery, J. R., Urich, M., Puddifoot, C. A., Johnson, N. D., Lucero, J., Huang, Y., Dwork, A. J., & Schultz, M. D. (2013). Global epigenomic reconfiguration during mammalian brain development. *Science, 341*(6146), 1237905.

Liu, F., Schafer, D. P., & McCullough, L. D. (2009). TTC, fluoro-Jade B and NeuN staining confirm evolving phases of infarction induced by middle cerebral artery occlusion. *J Neurosci Methods, 179*(1), 1-8.

Liu, Q. R., Rubio, F. J., Bossert, J. M., Marchant, N. J., Fanous, S., Hou, X., Shaham, Y., & Hope, B. T. (2014). Detection of molecular alterations in methamphetamine-activated Fos-expressing neurons from a single rat dorsal striatum using fluorescence-activated cell sorting (FACS). *Journal of neurochemistry, 128*(1), 173-185.

Liu, X. S., Wu, H., Ji, X., Stelzer, Y., Wu, X., Czauderna, S., Shu, J., Dadon, D., Young, R. A., & Jaenisch, R. (2016). Editing DNA methylation in the mammalian genome. *Cell, 167*(1), 233-247. e217.

Liu, Z., Fan, Y., Won, S. J., Neumann, M., Hu, D., Zhou, L., Weinstein, P. R., & Liu, J. (2007). Chronic treatment with minocycline preserves adult new neurons and reduces functional impairment after focal cerebral ischemia. *Stroke, 38*(1), 146-152.

Loane, D. J., & Byrnes, K. R. (2010). Role of microglia in neurotrauma. *Neurotherapeutics, 7*(4), 366-377.

Lobo, M. K., Karsten, S. L., Gray, M., Geschwind, D. H., & Yang, X. W. (2006). FACS-array profiling of striatal projection neuron subtypes in juvenile and adult mouse brains. *Nat Neurosci, 9*(3), 443.

Loh, Y.-H. E., Koemeter-Cox, A., Finelli, M. J., Shen, L., Friedel, R. H., & Zou, H. (2017). Comprehensive mapping of 5-hydroxymethylcytosine epigenetic dynamics in axon regeneration. *Epigenetics, 12*(2), 77-92.

Longa, E. Z., Weinstein, P. R., Carlson, S., & Cummins, R. (1989). Reversible middle cerebral artery occlusion without craniectomy in rats. *Stroke, 20*(1), 84-91.

Lyko, F. (2017). The DNA methyltransferase family: A versatile toolkit for epigenetic regulation. *Nature Reviews Genetics*, nrg. 2017.2080.

Maiti, A., & Drohat, A. C. (2011). Thymine DNA glycosylase can rapidly excise 5-formylcytosine and 5-carboxylcytosine potential implications for active demethylation of CpG sites. *Journal of Biological Chemistry, 286*(41), 35334-35338.

Maunakea, A. K., Nagarajan, R. P., Bilenky, M., Ballinger, T. J., D'Souza, C., Fouse, S. D., Johnson, B. E., Hong, C., Nielsen, C., & Zhao, Y. (2010). Conserved role of intragenic DNA methylation in regulating alternative promoters. *Nature, 466*(7303), 253.

May, J. M. (2012). Vitamin C transport and its role in the central nervous system *Water Soluble Vitamins* (pp. 85-103): Springer.

McCloy, R. A., Rogers, S., Caldon, C. E., Lorca, T., Castro, A., & Burgess, A. (2014). Partial inhibition of Cdk1 in G2 phase overrides the SAC and decouples mitotic events. *Cell cycle, 13*(9), 1400-1412.

Mellen, M., Ayata, P., Dewell, S., Kriaucionis, S., & Heintz, N. (2012). MeCP2 binds to 5hmC enriched within active genes and accessible chromatin in the nervous system. *Cell, 151*(7), 1417-1430. doi: 10.1016/j.cell.2012.11.022

Mergenthaler, P., Dirnagl, U., & Meisel, A. (2004). Pathophysiology of stroke: lessons from animal models. *Metabolic brain disease, 19*(3-4), 151-167.

Miao, Z., He, Y., Xin, N., Sun, M., Chen, L., Lin, L., Li, J., Kong, J., Jin, P., & Xu, X. (2015). Altering 5-hydroxymethylcytosine modification impacts ischemic brain injury. *Human molecular genetics, 24*(20), 5855-5866.

Miele, M., & Fillenz, M. (1996). In vivo determination of extracellular brain ascorbate. *J Neurosci Methods, 70*(1), 15-19.

Miltenyi, S., Müller, W., Weichel, W., & Radbruch, A. (1990). High gradient magnetic cell separation with MACS. *Cytometry, 11*(2), 231-238. doi: 10.1002/cyto.990110203

Mogensen, U. B., Olsen, T. S., Andersen, K. K., & Gerds, T. A. (2013). Cause-specific Mortality after Stroke: Relation to Age, Sex, Stroke Severity, and Risk Factors in a 10-Year Follow-up Study. *Journal of Stroke and Cerebrovascular Diseases, 22*(7), e59-e65. doi: https://doi.org/10.1016/j.jstrokecerebrovasdis.2012.04.006

Morris-Blanco, K. C., Kim, T., Lopez, M. S., Bertogliat, M. J., Chelluboina, B., & Vemuganti, R. (2019). Induction of DNA Hydroxymethylation Protects the Brain After Stroke. *Stroke, 50*(9), 2513-2521.

Morrison, H. W., & Filosa, J. A. (2013). A quantitative spatiotemporal analysis of microglia morphology during ischemic stroke and reperfusion. *Journal of neuroinflammation, 10*(1), 782. doi: 10.1186/1742-2094-10-4

Münzel, M., Globisch, D., Brückl, T., Wagner, M., Welzmiller, V., Michalakis, S., Müller, M., Biel, M., & Carell, T. (2010). Quantification of the sixth DNA base hydroxymethylcytosine in the brain. *Angewandte Chemie International Edition, 49*(31), 5375-5377.

Murphy, T. H., & Corbett, D. (2009). Plasticity during stroke recovery: from synapse to behaviour. *Nat Rev Neurosci, 10*(12), 861-872. doi: http://www.nature.com/nrn/journal/v10/n12/suppinfo/nrn2735_S1.html

Nakajima, M., Hirano, T., Terasaki, T., & Uchino, M. (2010). Signal change of the substantia nigra on diffusion-weighted imaging following striatal infarction. *Internal Medicine, 49*(1), 65-68.

O'Collins, V. E., Macleod, M. R., Donnan, G. A., Horky, L. L., van der Worp, B. H., & Howells, D. W. (2006). 1,026 experimental treatments in acute stroke. *Annals of neurology, 59*(3), 467-477.

Ohab, J., & Carmichael, S. (2008). Poststroke neurogenesis: emerging principles of migration and localization of immature neurons. *The Neuroscientist, 14*(4), 369-380.

Ohba, N., Kiryu-Seo, S., Maeda, M., Muraoka, M., Ishii, M., & Kiyama, H. (2004). Expression of damage-induced neuronal endopeptidase (DINE) mRNA in peri-infarct cortical and thalamic neurons following middle cerebral artery occlusion. *Journal of neurochemistry, 91*(4), 956-964.

Okano, M., Bell, D. W., Haber, D. A., & Li, E. (1999). DNA methyltransferases Dnmt3a and Dnmt3b are essential for de novo methylation and mammalian development. *Cell, 99*(3), 247-257.

Okano, M., Xie, S., & Li, E. (1998a). Cloning and characterization of a family of novel mammalian DNA (cytosine-5) methyltransferases. *Nature genetics, 19*(3), 219.

Okano, M., Xie, S., & Li, E. (1998b). Dnmt2 is not required for de novo and maintenance methylation of viral DNA in embryonic stem cells. *Nucleic acids research, 26*(11), 2536-2540.

Orset, C., Macrez, R., Young, A. R., Panthou, D., Angles-Cano, E., Maubert, E., Agin, V., & Vivien, D. (2007). Mouse model of in situ thromboembolic stroke and reperfusion. *Stroke, 38*(10), 2771-2778.

Özdemir, Y. G., Bolay, H., Erdem, E., & Dalkara, T. (1999). Occlusion of the MCA by an intraluminal filament may cause disturbances in the hippocampal blood flow due to anomalies of circle of Willis and filament thickness. *Brain research, 822*(1-2), 260-264.

Palmisano, I., & Di Giovanni, S. (2018). Advances and limitations of current epigenetic studies investigating mammalian axonal regeneration. *Neurotherapeutics, 15*(3), 529-540.

Paroush, Z., Keshet, I., Yisraeli, J., & Cedar, H. (1990). Dynamics of demethylation and activation of the α-actin gene in myoblasts. *Cell, 63*(6), 1229-1237.

Parry, L., & Clarke, A. R. (2011). The roles of the methyl-CpG binding proteins in cancer. *Genes & cancer, 2*(6), 618-630.

Percie du Sert, N., Alfieri, A., Allan, S. M., Carswell, H. V., Deuchar, G. A., Farr, T. D., Flecknell, P., Gallagher, L., Gibson, C. L., & Haley, M. J. (2017). The IMPROVE guidelines (ischaemia models: procedural refinements of in vivo experiments). *Journal of Cerebral Blood Flow & Metabolism, 37*(11), 3488-3517.

Perego, C., Fumagalli, S., & De Simoni, M.-G. (2011). Temporal pattern of expression and colocalization of microglia/macrophage phenotype markers following brain ischemic injury in mice. *Journal of neuroinflammation, 8*(1), 174. doi: 10.1186/1742-2094-8-174

Pettigrew, L. C., Kindy, M. S., Scheff, S., Springer, J. E., Kryscio, R. J., Li, Y., & Grass, D. S. (2008). Focal cerebral ischemia in the TNFalpha-transgenic rat. *Journal of neuroinflammation, 5*(1), 1.

Pfaffl, M. W. (2001). A new mathematical model for relative quantification in real-time RT–PCR. *Nucleic acids research, 29*(9), e45-e45.

Picascia, A., Grimaldi, V., Iannone, C., Soricelli, A., & Napoli, C. (2015). Innate and adaptive immune response in stroke: Focus on epigenetic regulation. *Journal of Neuroimmunology, 289*, 111-120. doi: http://dx.doi.org/10.1016/j.jneuroim.2015.10.013

Pollema-Mays, S. L., Centeno, M. V., Apkarian, A., & Martina, M. (2014). Expression of DNA methyltransferases in adult dorsal root ganglia is cell-type specific and up regulated in a rodent model of neuropathic pain. *Frontiers in cellular neuroscience, 8*, 217.

Pösel, C., Möller, K., Boltze, J., Wagner, D.-C., & Weise, G. (2016). Isolation and flow cytometric analysis of immune cells from the ischemic mouse brain. *JoVE (Journal of Visualized Experiments)*(108), e53658.

Razin, A., Szyf, M., Kafri, T., Roll, M., Giloh, H., Scarpa, S., Carotti, D., & Cantoni, G. L. (1986). Replacement of 5-methylcytosine by cytosine: a possible mechanism for transient DNA demethylation during differentiation. *Proceedings of the national academy of sciences, 83*(9), 2827-2831.

Reeves, M. J., Bushnell, C. D., Howard, G., Gargano, J. W., Duncan, P. W., Lynch, G., Khatiwoda, A., & Lisabeth, L. (2008). Sex differences in stroke: epidemiology, clinical presentation, medical care, and outcomes. *The Lancet. Neurology, 7*(10), 915-926. doi: 10.1016/S1474-4422(08)70193-5

Renno, T., Krakowski, M., Piccirillo, C., Lin, J. Y., & Owens, T. (1995). TNF-alpha expression by resident microglia and infiltrating leukocytes in the central nervous system of mice with experimental allergic encephalomyelitis. Regulation by Th1 cytokines. *The Journal of Immunology, 154*(2), 944-953.

Robinson, R. G., Shoemaker, W. J., Schlumpf, M., Valk, T., & Bloom, F. E. (1975). Effect of experimental cerebral infarction in rat brain on catecholamines and behaviour. *Nature, 255*(5506), 332.

Rubio, F. J., Li, X., Liu, Q.-R., Cimbro, R., & Hope, B. T. (2016). Fluorescence activated cell sorting (FACS) and gene expression analysis of Fos-expressing neurons from fresh and frozen rat brain tissue. *JoVE (Journal of Visualized Experiments)*(114), e54358.

Rudenko, A., Dawlaty, M. M., Seo, J., Cheng, A. W., Meng, J., Le, T., Faull, K. F., Jaenisch, R., & Tsai, L.-H. (2013). Tet1 is critical for neuronal activity-regulated gene expression and memory extinction. *Neuron, 79*(6), 1109-1122.

Schenk, J. O., Miller, E., Gaddis, R., & Adams, R. N. (1982). Homeostatic control of ascorbate concentration in CNS extracellular fluid. *Brain research, 253*(1-2), 353-356.

Schiesser, S., Hackner, B., Pfaffeneder, T., Müller, M., Hagemeier, C., Truss, M., & Carell, T. (2012). Mechanism and Stem-Cell Activity of 5-Carboxycytosine Decarboxylation Determined by Isotope Tracing. *Angewandte Chemie International Edition, 51*(26), 6516-6520.

Scorziello, A., Pellegrini, C., Forte, L., Tortiglione, A., Gioielli, A., Iossa, S., Amoroso, S., Tufano, R., Di Renzo, G., & Annunziato, L. (2001). Differential vulnerability of cortical and cerebellar neurons in primary culture to oxygen glucose deprivation followed by reoxygenation. *Journal of neuroscience research, 63*(1), 20-26.

Sharkey, J. (1993). Perivascular microapplication of endothelin-1: a new model of focal cerebral ischaemia in the rat. *Journal of Cerebral Blood Flow & Metabolism, 13*(5), 865-871.

Shen, J.-C., Rideout III, W. M., & Jones, P. A. (1994). The rate of hydrolytic deamination of 5-methylcytosine in double-stranded DNA. *Nucleic acids research, 22*(6), 972-976.

Sist, B., Winship, I. R., & Jesudasan, S. J. B. (2012). Diaschisis, Degeneration, and Adaptive Plasticity After Focal Ischemic Stroke. In J. C. G. Rodriguez (Ed.), *Acute Ischemic Stroke* (pp. 1-28). Croatia: INTECH Open Access Publisher.

Slepko, N., & Levi, G. (1996). Progressive activation of adult microglial cells in vitro. *Glia, 16*(3), 241-246.

Song, C.-X., Szulwach, K. E., Dai, Q., Fu, Y., Mao, S.-Q., Lin, L., Street, C., Li, Y., Poidevin, M., & Wu, H. (2013). Genome-wide profiling of 5-formylcytosine reveals its roles in epigenetic priming. *Cell, 153*(3), 678-691.

Soriano, M. A., Ferrer, I., Rodríguez-Farré, E., & Planas, A. M. (1996). Apoptosis and c-Jun in the thalamus of the rat following cortical infarction. *Neuroreport, 7*(2), 425-428.

Stöger, R., Scaife, P. J., Shephard, F., & Chakrabarti, L. (2017). Elevated 5hmC levels characterize DNA of the cerebellum in Parkinson's disease. *npj Parkinson's Disease, 3*(1), 6.

Stroke Association, *State Of The Nation: Stroke Statistics*, February 2018. (2018, 27/06/2019). [PDF] Retrieved from https://www.stroke.org.uk/sites/default/files/state_of_the_nation_2018.pdf

Szulwach, K. E., Li, X., Li, Y., Song, C.-X., Wu, H., Dai, Q., Irier, H., Upadhyay, A. K., Gearing, M., & Levey, A. I. (2011). 5-hmC-mediated epigenetic dynamics during postnatal neurodevelopment and aging. *Nat Neurosci, 14*(12), 1607-1616.

Szwagierczak, A., Bultmann, S., Schmidt, C. S., Spada, F., & Leonhardt, H. (2010). Sensitive enzymatic quantification of 5-hydroxymethylcytosine in genomic DNA. *Nucleic acids research, 38*(19), e181-e181.

Tahiliani, M., Koh, K. P., Shen, Y., Pastor, W. A., Bandukwala, H., Brudno, Y., Agarwal, S., Iyer, L. M., Liu, D. R., & Aravind, L. (2009). Conversion of 5-methylcytosine to 5-hydroxymethylcytosine in mammalian DNA by MLL partner TET1. *Science, 324*(5929), 930-935.

Takai, D., & Jones, P. A. (2002). Comprehensive analysis of CpG islands in human chromosomes 21 and 22. *Proceedings of the national academy of sciences, 99*(6), 3740-3745.

Tamura, A., Graham, D., McCulloch, J., & Teasdale, G. (1981). Focal cerebral ischaemia in the rat: 1. Description of technique and early neuropathological consequences following middle cerebral artery occlusion. *Journal of Cerebral Blood Flow & Metabolism, 1*(1), 53-60.

Tamura, A., Kirino, T., Sano, K., Takagi, K., & Hidemune, O. (1990). Atrophy of the ipsilateral substantia nigra following middle cerebral artery occlusion in the rat. *Brain research, 510*(1), 154-157.

Tan, L., & Shi, Y. G. (2012). Tet family proteins and 5-hydroxymethylcytosine in development and disease. *Development, 139*(11), 1895-1902.

Tanaka, T., Ueno, M., & Yamashita, T. (2009). Engulfment of axon debris by microglia requires p38 MAPK activity. *Journal of Biological Chemistry, 284*(32), 21626-21636.

Taylor, A. M., Blurton-Jones, M., Rhee, S. W., Cribbs, D. H., Cotman, C. W., & Jeon, N. L. (2005). A microfluidic culture platform for CNS axonal injury, regeneration and transport. *Nat Meth, 2*(8), 599-605. doi: http://www.nature.com/nmeth/journal/v2/n8/suppinfo/nmeth777_S1.html

Terragni, J., Bitinaite, J., Zheng, Y., & Pradhan, S. (2012). Biochemical characterization of recombinant β-glucosyltransferase and analysis of global 5-hydroxymethylcytosine in unique genomes. *Biochemistry, 51*(5), 1009-1019.

Thomson, J. P., Lempiäinen, H., Hackett, J. A., Nestor, C. E., Müller, A., Bolognani, F., Oakeley, E. J., Schübeler, D., Terranova, R., & Reinhardt, D. (2012). Non-genotoxic carcinogen exposure induces defined changes in the 5-hydroxymethylome. *Genome biology, 13*(10), R93.

Tong, Z., Segura-Feliu, M., Seira, O., Homs-Corbera, A., Del Río, J. A., & Samitier, J. (2015). A microfluidic neuronal platform for neuron axotomy and controlled regenerative studies. *RSC Advances, 5*(90), 73457-73466.

Town, T., Nikolic, V., & Tan, J. (2005). The microglial" activation" continuum: from innate to adaptive responses. *Journal of neuroinflammation, 2*(1), 24.

Trakhtenberg, E. F., & Goldberg, J. L. (2011). Neuroimmune communication. *Science, 334*(6052), 47-48.

Trueman, R. C., Diaz, C., Farr, T. D., Harrison, D. J., Fuller, A., Tokarczuk, P. F., Stewart, A. J., Paisey, S. J., & Dunnett, S. B. (2017). Systematic and detailed analysis of behavioural tests in the rat middle cerebral artery occlusion model of stroke: Tests for long-term assessment. *Journal of Cerebral Blood Flow & Metabolism, 37*(4), 1349-1361.

Tsenkina, Y., Ruzov, A., Gliddon, C., Horsburgh, K., & De Sousa, P. A. (2014). White matter tract and glial-associated changes in 5-hydroxymethylcytosine following chronic cerebral hypoperfusion. *Brain research, 1592*, 82-100.

Ünal-Çevik, I., Kılınç, M., Gürsoy-Özdemir, Y., Gurer, G., & Dalkara, T. (2004). Loss of NeuN immunoreactivity after cerebral ischemia does not indicate neuronal cell loss: a cautionary note. *Brain research, 1015*(1-2), 169-174.

Upadhyay, A. K., Horton, J. R., Zhang, X., & Cheng, X. (2011). Coordinated methyl-lysine erasure: structural and functional linkage of a Jumonji demethylase domain and a reader domain. *Current opinion in structural biology, 21*(6), 750-760.

Valinluck, V., & Sowers, L. C. (2007). Endogenous cytosine damage products alter the site selectivity of human DNA maintenance methyltransferase DNMT1. *Cancer research, 67*(3), 946-950.

Wang, F., Yang, Y., Lin, X., Wang, J.-Q., Wu, Y.-S., Xie, W., Wang, D., Zhu, S., Liao, Y.-Q., Sun, Q., Yang, Y.-G., Guo, C., Han, C., & Tang, T.-S. (2013). Genome-wide Loss of 5-hmC is a Novel Epigenetic Feature of Huntington's Disease. *Human molecular genetics*. doi: 10.1093/hmg/ddt214

Wang, M., Ji, X., Wang, B., Li, Q., & Zhou, J. (2018). Simultaneous Evaluation of the Preservative Effect of RNA later on Different Tissues by Biomolecular and Histological Analysis. *Biopreservation and biobanking, 16*(6), 426-433.

Wang, Q., Tang, X. N., & Yenari, M. A. (2007). The inflammatory response in stroke. *Journal of Neuroimmunology, 184*(1), 53-68.

Wang, Y., & Zhang, Y. (2014). Regulation of TET protein stability by calpains. *Cell reports, 6*(2), 278-284.

Watt, F., & Molloy, P. L. (1988). Cytosine methylation prevents binding to DNA of a HeLa cell transcription factor required for optimal expression of the adenovirus major late promoter. *Genes & development, 2*(9), 1136-1143.

Wei, L., Ying, D.-J., Cui, L., Langsdorf, J., & Yu, S. P. (2004). Necrosis, apoptosis and hybrid death in the cortex and thalamus after barrel cortex ischemia in rats. *Brain research, 1022*(1-2), 54-61.

Weng, Y.-L., An, R., Cassin, J., Joseph, J., Mi, R., Wang, C., Zhong, C., Jin, S.-G., Pfeifer, G. P., Bellacosa, A., Dong, X., Hoke, A., He, Z., Song, H., & Ming, G.-l. (2017). An Intrinsic Epigenetic Barrier for Functional Axon Regeneration. *Neuron, 94*(2), 337-346.e336. doi: https://doi.org/10.1016/j.neuron.2017.03.034

Wheldon, L. M., Abakir, A., Ferjentsik, Z., Dudnakova, T., Strohbuecker, S., Christie, D., Dai, N., Guan, S., Foster, J. M., & Corrêa Jr, I. R. (2014). Transient accumulation of 5-carboxylcytosine indicates involvement of active demethylation in lineage specification of neural stem cells. *Cell reports, 7*(5), 1353-1361.

Winship, I. R., & Murphy, T. H. (2008). In vivo calcium imaging reveals functional rewiring of single somatosensory neurons after stroke. *The Journal of Neuroscience, 28*(26), 6592-6606.

Winter, B., Juckel, G., Viktorov, I., Katchanov, J., Gietz, A., Sohr, R., Balkaya, M., Hörtnagl, H., & Endres, M. (2005). Anxious and Hyperactive Phenotype Following Brief Ischemic Episodes in Mice. *Biological Psychiatry, 57*(10), 1166-1175. doi: https://doi.org/10.1016/j.biopsych.2005.02.010

Witte, O. W., Bidmon, H.-J., Schiene, K., Redecker, C., & Hagemann, G. (2000). Functional differentiation of multiple perilesional zones after focal cerebral ischemia. *Journal of Cerebral Blood Flow & Metabolism, 20*(8), 1149-1165.

Wu, D., & Yotnda, P. (2011). Induction and testing of hypoxia in cell culture. *JoVE (Journal of Visualized Experiments)*(54), e2899.

Wu, J.-b., Song, N.-n., Wei, X.-b., Guan, H.-s., & Zhang, X.-m. (2008). Protective effects of paeonol on cultured rat hippocampal neurons against oxygen–glucose deprivation-induced injury. *Journal of the neurological sciences, 264*(1-2), 50-55.

Xu, Y., Wu, F., Tan, L., Kong, L., Xiong, L., Deng, J., Barbera, A. J., Zheng, L., Zhang, H., & Huang, S. (2011). Genome-wide regulation of 5hmC, 5mC, and gene expression by Tet1 hydroxylase in mouse embryonic stem cells. *Molecular cell, 42*(4), 451-464.

Yan, Y.-P., Lang, B. T., Vemuganti, R., & Dempsey, R. J. (2009). Galectin-3 mediates post-ischemic tissue remodeling. *Brain research, 1288*, 116-124. doi: https://doi.org/10.1016/j.brainres.2009.06.073

Yanev, P., & Dijkhuizen, R. M. (2012). In vivo imaging of neurovascular remodeling after stroke. *Stroke, 43*(12), 3436-3441.

Yen, R.-W. C., Vertino, P. M., Nelkin, B. D., Yu, J. J., El-Deiry, W., Cumaraswamy, A., Lennon, G. G., Trask, B. J., Celano, P., & Baylin, S. B. (1992). Isolation and characterization of the cDNA encoding human DNA methyltransferase. *Nucleic acids research, 20*(9), 2287-2291.

Yildirim, O., Li, R., Hung, J.-H., Chen, P. B., Dong, X., Ee, L.-S., Weng, Z., Rando, O. J., & Fazzio, T. G. (2011). Mbd3/NURD complex regulates expression of 5-hydroxymethylcytosine marked genes in embryonic stem cells. *Cell, 147*(7), 1498-1510.

Yin, R., Mo, J., Lu, M., & Wang, H. (2015). Detection of human urinary 5-hydroxymethylcytosine by stable isotope dilution HPLC-MS/MS analysis. *Analytical chemistry, 87*(3), 1846-1852.

Yu, H., Su, Y., Shin, J., Zhong, C., Guo, J. U., Weng, Y.-L., Gao, F., Geschwind, D. H., Coppola, G., & Ming, G.-l. (2015). Tet3 regulates synaptic transmission and homeostatic plasticity via DNA oxidation and repair. *Nat Neurosci, 18*(6), 836.

Yu, M., Hon, G. C., Szulwach, K. E., Song, C.-X., Jin, P., Ren, B., & He, C. (2012). Tet-assisted bisulfite sequencing of 5-hydroxymethylcytosine. *Nature Protocols, 7*, 2159.

Yushkevich, P. A., Piven, J., Hazlett, H. C., Smith, R. G., Ho, S., Gee, J. C., & Gerig, G. (2006). User-guided 3D active contour segmentation of anatomical structures: significantly improved efficiency and reliability. *Neuroimage, 31*(3), 1116-1128.

Zhang, H., Zhang, X., Clark, E., Mulcahey, M., Huang, S., & Shi, Y. G. (2010). TET1 is a DNA-binding protein that modulates DNA methylation and gene transcription via hydroxylation of 5-methylcytosine. *Cell Res, 20*(12), 1390-1393. doi: http://www.nature.com/cr/journal/v20/n12/suppinfo/cr2010156s1.html

Zhang, L., Szulwach, K. E., Hon, G. C., Song, C.-X., Park, B., Yu, M., Lu, X., Dai, Q., Wang, X., & Street, C. R. (2013). Tet-mediated covalent labelling of 5-methylcytosine for its genome-wide detection and sequencing. *Nature communications, 4*, 1517.

Zhang, Q., Deng, X.-X., Sun, X., Xu, J.-X., & Sun, F.-Y. (2013). Exercise promotes axon regeneration of newborn striatonigral and corticonigral projection neurons in rats after ischemic stroke. *PLoS ONE, 8*(11), e80139.

Zhang, R., Cui, Q.-Y., Murai, K., Lim, Y. C., Smith, Z. D., Jin, S., Ye, P., Rosa, L., Lee, Y. K., & Wu, H.-P. (2013). Tet1 regulates adult hippocampal neurogenesis and cognition. *Cell stem cell, 13*(2), 237-245.

Zhang, T., Gu, J., Wu, L., Li, N., Sun, Y., Yu, P., Wang, Y., Zhang, G., & Zhang, Z. (2017). Neuroprotective and axonal outgrowth-promoting effects of tetramethylpyrazine nitrone in chronic cerebral hypoperfusion rats and primary hippocampal neurons exposed to hypoxia. *Neuropharmacology, 118*, 137-147.

Zhang, Y., Xing, S., Zhang, J., Li, J., Li, C., Pei, Z., & Zeng, J. (2011). Reduction of β-amyloid deposits by γ-secretase inhibitor is associated with the attenuation of secondary damage in the ipsilateral thalamus and sensory functional improvement after focal cortical infarction in hypertensive rats. *Journal of Cerebral Blood Flow & Metabolism, 31*(2), 572-579.

Zhang, Z., Zhang, Z., Fauser, U., & Schluesener, H. J. (2007). Global hypomethylation defines a sub-population of reactive microglia/macrophages in experimental traumatic brain injury. *Neuroscience Letters, 429*(1), 1-6. doi: https://doi.org/10.1016/j.neulet.2007.09.061

Zhao, F., Kuroiwa, T., Miyasaka, N., Nagaoka, T., Nakane, M., Tamura, A., & Mizusawa, H. (2001). Characteristic changes in T2-value, apparent diffusion coefficient, and ultrastructure of substantia nigra evolving exofocal postischemic neuronal death in rats. *Brain research, 895*(1-2), 238-244.

Zhao, H., Wang, J., Gao, L., Wang, R., Liu, X., Gao, Z., Tao, Z., Xu, C., Song, J., & Ji, X. (2013). MiRNA-424 protects against permanent focal cerebral ischemia injury in mice involving suppressing microglia activation. *Stroke, 44*(6), 1706-1713.